FINAL DESIGN REPORT FOR THE

HEX BEAMLINE AT NSLS-II

Final Design Review date: 1 April 2019

Document No. NSLSII-27ID-RPT-002.

A Project in Collaboration with, and Financed by the
New York State Energy Research and Development Association (NYSERDA)
under contract 110960

Report Prepared by:

Andrew Broadbent
Brookhaven National Laboratory
P.O. Box 5000, Upton, NY 11973

Managed by Brookhaven Science Associates for the

U.S. Department of Energy, Office of Science, Basic Energy Science,
under contract DE-SC0012704

BROOKHAVEN
NATIONAL LABORATORY

Version History Log

Version	Date	Reason
A	23 March 2019	First Issue

Acknowledgments

This document was made possible through the hard work of many people. The editor would like to particularly thank the following staff who contributed chapters of this report.

- Mo Benmerrouche (Shielding calculations)
- Oleg Chubar (Calculations for the wiggler output spectrum, fan etc.)
- Raj Gutta (Cost estimates, contingency analyses, project management information)
- Charlie Hetzel (Straight and X-ray beam extraction)
- Mike Lucas (Drawings)
- Brian McCaffrey and Tom Joos (satellite building design)
- Sushil Sharma (Front End)
- Chris Stebbins (utilities and protection systems)
- Lori Stiegler (ES&H)
- Toshi Tanabe (SCW)
- Rob Todd (Vacuum)
- Zhijian Yin (Controls)
- Zhong Zhong (Filters, Laue mono, Diagnostics, End-stations)

Additionally, it is appropriate to thank the following people who have contributed significantly to this project.

- Members of the Beamline Advisory Team, especially Mark Croft (Rutgers University) and Yan Gao (GE Research) for their vision and efforts to propose this beamline in the first round of Beamline Development Proposals, before NSLS-II was completed.
- Eric Dooryhee Diffraction Program Manager for advice and support.
- Erik Johnson and Paul Zschack for significant overall guidance.
- Many other members of the NSLS-II staff who have been patient with my constant questioning and requests for many different forms of information – technical, financial, procedural etc.

Table of Contents

List of Abbreviations

ALARA	As Low As Reasonably Achievable
APS	Advance Photon Source (Argonne, IL)
ADXD	Angle Dispersive X-ray Diffraction
BESAC	Basic Energy Sciences Advisory Committee
BM	Bending Magnet
BMPS	Bending Magnet Photon Shutter
BNL	Brookhaven National Laboratory
BORE	Beneficial Occupancy Readiness Evaluation
BPM	Beam Position Monitor
BR	Bremsstrahlung Radiation
BRS	Bremsstrahlung Stop
BSA	Brookhaven Science Associates
BTF	Burn-Through Flange
CA	Channel Access
CABS	Crotch Absorber
CCG	Cold Cathode Gauge
CFR	Code of Federal Regulations
CHESS	Cornell High Energy Synchrotron Source (Ithaca, NY)
CRL	Compound Refractive Lens
CSS	Control System Studio
CT	Computed Tomography
CuCrZr	Copper/Chromium/Zirconium (a special copper alloy)
CCG	Cold Cathode Gauge
CDR	Conceptual Design Review
DAMA	Data Acquisition, Management and Analysis
DOE	Department of Energy
DI	De-Ionized (water)
DP	Differential Pump
DW	Damping Wiggler
EA	Environmental Assessment
EDXD	Energy Dispersive X-ray Diffraction
EPICS	Experimental Physics and Industrial Control System
EPS	Equipment Protection System
ESD	Emergency Shutdown
ES&H	Environment, Safety, and Health
ESRF	European Synchrotron Radiation Facility (Grenoble, France)
EVG	Event Generator
EVR	Event Receiver
FDR	Final Design Review
FE	Front End
FEA	Finite Element Analysis
FEP	Fluorinated Ethylene Propylene
FOE	First Optics Enclosure
FOM	Figure of Merit
FOV	Field of View
FPPS	Front-end Personnel Protection System
FWHM	Full Width at Half Maximum
GB	Gas Bremsstrahlung
GE	General Electric
GHe	Gaseous Helium
HEX	High-energy Engineering X-ray (Beamline)
HMI	Human-Machine Interface
HTS or HTSC	High Temperature Superconductor
HV	High Voltage
HXN	Hard X-ray Nanoprobe (NSLS-II Beamline)
ID	Insertion Device
ID	Inside Diameter

IMBL	Imaging and Medical Beamline (Australian Synchrotron)
IOC	Input/Output Controller (a rack mounting computer)
IRR	Instrument Readiness Review
ISM	Integrated Safety Management
KB	Kirkpatrick-Baez (mirror)
keV	kilo electron Volt
KPM	Key Performance Metric
LAN	Local Area Network
LCO	Lead Collimator
LHe	Liquid Helium
LIMS	Laboratory Information Management System
LOB	Laboratory Office Building
MCA	Multiple Channel Analyzer
NEG	Non-Evaporable Getter
NFPA	National Fire Protection Association
NSLS	National Synchrotron Light Source (now closed)
NSLS-II	National Synchrotron Light Source II
NYSERDA	New York State Energy Research and Development Association
OD	Outside Diameter
ODH	Oxygen Deficiency Hazard
OPI	Operator Interface
PDF	Pair Distribution Function
PDR	Preliminary Design Review
PLC	Programmable Logic Controller
PPS	Personnel Protection System
PS	Photon Shutter
PSD	Photon Stimulated Desorption
PV	Process Variable
QA	Quality Assurance
QRGA	Quadrupole Residual Gas Analyzer
RAV	Right Angle Valve
RCO	Ratchet-wall Collimator
RF	Radio Frequency
RGA	Residual Gas Analysis
RMS	Root Mean Square
RSI	Requirements, specification and Interfaces (document)
RW	Ratchet Wall
SAD	Safety Assessment Document
SAXS	Small Angle X-ray Scattering
SBM	Side Branch Monochromator
SBMS	Standards Based Management System
SC	Superconductor
SCW	Superconducting Wiggler
SGV	Slow Gate Valve
SiC	Silicon Carbide
SNS	Spallation Neutron Source (TN)
SR	Storage Ring
SR	Synchrotron Radiation
SS	Safety Shutter
TIG	Tungsten Inert Gas (welding)
TSP	Titanium Sublimation Pump
UHV	Ultra High Vacuum
VFM	Vertical Focusing Mirror
VME	Versa Module Europa (bus)
WBS	Work Breakdown Structure
WBS	White Beam Stop
XPD	X-ray Powder Diffraction (beamline)
YAG	Yttrium Aluminum Garnet

List of Figures

1. Project Overview

1.1. Introduction

The New York State Energy Research and Development Association (NYSERDA) has provided funding ($25M) for the development of an x-ray beamline at the National Synchrotron Light Source II (NSLS-II) facility at Brookhaven National Laboratory. NSLS-II will contribute a further $5M to cover the oversight costs. This beamline will be used for in-situ and in-operando studies of sustainable energy materials and devices; in order to penetrate thick metallic samples and the equipment required for various sample environments, the x-rays will be of high energy.

Typical samples to be studied at the beamline include fully assembled and functioning batteries, photovoltaic materials, fuel cells, and a wide range of engineering materials including gas turbine blades, composite structures, and a wide range of materials under extreme conditions (stress, temperature, chemical environments etc). The scientific techniques possible at the beamline will include both imaging and diffraction; the high energies will make this a unique beamline at NSLS-II and one of perhaps a dozen such beamline worldwide – many of which are highly oversubscribed.

The scientific objectives fit with the stated mission needs for the US Department of Energy.

1.2. Mission Statement

The mission of the HEX beamline is to help advance clean energy technologies and creative energy storage solutions. This facility will provide world-leading x-ray imaging capabilities to support engineering materials development in NY State and beyond

1.3. Background

Over the past decade, the DOE BES research needs have been defined and documented by the scientific community in ten “Basic Research Needs” Workshop Reports in the areas of hydrogen economy, solar energy utilization, superconductivity, solid state lighting, advanced nuclear energy systems, combustion of 21st century transportation fuels, electrical-energy storage, geosciences related to the storage of energy wastes (the long-term storage of both nuclear waste and carbon dioxide), materials under extreme environments, and catalysis for energy applications. These were followed by a report from the BES Advisory Committee (BESAC), “New Science for a Secure and Sustainable Energy Future,” which summarized the magnitude of the challenges facing the U.S. in the realm of energy and environment and emphasized the importance of fundamental science for finding transformational solutions. Collectively, these reports underscore the need to develop new tools that will allow characterization of the atomic and electronic structure, chemical composition, and magnetic properties of materials with nanoscale resolution.

1.4. Previous Work at NSLS

The NSLS facility, closed in 2014 as the new NSLS-II came on stream, had one high energy beamline, which ran successfully for ~25 years. X17 that specialized in much of the work planned for HEX. A number of enthusiastic X17 Users, as well as beamline staff, first proposed the HEX beamline in a call for

Beamline Development Proposals in 2011. Significant developments in high energy x-ray optical systems and experimental techniques were made at X17; it is anticipated that the developments will be a stepping stone to a new world-class, high-energy facility.

1.5. Scope

The scope of the project includes a superconducting wiggler, optimized for high energies, any necessary modifications to the NSLS-II storage ring, and the Front End inside the storage ring tunnel which collimates the beam, allows switching of the beam sizes, and allows the beam to be safely switches off.

Outside the storage ring tunnel the beamline, comprising optics, diagnostics, safety components and sections of shielded transport pipe, passes through a series of lead hutches (rooms) to an external satellite building housing an experimental station within a concrete bunker (approx. 20m x 5m wide).

The initial scope will include the single central branch running to the satellite building. Affordances will be made in the design for the later addition of two side branches which use parts of the wide wiggler fan and would increase the utility of the beamline as much as three-fold.

The scope is documented in the WBS structure, and in detail in this document.

1.6. Schedule

The schedule was agreed in the formal contract between NYSERDA and BNL. Following a relaxation of the funding profile, an accelerated schedule was agreed, which is expected to save ~6 months.
The planned milestone dates listed below in Table 1 reflect this accelerated schedule.

HEX Project Milestone Dates	**Contract dates**	**Actual / Planned**
Project Start	Aug-17	12-SEP-17
HEX Beamline Conceptual Design Review	Nov-17	25-OCT-17
HEX Beamline Preliminary Design Review – **Go/No go 1**	Apr-18	26-APR-18
Superconducting Wiggler Procure / Make Decision– **Go/No Go 2**	Aug-18	30-AUG-18
Front End Design Review	Oct-18	25-SEPT-18
Hutches Procured	Mar-19	10-JAN-19
HEX Beamline Final Design Review– **Go/No go 3**	May-19	1&2-Apr-19
Satellite Building Contract Placed	Jul-19	14-DEC-18
Optical Components Procured	Sep-19	Jul-19
Beamline Hutches Installed and Complete	Apr-20	Feb-20
Satellite Building Beneficial Occupancy	Jul-20	Jul-20
End Station Components Procured	Sep-20	Jan-20
Optical Components Installed	Sep-21	Mar-21
HEX Beamline Utilities Complete		Feb-21
HEX Beamline Components Testing Complete		Mar-21
SCW Installation Complete	Apr-22	May-21
Instrument Readiness Review (IRR)	Jun-22	Nov-21
HEX Beamline Project Complete	July-22	Dec-21

Table 1: List of Project Milestones

1.7. Performance

The Key Performance Metrics (KPMs) and design parameters for the HEX beamline are taken directly from the NYSERDA / BNL contract for HEX; these are as follows:

Key Performance Metric	Objective	Objective Measure
Beamline design	Flexible hard x-ray beamline design for one functional branch line with affordances for a total of three branch lines.	Fully documented in the Final Design Review.
SCW source	Capable of producing photons of at least 150 keV.	Analysis of the measured parameters of the final SCW.
Photon Delivery System	Capable of delivering monochromatic or white (non-monochromatic) x-ray beam.	Successful completion of the IRR (Instrument Readiness Review).
Satellite End Station	At least 3000 GSF building housing integrated experimental end station enclosures (hutches).	Evaluation of the completed structure and successful completion of the BORE (Beneficial Occupancy Readiness Evaluation).

Table 2 The Key Performance Metrics (KPMs) and design parameters for the HEX beamline

The project objectives are considered to have been achieved when the above criteria are met.

The project team have a number of non-contractual goals for the project, which we plan to achieve during x-ray commissioning. These are as follows:

Monochromatic beam energy range	30 – 150 keV. Test experiments at 30, 70, 100, 150 keV to characterize the imaging mono. Diffraction from NIST standard (Al_2O_3) gives energy, flux measured with ion chamber at specific energies – confirmed by calculation.
White beam energy range	20 – 250 keV
Maximum beam size at F-hutch	20 mm (V) x 100 mm (H). To be measured with a burn paper or preferably use an x-ray eye type device to measure beam homogeneity, profile and size more accurately
Demonstration imaging experiment	Standard AA battery Stretch goal: image a machine screw
Demonstration EDXRD experiment	Standard AA battery.
International benchmarking	Late in commissioning, compare results against measurements of the same samples done at other facilities

.

2. HEX Beamline Scientific Programs and Technical Scope

This section will be added later.

3. HEX Beamline Design

3.1. HEX Beamline Design Overview

HEX is a hard x-ray beamline and will operate in the 20-250 keV range. The planned mature scope includes three independent branches capable of simultaneous operations. The scope of the current project is for the construction of the central branch only, with the satellite building and the experimental station. The design includes the affordances for building the two side branches in the future, without adding significantly to the cost, and ideally without causing major future disruption. The mature scope additions are discussed in greater detail in Section 3.13.

This section describes the source of the x-rays, in this case a Superconducting Wiggler (SCW) located in one of the thirty straights of the storage ring, the Front End (the part of the beamline located inside the Storage Ring tunnel, and including a shutter to turn the x-ray beam on and off, the beamline itself including the optics, diagnostics and vacuum, as well as the shielding and safety component design.

Figure 1 below shows the (initial, in-scope) central branch. White beam x-ray radiation passes from the wiggler source through the apertures and shutters that comprise the Front End, and then through the ratchet wall and onto the experimental floor. Substantial filtering of the beam then occurs in order to remove the lower energies which are not useful for this beamline, and which beneficially also removes a significant fraction of the beam power, before the beam touches any optical element (the monochromator).

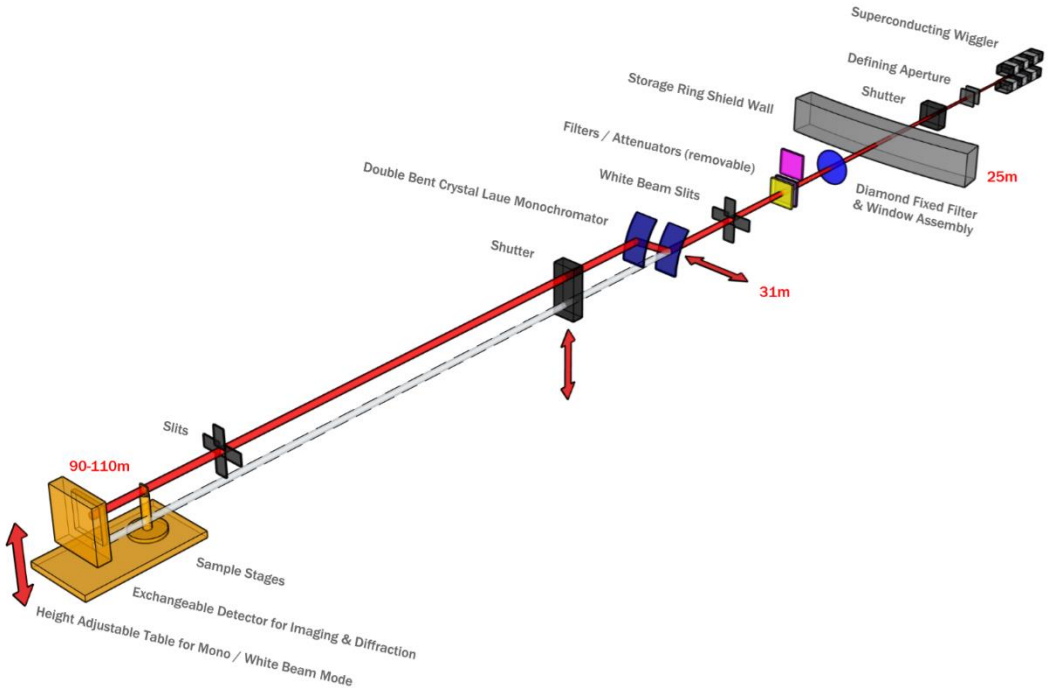

Figure 1 Schematic layout of the HEX beamline

3.2. HEX Initial Scope Beamline Layout

Figure 2 shows the initial scope layout of the HEX First Optics Enclosure (FOE) components, viewed from above. The design of HEX optics, for the initial scope, includes the center-branch imaging monochromator.

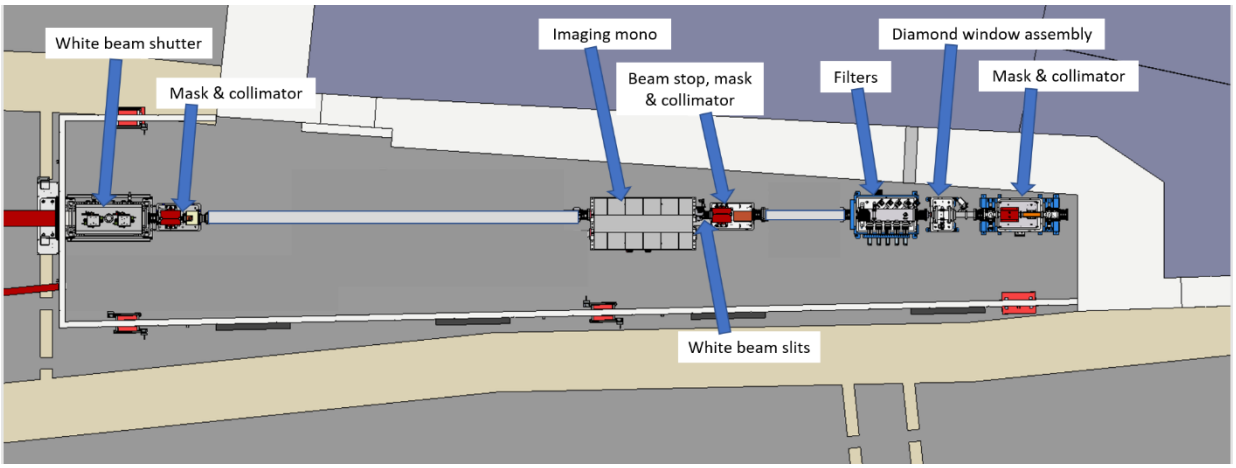

Figure 2 Initial scope layout of the HEX optics in the horizontal plane

The imaging mono has a meridionally bent crystal for imaging with a large beam fan in the F experimental enclosure. Since this center branch is white-beam compatible, we will use a small offset of 25 mm to allow compact design and facilitate beam stability.

The imaging monochromator will use meridionally-bent, asymmetric crystals. This is a proven design having been used at X17B1 of the NSLS, JEEP beamline at the Diamond Light Source, the Imaging Beamline at the Australian Light Source, and the BMIT facility at the Canadian Light Source. Water-cooled slits are upstream of the imaging monochromator.

3.3. HEX Mature Scope Beamline Layout

Figure 3 shows the mature scope layout of the HEX First Optics Enclosure (FOE) including all the optics, viewed from above. The design of HEX optics includes the side-bounce monochromator for the monochromatic beam branch, the center-branch imaging monochromator, and a (sagittal) focusing monochromator, also for the middle branch. The reason for placing the side-bounce monochromator at the upstream end of the optics is that the inbound white beam can be stopped immediately after the side-bounce monochromator, thereby greatly easing the design of the focusing monochromator and mirrors downstream. The monochromatic beam from the side-bounce monochromator crosses the white beams of the center branch and outboard white-beam branch. There is a mirror chamber, hosting two vertically-focusing mirrors for the central branch and the monochromatic side branch, downstream of the sagittal-focusing monochromator.

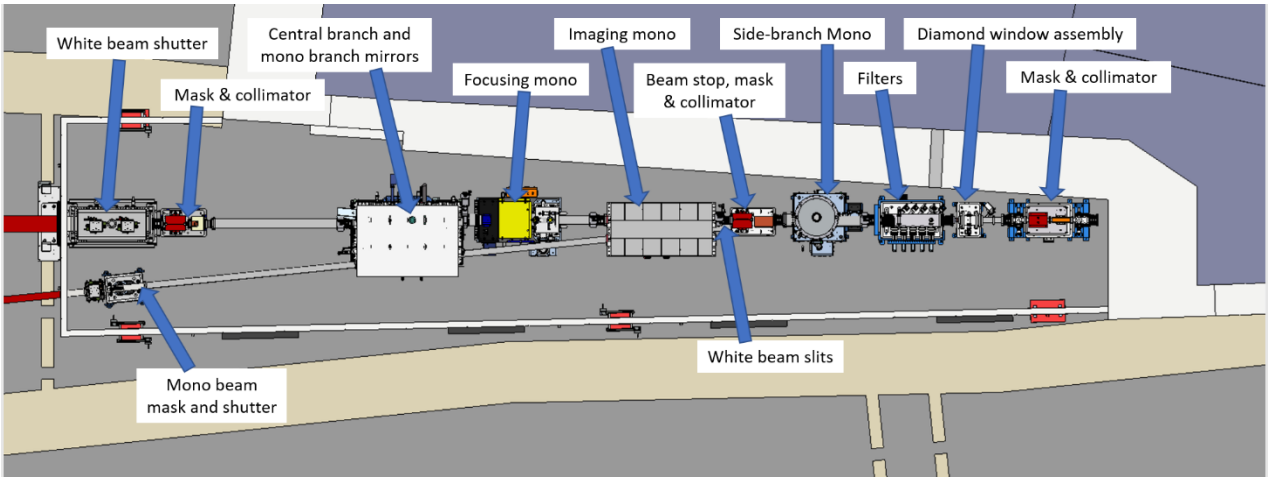

Figure 3 Mature scope layout of the HEX optics in the horizontal plane

Two bent-Laue monochromators will serve the center branch: the imaging mono was described above, and sagittal-focusing Laue monochromator for ADXD with focused beam in the E enclosure. Again, we will use a small offset of 25 mm to allow compact design and facilitate beam stability. The sagittal-focusing monochromator was invented at the NSLS, and is a proven design having been used successfully over the past decade at the X17B1, C, X7B beamlines at the NSLS, the XPD beamline at the NSLS-II, and the high-energy beam line at CHESS.

The sagittal-focused beam for the center branch will be vertically focused by a vertical-focusing mirror with approximately 1 mrad incident angle. Since the monochromatic beams have a 25 mm vertical offset in the upward direction, and the mirror bouncing the beam in the downward direction. This minimizes the distance between the three beams (white beam, imaging monochromatic beam, and focused monochromatic beam) allowing for a single large aperture white-beam shutter at the downstream end of the FOE to control the three beams. A similar shutter at the end of E experimental enclosure controls the three beams in the F enclosure.

We note that only the imaging monochromator is in the current scope of the project. However, the design of the beamline (FOE layout, beam transport, hutches) must accommodate future addition of a focusing monochromator, two focusing mirrors and future utilization of the outboard white beam branch. Table 3 summarizes the optics being considered. The optics shown in grey are not in the current scope; these mature scope items are described in detail in Section 3.13.

	Side branch	Center Branch	White-beam Branch
Monochromator	One-bounce bent-Laue	Sagittal focusing mono Imaging mono	N/A
Mirror	Vertical-focusing	Vertical-focusing	N/A
Mode	Monochromatic	White/Monochromatic	White

Table 3 Summary of the HEX beamline optics

Figure 4 shows the paths of the three beams (in green) in the mature scope configuration. Of note is the close proximity of the center branch and the white beam branch (in the same vacuum pipe on exit from the FOE).

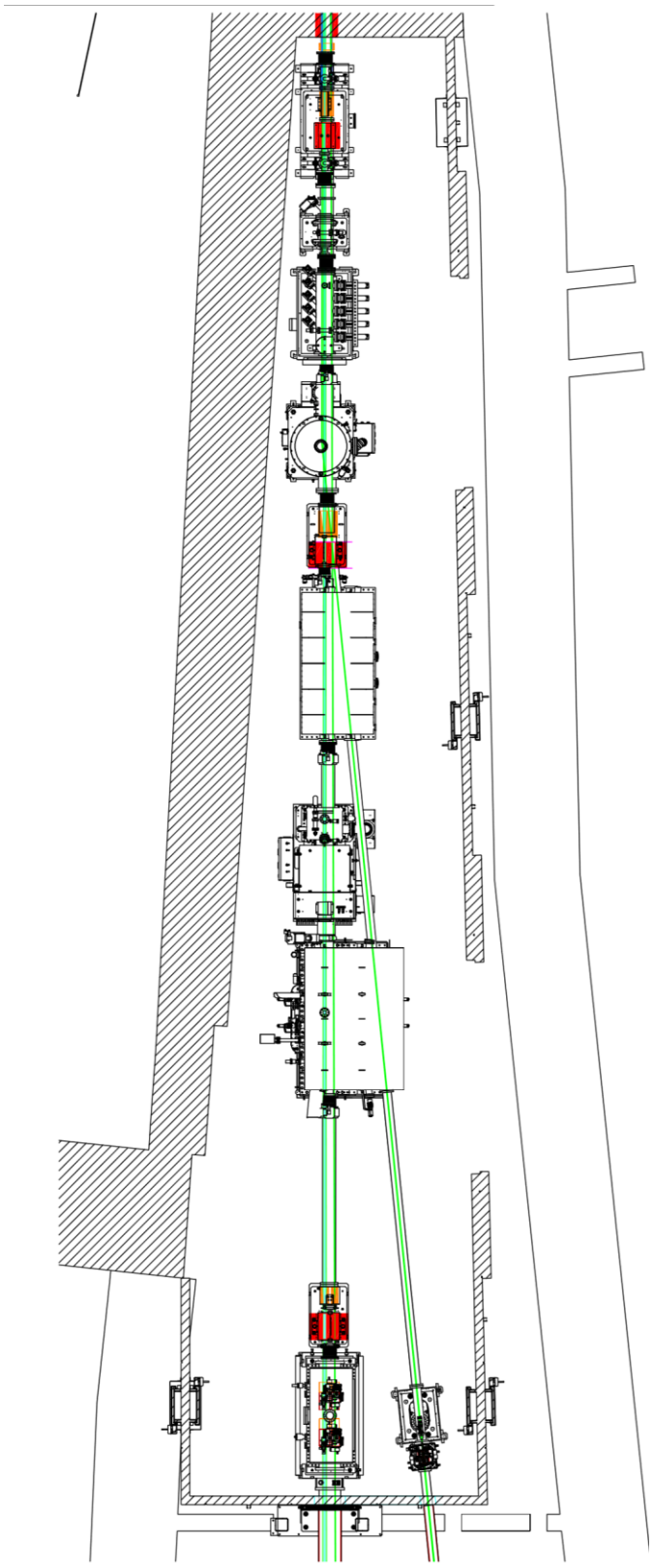

Figure 4 Mature scope layout showing the paths of the three beams in the horizontal plane

3.4. Beamline Component Listing

Table 4 shows a listing of the Beamline Components for the initial scope, and for the mature scope. Since some gate valves are not required in the initial build-out (since the components they will isolate will not be present), we seek to avoid renumbering the vacuum sections as the beamline is built out; the table defines the initial and final vacuum section numbers.

Location	Vacuum section (Initial)	Vacuum Section (Mature)	Initial Scope (Central Branch)	Mature scope
FOE	1	1	Mask/Collimator/Diamond Filter Assembly	
FOE	2	2	Diamond Window/Filter Assembly (suitable for 3 beams), 2 x brazed windows. Includes quartz viewport and shielded camera.	
FOE	3	3	SiC Filter Assembly (suitable for 3 beams). Includes quartz viewport and shielded camera.	
	3	3	Removable filter assembly for central branch, provision for extra filters for side branches.	Additional filters / actuators for side branches.
FOE		*		8" All Metal Gate Valve
FOE	3	4	8" Spool Section for Future SBM	Side Branch Mono
FOE	3	4	Beam Stop/Center Branch Pass Through & Collimator	
FOE	3	4	White Beam Slits	
	*	*	8" All Metal Gate Valve	
FOE	5	5	Imaging Mono (designed to allow future SBM beam to pass). Includes coated (removable) beamstop, quartz viewport and shielded camera.	
	5	5	Removable diagnostic flag for mono beam in monochromator chamber, including quartz viewport and shielded camera.	
		*		8" All Metal Gate Valve
	5	6	8" Spool Piece (Future Double Laue (focusing) Mono)	Focusing Mono
FOE		*		8" All Metal Gate Valve
FOE	5	7	8" Spool Piece (Future VFM) with ion pump	Vertically focusing mirrors for center branch and/or side branch.
FOE	*	*	8" All Metal Gate Valve	All Metal Gate Valve
FOE		20		Spool piece
FOE		20		Mask (mono beam)
FOE		20		Mono beam shutter
Hutch A-B		20		Transport Pipe
Hutch B		20		Pumping cross with gauges
Hutch B		*		All Metal Gate Valve
FOE	6	8	Mask/Collimator Assembly	
FOE	6	8	White Beam Shutters in vacuum vessel with ion pump, vacuum gauges, and diagnostic (coated copper block, with quartz viewport and camera). These two dual shutters independently control center branch & white-beam branches	

Hutch A-C	6	8	10” Shielded Transport Pipe	
Hutch C	6		Pumping cross with gauges	
Hutch C	*	*	10” All Metal Gate Valve	
Hutch C	9	9	Mask/Collimator Assembly	
Hutch C	9	9	4” Transport pipe (shielded)	4” Transport pipe (shielded)
Hutch D	9	9	4” Shielded Beam Pipe	
Hutch D	9	9	Beam stop and Bremsstrahlung Stop Assembly	
Hutch E	9	9	Pumping cross with gauges	
Hutch E	*	*	4” All Metal Gate Valve	
Hutch E	10	10	4” Un-Shielded Beam Pipe	
Hutch E	*	*	4” All Metal Gate Valve	
Hutch E	11	11	Mask/collimator assembly	
Hutch E	11	11	White Beam Shutter with ion pump, vacuum gauges, and diagnostic (coated copper block, with viewport and camera)	
Hutch E-F	11	11	Transport Pipe (shielded), with 1 x pumping box (6” diameter x 6 sections, 10” diameter x 3 sections, 3.5m per section).	
Hutch F	11	11	KB mirror system (located on beam conditioning table)	
Hutch F	11	11	Beam conditioning module incl attenuators / primary WB slits / window / fast shutter / cleanup slit / segmented ion chamber. All mounted on a rigid 5-axis support table	
Hutch F			White beam stop and Bremsstrahlung stop (300mm x 300mm)	

Table 4 Beamline Component Listing

3.5. Source

3.5.1. Source Requirements

The source requirement for the HEX beamline is for a broadband x-ray spectrum extending up to ~200keV for white beam. With an electron beam energy of 3 GeV for the NSLS-II ring, only a superconducting wiggler (SCW) producing greater than 4T peak field can cover this range with a sufficient number of photons.

A wiggler device consists of alternating vertical magnetic fields which will cause the electron beam in the storage ring, encountering these fields, to "wiggle" from side to side, emitting x-ray radiation over a horizontal fan in the forward direction. For the proposed imaging and micro-focusing applications at HEX, the brightness needs to be as high as possible; this means the wiggler should have as many magnetic poles as possible, or, for a given device length, the period length should be as small as possible. Such devices are available commercially.

The final choice of wiggler parameters is a careful trade-off between field, period and device length.

- The ideal device has a high field and small period,
- There is a practical limitation on increasing the magnetic field and decreasing the period due to the space available for coils and associated performance constraints on the superconductor,
- The size of the fan of x-rays produced by the device is a linear function of period and field. The extent of the fan is constrained by the exit port size from the ring (see Section 3.6 for a full description of these challenges). This therefore sets a maximum period for a given field.
- The power emitted by the device is proportional to the device length, and to the square of the magnetic field. Given the significant power produced (many 10s of kilowatts), this is not a trivial problem for the windows, filters and optics and great care has to be taken to ensure the power can be safely accommodated.
- Finally the source size, when viewed off-axis, increases with the wiggler length. For imaging applications the source size needs to be small.

The constraints listed above dictate in favor of a 4.3T magnetic field, 70mm period, and 1m magnetic length.
Figure 5 shows both the variation of brightness over the spectral range of interest, on-axis and off-axis (i.e. as seen by the central branch and a side-branch), and the concentration of the higher energies in the center of the fan.

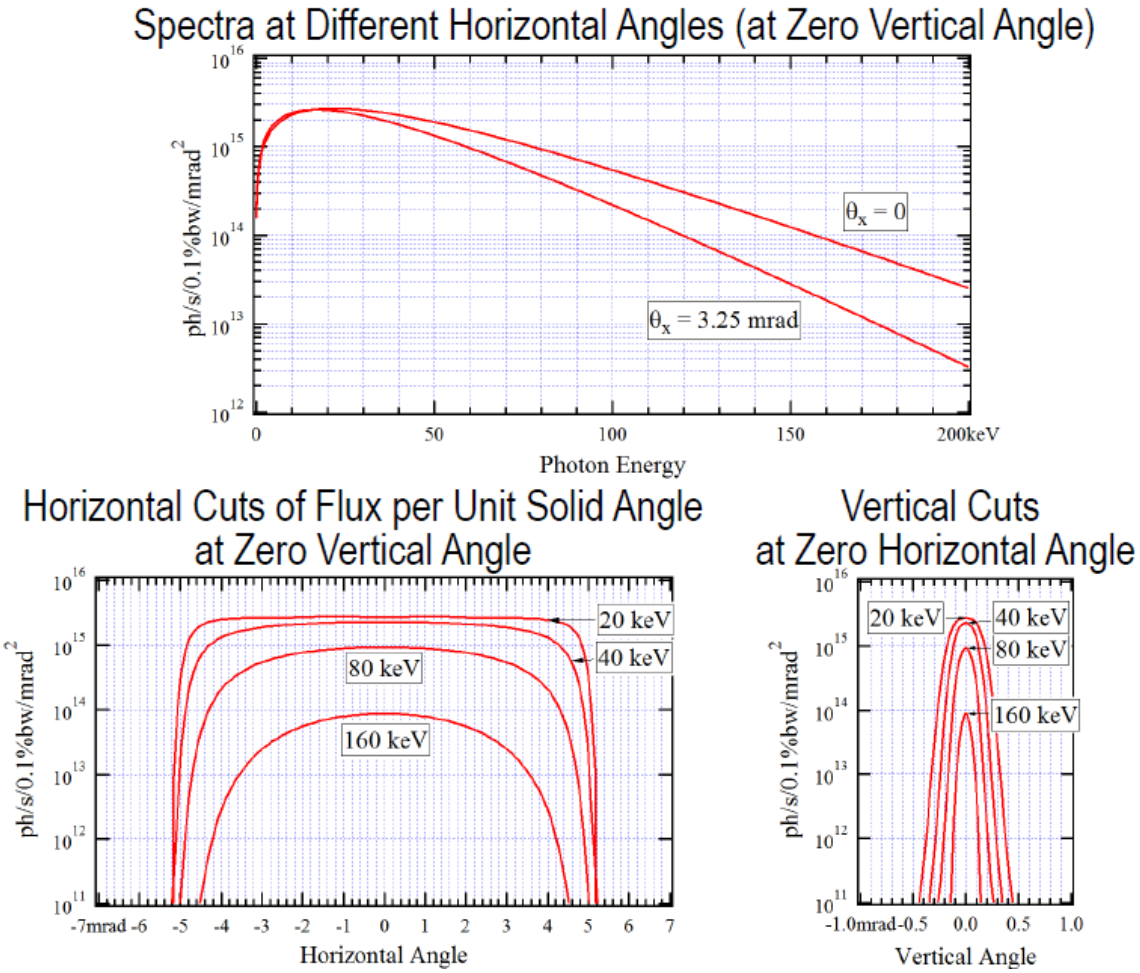

Figure 5 Spectral angular distribution of x-rays from the SCW70 device.

Ideally the wiggler should be installed in the center of a short straight section in the NSLS-II ring. However, HEX-SCW will be installed by 1m downstream from the straight center in order to minimize the exit fan size. Beam physics simulations have been conducted to ensure that the lattice can be compensated [1], and dynamic aperture degradation is acceptable. The final specifications of the SCW are shown in Table 5.

Beamline	HEX
Type	SCW
Device envelope length	~1.8 m
Magnetic Length	1.2m nominal (29 main and 4 partial poles)
Canted	No
Period: nominal	70 mm
Nominal (minimum) gap of vacuum bore tube	10 mm
Peak field nominal	4.3 T
K_{eff}: nominal	28.1[*1]

Energy Range:	8 keV –200 keV
Power total: nominal	55.7 kW[*1]
Max. power per unit solid angle: nominal	28.4 kW/mr^2 [*1]
Straight	Low beta
Device center[*2]	Offset by 1m to downstream
Fan angle [*3] (mrad H) : nominal (maximum)	9.87 (10.15)
Fan angle [*3] (mrad V) : nominal (maximum)	0.88 (1.47)
Gap scanning and other requirements	Current adjustment 0 – 100%

Table 5 Specifications for the Superconducting Wiggler (SCW)

Note 1: Assumes of sinusoidal magnetic field distribution in central part of wiggler.

Note 2: The ray tracing should accommodate axial movements of the IDs by +/-5mm, which might be required in the design of the straight.

Note 3: The fan angles of the radiation quoted here are as seen at 16m from the source, and it takes the effects of source length into account; the worst-case fan size is taken. The two values quoted are for the points where the power density falls to values that are 1% and 0.1% of the central value. Designs of the fixed mask entrance shall take these fringe power loads into account.

3.5.2. Superconducting Wiggler Design

A reference magnetic design in a left-handed coordinate system is given in Figure 6, and the expected spectra of the HEX-SCW (SCW70) as well as other similar devices are shown in Figure 7Figure 7 Spectra of HEX-SCW and those of other similar devices..

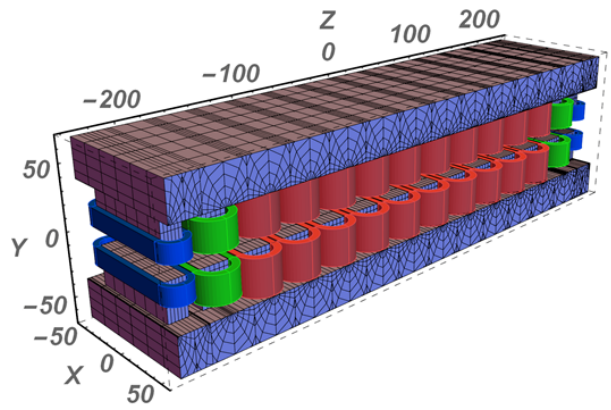

Magnetic Length	1.2m nominal (29 main and 4 partial poles)
Period: nominal	70 mm
Yoke Gap	15.2 mm
Peak field: nominal	4.3 T
Pole width	80mm
Main (red) Coil Height	29.5mm
Main Coil Thickness	6.3mm
Main Yoke Thickness	22.4mm
End Yoke Thickness	14.336mm
Green Coil Height	22.125mm
Blue Coil Height	14.16mm
Yoke Material	1006 Steel
Nominal Engineering Current Density@4.3T	900A/mm^2

Figure 6 Reference Magnetic Design of HEX-SCW Magnetic Circuit

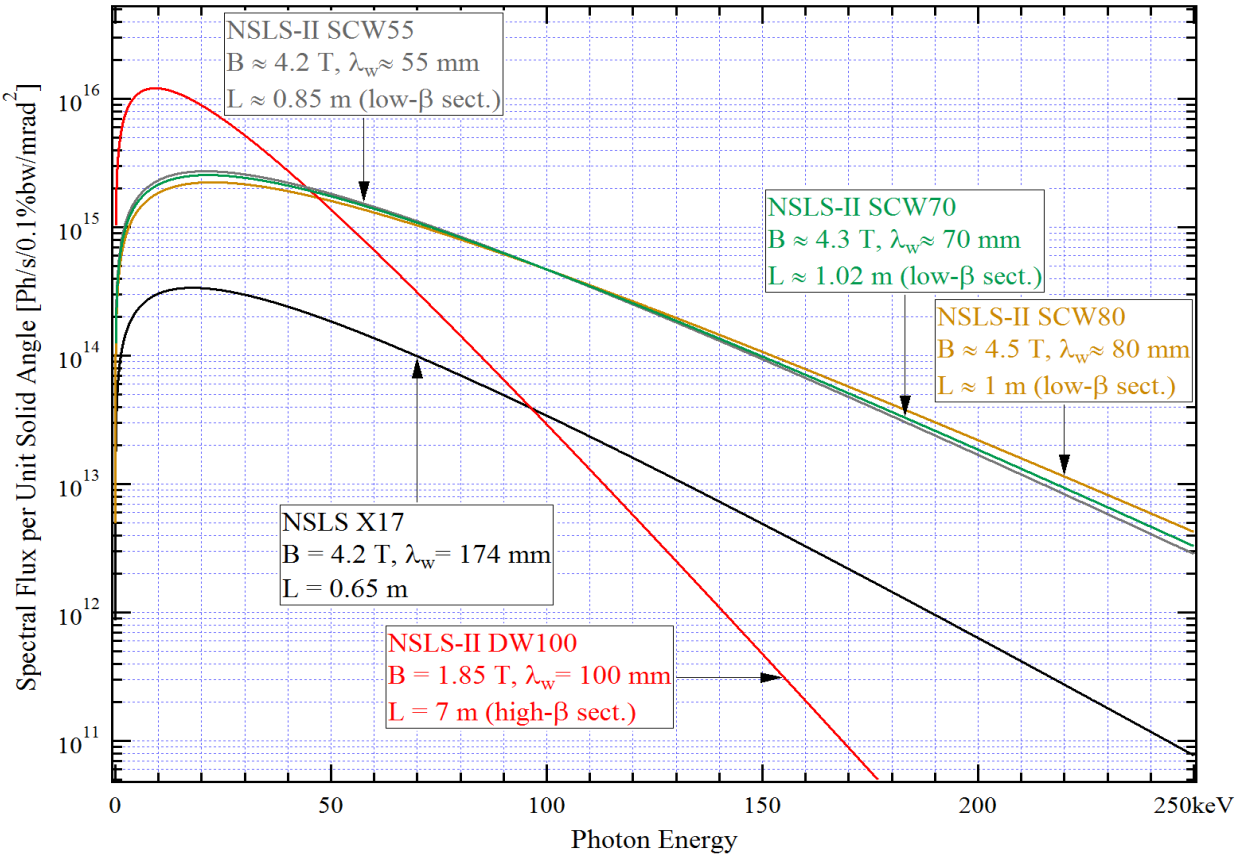

Figure 7 Spectra of HEX-SCW and those of other similar devices.

Figure 8 shows a typical design of a SCW by Budker Institute, Russia. It utilizes four cryocoolers with three stage (4K, 20K and 60K) heat shields. The vacuum chamber is made of stainless steel with copper liner inside. The copper liner is kept at 20K to shield 4K cold mass from heat generated by electron beam. At the ends of the electron beam vacuum chamber, solid tapered transition at ends of the narrow gap section is necessary to bring the internal vertical cross section of 10 mm (V) and 76mm (H) to the storage ring cell chamber cross-section of 25 mm vertical and 76 mm horizontal. Liquid He free design is also considered as long as the recovery time from a quench is acceptably short.

The expected beam induced heat load to the copper liner is set to be 30W/m. The contribution from resistive wall impedance is found to be small [2]. However, various measurements done at Diamond Light Source (DLS)indicate that hear load from geometric impedance is greater than that from resistive wall [3]. This value has been derived from the measured value of heat load at the DLS with scaling to NSLS-II ring parameters.

The cryostat must be designed to prevent this beam-induced heat and other heart sources such as current leads, radiation, conduction via suspension and bore tubes from affecting the temperature of the cold mass.

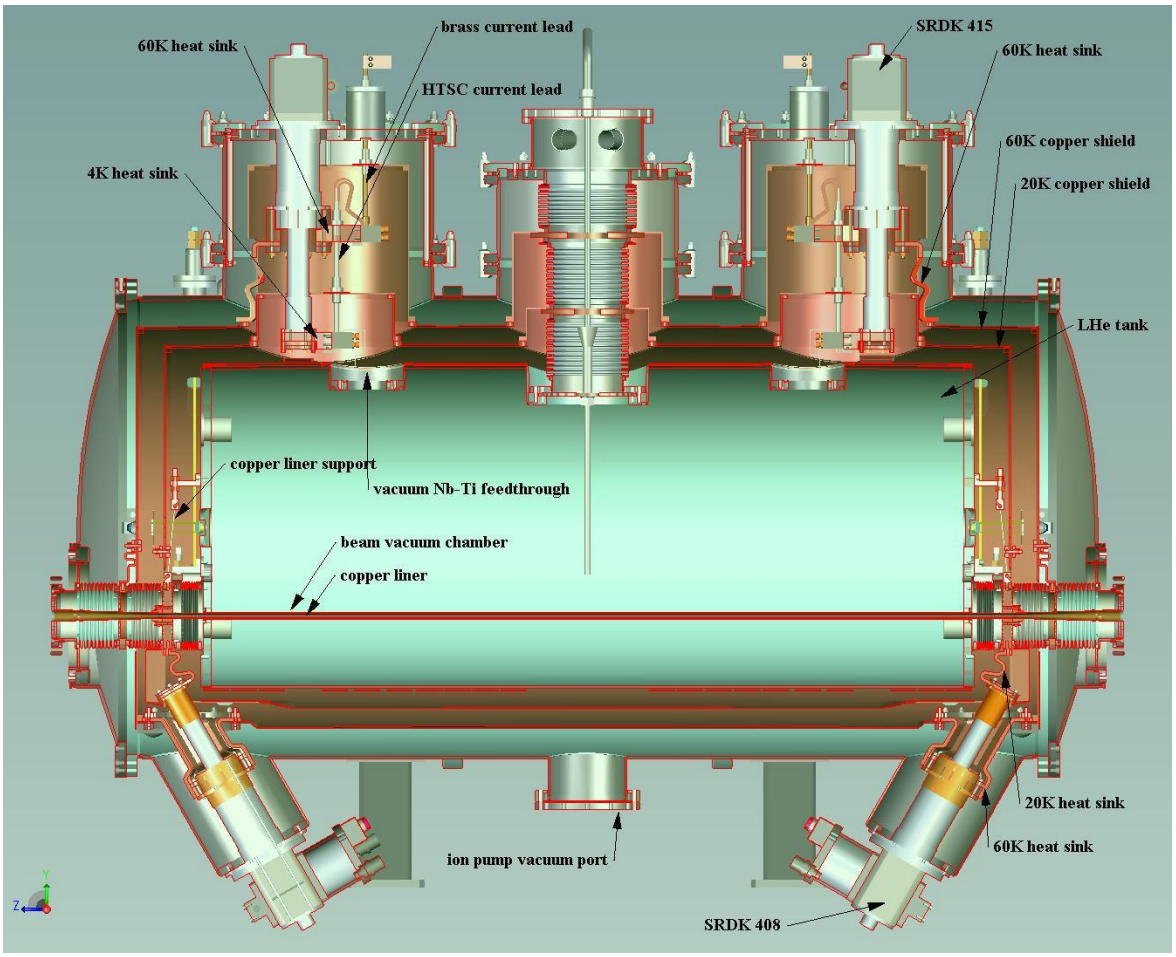

Figure 8 Cross sectional view of a superconducting wiggler with LHe bath made by Budker Institute.

3.5.3. SCW Control System

The control system includes the interface to the Input Output Controller, the design of the EPICS functionality in the IOC, and the development of the user interface. Main functions of the SCW control system are: cryostat monitoring, Interlock protection, Power supply units control (current control) and cryo-compressors state monitoring. Cryostat monitoring includes temperature probes, LHe level sensor, GHe pressure sensor and vacuum gauge. The interlock will be implemented to detect quench of magnets and HTSC current leads overheat. It will be realized in a PLC based subsystem or other hardware and not in the IOC. The PLC must be capable of interfacing with the BNL designed and built EPS system for monitoring of relevant parameters.

3.5.4. SCW References

[1] Y. Li and W. Guo, “Lattice Schemes for the HEX Beamline at Cell27,” NSLS-II tech note #289

[2] V. Smalyuk, et. al., “Beam-induced power in HEX SCW,” NSLS-II tech note #282

[3] R. Voutta, et. al., “Cold vacuum chamber for diagnostics: Analysis of the measurements at the Diamond Light Source and impedance bench measurements,” Phys. Rev. Acc.&Beams, 19, 053201 (2016).

3.6. Storage Ring Straight and X-ray Beam Exit.

3.6.1. Storage Ring Overview.

The NSLS-II storage ring is divided into 30 repeating 'cells' approximately 19m in length. These cells are separated by straight sections (numbered 1 - 30) which are used to accommodate insertion devices (that generate x-rays for experiments) as well as injection from the booster ring and RF acceleration.

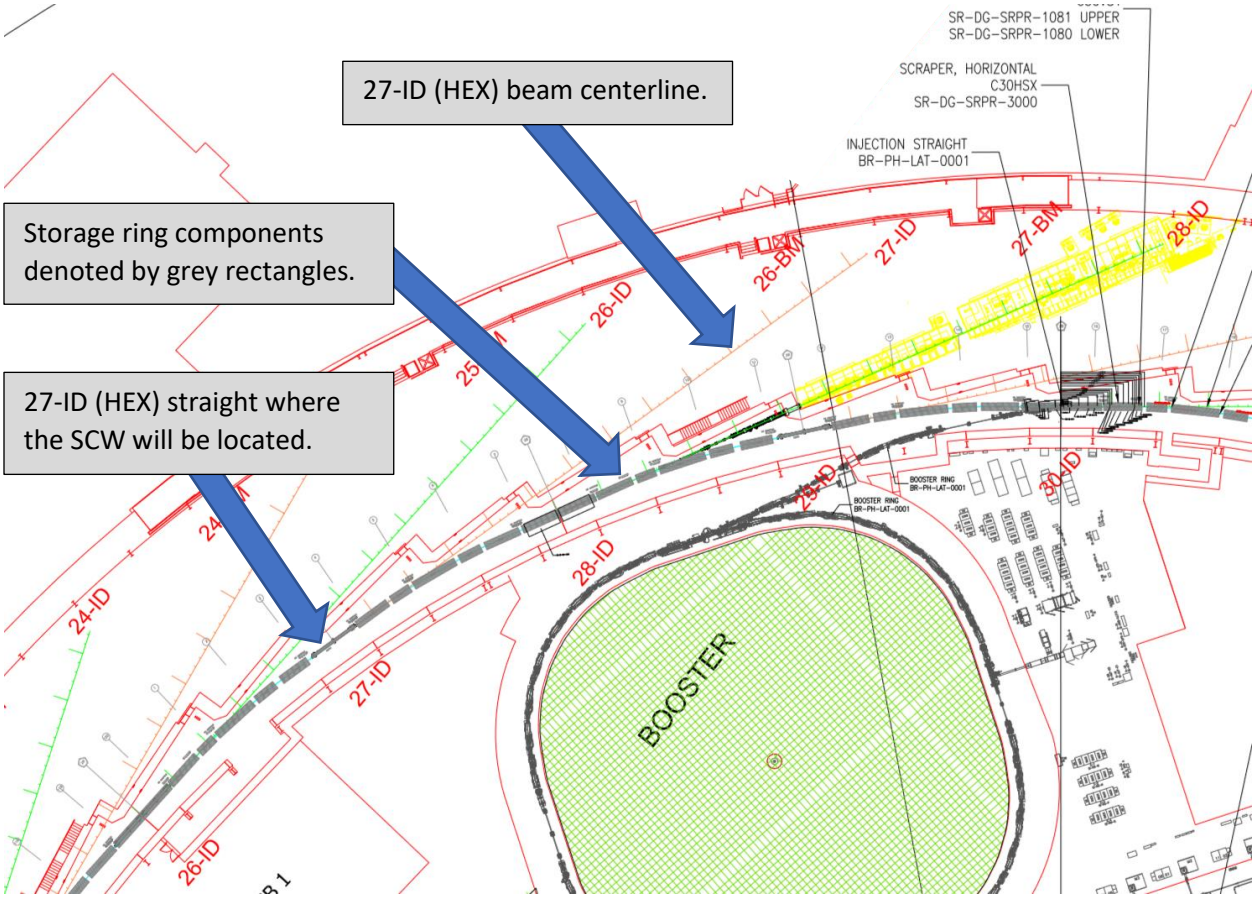

Figure 9 Section of Storage Ring adjacent to HEX

Each cell consists of 5 independent girder assemblies which include the accelerator magnets as well as the vacuum chambers used to circulate the electron beam. A layout of a typical storage ring cell and the preceding straight is shown in Figure 10. The two dipole girders are used to bend the electron beam by 12° per cell, thus providing a closed polygonal orbit through 30 cells. The three multipole girders are used to keep the electron beam focused resulting in high photon flux from the insertion devices.

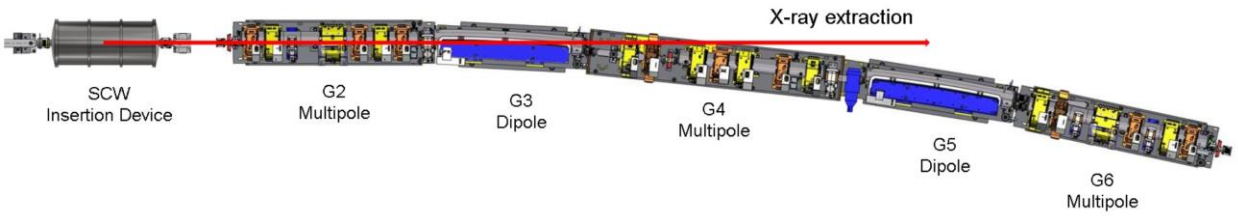

Figure 10 A storage ring cell

Once the x-rays are generated, they travel along the same path as the electron beam up until the first dipole girder. At this point the electron beam is bent due to the magnetic field and the x-rays continue along a straight line to the front end then out to the experimental hall and eventually to an end station where experiments are performed. The power contained in these intense x-ray beams varies depending on the type of insertion device installed. It is imperative that the x-ray beam does not impinge on any unprotected surface in order to prevent a catastrophic vacuum failure.

The cross section of a typical multipole and dipole vacuum chamber are shown in Figure 11. The electron beam channel, which is on the left is 76mm wide and 25mm high. The larger chamber on the right provides room distributed vacuum pumping and the slot between them provides clearance for the x-ray beam. The x-ray beam passes between the beam channel and pumping chamber through the 15mm high slot in the dipole chamber.

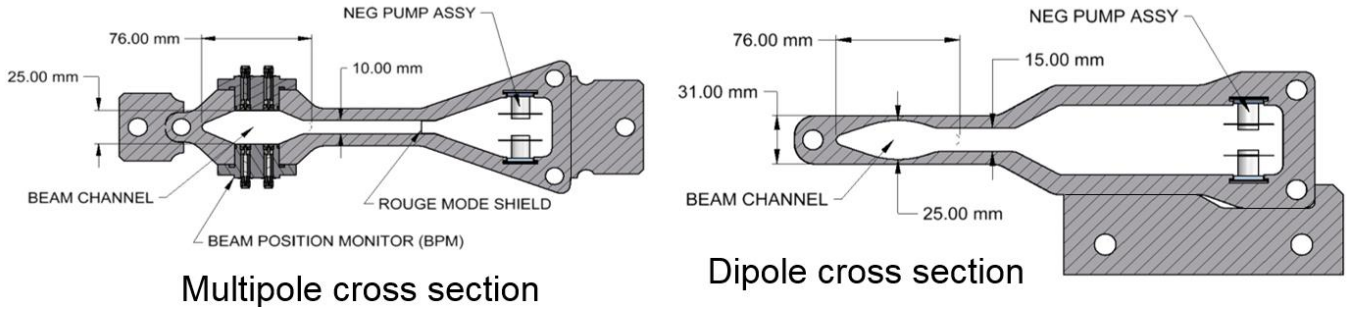

Figure 11 Storage ring vacuum chamber cross-sections

The super conducting wiggler source which will be used for HEX introduces several challenges to the existing storage ring which need to be overcome. The x-ray beam generated by this device will be the widest of any device installed at NSLS-II to date. In fact, this fan will be more than 50% wider than the previous record holder. In addition, the power density in this beam is relatively uniform across the entire width. This means that there is a still a lot of power all the way to the edges of the fan. Special attention needs to be paid to all components which may come into contact with the x-ray beam.

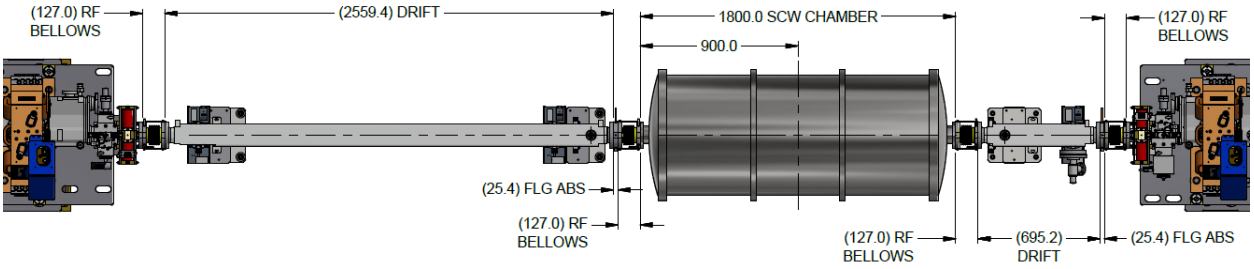

Figure 12 Plan view of straight layout with SCW

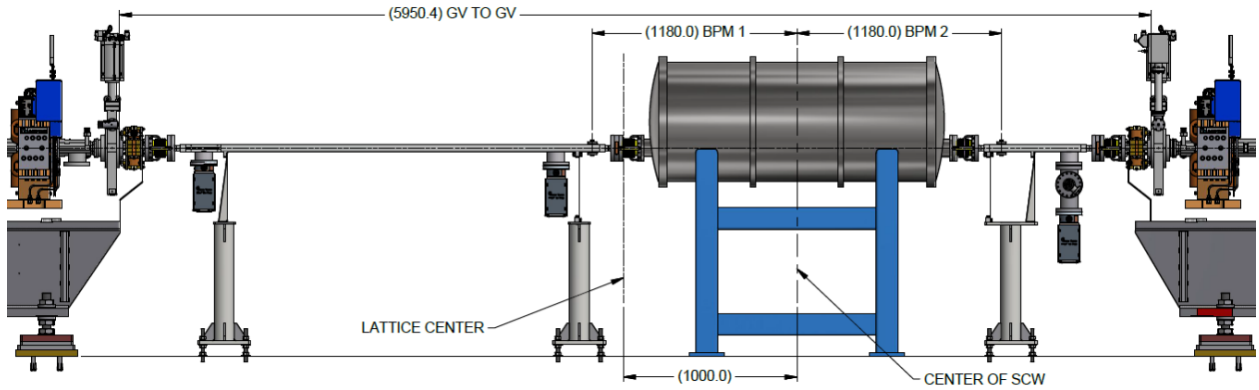

Figure 13 Elevation view of straight layout with SCW

The HEX insertion device will be placed in a short straight section which has a length of approximately 6.6m (see

Figure 12 and Figure 13). From a machine physics standpoint, the ideal position for the device would be in the center of the straight. The generated x-ray beam has a fixed opening angle, so it continues to get wider the further you move from the source. Placing the device in the center of the straight would require significant modifications to the first multipole chamber. This would not only be very expensive but time consuming as well since it would require the disassembly of multiple storage ring magnets. The best way to minimize the impact to the storage ring would be to place the SCW as close to the end of the straight as possible. This would minimize the width of the x-ray fan as it passes through the storage ring vacuum chambers. After extensive simulations and ray tracings it was agreed to shift the device towards the downstream end of the straight by 1m.

3.6.2. Storage Ring Components and Modifications.

The following sections detail the design and new components and modifications that are required to

- The G2-G3 chamber interconnect
- Crotch absorber (CABS) at the downstream end of the G3 chamber
- Exit flange on the G3 chamber
- Undulator absorber at the start of the G4 chamber

3.6.2.1. First Multipole Chamber.

This shift of the SCW described in the previous section results in an acceptable disturbance to the electron beam and reduces the size of the x-ray beam at any given downstream location. This shift eliminates the need to modify the first multipole chamber. The difference in the size of the x-ray beam is shown in Figure 14. If the SCW were centered in the straight section the x-ray beam would touch the interior walls of the chamber (this would certainly cause local damage to the chamber walls due to the very high power densities involved).

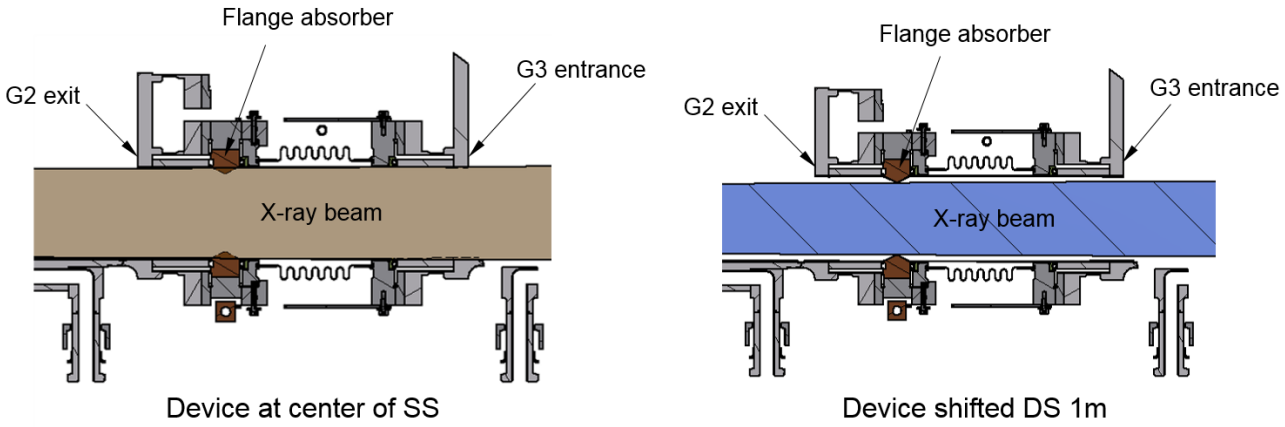

Figure 14 Effect of SCW location on the beam size at the G2/G3 interface

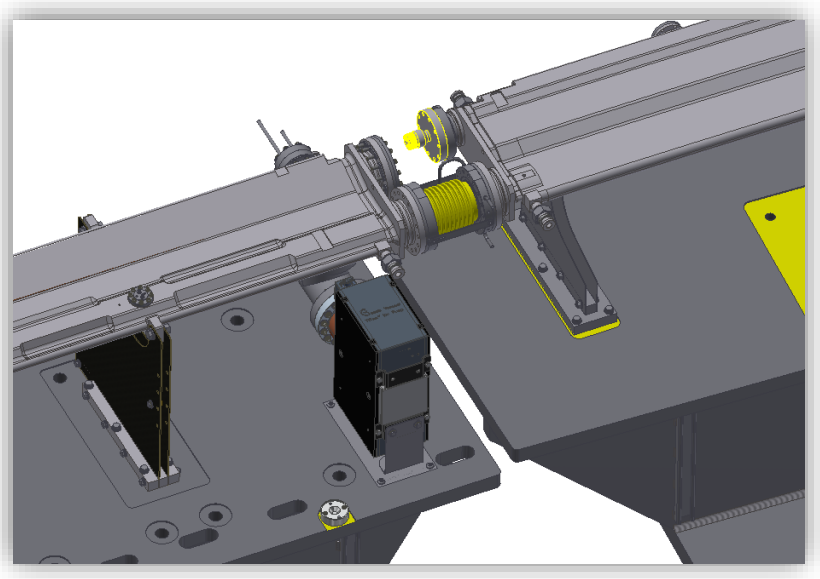

Figure 15 Solid model of the G2-G3 interface

3.6.2.2. Crotch Absorber (CABS).

The next component the x-ray beam comes into contact with is the crotch absorber (CABS) which is located at the downstream end of the dipole chamber. This element is used to protect non-water-cooled components in the storage ring from the x-rays which are generated by the dipole magnet. This

component also provides an aperture to allow the x-rays from the insertion device to continue along to the front end. The existing NSLS-II CABS provides a maximum opening of 75mm. This limit provides shielding for the exit flange, preventing x-rays from hitting uncooled surfaces and causing damage. With the distance from the source approaching 9m, the x-ray beam is almost 90mm wide by the time it reaches the CABS. Given the limited cooling capacity of the CABS and the amount of power contained in the edges of the fan, the aperture had to be enlarged. Fortunately, the existing CABS design can accommodate a wider aperture (see Figure 16 and Figure 17 below), however this change then requires an increase in the width of the next component downstream, the exit flange.

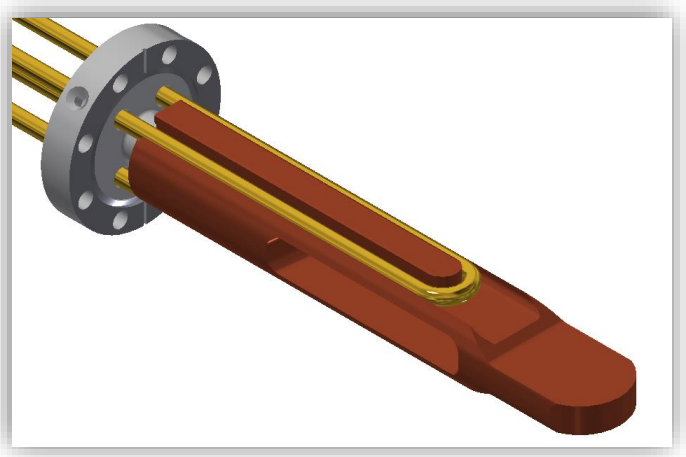

Figure 16 CABS component showing cooling and aperture arrangement

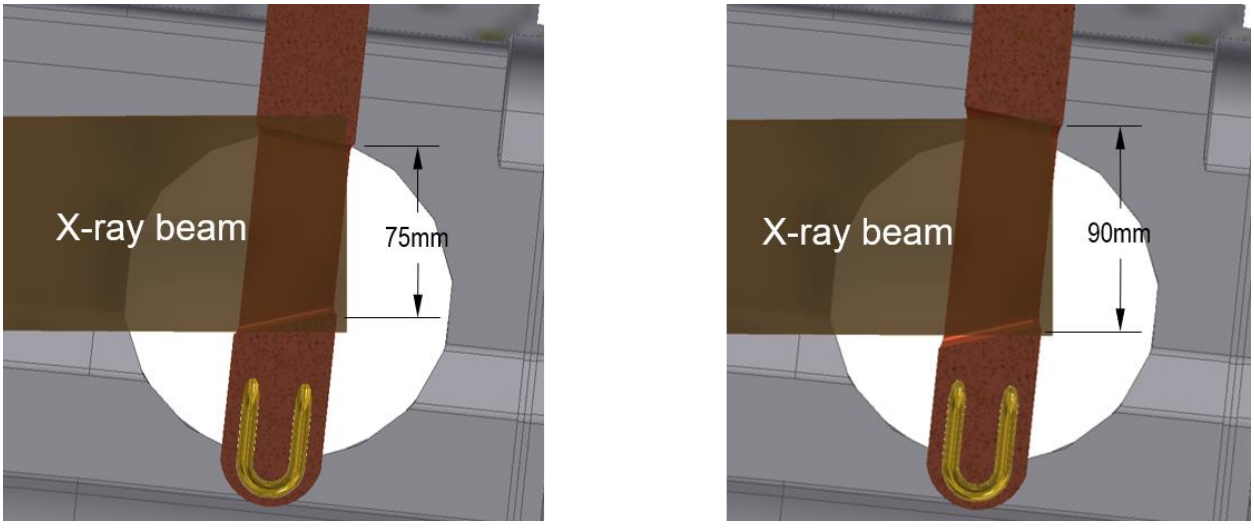

Figure 17 Showing the enlargement of the CABS aperture

3.6.2.3. Dipole Chamber Exit Flange.

After several design considerations it was determined that the existing dipole chamber can be reworked and a custom flange with an elliptical neck added. With this new flange, the opening could be increased to allow a wider fan to exit the dipole vacuum chamber. Figure 18 shows an illustration of the enlarged opening as well as a proof of concept flange assembly which was fabricated at BNL. Special fixturing will be required to hold the curved 3.5m long vacuum chamber during machining. After modifying the chamber and welding the new flange the entire assembly will need to be cleaned and processed to achieve the required UHV levels for installation back in the storage ring.

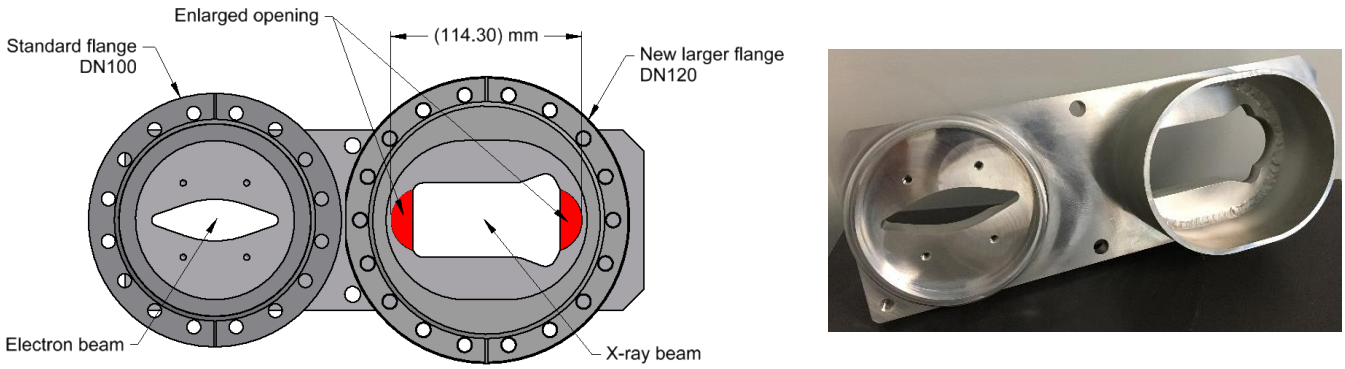

Figure 18 Dipole chamber exit modifications

3.6.2.4. Undulator Absorber.

After exiting the dipole chamber, the unused portion of the x-ray fan must be trimmed to a size which can fit through the nearby storage ring magnets. This will be accomplished by a large water-cooled copper absorber. Long shallow tapers will be used to reduce the peak power density (>300 W/mm^2) to manageable levels. The water cooling must be adequate to absorb approximately 20kW of power which will be removed from the beam at this location. A short bellows will be installed between the absorber and the dipole chamber to allow independent alignment of the 2 components. The trimmed x-ray beam will travel inside a thin walled vacuum pipe after exiting the absorber in order to maintain the UHV environment of the storage ring. Figure 19 shows a rendering of the absorber and the exit pipe which will connect the storage ring to the front end.

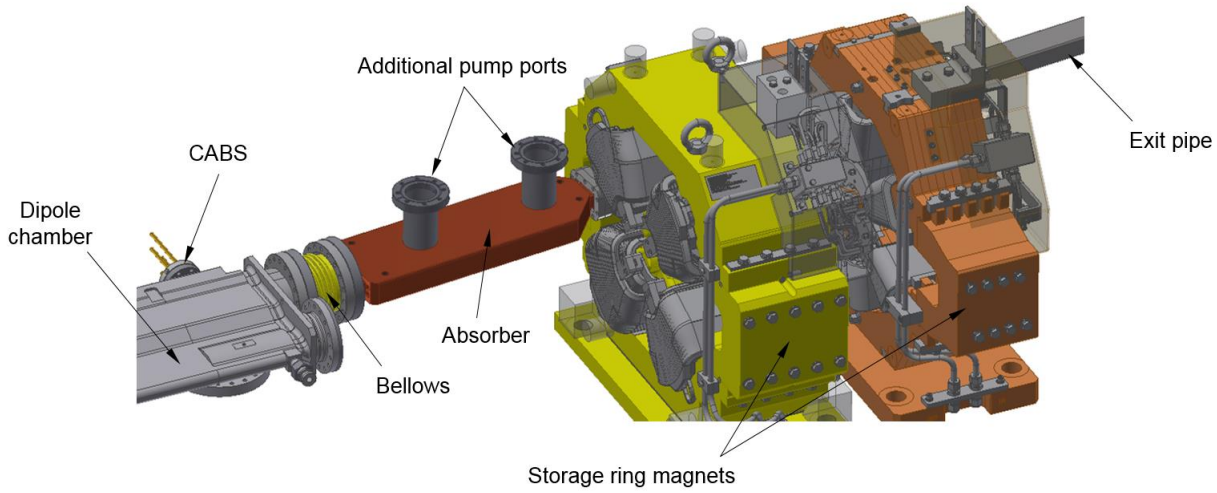

Figure 19 Absorber at the Storage Ring to Front End transition

The absorber will be fabricated out of CuCrZr which is a readily available copper alloy that has greater yield and fatigue strength compared to oxygen free copper. This material also maintains it structural integrity at elevated temperatures and is used extensively in high temperature fusion reactor components. While it does have many attractive features, there are some limits on the joining methods which can be employed. At temperatures above 400°C, CuCrZr starts to lose some of its most useful properties including hardness and tensile strength. For these reasons it is important to minimize the heat affected zone and preserve the properties of the bulk material. One technique is to employ TIG welding to join various components together while maintaining a leak tight seal. To prove this as a viable option a small development project was undertaken at BNL. Multiple test samples were fabricated to develop the techniques required to join stainless steel to CuCrZr utilizing standard TIG welding equipment. Figure 20 shows some of the results of this development project.

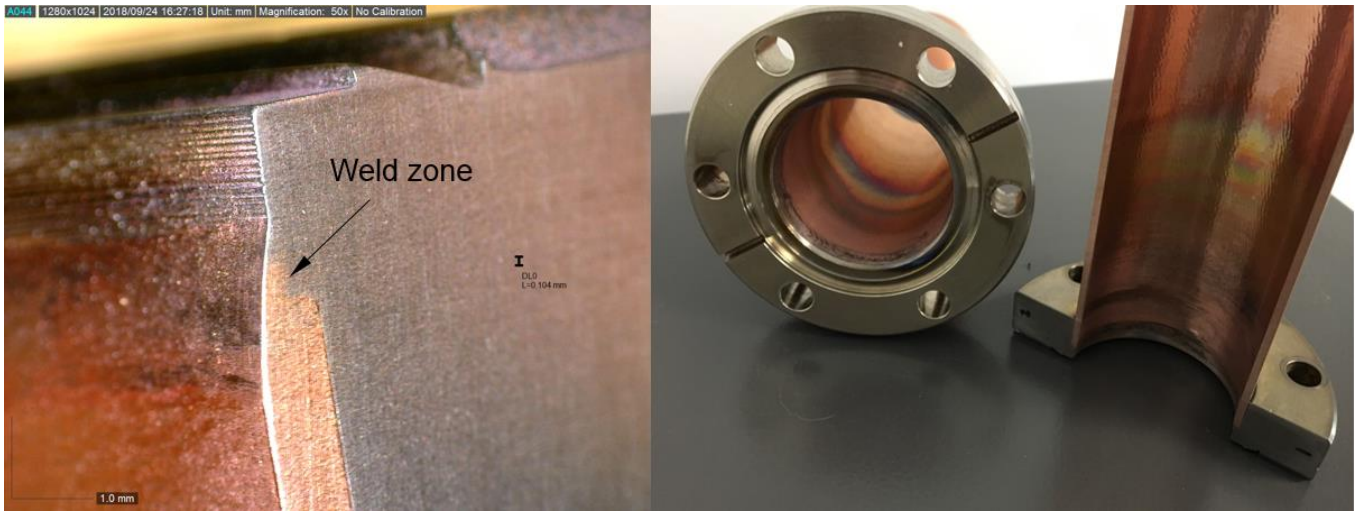

Figure 20 Stainless steel to CuCrZr weld test specimens

3.6.2.5. Summary.

A detailed study of the impacts to the storage ring resulting from the wide x-ray fan produced by the superconducting HEX wiggler has been completed. Several areas of concern, which were identified earlier, have been addressed and mitigation strategies have been developed that are both practical and relatively cost effective. In order to eliminate risk, prototypes of the most challenging components have been fabricated. At this point the costs and technical risks are well understood. Details for the individual components are almost complete and fabrication will begin once the drawings are reviewed and released to manufacturing.

3.7. Front End

3.7.1. Introduction.

The HEX front end serves as an interface between the storage ring (SR) and HEX users beamlines. It is located inside the ratchet wall between 15-25 meters from the center of the ID (HEX wiggler) as shown in the front-end layout (Figure 21). The primary function of the front end is to trim the sizes of the x-ray fan and the Bremsstrahlung radiation (BR) fan. The x-ray fan is generated by the HEX wiggler whereas the BR fan is generated by the collision of the SR electron beam with the residual gases in the vacuum chambers. The front end can also stop the x-ray and BR fans completely to allow access to the beamline enclosures for installation and maintenance activities during machine operation.

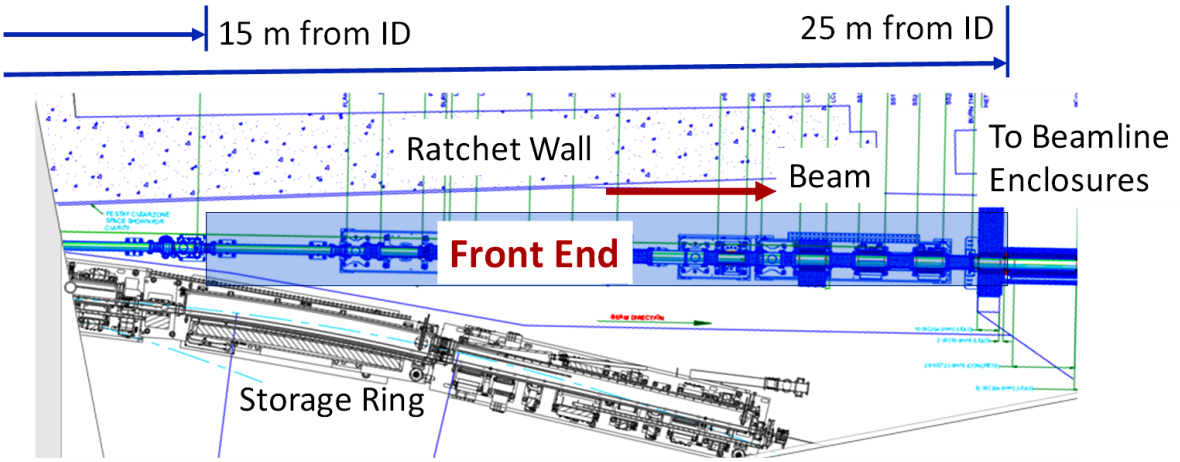

Figure 21 HEX front end located inside the ratchet wall at ~ 15-25 m from the ID (HEX wiggler).

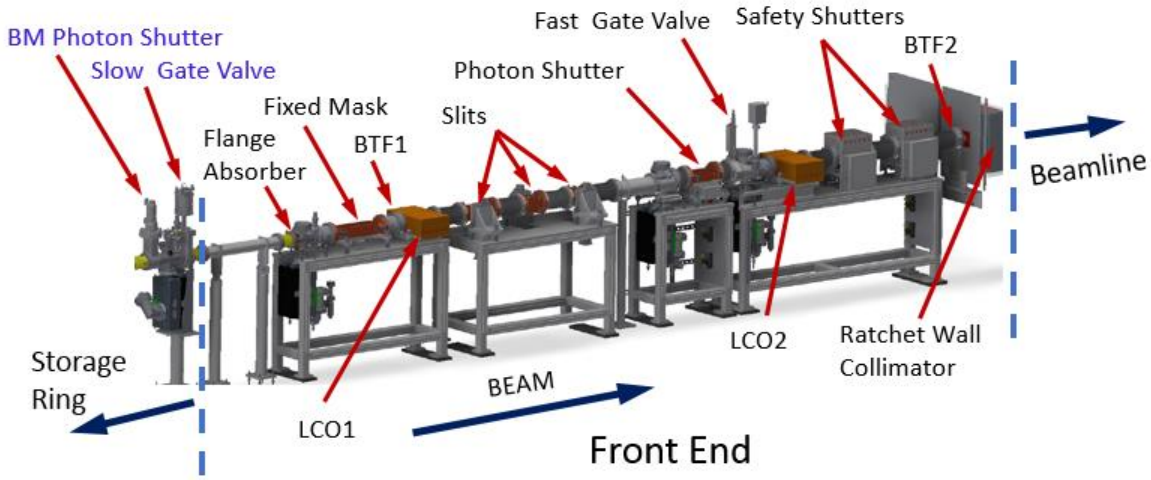

Figure 22 HEX Front End components

As shown in Figure 22, the HEX front end begins downstream of BM photon shutter (BMPS) and a slow gate valve (SGV). BMPS and SGV are used to isolate the front end from the storage ring for trouble-

shooting and maintenance. The main components of the front end are: (1) flange absorber (2) fixed mask, (3) burn-through flanges (BTF1 and BTF2), (4) lead collimators (LCO1 and LCO2), (5) three slits, (6) photon shutter, (7) fast gate valve, (8) safety shutters, and (9) ratchet wall collimator. Except for the fast gate valve all other components trim (or block) either the x-ray fan or the BR fan. The trimming of the fans is shown in front end raytracing drawings and forms the basis on which the apertures of the front end components are determined. In the following sections we describe front-end raytracing and the main front-end components covering their functional requirements, designs and analyses.

3.7.2. Front-End Raytracing

The front-end raytracing depicts how the x-ray and BR fans propagate from their sources and how they are trimmed or blocked as they propagate through the front-end components. Raytracing drawings are produced following a very detailed and prescriptive procedure [1] based on source definitions and guidelines [2, 3]. In this section we cover the basic concepts without going through procedural details.

3.7.2.1. Source Definitions

The starting point for the raytracing is the sources from which the rays start and propagate toward the front ends. The x-ray source location is defined to be at the center of the magnetic length of the HEX wiggler which has an offset from the center of the ID straight section. The BR source is located at the end of the ID straight which is 2.5 m from the center of the ID straight. The X-ray fan size generated by the HEX wiggler is ± 4.94 mrad (horizontal) by ± 0.44 mrad (vertical). Electron beam deviations are added to the fan size to ensure the safety of the front-end components from extremal rays. The source size is thus dependent on electron beam deviation envelope allowed by the beam position monitoring (BPM) system. The x-ray fan from this source is referred to as the interlocked fan or the EPS (equipment protection system) fan. At NSLS-II the beam is assumed to be un-interlocked for radiation safety components (lead collimators and the ratchet wall collimator), thereby leading to a larger x-ray source size and fan angles. For additional safety of these collimators the x-ray fan (named as Max Fan) is assumed to start from the end of the ID device and is not trimmed by the fixed mask. A set of formal raytracings drawings consists of 7 separate drawings, one for the front-end layout and two each for horizontal and vertical fans of the interlocked, un-interlocked (max) and Bremsstrahlung beams. The source sizes for the x-ray and BR fans as defined in [2, 3] are summarized in Table 6.

Table 6 Source definitions for x-ray and Bremsstrahlung radiation (BR) fans

	Source Location	Horizontal*		Vertical*	
		Position (mm)	Angle (mrad)	Position (mm)	Angle (mrad)
HEX wiggler beam	1 m downstream of the center of ID straight	0	± 4.94	0	± 0.44
Electron Beam Deviations -Interlocked Fan	1 m downstream of the center of ID straight	$\pm$ 0.50	$\pm$ 0.25	$\pm$ 050	$\pm$ 0.25
X-ray Max Fan	1.6 m downstream of the center of ID straight	$\pm$ 38 (ID Chamber Aperture)	**	$\pm$ 5 (ID Chamber Aperture)	**
BR Fan	2.5 m downstream of the center of ID straight	+38 / - **	**	$\pm$ 12.5	**

* The outboard/inboard dimensions are denoted by +/- signs. ** See Sections 3.7.2.2 and 3.7.2.3.

3.7.2.2. X-Ray Raytracing

The basic approach for the interlocked (EPS) x-ray raytracing is shown schematically in Figure 23 which illustrates trimming of the interlocked x-ray fan in both the horizontal and vertical planes. In the horizontal plane (Figure 23(a)), the x-ray fan is bounded by the extremal rays OA and ID starting at O (+ 0.5 mm) and I (-0.5 mm) at angles of + 5.19 mrad and – 5.19 mrad, respectively, which include the wiggler beam size and the electron beam deviations (see Table 6 Source definitions for x-ray and Bremsstrahlung radiation (BR) fans). This fan for the HEX wiggler, unlike the fans of typical undulator beams, is too wide to fit inside the exit-port chamber upstream of the front end. It is, therefore, trimmed by an exit absorber placed upstream of the front end. The trimmed fan entering the front end is bounded by extremal rays, OE and IB. It is further trimmed by the fixed mask to a size defined by the extremal rays OF and IC. The downstream trimming aperture of the fixed mask is determined by the nominal x-ray beam size requested by the beamline user [2]. Inside horizontal apertures of the burn-through flanges, BTF1 and BTF2, are required to be larger than the fan size passing through them as shown in the figure below.

Figure 23 Raytracing for the interlocked (EPS) fan

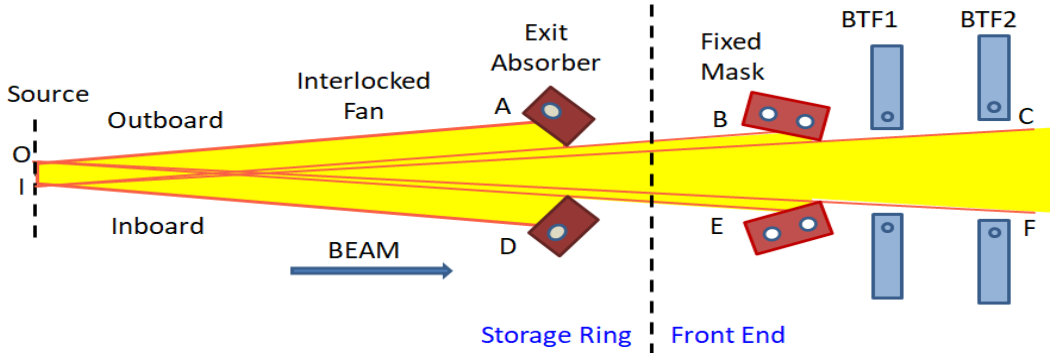

(a) The wide horizontal x-ray fan (± 5.19 mrad) is trimmed by a storage ring exit absorber and the front end fixed mask. Inside horizontal apertures of the burn-through flanges, BTF1 and BTF2 are outside

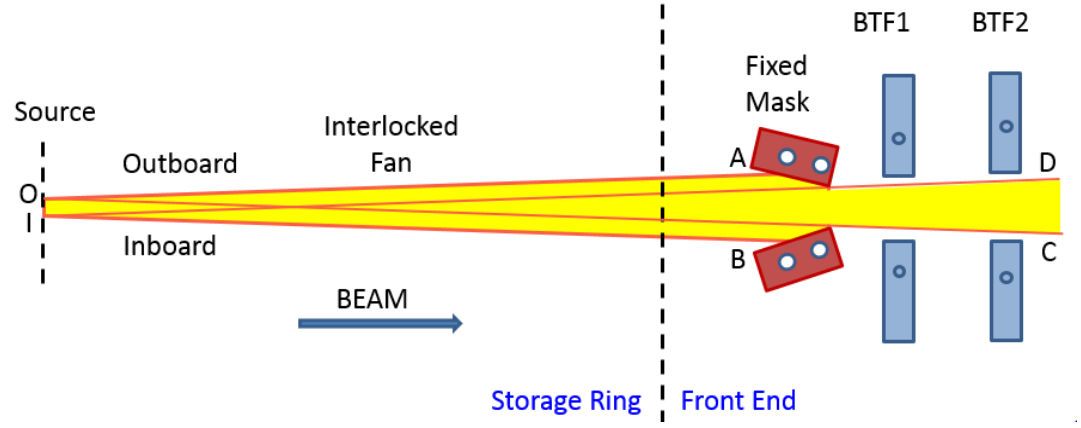

the trimmed fan.

(b) Inside vertical apertures of BTF1 and BTF2 are larger than the vertical fan trimmed only by the fixed mask.

Upstream apertures of the slits and photon shutters are made larger than the fan size at their respective locations. It is customary not to include slits and the photon shutter in the raytracing because they are designed to intercept the full beam power exiting the fixed mask. In addition, the inside apertures of the various vacuum components, such as bellows, spool pieces, bellows, crosses (also customarily not shown in raytracing), are made larger than the fan size.

Interlocked (EPS) x-ray raytracing in the vertical plane is done similarly (Figure 23(b)). It is simpler because the HEX wiggler beam is small vertically (± 0.44 mrad) and the x-ray fan, bounded by extremal rays OA and IB, does not require trimming by the exit absorber. Vertical inside apertures of BTF1 and BTF2 are made larger than the fan trimmed by the fixed mask (bounded by the extremal rays OC and ID).

Max fan raytracing is shown schematically in Figure 24 and is representative of raytracing in both the horizontal and vertical planes. The source size is defined by the geometric envelope for the electron beam which conservatively can be as large as the aperture of the vacuum chamber at the source location. Max fan source points O and I are thus located at the outboard and inboard ends of the aperture. The angles of the extremal rays, OA and IB, can also be very large (up to 10 mrad). However, max fan raytracings are relevant to only LCO1, LCO2 downstream of BTF1, and RCO downstream of BTF2. It is, therefore, customary to ignore the max fan before BTF1 and show only the extremal rays OD and IC for the fan exiting BTF1, and extremal rays OF and IE for the fan exiting BTF2. As shown in Fig. 4, inside apertures of the vacuum chambers of LCO1, LCO2 and RCO are required to be outside these fans.

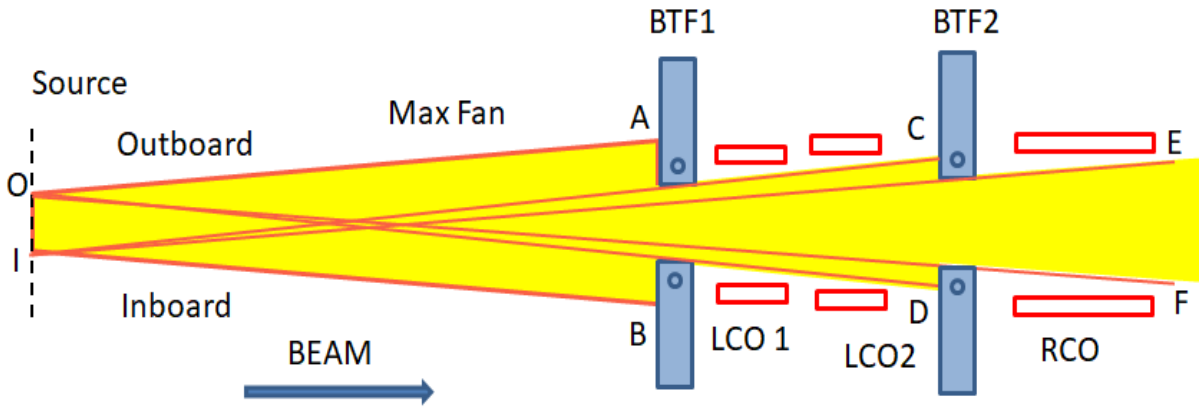

Figure 24 Max fan is trimmed by BTF1 and BTF2. Vacuum chambers of LCO1, LCO2 and RCO are outside the fans trimmed by their upstream BTF, respectively

3.7.2.3. Bremsstrahlung Raytracing

Bremsstrahlung raytracing guidelines [3] are used to establish source points for the extremal rays of the BR fan and for trimming of the BR fan by lead stacks in LCO1, LCO2, RCO and the ratchet wall (RW).

Figure 25 illustrates trimming of the BR fan in the horizontal plane. A compressed horizontal to vertical scale (~ 1:200) is used in the figure for clarity. A line is drawn passing through the upper upstream-inside corner (A) of the RCO to the lower upstream-inside corner (B) of LCO1. The intersection of this line with the dotted line at the BR source location, (I), becomes the new inboard source for the BR fan.

The outboard source (O) is located at 38 mm (half aperture of the SR chamber) as specified in the guidelines. Another line is drawn joining the lower upstream-inside corner (C) of RCO with the outboard source (O). The extremal rays IA and OC define the BR fan exiting into the beamline hutch.

From the source points O and I, lines are drawn joining lower and upper inside-upstream corners of LCO1, (B and D), and LCO2 (H and G) respectively. The BR rays represented by OB and ID are intercepted at E and F by lead of collimator LCO2. Similarly, the rays represented by OH and IG are intercepted by lead of RW.

For Bremsstrahlung shielding in the horizontal plane, the guidelines also require that there be no line of sight from the beamline hutch to the inboard side of the front end. To insure this, lines are drawn from A to lower upstream-inside corners of RW and LCO2, (M and H), respectively. These lines are intercepted at points P and Q of LCO2 and LCO1. As shown in the figure below LCO1, the intersection points such as Q must be at least 3 Moliere radii (36 mm) away from the outer edge as per the shielding guidelines. These requirements, together with the minimum length along the beam direction (305 mm), determine the dimensions of the lead stacks in all collimators.

Figure 25 does not show the lead stacks of the safety shutters to avoid cluttering. In the formal raytracing drawing these lead stacks are included in their closed position to show that the exit BR fan is completely stopped following the 3 Moliere radii guideline.

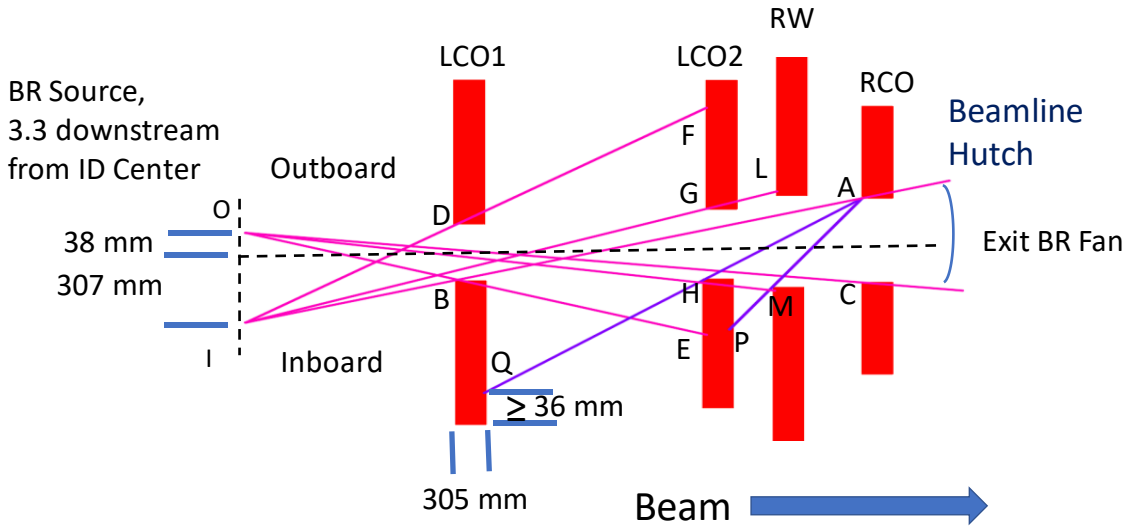

Figure 25 Bremsstrahlung radiation (BR) raytracing in the horizontal plane shows source points (O and I), trimming of the various extremal BR rays by LCO1, LCO2, RW (ratchet wall) and RCO, and BR fan exiting to the beamline hutch

BR raytracing in the vertical plane is done in a similar manner with two simplifications. Both the outboard and inboard source locations are at the ends of the vertical aperture (25 mm) of SR chamber. There is also no requirement for blocking the line of sight from the beamline hutch. As shown in Figure 26, the exit BR fan is bounded by the extremal rays IA and OB, where A is the upper upstream-inside corner of the RCO and B is its lower upstream-inside corner. The rays from I and O to the upstream-inside corners of LCO1 (C and D) and LCO2 (E, F) are intercepted are at (G, H) and (L, M) of LCO2 and RW, respectively. As in Figure 25, the lead stacks of the safety shutters are not included in Figure 26.

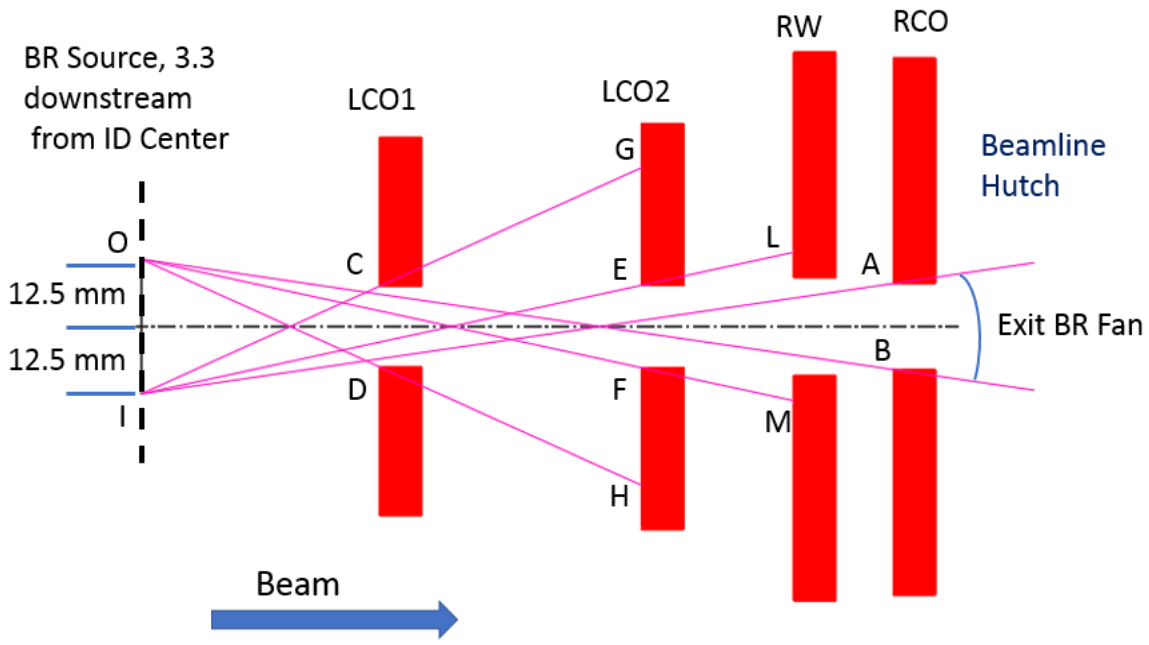

Figure 26 Bremsstrahlung raytracing in the vertical plane shows source points O and I of the vertical BR fan, trimming of the BR fan by the lead stacks of LCO1, LCO2, RW (ratchet wall) and RCO, and the BR fan exiting to the beamline hutch

3.7.3. Front End Components

The ray-tracings described in Section 2 above are done iteratively to determine optimum locations of the front-end components and to determine their optimum basic dimensions (length, cross section, and upstream and downstream apertures).

For the x-rays intercepting components (flange absorber, fixed masks, slits, photon shutter and burn-through flanges), detailed thermal analyses are usually performed to ensure their long-term survivability. These components are made from a copper alloy CuCrZr which is readily available and has thermal performance comparable to that of Glidcop (used in previous NSLS-II front ends). Specifically, the fatigue life of CuCrZr under thermal cycles is about the same as that of Glidcop [4]. We can therefore use the same maximum temperature rise criteria for design, namely, 300 ^{o}C for 30,000 thermal cycles, and 400 ^{o}C for upset conditions such as a large beam deviation. CuCrZr is weldable to itself and to stainless steel which makes it possible to eliminate the brazing steps in the fabrication [5].

3.7.3.1. Flange Absorber

A flange absorber, shown in Figure 27(a), is provided in all ID front ends to intercept the wide x-ray fans of two upstream dipoles, one upstream of the HEX wiggler and the other downstream of it. Even though the dipole beam power, ~ 23 W/mR, is low and their source distances are large (22.7 m and 8.6 m), this flange absorber is used to intercept the two beams to protect un-cooled upstream surfaces of the fixed mask.

The flange absorber is custom made from CuCrZr alloy and is of approximately the size of a 150 mm Conflat flange. It has an aperture of 98.6 mm (H) x 29.3 mm (V) as a pass-through for the wiggler

beam. Two horizontal channels of 8 mm diameter, ± 26 mm from the center, provide water cooling. An FE thermal analysis (Figure 27(b)) shows a maximum temperature rise of 22.5 ^{o}C which is quite low compared to the safe design criteria of 300 ^{o}C.

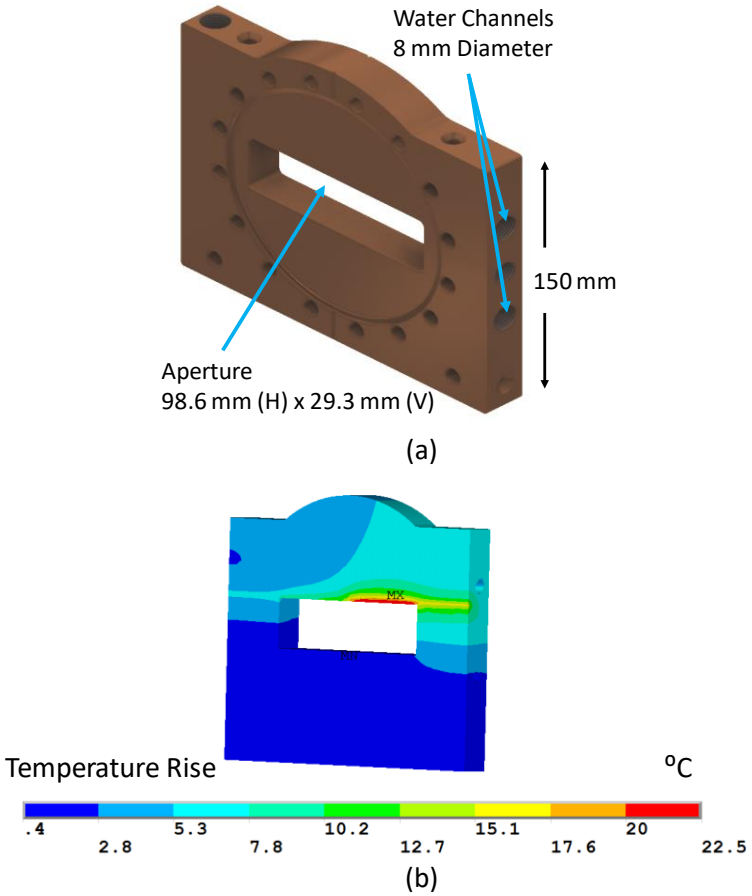

Figure 27 Front end flange absorber, (a) the wiggler beam passes through the central aperture of 98.6 mm (H) x 29.3 mm (V), (b) x-ray beams from the two upstream dipoles are intercepted by the flange absorber resulting in a maximum temperature rise of 22.5 ^{o}C

3.7.3.2. Fixed Mask

The HEX fixed mask has two main functions, namely, shadow the downstream burn-through flanges and upstream apertures of the slits and the photon shutter from the interlocked beam, and (2) split the main wiggler beam into three beams of specific dimensions and separations, shown in Figure 28(a), as per the users' requirements [2]. The separation between the inboard beam and the center beam is only 0.55 mR. Any partition in this angular separation will be too narrow for effective water cooling considering the electron beam deviation of up to 0.25 mR. A new mask design was developed at NSLS-II [5] for such cases and a mask of this design is already in use at 7-ID (SST) front end. In this design the ID beam is intercepted only by the top and bottom inclined surfaces of the fixed mask (Figure 28(b)). The exit apertures are machined (by electric-discharge machining) at the downstream end where the two surfaces meet.

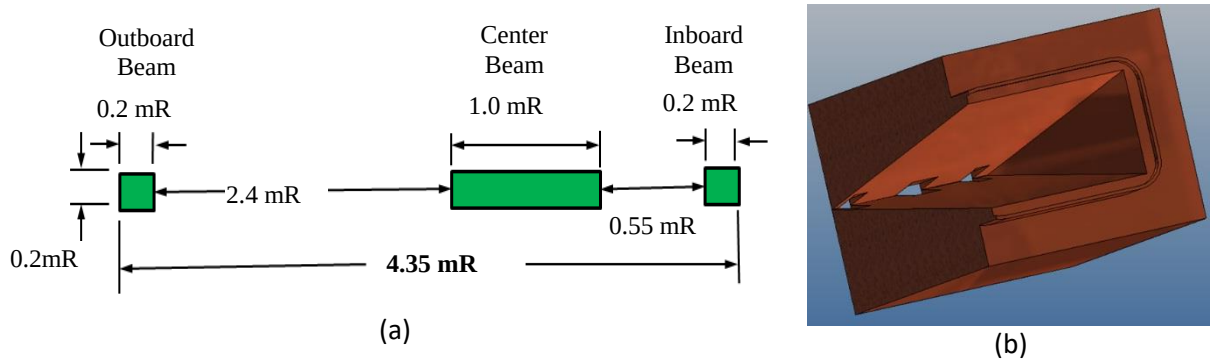

Figure 28 Splitting of the wiggler beam by the fixed mask, (a) dimensions and spacings of the three beams, (b) ID beam is intercepted only by the top and bottom surfaces in the new mask design

Figure 29 shows the power density plots of the full HEX wiggler beam and of the 3 beams split by the fixed mask. Upstream of the fixed mask, an exit absorber in the storage ring trims the ± 4.94 mR fan (Figure 29(a)) to ± 0.252 mR reducing the total beam power from 55.7 kW to 40.8 kW. The 3 beams exiting the fixed mask are shown in Figure 29(b)). The total power in the three beam is ~ 7.7 kW with the rest intercepted by the fixed mask.

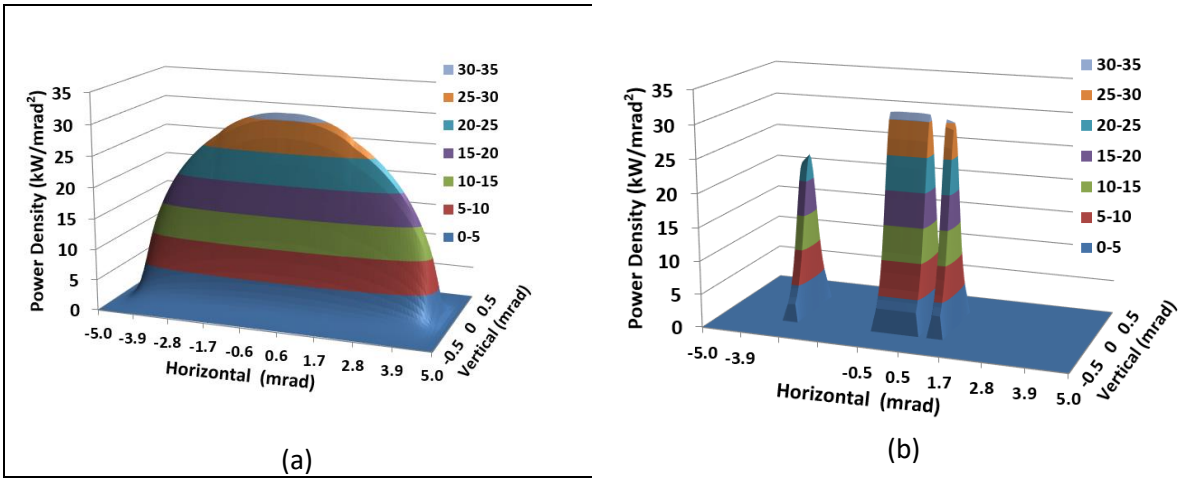

Figure 29 HEX wiggler beams, (a) full fan upstream of the fixed mask, (b) trimmed fans of the 3 beams downstream of the fixed mask

The main dimensions of the fixed mask are shown in the CAD model of Figure 30. The overall length of the mask between flanges is 584 mm long (Figure 30(a)) including two CuCrZr flanges of 202 mm diameter welded to the main body. The upstream aperture of the mask is 106 mm x 34 mm which accounts for both the wiggler beam size and the interlocked deviations of the electron beam. The top and bottom beam-intercepting surfaces are inclined at an angle of 1.875^{o} over a length of 492 mm (Figure 30 (b)). Water cooling is provided by 6 round channels of 12.7 mm diameter. Three water channels on each side run parallel to the top and bottom surfaces.

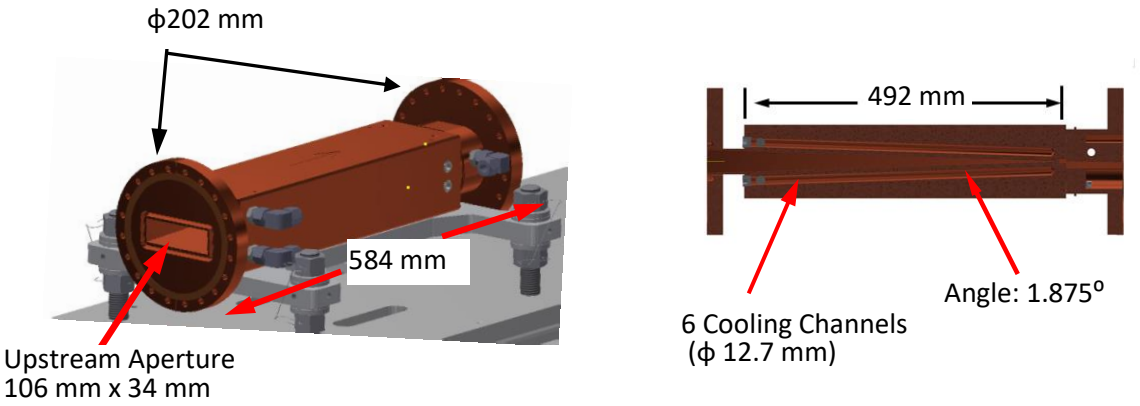

Figure 30 HEX fixed mask made of CuCrZr alloy, (a) the mask welded to two 202 mm diameter flanges has an overall length of 584 mm. The upstream aperture is 106 mm x 34 mm. The mask is water-cooled by 6 cooling channels shared by two top and bottom surfaces inclined at 1.875°

Detailed FE thermal analyses were performed for the HEX mask to ensure that the maximum temperature rise under the wiggler beam power of 40.8 kW would be in the acceptable range. The downstream aperture is not included in the FE models which makes them simpler and conservative. Temperature contours for the nominal beam position are shown in Figure 31(a) and (b) looking from upstream and downstream sides, respectively. A maximum temperature rises of 281.2 °C is obtained which is lower than the acceptable design value of 300 °C. In other analyses (not shown) the beam was placed at different locations of the mask's inclined surfaces. In all such case the maximum temperature rise was lower than the nominal case. Also, in the nominal case the temperature rise would have been lower if the beam apertures were included in the model thereby reducing the total intercepted power by ~ 7.7 kW.

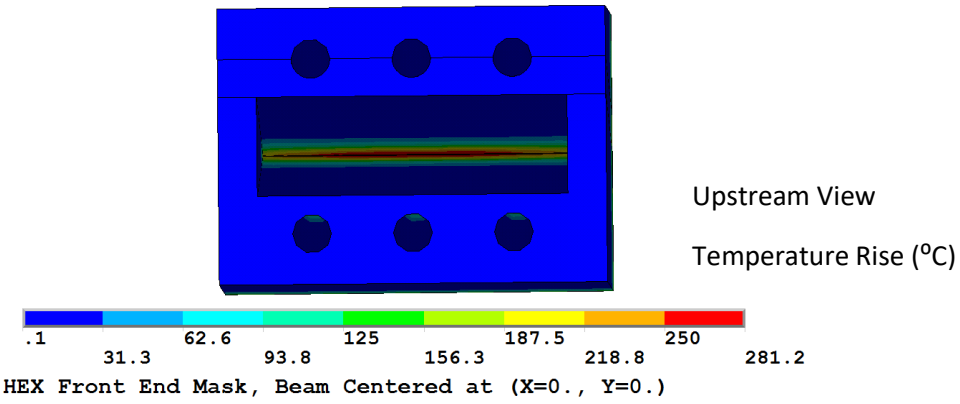

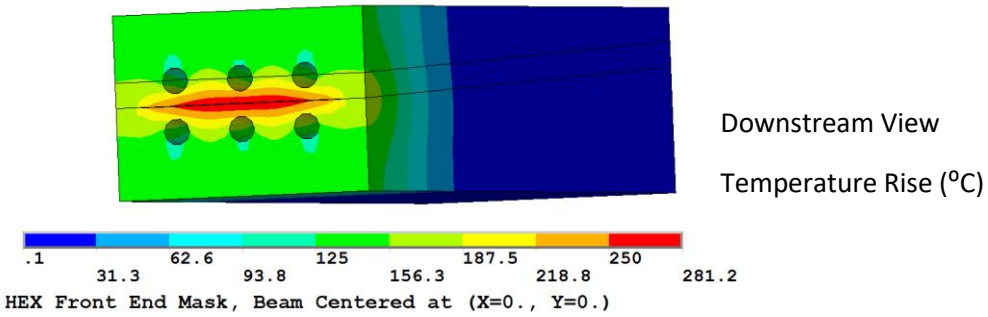

Figure 31 Temperature rise contours in the HEX mask under the wiggler beam power of 40.8 kW, (a) upstream view, (b) downstream view. The maximum temperature rise is 281.2 °C, lower than the acceptable design temperature of 300 °C.

3.7.3.3. Burn-Through Flanges

As described in Section 3.7.2.2, the burn-through flanges, BTF1 and BTF2, are protected by the fixed mask from the wiggler fan when the electron beam is interlocked (i.e., from the interlocked fan). These flanges in turn protect the collimator chambers, LCO1, LCO2 and RCO, from the wiggler fan when the electron beam is not interlocked (Max Fan). This is illustrated schematically in Figure 32 in which both fans are depicted. The burn-through flange is in the shadow of the fixed mask from the extremal rays of the interlocked fan AB. The max fan, CD, is intercepted by the burn-through flange before it can strike the collimator chamber.

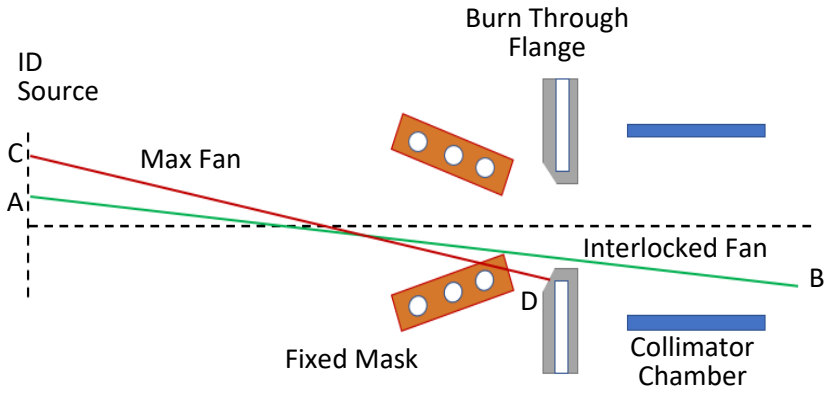

Figure 32 A burn-through flange, in the shadow of the mask from the interlocked fan (AB), protects the collimator chamber from the max fan (CD)

HEX burn-through flanges are made from standard 202 mm (8-inch) diameter 304 stainless steel (SS) flanges. Figure 33 shows CAD model of the BTF1. A nominal aperture of 78.6 mm (H) x 7.3 mm (V) is machined at the center of the flange with a large upstream chamfer of 4.5 mm length at 60° (Figure 33(a)). Four through holes of 6.35 mm diameter are drilled around this aperture close to the chamfer as shown in the half-section view of Figure 33(b). The minimum distance between the chamfer's taper surface and the through holes is 0.8 mm.

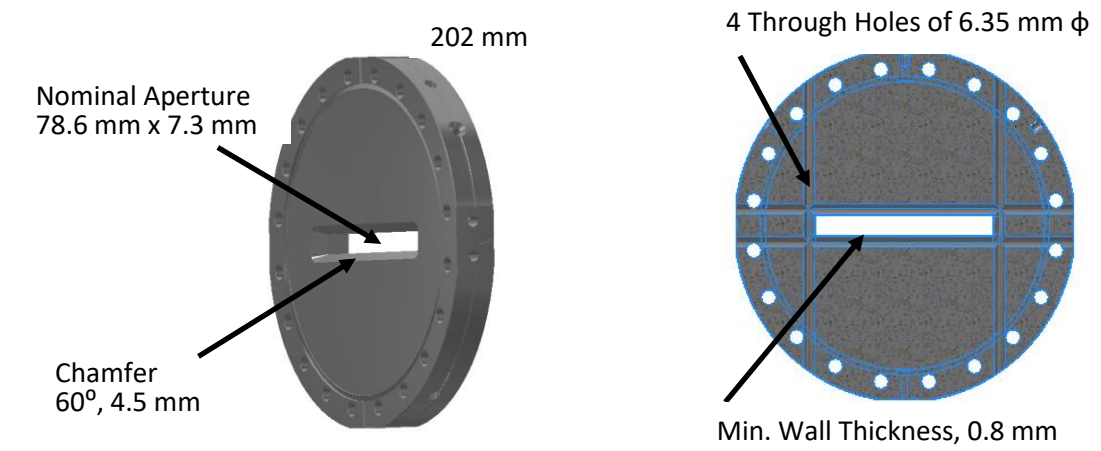

Figure 33 HEX burn-through flange, (a) nominal aperture with a large chamfer, (b) four through-holes of 6.35 mm diameter drilled around the nominal aperture

In a very rare event of electron beam deviation exceeding the interlocked limits the wiggler beam can strike the chamfered surfaces. A transient FE analysis was performed to estimate the maximum surface temperature rise for such a case. As shown in Figure 34 (a), the temperature reaches melting point (~ 1450 ^{o}C) of 304 stainless steel in ~ 7 milliseconds. The high temperatures are limited to a very small volume (Figure 34(b)) because of the low thermal conductivity (0.016 W/mm.K) of stainless steel. Even before the melting of the thin wall occurs the atmospheric pressure would cause the thin wall to breach. The air then would rush into the storage ring causing a beam dump.

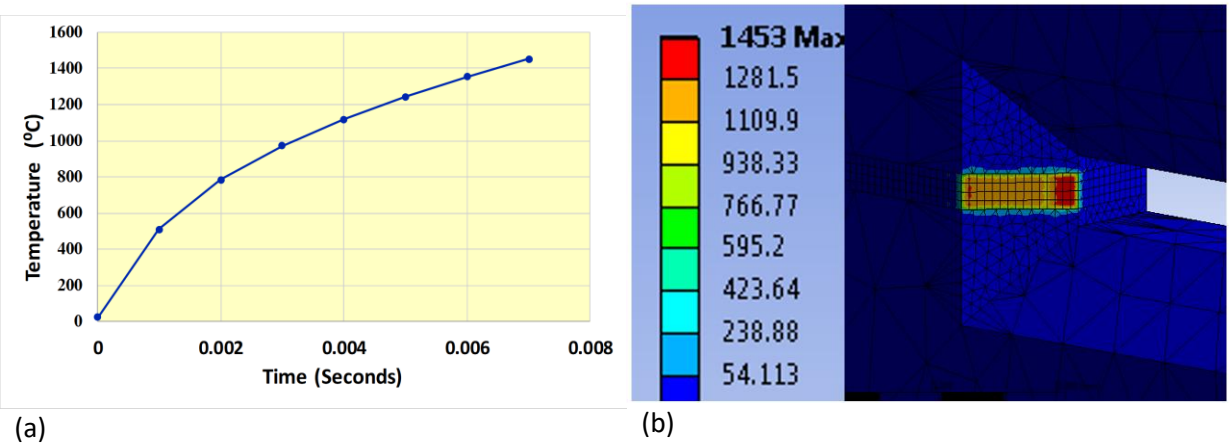

Figure 34 A transient FE analysis of the HEX burn-through flange, (a) temperature-time curve showing melting point reaching in ~ 7 milliseconds, (b) temperature contours in the beam-strike region

3.7.3.4. Lead Collimators, LCO1 and LCO2

The lead collimators, LCO1 and LCO2, consist of lead stacks assembled from 50.8 mm thick lead bricks around commercially-available rectangular 304 stainless steel (SS) tubes (see Figure 35). The lead bricks of 150.4 mm length and of various width are slotted to fit around the tube in a staggered configuration (Figure 35(a)) to prevent any line of sight through the mating surfaces. The total length of

the lead stack is at least 304.8 mm as required by the shielding guideline [3]. The lead stack is covered by a protective and configuration-controlled sheet metal enclosure (as shown in the inset) to prevent any change in the lead stack.

The 304 SS tube of 2 mm wall thickness has an inside aperture of 96 mm (H) x 16 mm (V) for LCO1 (Figure 35 (b)) and of 123.9 mm (H) x 44.7 mm (V) for LCO2. The tube is welded to two 304 SS flanges of 202 mm diameter. The overall length of the tube assembly is 403.5 mm for both the collimators.

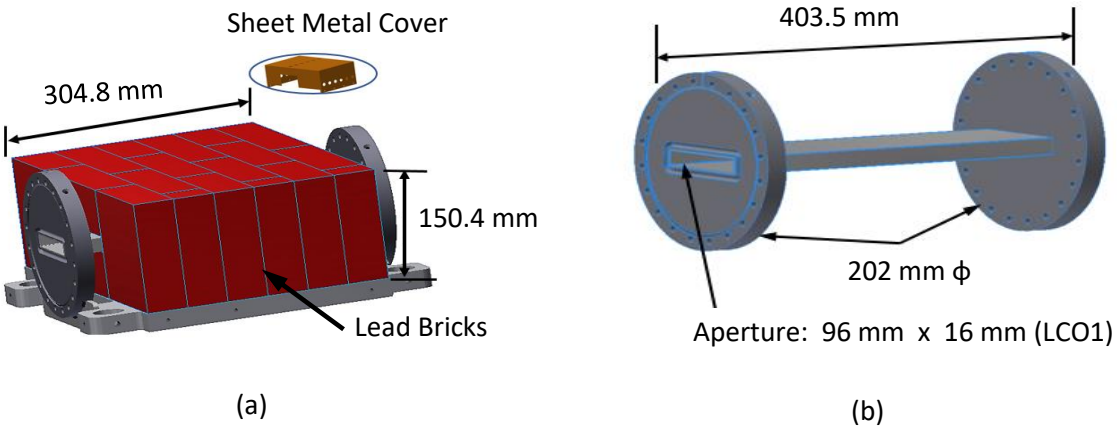

Figure 35 Lead collimator assembly for HEX front end, (a) assembly with lead bricks stacked around a 304 SS tube, (b) overall dimensions of the 2 mm thick tube welded to two 202 mm diameter 304 SS flanges.

3.7.3.5. Slits

Slit Assembly

Three slits (Figure 36) are provided in the HEX front end to reduce the beam size for each beamline independently. The inboard, outboard and center slits are located at 7.03m, 7.40 m and 7.59 m, respectively, from the source (center of the wiggler). Their overall lengths are 236 mm (inboard slit), 236 mm (outboard slit) and 359 mm (center slit), as shown in Figure 36(a). The center slit is longer since it can intercept 1 mR(H) of the wiggler beam compared to 0.2 mR(H) for the inboard and outboard slits.

At their source distances the inboard and the center beams, nominally 0.55 mR apart, are too close to allow any vertical partition with cooling channels. The conventional design of a pair of L-shaped slits is not possible for these closely beams because there is no room for any significant horizontal travel. As a compromise it was decided that the HEX slits will have only four discreet apertures [2] located vertically as listed in Table 7. The slits are required to operate independently, thus selecting an aperture in one slit does not affect the other two beams. Each slit is also required to act as an independent beam stop. The three slits are connected by 202 mm diameter edge-welded bellows which can allow large relative displacements between the slits.

Because of small beam separations only a pass-through design is feasible in which each slit has the specified apertures for its designated beam and two pass-through apertures for the other two beams. The four apertures in slits are 58 mm apart vertically. A high precision vertical stage, Parker Model 406 XR, with 100 mm travel is used for each slit (Figure 36(b)) with a support bracket. This stage, with 25 mm diameter ball screw and 2 square rail bearings can carry the weight of the center slit (36 Kg) and

resist the large bellows forces (980 N) at their full travel. The fatigue life of this stage at full travel and an offset of 131 mm (see Figure 36(b)) is greater than 40 million cycles.

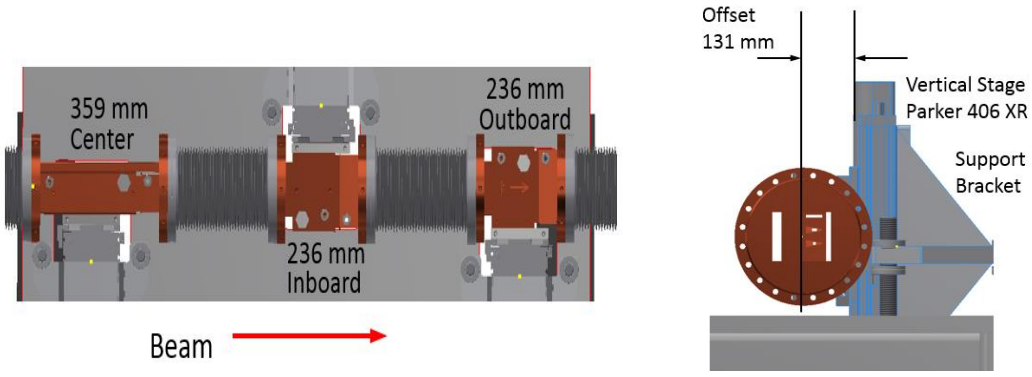

(a) (b)

Figure 36 Slits in the HEX frontend, (a) 3-slits assembly of the inboard, outboard and center slits, (b) center slit attached to a vertical stage, Parker 406 XR, at an offset of 131 mm

Table 7 Discrete apertures of the three HEX slits located vertically

Aperture No.	Inboard Slit Aperture (H, V)	Center Slit Aperture (H, V)	Outboard Slit Aperture (H, V)
1	0.2 mR x 0.2 mR	1.0 mR x 0.2 mR	0.2 mR x 0.2 mR
2	0.1 mR x 0.2 mR	0.4 mR x 0.2 mR	0.2 mR x 0.1 mR
3	0.05 mR x 0.2 mR	0.2 mR x 0.2 mR	0.2 mR x 0.05 mR
4	0.05 mR x 0.05 mR	0.05 mR x 0.05 mR	0.05 mR x 0.05 mR

Slit Design

The design of only the center slit is described in this section. The inboard and outboard slits are similar in design but simpler because these slits intercept much lower beam power. A CAD model of the center slit is shown in Figure 37. The main body (Figure 37(a)) is made from CuCrZr by conventional machining. Apertures for the center and inboard beams are then made by electric-discharge machining (EDM). Figure 37(b) shows the apertures looking into the beam direction. For clarity the upstream flange (ϕ 200 mm) is removed. Beam apertures for the center beam are created on a surface (A) inclined at 10.8º from the vertical plane. Each aperture also has top and bottom tapered surfaces to further reduce the incident beam power density. The inboard beam aperture is a simple rectangular pass-through opening. A separate rectangular chamber is machined for the outboard beam mainly to avoid water-to-vacuum joints on surface (B). This part is also made from CuCrZr. The two parts are then edge welded to the upstream and downstream CuCrZr flanges.

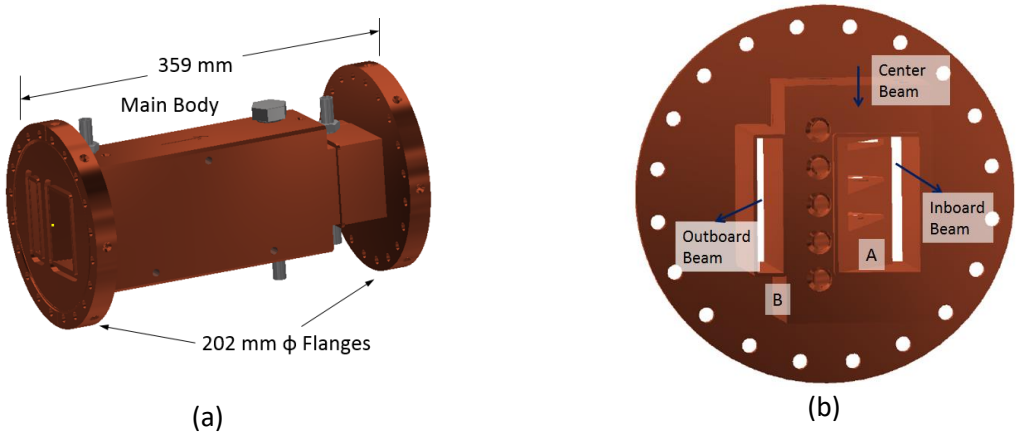

Figure 37 Center beam slit in HEX front end, (a) the main body is made from CuCrZr and welded to two 202 mm φ custom CuCrZr Conflat flanges. Central beam apertures and inboard beam pass-through apertures are made into the main body by EDM. The pass-through aperture for the outboard beam is made in a separate channel

High power density of the wiggler beam require requires the cooling channels to be within a 3-8 mm range from the beam footprint. This is achieved by a cooling channels configuration shown in Fig. 18. Cooling channels C (Figure 38(a)) of 9.5 mm diameter are blind-drilled parallel to the inclined surface A (Figure 37). Another set of channels D of the same diameter are blind-drilled perpendicular to surface B to connect with channels C. Both sets of channels are plugged at the entrances. Channels E and F are then drilled parallel to surface B to interconnect channels C and D, respectively. These channels are of 16 mm diameter except at the entrances where the standard geometry for a 16 mm tapered plug is used. Custom tapered plugs are used for these channels as shown in (Figure 38(b)). The stems of these plugs have two diameters, 6 mm in the middle to connect 2 water channels of 9.5 mm diameter in series, and 16 mm at the end to plug the channels of 16 mm diameter. Two of the plugs have through holes for water inlet and outlet.

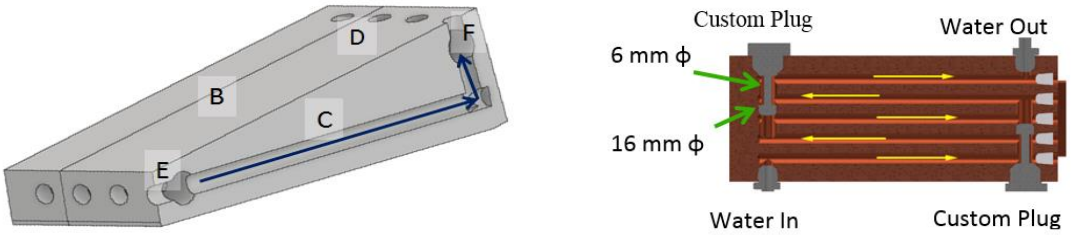

Figure 38 Cooling channel configuration in the center slit, (a) channels C run parallel to the inclined beam-intercepting surface, (b) the channels are connected in series using custom plugs

Thermal Analysis

An ANSYS finite element (FE) analysis was carried out to determine the maximum temperature rise in the center slit. The wiggler beam was positioned at different parts of the slits to ensure that the worst condition was not missed. Heat transfer film coefficient for the cooling channels was assumed to be 0.01 W/mm^2.K. Temperature contours are shown in Figure 39 for three different cases. Case 1 is for normal operation when the central part of the wiggler beam passes through one of the apertures, 0.2 mR (H) x 0.2 mR (V) aperture for instance. In this case a maximum temperature rise, ΔTmax, of 99. 5°C is obtained (Figure 39(a)).

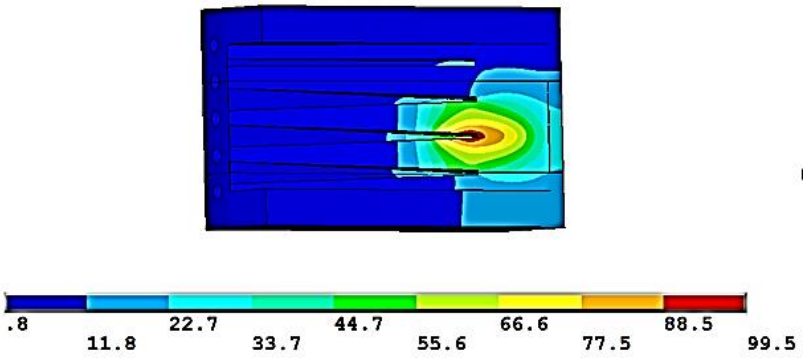

(a)

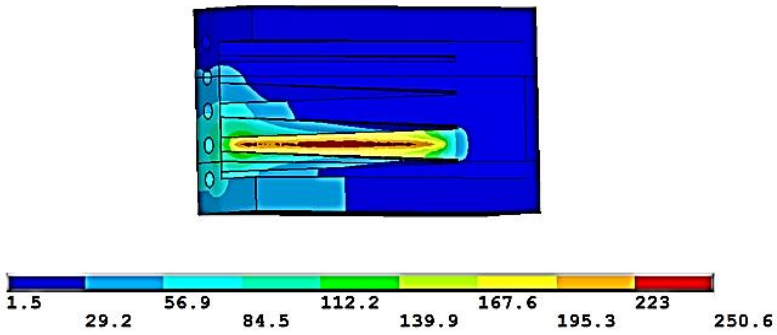

(b)

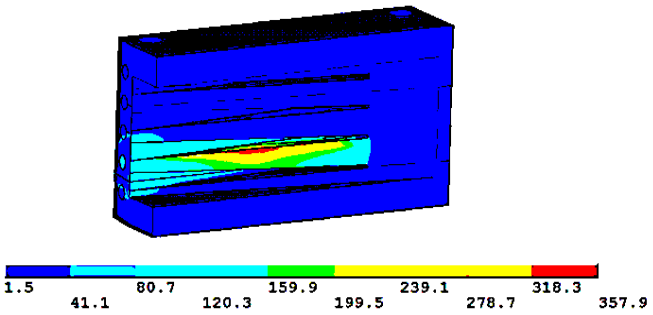

(c)

Figure 39 Temperature rise (ΔT in ^{o}C) contours for the center slit, (a) beam at the center of an aperture, (b) beam on a beam-stop position, (c) beam on an inclined edge (upset condition)

In case 2 the slit is used as a beam stop. The wiggler beam is parked on the inclined surface between any two apertures. For this case a ΔTmax of 250.6°C is calculated (Figure 39(b)) which is sufficiently lower than the acceptable value of 300°C. The third case is for upset conditions such as a failure of the vertical motion stage or its controller. In this case the beam can be incident on an inclined edge resulting in a ΔTmax of 357.9°C. This is also lower than the acceptable value of 400°C for upset conditions.

3.7.3.6. Photon Shutter

HEX photon shutter (PS), shown in Figure 40, protects the downstream safety shutters and their bellows from the wiggler beams when the safety shutters are in their down positions to block the BR fan. A single PS is used to stop all three beams simultaneously to use a simple design in the restricted space of the front end. The PS, 325 mm in length and located at ~ 21.1 m from the source (center of the wiggler), is similar in design as the fixed mask with the addition of a vertical pneumatic actuator and limit switches (Figure 40 (a)). The main body is made from CuCrZr and is welded to two 202 mm diameter Conflat flanges.

The main body (see sectional view in Figure 40 (b)) has an upstream aperture 101 mm (H) x 39.6 mm (V) and a downstream aperture of 101 mm (H) and 30.2 mm (V). The PS has only one inclined surface at 2.5^{o} on the top that intercepts the beams in its down position. Two water-cooling channels (not shown) of 12.7 mm diameter and 50.4 mm apart run parallel to the inclined surface.

The PS is mounted on a vertically oriented pneumatic actuator, SMC model MGPLF-Z (guided cylinder, ball bushing bearings), with a bore size of 63 mm and a maximum travel of 20 mm. At a nominal air pressure of 621 kPa (90 psi), the actuator has a force capacity of 177 kgf. This is more than double the combined force of 78 kgf due to the weight of the PS (45 kg) and a force (33 kgf) exerted by the 202 mm bellows under vacuum displaced by 20 mm. A mode detailed analysis of the actuator that covers off-axis bellows forces is presented in [6].

The PS up and down positions are monitored with redundancy by 5 safety-rated limit switches, 3 on the inboard side (Figure 40 (a)) and 2 on the outboard side. The switches are from two different suppliers, Allen Bradley (440-MRPB22E plunger type and 400P-MMHB04E lever type) and Siemens (3SE5112-0PA00 body, 3SE5112-0AD02 plunger) as specified by the NSLS-II PPS Group. The electron beam in the storage ring is dumped if a proper contact is not made by any of the limit switch.

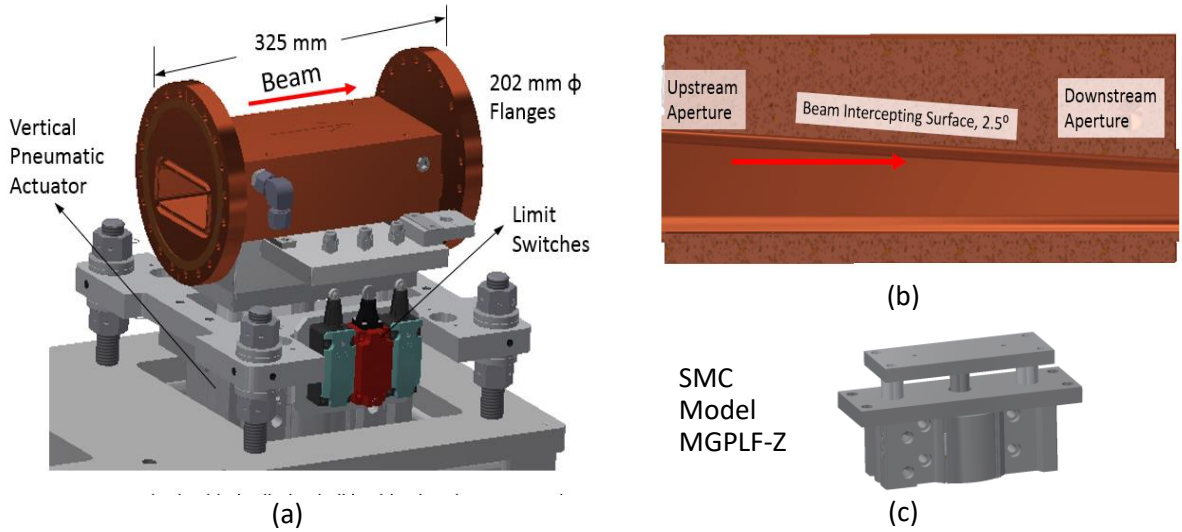

Figure 40 HEX front end photon shutter, (a) main body made from CuCrZr is welded to 2 CuCrZr conflat flanges of 202 mm diameter, 5 limit switches monitor the PS up and down positions, (b) tapered aperture of the PS, (c) pneumatic actuator SMC Model MGPLF-Z (63 mm bore).

An FE analysis of the photon shutter was performed to ensure that the maximum temperature rise under the combined heat load of the three beams, 7.72 kW, would be acceptable. The photon shutter

intercepts a total power of 7.72 kW of the three beams trimmed by the fixed mask. Several cases of beam deviations were analyzed to capture the worst case of thermal loading. Temperature-rise contours for the nominal case (without beam deviations) and for the worst case (vertical offset of 3 mm) are shown in Figure 41(a) and (b), respectively. The maximum temperature-rise of 198.7 ^{o}C for the latter case is substantially below the design criteria, $\Delta T_{max} \leq 300\ ^{o}C$.

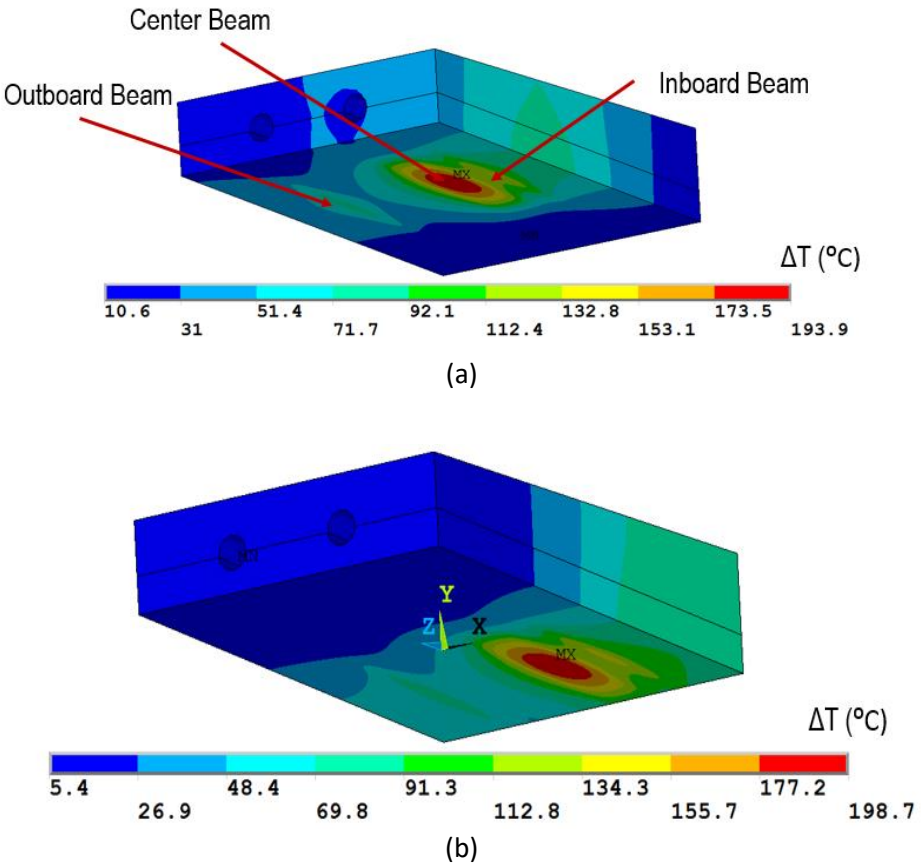

Figure 41 FE analysis results for the HEX photon shutter, (a) temperature-rise contours for nominal beam intercept, (b) temperature-rise contours for the worst case of beam deviation (vertical offset of 3 mm).

3.7.3.7. Fast Gate Valve

A fast gate valve, located at 21.5 m from the source (center of the wiggler), is used in the front end to prevent venting of the storage ring in the case of an accidental vacuum breach in the beamline. This is a commercial 8-inch flange (nominal ID of 160 mm) VAT 773 series all-metal gate valve with a closing time of less than 10 milliseconds. The fast gate valve is interlocked with the EPS system. The electron beam in the storage ring must be dumped before the fast valve is closed since its shutter cannot be exposed to the wiggler beam.

3.7.3.8. Safety Shutters

In normal operation a significant fraction of the Bremsstrahlung radiation (BR) fan exits into the beamline hutch through the ratchet wall collimator (RCO), as shown in Figure 25 and Figure 26. Front end safety shutters, SS1 and SS2 (Fig. 22 (a)), located upstream of the RCO between 22.8 m to 23.5 m from the

source, are used to stop this fan for safe access to the beamline hutches. One SS is sufficient to the stop the BR fan but two are used for redundancy. Edge-welded bellows of 202 diameter (8-inch) are used to connect SS-1 to LCO2 and SS-2, and SS-2 to RCO.

The SS of NSLS-II front ends use a unique design as illustrated in Figure 42 (b). The lead stack for stopping the BR fan is assembled on top of the SS rectangular vacuum chamber. In the open position of SS both the x-ray fan and the BR fan pass through the vacuum chamber. The upstream PS is closed first before closing the SS. In the closed position the whole SS assembly is displaced down bringing the lead stack into the path of the BR fan. Special edge-welded bellows are used that allow a large transverse displacement (~ 80 mm) for large number of cycles (> 30,000 as per RSI [2]). Although the upstream PS protects the lead stack from the wiggler beam, this design is fail-safe in the following way. Before the wiggler beam can hit the lead stack, it must pass through the flexible bellows burning a hole through its convolutions. This would result in venting of the storage ring and a beam dump fast enough to protect the lead stack [7].

A CAD model of the HEX SS is shown in Figure 43. The stack of lead with an overall length of 305 mm consists of 6 bricks, each brick 50.8 mm (2 in) thick, 165 mm (6.5 in) high and 254 mm (10 in) wide (Figure 42(a)). The bricks are stacked on a 304 SS vacuum chamber with in internal aperture of 134 mm (H) x 34 mm (V), 3 mm wall thickness, and an overall length of 388 mm including two 304 SS flanges of 202 mm diameter (Figure 42 (b)).

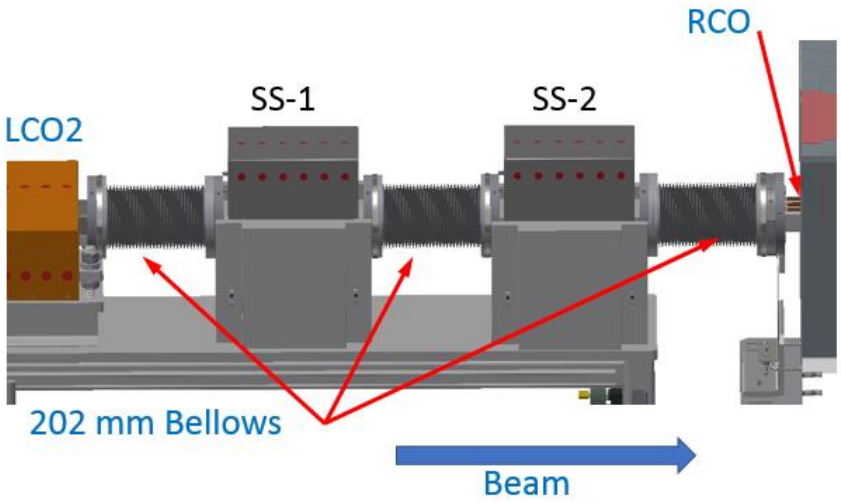

(a)

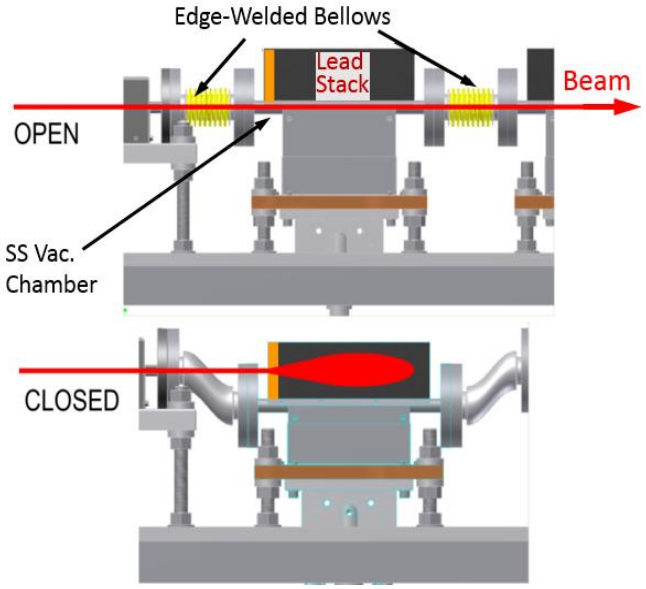

Figure 42 Safety shutters (SS) in the HEX front end, (a) safety shutters between LCO2 and RCO are interconnected by 202 mm diameter flexible (Edge-welded) bellows, (b) x-ray and BR fan pass through the vacuum chamber in the open SS position; the lead stack is lowered into the path of BR fan in the close-position of SS (after upstream PS is closed)

Each SS is mounted on a vertically oriented pneumatic actuator, SMC model MGPLF-Z (guided cylinder, ball bushing bearings), with a bore size of 100 mm and a maximum travel of 83 mm. At a nominal air pressure of 621 kPa (90 psi), the actuator has a force capacity of 497 kgf. This is 60% higher than the combined force of 309 kgf due to the weight of the SS assembly (172 kg) and a force (137 kgf) exerted by the 202 mm bellows under vacuum displaced by 83 mm. A mode detailed analysis of the actuator forces with different combination of bellows forces (SS-1 and SS-2 can be operated independently during testing) is presented in [6].

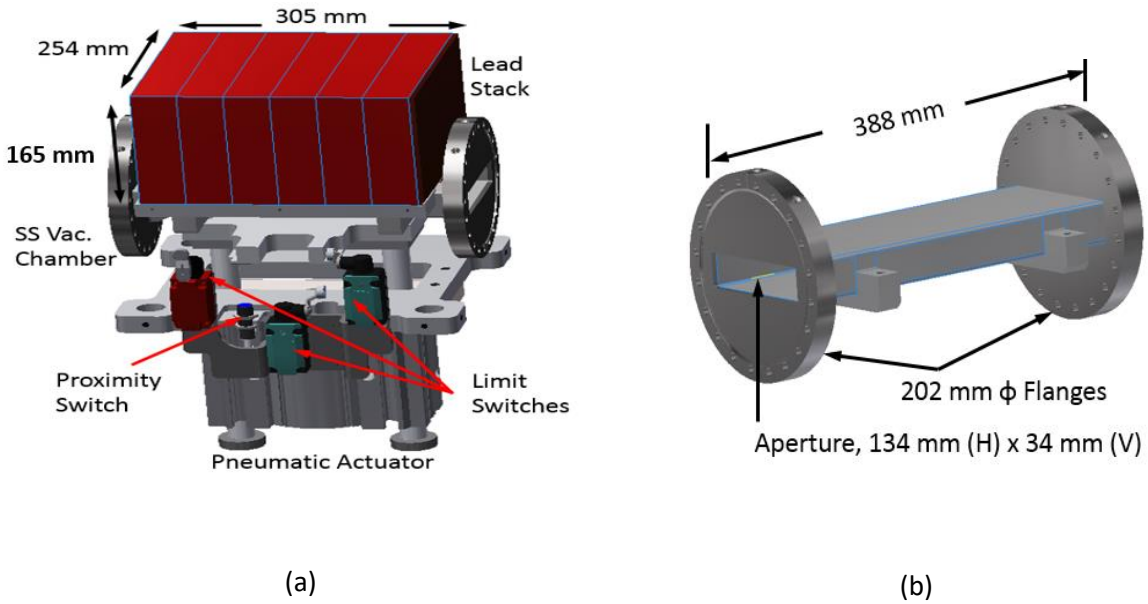

Figure 43 CAD models of the HEX SS, (a) the lead stack consisting of 6 bricks 50.8 mm x 165 mm x 254 mm is assembled on a 304 SS vacuum chamber mounted on a pneumatic actuator with limit and proximity switches, (b) the vacuum chamber with an internal aperture of 134 mm x 34 mm, 3 mm wall thickness and overall length of 388 mm

The up and down positions of the SS are monitored with redundancy by 4 safety-rated switches on the outboard side (Figure 43(a)). The switches are from three different suppliers as specified by the NSLS-II PPS Group. Two limit switches are from Allen Bradley (440-MRPB22E plunger type and 400P-MMHB04E lever type), one limit switch is from Siemens (3SE5112-0PA00 body, 3SE5112-0AD02 plunger) and the proximity switch is from Klaschka (IAB-12mg40b2-3NT1A). The electron beam in the storage ring is dumped if a proper contact is not made by any of these 4 switches.

3.7.3.9. Ratchet Wall Collimator (RCO)

The concrete ratchet wall penetration from the front end to the beamline hutch is ~ 1.45 m long with un upstream aperture of 1.40 m (H) x 0.51 m (V) for a length of 0.254 m and a downstream aperture of 0.41 m (H) x 0.20 (V) for the remaining length (see Figure 44 (a)). The RCO will be installed in this penetration (presently filled with lead bricks) during the installation of the front end.

The RCO is built in a chassis made from 12.7 mm thick aluminum plate for ease of installation (Figure 44 (b)). The chassis has an overall length of 1.07 m, width of 0.29 m and height of 0.14 m. It is supported on the floor of the penetration with alignment pads. The vacuum tube of the RCO (Figure 44 (b)) is made from a commercial rectangular tube of 304 SS. The tube has a wall thickness of 3 mm and inside aperture of 123.9 mm (H) x 44.7 mm (V). It is welded to 2 Conflat flanges of 202 mm diameter at the two ends providing a total length of 1,582 mm.

Concrete and lead bricks of 50.8 mm thickness and of various widths and heights are stacked around the vacuum tube to intercept the BR fan. The lengths of the upstream concrete stack and downstream lead stack are 711 mm and 305 mm, respectively. Stackings of both the concrete and lead bricks are done according to a formal procedure that ensures no line-of-sight through the stacks. After the installation of the RCO chassis into the penetration the upstream penetration aperture is filled with

modified lead bricks. Poly and lead shims are then used to fill in all gaps between the RCO and the penetration.

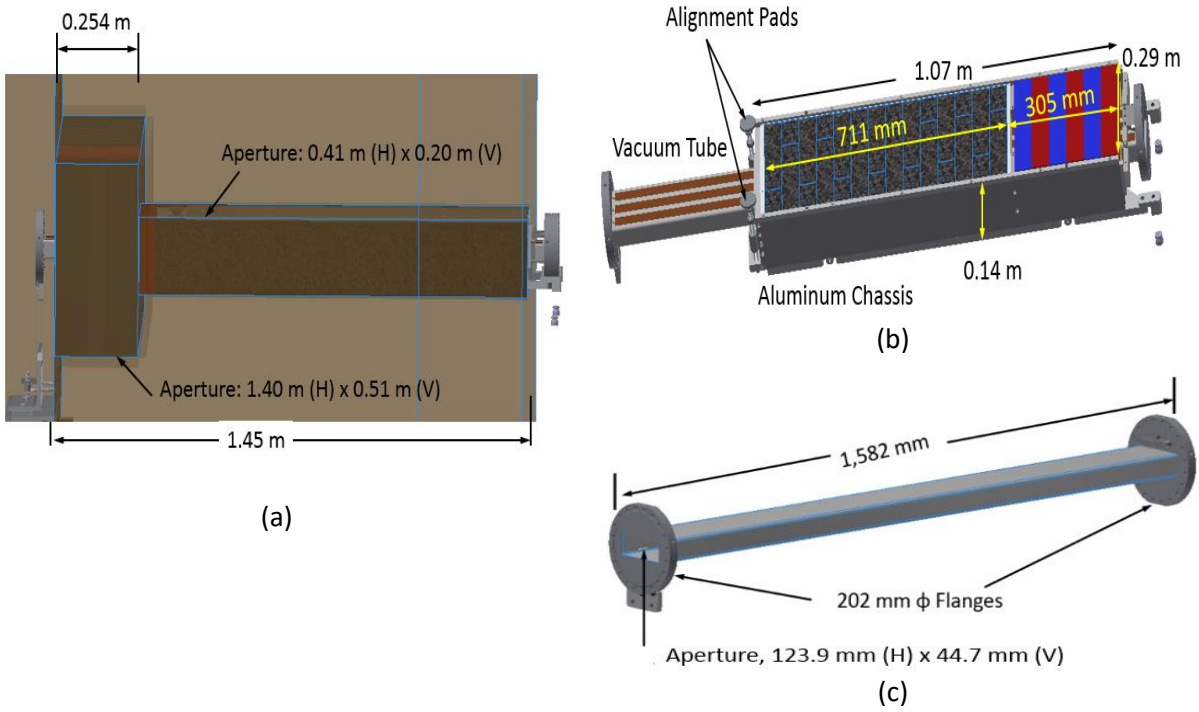

Figure 44 HEX ratchet wall collimator (RCO), (a) ratchet wall penetration with upstream and downstream apertures, (b) RCO assembled with concrete and lead bricks in an aluminum chassis for ease of installation, (c) RCO vacuum chamber.

3.7.3.10. References

[1] NSLS-II Procedure: Insertion Device Front End Ray Tracing, NSLSII-MEG-PRC-006, Revision 5, November 9, 2018

[2] RSI for Superconducting Wiggler Source and Front End for the HEX Beamline, NSLSII-27ID-RSI-001, Version 4, November 2018.

[3] Bremsstrahlung Ray Tracing Guidelines for NSLS-II Beamline Front Ends, PS-C-ESH-STD-003, Version 3, August 4, 2014.

[4] Li M. and Zinkle S.J. "Physical and Mechanical Properties of Copper and Copper Alloys," Comprehensive Nuclear Materials, Vol. 4, pp. 667-690 (2012).

[5] Sharma et al., "A novel design of high power masks and slits, MEDSI2014, Melbourne, Australia.

[6] M. Breitfeller, " A load analysis of NSLS-II front end pneumatic actuators," Tech Note in progress, December 2018.

[7] Front End Personal Protection Task Force – Final Report, July 2013 (https://ps.bnl.gov/acc/mech/frontends/Frontend%20IRRARR/Forms/AllItems.aspx)

3.8. Power Filtering Scheme

The design of the white-beam conditioning components, including diamond filters, diamond windows, and SiC filters, closely follows the design used by the XPD and PDF beamlines at NSLS-II. The filtering scheme described in this section applies to all three branches of the beamline, and is included in the beamline base scope.

Figure 45 shows the design of the diamond filter/window module, followed by fixed SiC filter. This diamond window/filter module is located downstream of the fixed mask in the FOE. The function of the diamond filter module is to filter the white beam, firstly using a water-cooled clamped diamond filter, to a low enough power density to minimize risk of damage to the downstream water-cooled diamond double window assembly. The diamond windows serve to isolate the beamline vacuum from the ring vacuum and to further filter the beam. The fixed SiC filter is designed to ensure that the heat load on the downstream monochromator crystal is reasonable in the worst-case event that all removable filters are removed and the slits are opened to the maximum position. The removable filters are located between the fixed SiC filter and the monochromator crystal.

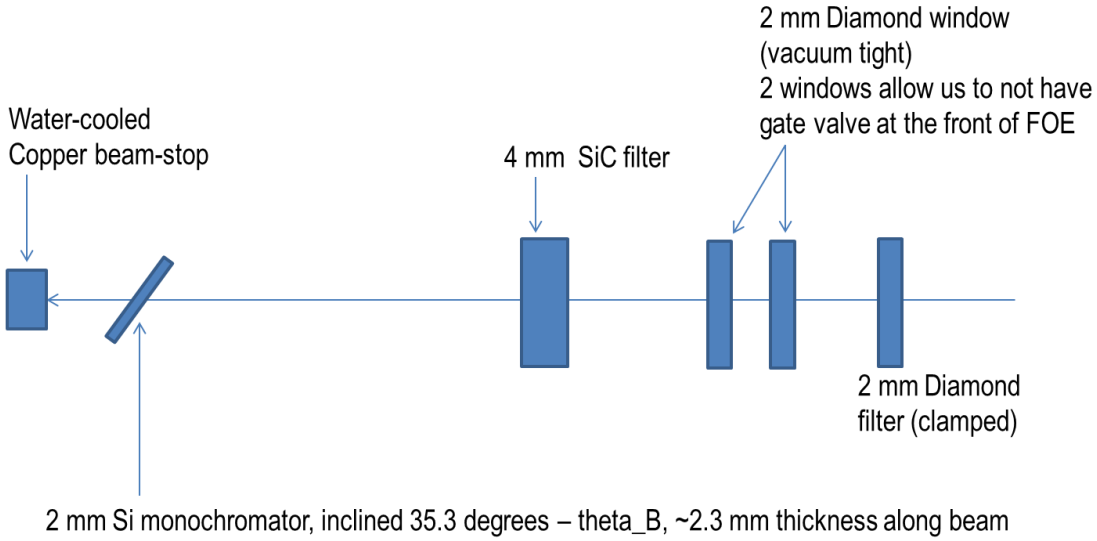

Figure 45 Design of the diamond filter/window module, followed by SiC fixed filter module.

To assure survivability of the filters and windows, worst-case power loads were calculated for each component, and FEA was performed based on the power load.

The XOP application "Wiggler Spectrum" was used to simulate the wiggler spectrum. 3 GeV ring energy, 500 mA ring current was assumed for the storage ring. A superconducting wiggler of 7 cm period and 14 periods was assumed. The field was assumed to be 4.3 T, with K_y being 28.22. The simulation shows that the wiggler provides x-rays with a total power of 55 kW, with on-center power density being 23.6 kW/mrad^2. This spectrum is then used to simulate the power load on windows, filters, monochromators, as well as to simulate the performance of optics.

A program was then written in IDL programming language to calculate the worst-case absorbed power from windows/filters. To be conservative, absorbed power is assumed to be incident power minus the

transmitted power, hence ignoring the scattered x-ray power. The spectrum from the center 0.1 x 0.1 mrad^2 is used.

Figure 46 shows the simulated incident spectra on the window and filtering elements. The monochromator is assumed to be 2 mm thick Silicon crystal, inclined at 35.3 degrees minus the Bragg angle of reflection (about 2 degrees), resulting in an effective thickness of 2.3 mm along the beam path. It shows that the filtering elements progressively remove power, particularly at x-ray energies below 20 keV, while preserving most of the high-energy x-rays above 50 keV. Diamond, being low-Z, is effective at filtering unwanted x-rays below 10 keV, while SiC, with a higher Z value than carbon, is effective at filtering unwanted x-rays in the 10-30 keV range. The combination of diamond and SiC filters is ideal for conditioning the HEX beams, to reduce the power density of the beam incident on monochromator while preserving the high-energy x-ray flux.

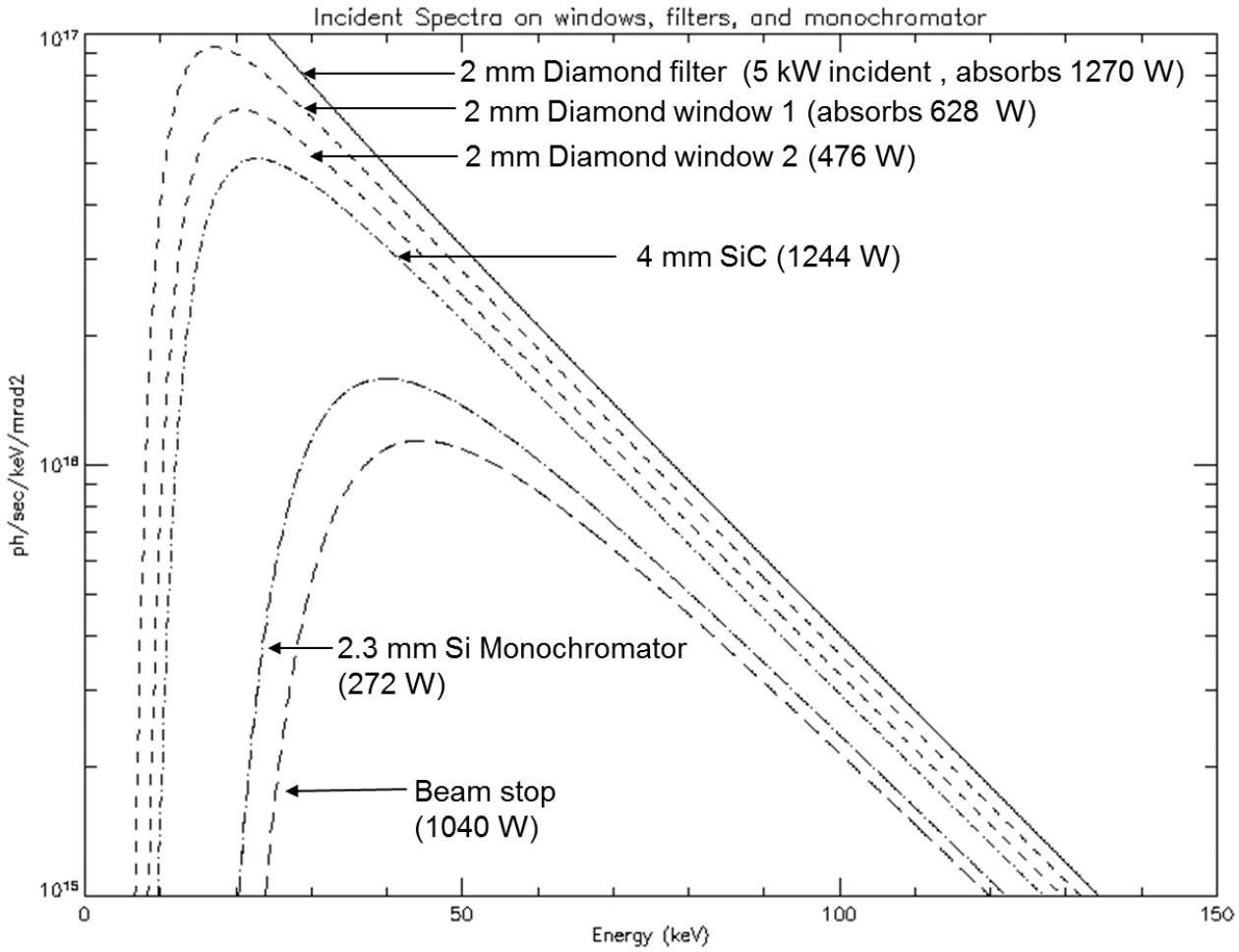

Figure 46 Simulated incident spectrum on each window, fixed filter and the monochromator.

Figure 47 shows the simulated absorbed spectrum for each of the diamond filter/windows and SiC filter, as well as for the monochromator.

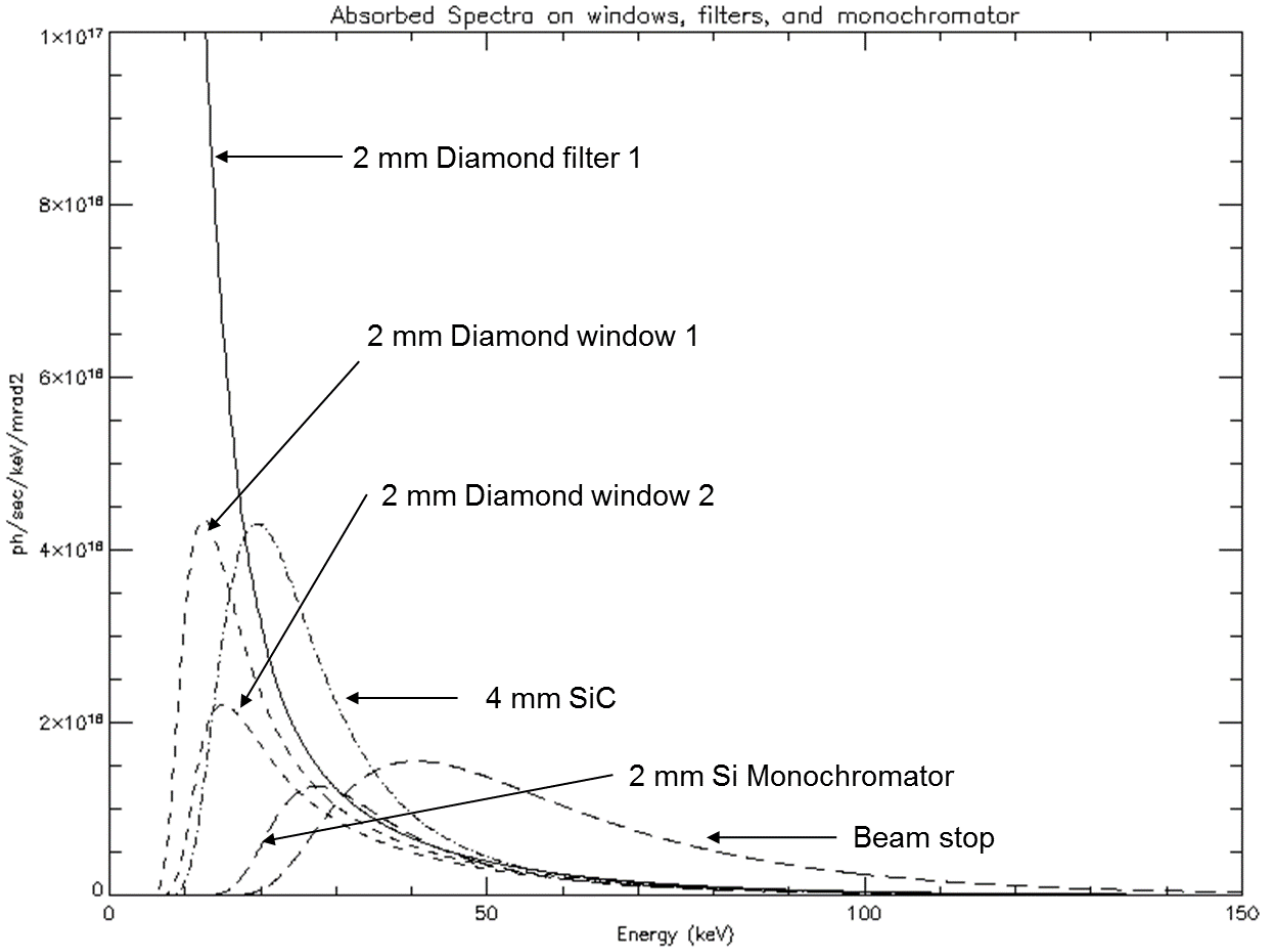

Figure 47 Simulated absorbed spectrum on each window, fixed filter and monochromator.

The absorbed power density is then calculated using the data shown in Figure 45. Table 8 shows the results of power load simulation.

	Material	Thickness Along Beam (mm)	Incident Power Density (kW/mrad^2)	Absorbed Power Density (kW/mrad^2)	Maximum Absorbed Power (W)
Diamond filter*	Diamond	2	25.1	6.37	1270
Diamond window 1	Diamond	2	18.7	3.14	628
Diamond window 2	Diamond	2	15.6	2.38	476
SiC filter*	SiC	4	13.2	6.22	1244
Monochromator*	Si	2.3	7.0	1.36	272
Beam stop	Cu	N/A	5.7	5.70	1140

*Table 8 Results of the power simulation. FEA has been performed for components denoted by * to assure survivability.*

As seen in the table above, of the three diamond filter/windows, the diamond filter has the worst-case heat load at 6.37 kW/mrad^2. The power load on the first diamond window is approximately half that of the diamond filter. FEA simulations have been performed for the diamond filter based on the simulated

power load with mechanical and cooling models of filters from XPD filter design. The results in Figure 48 shows that the maximum temperature is 305°C with a conservative surface heat load of 1270W.

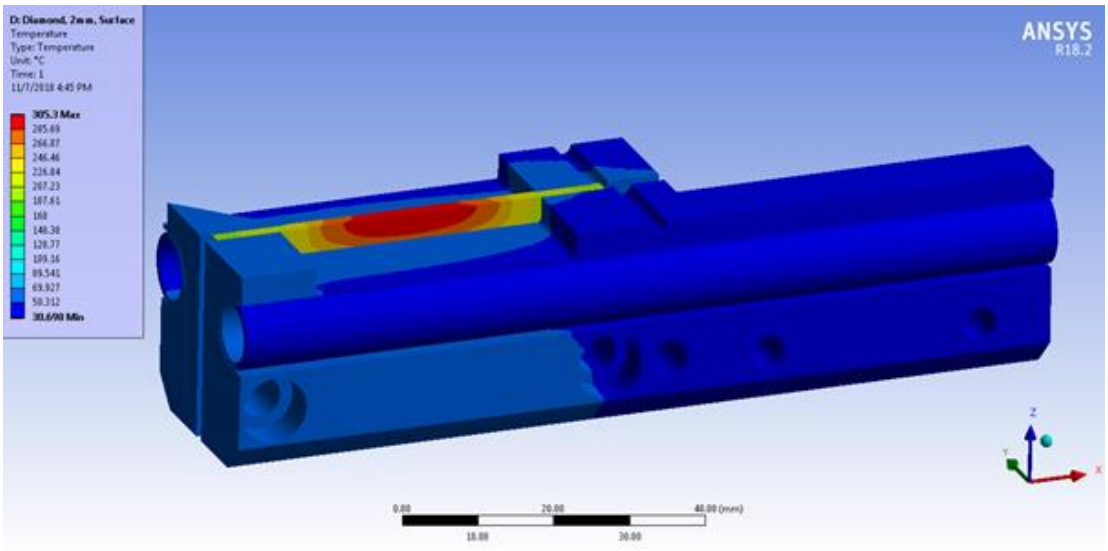

Figure 48 FEA result of the diamond filter with 1270W power load

The SiC filter, 4 mm in thickness, absorbs similar power load as the diamond filter. FEA simulations have been performed for the 4-mm SiC filter (Figure 49) resulting in a maximum temperature of 560°C assuming uniform volumetric loading, and a maximum temperature of 642°C assuming surface loading. The maximum temperature, estimated to be 600°C, is in between the two scenarios. A contact conductance between SiC and Cu cooling block, of 0.002 W/mm^2-C, was assumed for the FEA. Figure 49 shows the model used for the simulation.

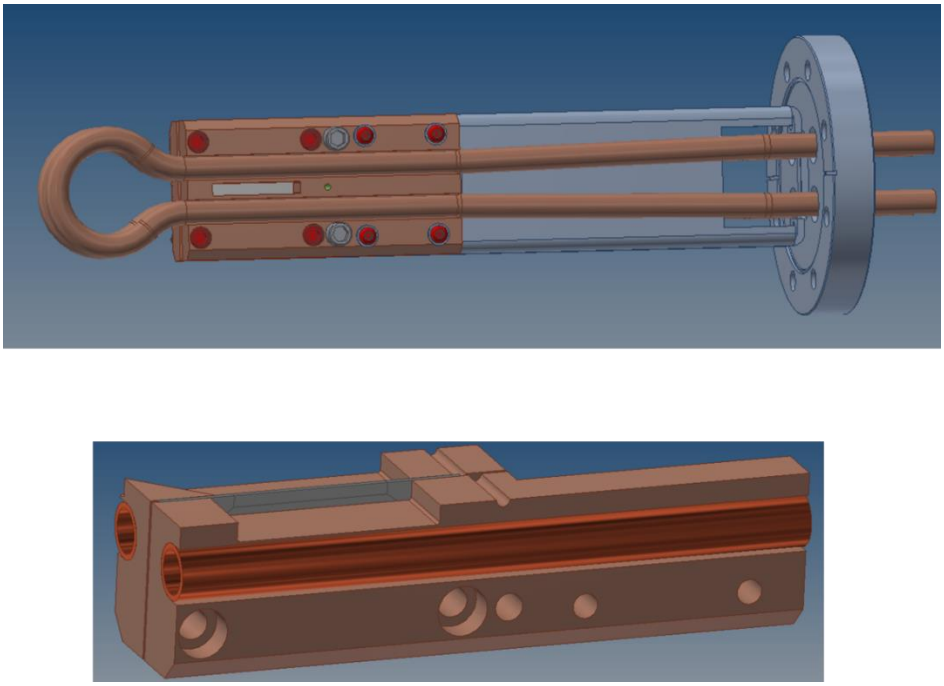

Figure 49 Design of the SiC filter with the single-crystal wafer sandwiched between water-cooled copper blocks.

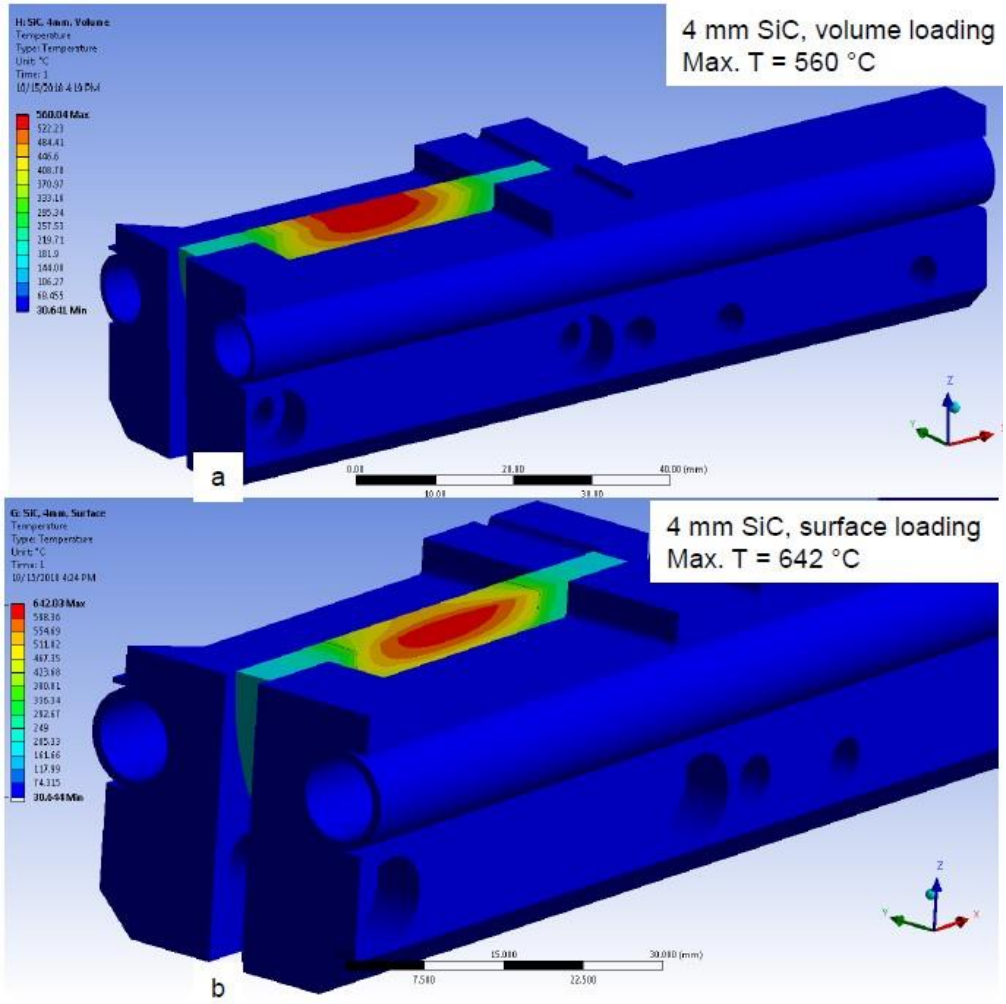

Figure 50 FEA result of 4 mm SiC filter: Temperature distribution assuming a) uniform volumetric power loading through the SiC thickness, and b) surface loading.

The preliminary design, shown in Figure 49, has been optimized based on the simulation results. Based on experience at the XPD and at the JEEP beamlines, we are confident that the design assures survivability of the filters and the monochromator and windows downstream that these filters are designed to protect.

The filtering scheme presented in the PDR uses 4 mm (total) of diamond followed by 1 mm and 3 mm SiC. For 1 mm SiC, 850 W, the maximum temperature was simulated to be 810°C assuming surface heating, and 800°C assuming uniform volumetric heating. We received advice (Thomas Connolley, Diamond Light Source) that 810°C on SiC was too high; the JEEP beamline experience SiC cracking around these temperatures. The suggestion was to limit the temperature to around 600°C. The cyclic thermal loading can cause stress cracking, even though 810°C is far below the melting temperature of SiC.. In order to lower the temperature of SiC filter, the current design uses 6 mm diamond to filter the beam. The final design also uses thicker SiC to achieve a lower average volumetric power loading on SiC than in the PDR.

The final design layout for the filters is shown below in Figure 51; note the three beams passing from Right to Left, and all passing through the (one) clamped and (two) brazed diamonds, as well as the SiC filter before the central beam can be further filtered by and additional three removable filters, and the side branches can each be filtered by one extra filter.

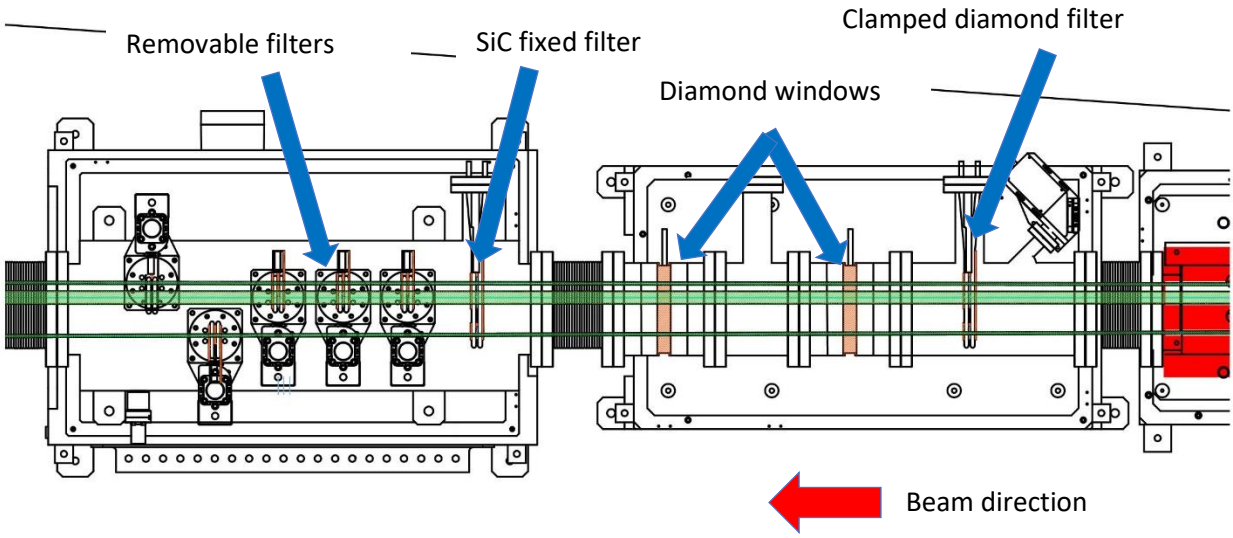

Figure 51 High-power filter layout

3.9. Center Branch Imaging Monochromator

HEX will be designed with a new high-energy non-focusing x-ray monochromator for full-field imaging. The design/construction/installation/commissioning of the imaging monochromator is in the current scope. Here we describe the design and specification of the imaging monochromator.

High-energy x-rays are especially suitable for imaging batteries, engineering materials, and earth science samples. Simulations show that bent-Laue crystal monochromator can be used at HEX to provide high-energy x-rays at a flux on the order of 10^{11} ph/s/mm^2. It will allow EDXD (high spatial resolution and depth resolution, low angular resolution) and imaging on the same sample, greatly enhancing the HEX scientific programs. In the initial scope configuration (without the focusing monochromator), the monochromatic beam size can be reduced by the use of slits, to allow the non-focused beam to be used for ADXD.

The design of the HEX imaging monochromator will consist of two identical bent crystals with the first crystal being water-cooled. Both crystals have pitch and roll angular adjustment and the second crystal can be translated along the white-beam direction to allow for energy change while maintaining a fixed exit beam height. This design is similar in concept to the high energy monochromator currently in use at beamline I12 at the Diamond Light Source (UK), see Figure 52 below.

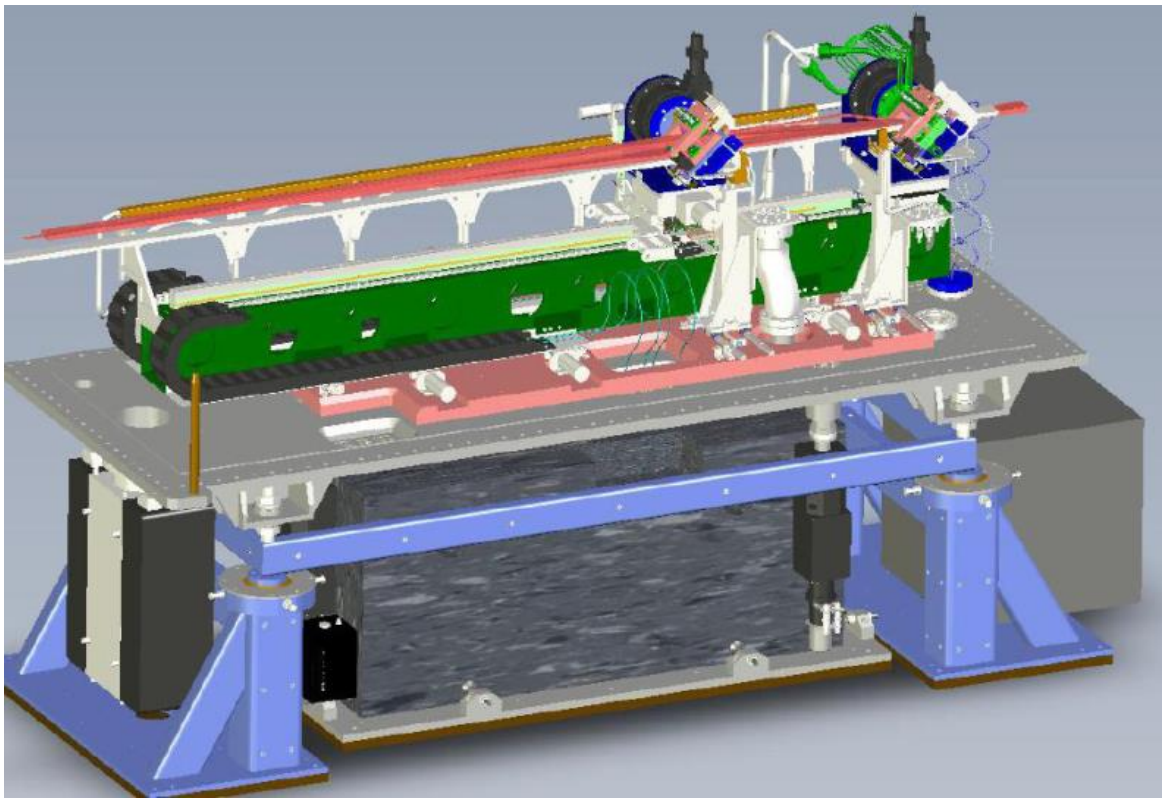

Figure 52 Design of a similar High-Energy Monochromator (DLS, UK)

3.9.1. Design Ideas and Goal

The following design ideas apply to the imaging monochromator:

1. The HEX center branch is white-beam compatible. Thus, a small offset of 25 mm is chosen to minimize the distance between the two crystals and between the monochromatic and white beam heights. This affords compact design and higher stability.
2. The XPD monochromator has the second crystal/bender in the air. We will also consider this option.
3. The monochromator and beam stop must be removable and EPS interlocked to allow white-beam operation. We will propose a design that allows both to move together to simplify the mode change.
4. The vacuum tank needs to accommodate future addition of a one-bounce monochromator on the inboard side. We prefer the monochromator tank to be opened from the side for easy access and alignment.

The monochromator is located in the FOE with the following parameters:

- source to monochromator distance (f1) is 31 m;
- Monochromator to sample distance (f2) is 73 m.

The design goal is to provide a large (100 mm x 20 mm) field of view at the F-station in the satellite building.
The required x-ray energy range needs to be variable over 30 to 150 keV. It is desirable to achieve energy-change without readjusting the bending.

We note that energy resolution is not important for imaging. However, if possible, the monochromator should offer a high-resolution mode, at about 10^{-3} dE/E, allowing it to be used for diffraction in the future.

3.9.2. Monochromator Design Considerations

Figure 53 shows the geometry for a cylindrically bent Laue monochromator. The plane of diffraction is in the plane of the figure. X rays from a point source are diffracted by the lattice planes in the bent crystal and are focused at a virtual focal point.

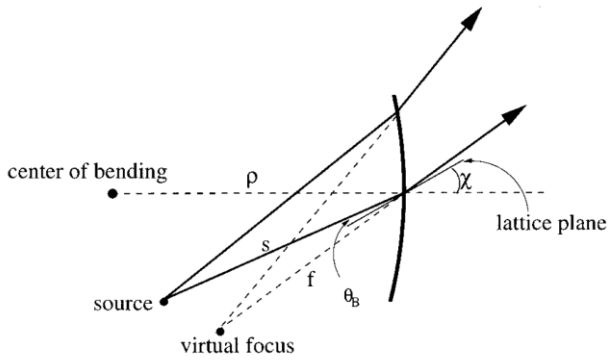

Figure 53 Geometrical optics considerations for a cylindrically-bent Laue crystal

The asymmetry angle x is defined as the angle between the normal to the crystal's surface and the lattice planes used for reflection of x rays; θ_B (the Bragg angle) is the angle required by the Bragg's law, $\lambda=2d\sin\theta_B$, for a given x-ray wavelength λ and crystal lattice spacing *d*. The distance between the source and the center of the crystal is s and the distance between the virtual focus and the crystal is f (f is negative for a virtual focal point, as is the case in Figure 53). Geometrical considerations give the following relationship between s and f:

$$\frac{2}{\rho} = \frac{\cos(\chi \mp \Theta_B)}{s} - \frac{\cos(\chi \pm \Theta_B)}{f} \qquad \textit{Equation 1}$$

where ρ is the bending radius of the bent crystal. ρ is positive when the source point is on the concave side of the crystal, as shown in figure above, and negative with the source on the convex side. The upper sign corresponds to when the source and the center of bending are on the same side of the crystal's lattice plane (as shown in figure above). For the lower sign, the source and the center of bending are on different sides of the lattice plane. The upper sign case will be the case for our monochromator.

The variation of the x-ray's angle of incidence θ along the crystal surface for a monochromator length L is:

$$\Delta\theta = L/2\left[\frac{\cos(\chi - \Theta_B)}{s} + \frac{\cos(\chi + \Theta_B)}{f}\right] \qquad \textit{Equation 2}$$

According to the Bragg's law, the diffracted beam energy bandwidth (FWHM) is:

$$\frac{\Delta E}{E} = cot\Theta_B\sqrt{\Delta\theta^2 + {\omega_0}^2 + (\sigma_s/s)^2} \qquad \textit{Equation 3}$$

where ω_0 is the angular width of acceptance of the bent crystal diffraction, and σ_s is the size of the x-ray source in the plane of diffraction.

For the special case of zero variation of the angle of incidence along the crystal surface, the diffracted beam will exhibit no energy broadening due to the geometry [i.e., with the highest monochromaticity, and $\Delta\theta = 0$ in the above equation]. The condition for producing such a beam is

$$s = \rho\cos(\chi - \theta_B) \qquad \textit{Equation 4}$$

and

$$f = -\rho.\cos(\chi + \theta_B) \qquad \textit{Equation 5}$$

In this case, commonly referred to as the inverse Cauchois geometry, both the source and the focal point are on the Rowland circle, a circle whose diameter is equal to the bending radius of the crystal. This mode has been used to produce a diverging monochromatic beam.

Both crystals are bent towards the source to minimize energy difference between the top and bottom parts of the beam. Inverse Cauchois geometry, at approximately 40 m bending radius for our first crystal, gives zero energy difference. However, 10-20 m bending radius yields acceptable energy difference, with larger bandwidth and higher intensity.

For bent Laue crystals, the bandwidth of the monochromatic beam is proportional to $\tan(\chi-\theta_B)$, where χ is the asymmetry angle defined as the angle between the diffraction vector and crystal surface. θ_B is typically small for high energy x-rays using Si 111 reflection. Thus, asymmetric crystals with asymmetry angle from 10 to 45 degrees are typically chosen to enhance bandwidth.

3.9.3. Optimization

The monochromator design choice involves a large parameter space that includes asymmetry angle, crystal thickness, and bending radius. The above factors also depend on the desired operating x-ray energy. Generally, larger asymmetry angle results in higher bandwidth and higher flux. However, if the asymmetry angle is too large, the beam footprint on the crystal increases. A thicker crystal results in larger bandwidth and higher flux at high x-ray energy. However, thicker crystals affect performance at low x-ray energy due to the crystal's self-absorption. As mentioned above, setting both crystals to a bending radius of approximately 40 m gives best energy resolution, while 10-20 m gives higher flux.

To explore the parameter space to guide an intelligent choice of crystal parameter that suits the unique requirement for imaging at HEX beamline, an IDL program was written, using lamella model for bent-crystals, to explore the parameter space.

Figure 54 shows result of the optimization at 50 keV for various imaging monochromator parameters: asymmetry angle, thickness, and bending radius. The figure of merit (FOM), represented by grayscale in this figure (lighter color means higher FOM), is the reflectivity multiplied by the integrated reflectivity in milli-radians. This FOM is proportional to the output flux of the two-crystal monochromator system.

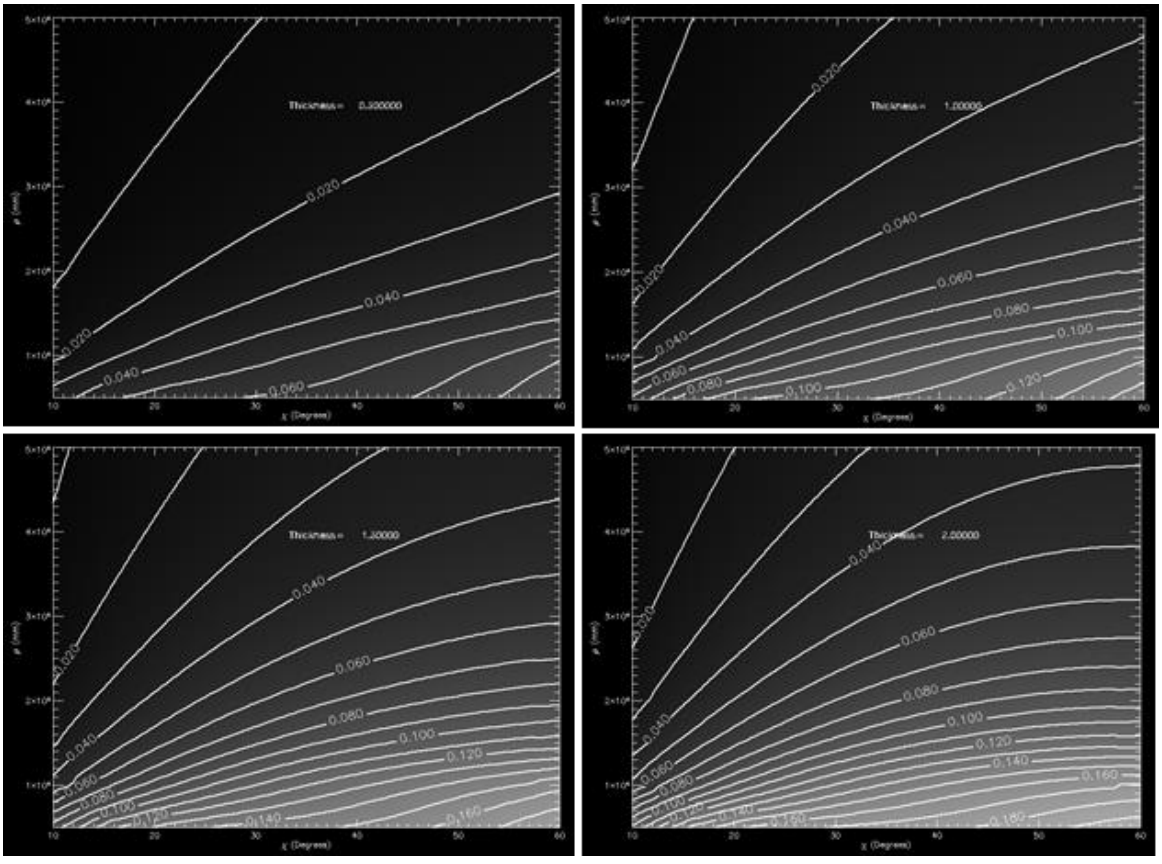

Figure 54 Result of the optimization at 50 keV for various imaging monochromator parameters: asymmetry angle, thickness, and bending radius

Similar simulations were performed at 30 and 150 keV to assess the effects of the parameters on the performance across the desired energy range. The results for 30 keV are shown in Figure 55.

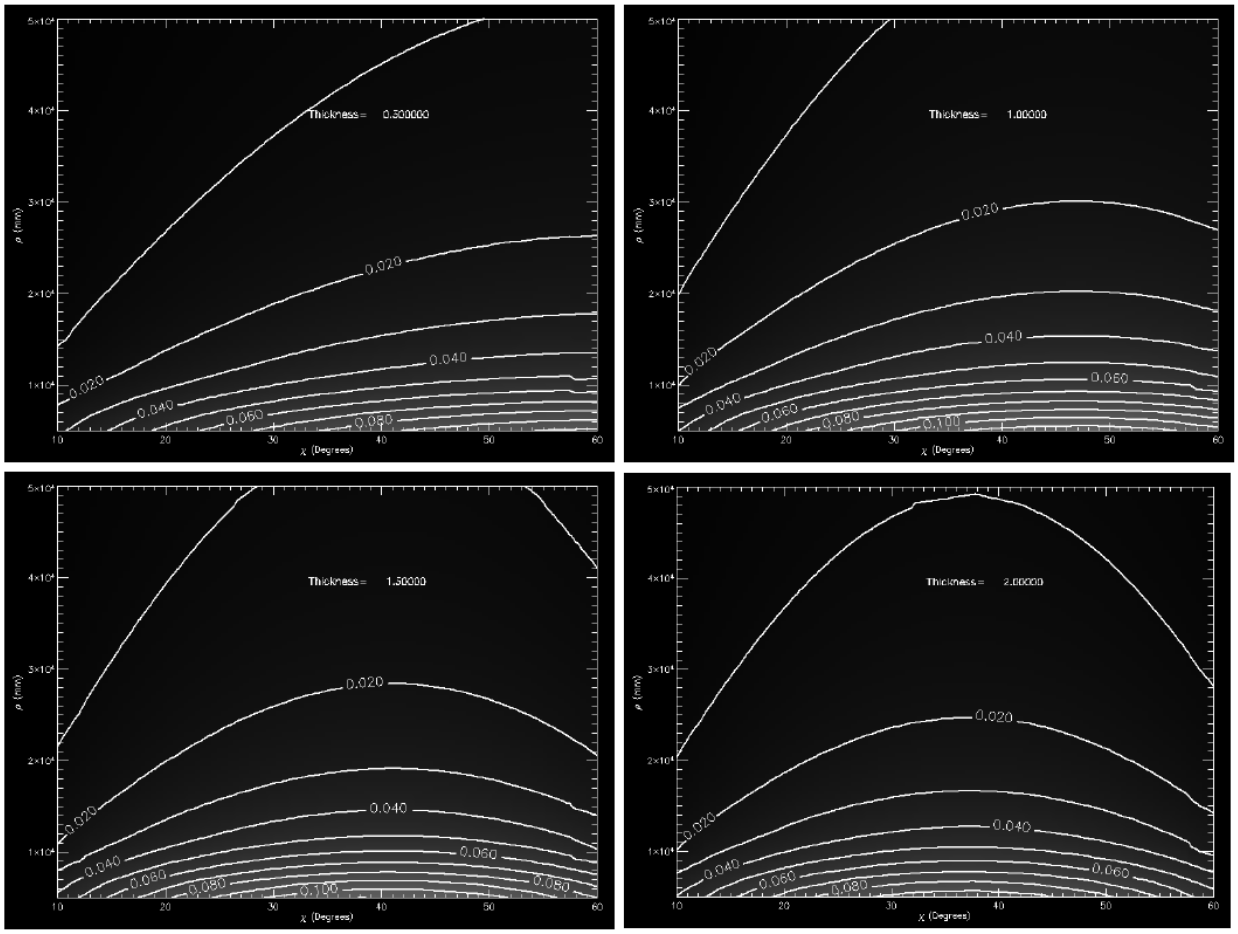

Figure 55 Result of the optimization at 30 keV for various imaging monochromator parameters: asymmetry angle, thickness, and bending radius

Analysis of optimization results in Figure 54 and Figure 55 show that the benefit of larger asymmetry angle levels off after about 40 degrees. Therefore, the symmetrical crystal cut of 35.3 degrees asymmetry angle, with crystal surface being 100, shown in Figure 56, is an appropriate choice.

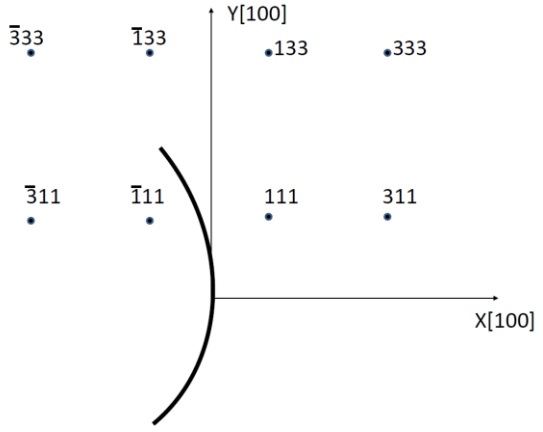

Figure 56 Reciprocal space configurations of a Laue crystal with surface normal being 100, and the 111 reflection at 35.3 degrees asymmetry angle

The advantages of a 100 crystal are:

1. Simple symmetrical crystal design minimizes confusion. For example, accidental or deliberate flipping the crystal would have no negative consequences.
2. 111 reflection at 35.3 degrees asymmetry angle has high flux for imaging and no second harmonics.
3. On the same crystal, it is shown in Figure 56 that the 022 is a symmetrical reflection with 0 asymmetry angle. At 0-degree asymmetry angle, bending the crystal does not broaden the rocking-curve width. This reflection is a thus good choice for very high resolution, and consequently lower flux, beam.
4. The 311 reflection on the same crystal has high resolution and moderate flux, with no second harmonics. This reflection is a good candidate for diffraction studies that require high resolution.

We note that the 022 and 311, both about 30 degrees from nominal 111 position, may not be accessible if we use an InGa-filled trough on top of the crystal for cooling.

As for the choice of crystal thickness, the optimization studies show that 1.5- 2 mm allows reasonable 30 keV performance, while thicker crystals benefit higher energies. We choose 2 mm average thickness for the first and second crystal in our baseline design due to the desire to image at 30 keV.

As expected, smaller bending radius results in higher flux at the cost of larger energy difference between the top- and bottom- parts of the beam. The flux benefit levels off at smaller than 10 m radius.

According to the lamellar model, as a result of the systematic change of the angle of lattice plane from the front to the back of the crystal along the beam path, the bent-Laue crystal's rocking curve is typically rectangular in shape. The rocking curve between two identical crystals is the convolution of two rectangles, resulting in a triangular rocking curve. Operating the monochromator with a triangular rocking curve results in the intensity fluctuation as the relative angle between the crystals changes. Since the rocking curve width is proportional to the crystal thickness, if the second crystal is slightly thicker than the first crystal, then the rocking curve would be a trapezoid, resulting in better intensity stability of the monochromatic beam. Thus, we will consider the second crystal having slightly larger thickness than first crystal to achieve a flat-top in the rocking curve. This concept was successfully implemented by the MECT monochromator at X17B beamline of the NSLS.

3.9.4. Crystal Cooling

Since the micro-imaging program does not require x-rays less energetic than 30 keV, diamond windows and SiC filters can be effectively used for reducing the heat load by removing the lower energies present in the white beam. The design uses three diamond windows (2 mm each) and 4 mm of SiC followed by a set of removable SiC filters. The diamond windows serve both as heat filters and as a vacuum barrier while providing added reliability because each is capable of carrying the full power load. The removable SiC filters can be selected to adjust the tradeoff between transmitted power and transmitted flux in real time. The filtering proposed for the HEX imaging monochromator is similar to the scheme chosen for the sagittal-focusing monochromator at the XPD beamline at NSLS-II.

We used FEA to study the thermal impact of the filtered white-beam on the first crystal of the bent-Laue monochromator.

Figure 57 shows the model used for the FEA simulation. The active area of the Laue crystal is limited to 12 mm (this is the minimum required to intercept 6 mm high white beam at inclined angles) vertically to facilitate heat dissipation to the water-cooled copper block. The top and bottom portions of the crystal are extended to 5 mm thick blocks for two purposes:

1. To create a rigid bar, so that the leaf springs, mounted on the inboard and outboard sides of the crystal, can realize cylindrical bending in the active region of the Laue crystal;
2. To minimize the strain (due to clamping) from propagating to the active region.

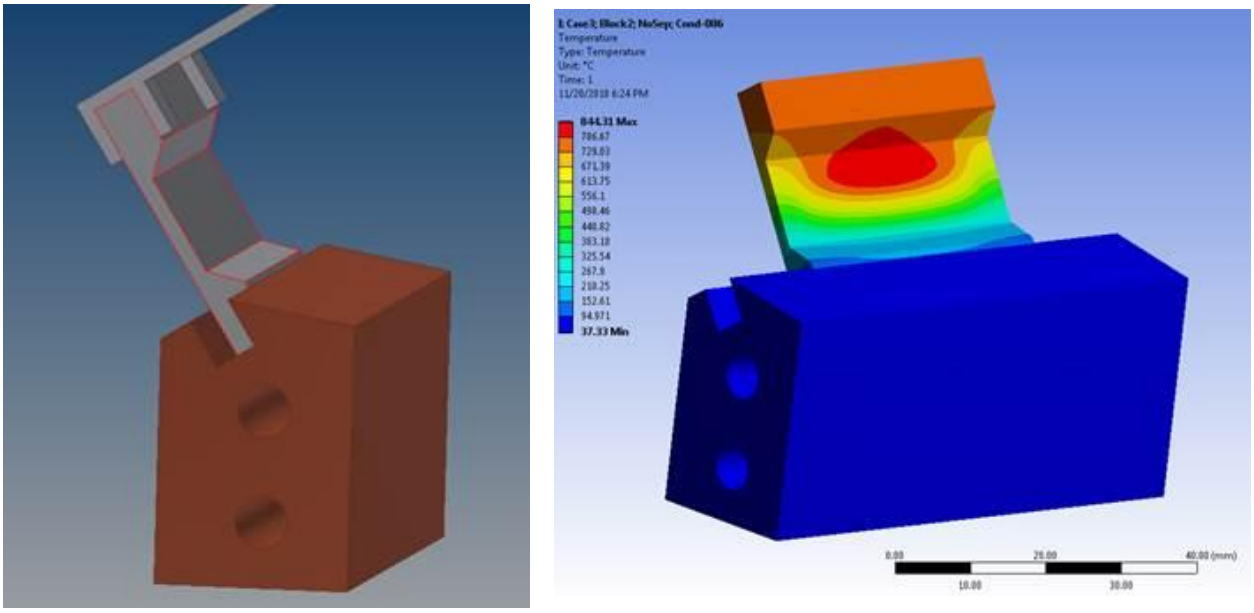

Figure 57 Model used for FEA simulation of the bent-Laue crystal

One can restrict the horizontal aperture on the monochromator when operating without SiC filter to limit the total power on the monochromator at low x-ray energies. This strategy is consistent with full-field imaging in that samples that use low x-ray energies are typically small samples requiring small field of view. For larger samples that require the full horizontal field of view and accordingly higher x-ray energies, the monochromator can utilize additional SiC or Copper filtering to further reduce heat load and improve thermal stability at higher x-ray energies above 50 keV. Based on this strategy of applying more filters at larger field of view, we simulated three representative cases for using the monochromator (all examples consider the central branch beam in the F-hutch):

- Case 1. 1 mm x 1 mm beam (FE aperture #4, with additional slitting of beam) for ADXD applications with default fixed filter (6 mm diamond + 4 mm SiC).
- Case 2. 10 mm x 10 mm beam (FE aperture #3, with additional slitting of beam) for imaging of typical samples up to 10 mm in diameter, with default filter.
- Case 3. 20 mm x 100 mm beam (FE aperture #1, with NO additional slitting of beam) for imaging of large samples up to 100 mm in diameter, with 15 mm additional SiC filter.

Additionally, worse-case thermal loading under fault conditions (20 mm x 100 mm beam, default filter) is also simulated. Table 9 summarizes the beam size, filter condition, simulated absorbed power by the first crystal at a typical operating inclination angle of 33 degrees, and FEA-simulated maximum temperature at the active area of the Laue crystal. The FEA simulation assumes a conservative thermal conductance of 0.002 W/mm^2.°C and a conservative thermal convection coefficient of 0.01 W/mm^2.°C.

Mode	Absorbed Power Density (kW/mrad^2)	FE Aperture	Additional Filter	Beam Area at 100 m (mm x mm)	Maximum Absorbed Power (W)	Max Temp. (°C)
Case 1: Diffraction	1.36	#4	None	1 x 1	0.136	30
Case 2: Imaging small Beam	1.36	#3	None	10 x 10	13.6	68
Case 3: Imaging Large beam	0.24	#1	15 mm SiC	20x100	48	129
Worst-Case	1.36	#1	None	20 x 100	272	1227

Table 9 Summary of FEA simulation results for three typical modes of using the imaging monochromator, and the worst-case fault condition

The simulations shown above assume a conservative thermal conductance, between Silicon and Copper, of 0.002 W/mm^2.°C and a conservative thermal convection coefficient of 0.01 W/mm^2.°C. To estimate the effect of thermal conductance and convection coefficient, additional simulations were performed assuming an optimistic convection coefficient of W/mm^2.°C and/or higher thermal conductance (perfect condition and more optimistic 0.006 W/mm^2.°C). The results, listed in Table 10, show that the impact of convection coefficient is small, and that the thermal conductance plays an important role in the thermal management of the Laue crystal. For example, for case 3 (Imaging with large beam) with 15 mm additional SiC filter, using an achievable thermal conductance of 0.006 W/mm^2.°C lowers the maximum temperature to 98 °C from 129 °C, an approximately 30% lowering of temperature rise (relative to cooling water). Based on these results, we will pay close attention to maximizing the thermal conductance in the engineering design of the monochromator.

	Beam Size	Total Power [W]	Power Density [W/mm3]	Convection Coefficient [W/mm^2-°C]	Contact Condition	Thermal Conductance [W/mm2-°C]	Maximum Temperature [°C]
Case 1	0.31 mm x 0.31 mm	0.136	0.657	0.01	*No Separation*	*perfect conduction*	29.9
Case 2	3.1 mm x 3.1 mm	13.6	0.657	0.01		*perfect conduction*	55.7
		13.6	0.657	0.01		0.002	67.9
Case 3	6.2 mm x 31.0 mm	272	0.657	0.01		*perfect conduction*	567.5
		272	0.657	0.01		0.006	844.3
		272	0.657	0.01		0.002	1227.4
		272	0.657	0.015		0.006	832.1
		272	0.657	0.015		0.002	1218.5
		102	0.246	0.01		0.006	203.5
		102	0.246	0.01		0.002	280.3
		48	0.116	0.01		0.006	98.0
		48	0.116	0.01		0.002	129.2
Perfect Conduction: To show the limiting value (lowest possible temperature)							
Good Conduction = 0.006 W/mm2-°C (approximately)							
Poor Conduction = 0.002 W/mm2-°C (approximately)							

Table 10 FEA results for the three typical usage cases and worse-case, assuming more optimistic convection coefficient and/or thermal conductance

Thermal distortion of the Laue crystal results in broadening of the rocking curve, making it more difficult to match the rocking curve of the second crystal with that of the first crystal. This can lead to intensity loss of the monochromator output and non-uniformity of the imaging field. Figure 58 shows the temperature distribution at the center of the Laue crystal for case 2 (10 mm x 10 mm beam in hutch F, no additional filter), resulting in a maximum temperature of 68 °C.

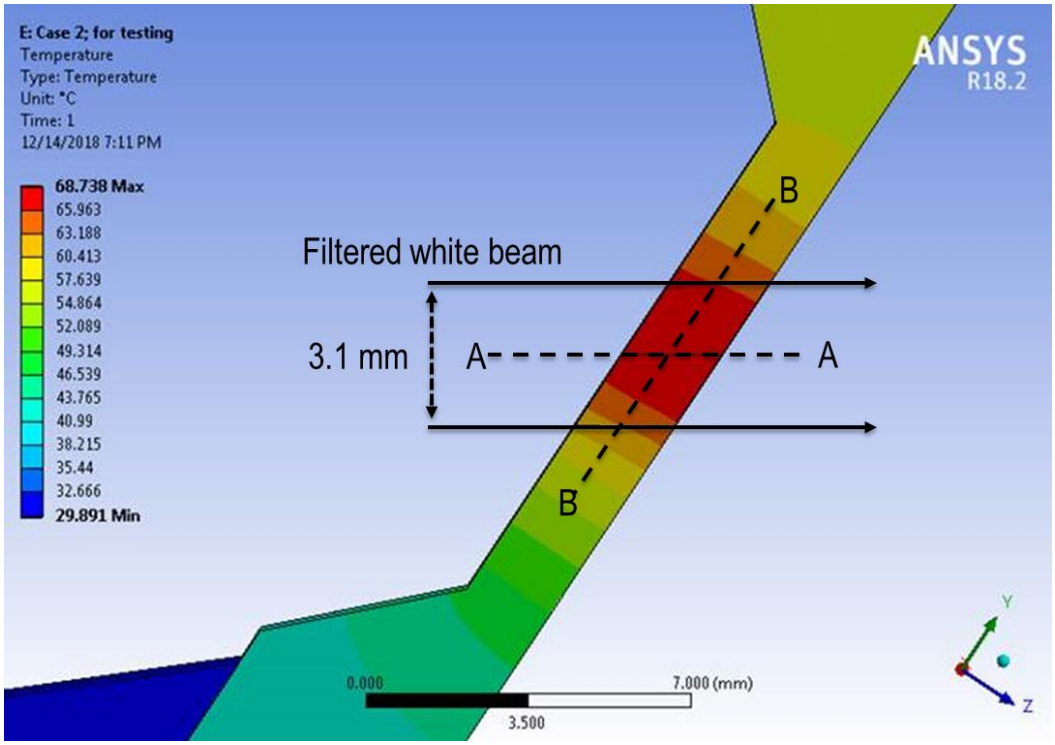

Figure 58 Temperature distribution in a cross-section at the center of the crystal for case 2

To estimate the impact of thermal distortion on the performance of the bent-Laue monochromator, we tracked the distortion of a straight-line, A-A shown in Figure 58 above, in the crystal along the path of x-ray beam. The blue line in Figure 59 below shows the Y (along the surface of the crystal in the diffraction plane) displacement going from the front-side to the back-side of the crystal. It is seen that the relative displacement is small at about 0.008 microns. The impact on x-ray diffraction by the lattice planes in the Laue crystal is represented by the relative in-plane angular change (typically called slope error) of the straight line, AA. The slope error is calculated by first-order derivative of the Y-displacement vs. position along x-ray beam. The brown line in Figure 59 shows the slope error as a function of position along the beam centerline. The absolute magnitude of the slope error along the beam is about 10 micro-radians. The slope error as a function of position can be represented by a superposition of a linear slope, shown by the black line, and residual slope error, shown by dashed lines in Figure 59.

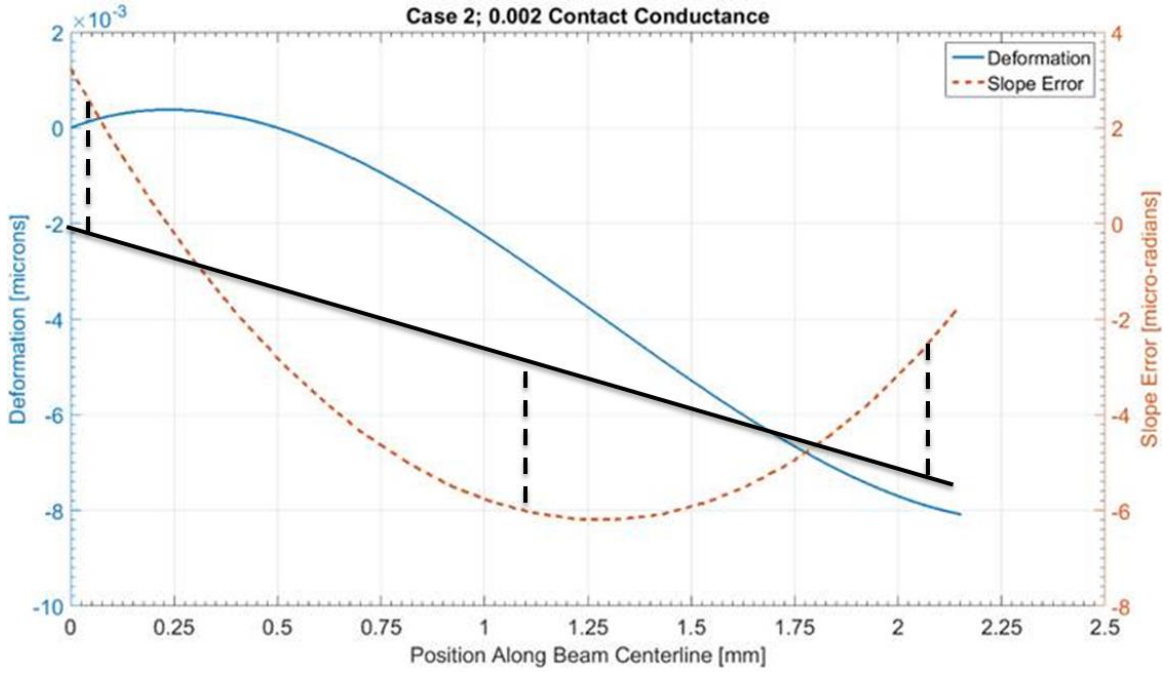

Figure 59 Displacement (along Y direction) of a straight line (AA) along the white-beam centerline, and the slope of the distorted AA line, as a function of depth in the crystal for case 2

The linear slope of approximately 4 micro-radians change across the length of 2.1 mm represents a cylindrical bending radius of 525 meters. This additional bending is insignificant compared to the crystal's designed bending radius of 10 m (for maximum output intensity) to 30 m (for best energy resolution with inverse-Cauchois geometry). This slope error can therefore be compensated for by adjustment of bending if necessary.

The residual slope error shown by the dashed lines in Figure 59, of approximately 3 micro-radians in magnitude, cannot be compensated by adjustment of bending. The effect on x-ray intensity loss can be estimated by comparing the slope error with the rocking-curve width of the bent-Laue crystal. According to the Lamella model, the bent crystal's rocking curve width is $T/\rho\tan(\chi-\theta B)$, where T (1.8 mm) is the thickness of the crystal, ρ (10-30 m) is the bending radius of the crystal, χ (35.3 degrees for the 111 reflection) is the asymmetry angle, and θ_B (a few degrees) is the Bragg angle. The rocking curve width is

thus calculated to be 100 to 300 micro-radians. The residual slope error of 3 micro-radians is insignificant compared to the operating rocking curve width, and this is unlikely to impact the intensity and uniformity of the diffracted x-ray beam.

For case 3 (large beam with 15 mm SiC filter) which results in a temperature of 129 °C, similar FEA simulations of the distortion and slope-error of the white-beam centerline were performed. Figure 60 below shows the displacement (blue line) and slope error (brown line) as a function of position along the centerline. It is seen that the relative displacement, though larger than that seen in case 2, is still small at about 0.08 microns. The absolute slope error, about 20 micro-radians, is also larger than the slope error seen in case 2.

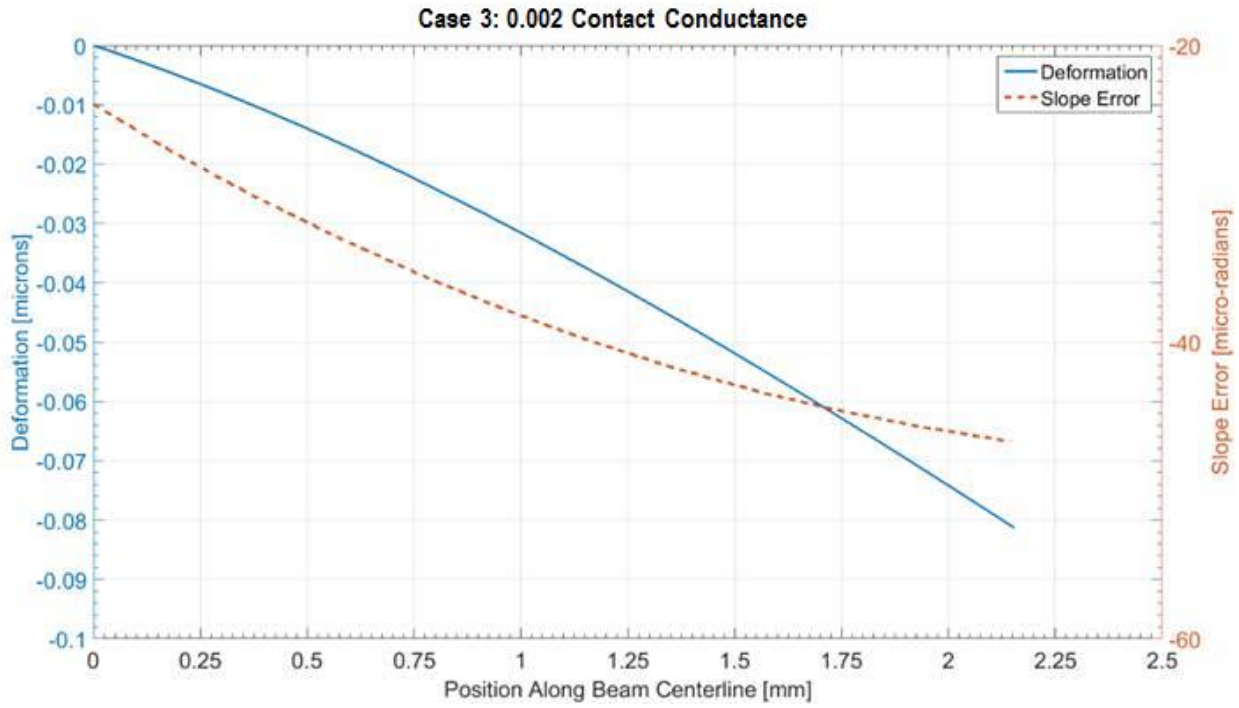

Figure 60 Y-displacement and the slope of the distorted AA line, as a function of depth in the crystal for case 3 with 15 mm SiC filter

As in case 2, the slope error is represented by a linear component and residual. The yellow line in Figure 61 shows the result of linear least-square fitting to the slope error. The yellow line represents an additional bending with a radius of about 100 m. Though not insignificant, this additional bending due to the thermal distortion is still small compared to the designed bending radius of the crystal (10-30 m), and this can be compensated for by small adjustment of the crystal bending, if necessary.

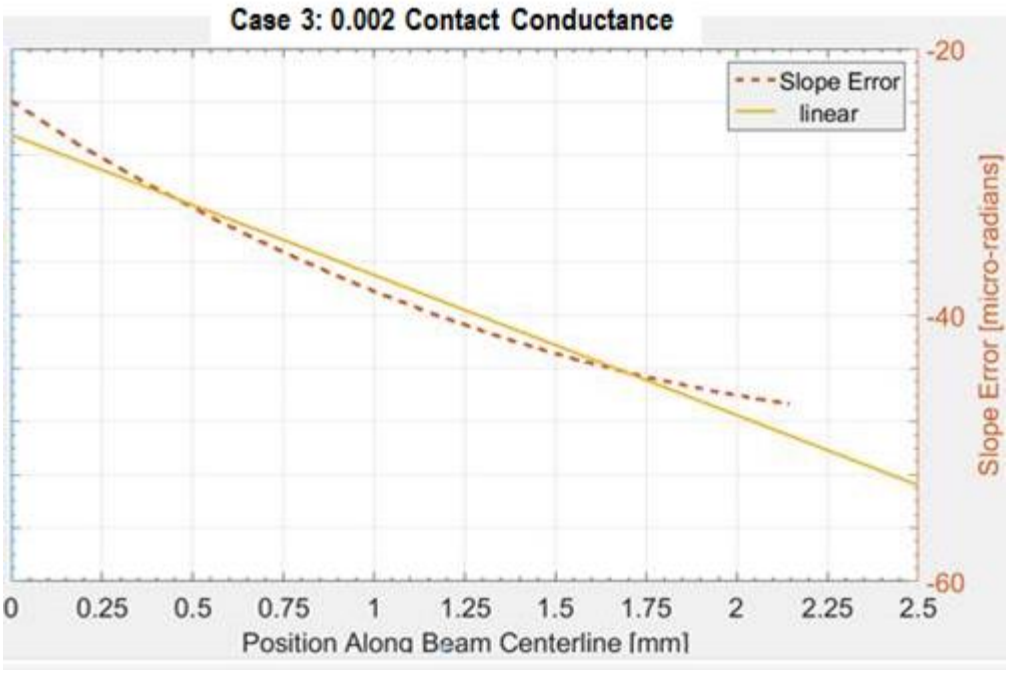

Figure 61 Result of linear least-square fitting of the slope-error vs. position along beam

Figure 62 shows the residual slope error after subtracting the linear component. The residual slope error is about 2.5 micro-radians in deviation. It is interesting that the residual slope error for case 3 is similar to that of case 2, even though the maximum temperature for case 3 is twice that of case 2. This is due to the larger 6.2 mm vertical beam size in case 3 resulting in smoothing out of the distortion field. Again, the residual slope error is insignificant compared to the 100-300 micro-radians rocking curve width expected of the bent-crystal.

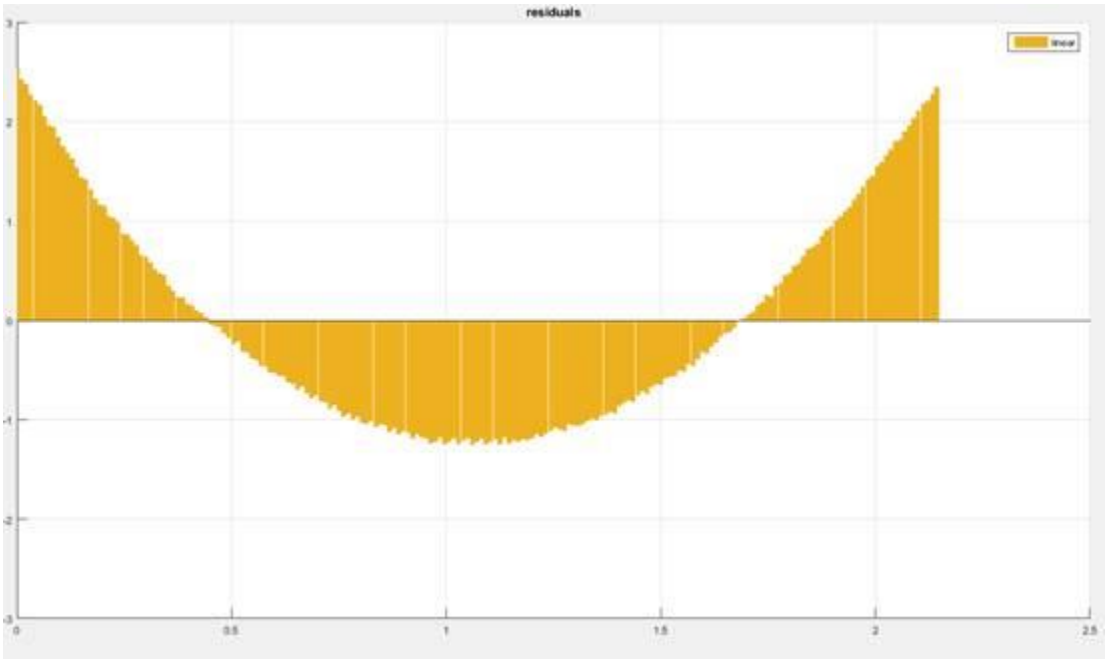

Figure 62 Residual slope error (after subtracting the linear component) vs. position along beam

The thermal distortion of case 1 (maximum temperature of 30 degrees) is expected to be much less than that of cases 2 and 3. Based on our analysis of slope errors for cases 2 and 3, we conclude that with one-side water-cooling of the crystal, thermal distortion is unlikely to impact the intensity and uniformity of the diffracted x-ray beam for all three practical-use cases. Thus, water-cooling (instead of liquid nitrogen cooling) will be specified for the imaging monochromator to reduce cost and simplify operations.

The simulations presented above assume one-sided cooling of the crystal. Typical two-sided cooling of both the top and bottom parts of the crystal requires an In-Ga-filled trough on the top of the crystal. This is incompatible with our desire to rotate the crystal by +- 35 degrees from the default 111 reflection position to utilize the 220 and 311 reflections. However, there are significant advantage to two-sided cooling: the resulting thermal distortion is more symmetric; and the absolute distortion is lower. Thus, we will specify a cooling scheme that is in-between one-sided and two-sided cooling. The cooling scheme will involve indirect cooling of the top leaf of the crystal, where the bender is attached, by flexible foil with high thermal conductivity.

3.9.5. Optimized Monochromator Parameters

Our optimization study suggests the following parameters for our baseline imaging monochromator design: 35.3 degrees asymmetry angle, approximately 1.8 mm first crystal thickness and 2.2 mm second crystal thickness, 10-50 m bending radius, 25 mm offset between white beam and monochromatic beam, ±35 degrees pitch angle range if allowed by the cooling arrangement.

For the motion control specifications, each crystal needs independent adjustments on the inboard and outboard sides of the crystal. The roll of both crystals, and pitch of the second crystal should be adjustable. In addition, the second crystal should be able to translate along the white-beam direction to allow for energy change with a fixed beam offset.

3.9.6. Performance

The photon flux and energy resolution in the experimental station F were simulated for various bending radii using the baseline crystal specification listed above. Figure 63 and Figure 64 show the photon flux results for 30 m, and 10 m bending radii, respectively.

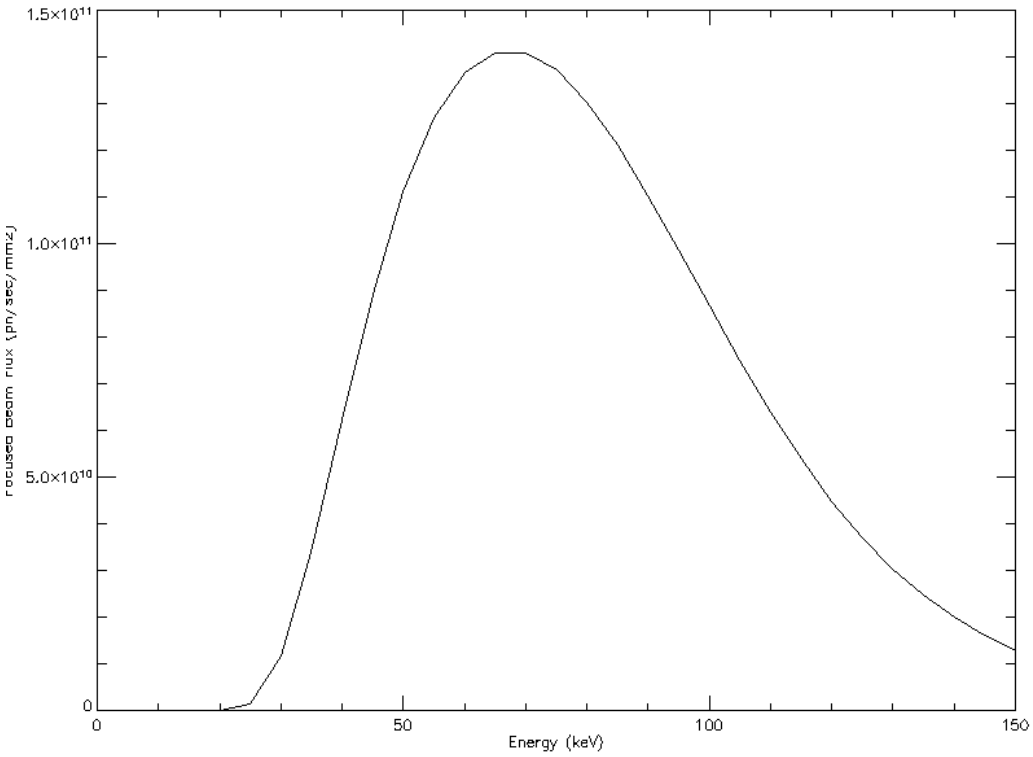

Figure 63 Performance of the imaging monochromator with 30 m bending radius

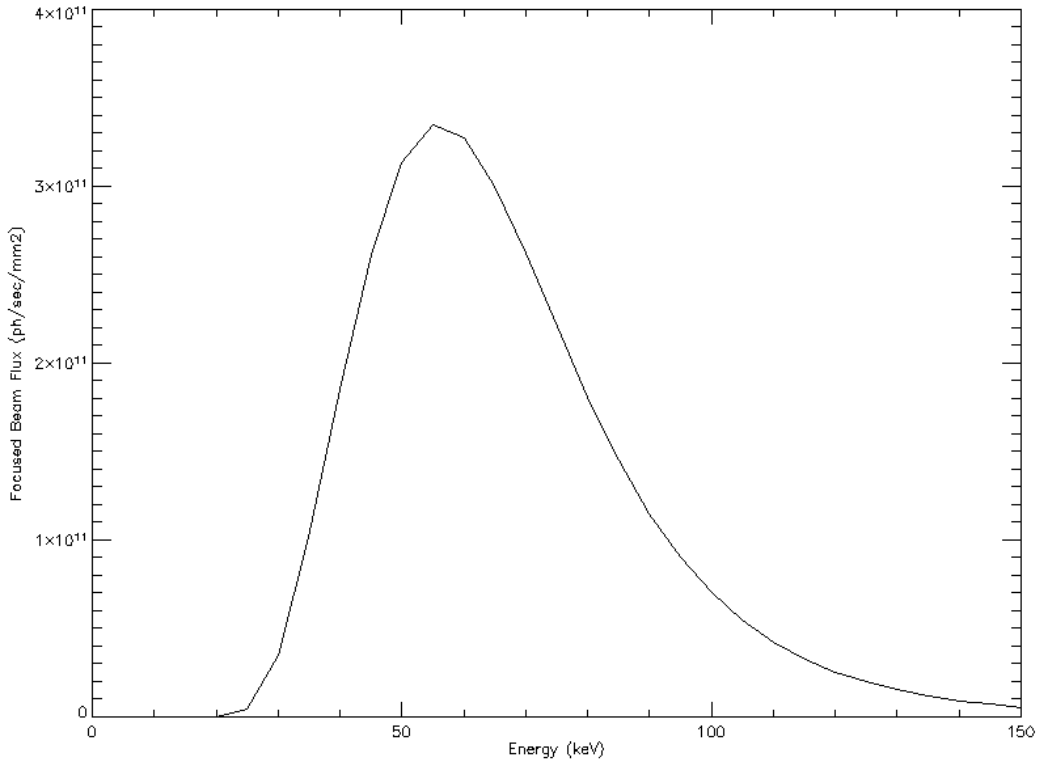

Figure 64 Performance of the imaging monochromator with 10 m bending radius

3.9.7. Comparison with similar monochromators

Table 11 shows parameters and cooling mechanisms for double bent-Laue monochromators at other facilities, along with data for the proposed HEX imaging monochromator. We note that JEEP and Shanghai monochromators were not designed exclusively for imaging, and thus have larger crystal-thickness of 4 mm, compared to imaging monochromators that use typically 1-2 mm thickness crystals.

	BMIT (Canada)	JEEP (Diamond)	UHX (Shanghai)	IMBL (Australia)	CAMD (USA)	HEX (NSLSII)
Asymmetry angle (deg.)	15	44	45	15	35.3	**35.3**
Reflection	111 & 220 (either/or)	111	111	111, 311 via rotation	111	**111, 220 & 311 via rotation**
Thickness (mm)	2.0	4.0	4.0	1.0	0.7	**1.8 1st crystal 2.2 2nd crystal**
Offset (mm)		50	50	20	8-25	**25**
Energy range (keV)	25-150	53-150	45-150	30-100	30-80	**30 – 150**
Cooling	Water, In-Ga trough	Cryogenic	Cryogenic	Water, In-Ga bath	Water, one-side	**Water, one-side**
Bender	2 Leaf Springs	2 Leaf Springs	2 Leaf Springs	2 Leaf Springs	2 Leaf Springs	**2 leaf springs**

Table 11 Parameters and cooling mechanisms by other facilities for double bent-Laue monochromators, along with that for the proposed HEX imaging monochromator

3.9.8. Specifications of the crystals

Figure 65 shows the design of the first crystal, with the active area being 1.8 mm thick. The design of the second crystal is similar with a 2.2 mm thick active area. The crystals should be cut from floatzone Si crystal. The surface should be perpendicular to the 100 direction. The sides should be perpendicular to 0-11 and 011 directions. Crystallographic designations (111, 100, 011, and 0-11) in the drawing are reflection directions, not lattice planes. For Laue crystal, the azimuthal direction is as important as the surface 100 direction. The thin (~2 mm) portion of the crystal should be polished on both sides.

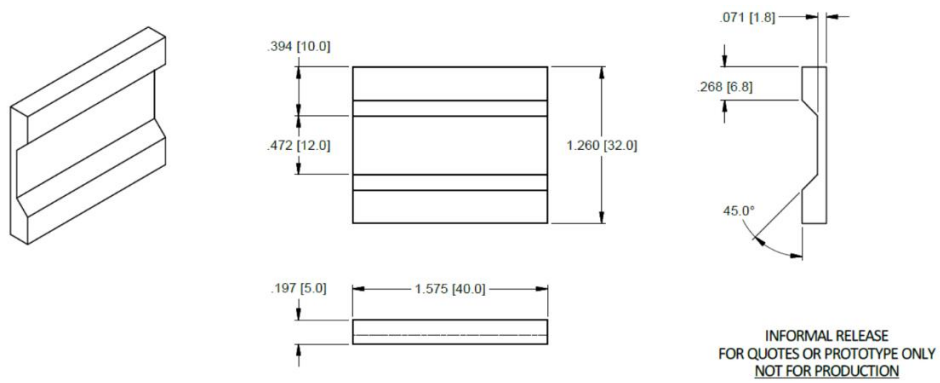

Figure 65 Design of the first crystal for imaging monochromator

3.9.9. Specifications of the imaging monochromator

The imaging monochromator consists of the following components: disaster mask, water-cooled removable first crystal, second crystal, Compton shield, removable beam-stop, and diagnostic shield. These components are housed in a vacuum chamber of about 1.5 m along the beam.

Along the beam path, the first component in the monochromator is a water-cooled Copper mask. The mask moves vertically +5 mm (up) to -40 mm with, together with the first crystal, to protect the bender of the first crystal when it is translated in and out of the white beam. The white beam on the mask can be normal-incidence.

The first crystal rotates via a cradle. The cradle should have an angular range of +/- 36 degrees rotation in plane with a resolution of 0.001 degree. The bending of the crystal (towards source) is adjustable via a two leaf-spring bender to a radius of 10 m – infinity. The two leaf springs are individually adjustable.

+5 mm (up) to -40 mm to move the first crystal out of the beam. The position of the first crystal with respect to the white, and monochromatic beams, is shown in Figure 66.

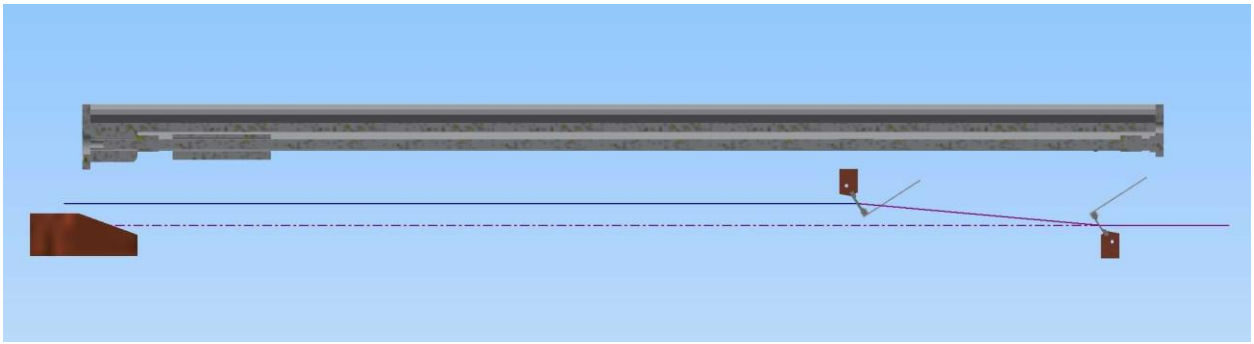

Figure 66 Simplified design layout of the imaging monochromator

The second crystal active area is 12 mm (V) by 40 mm (H) with 2.2 mm thickness. The bending radius (towards source) is the same as that of first crystal, with a range of 10 m to infinity. The second crystal cradle should have a range of +- 36 degrees rotation in plane with 0.0001 deg. resolution. In addition to in-place rotation, the second crystal should have a +/- 2 deg roll adjustment with 0.001 deg. resolution. The roll adjustment allows accurate adjustment of the horizontal position of the monochromatic beam. The 2 leaf-spring bender for the second crystal is of the same design as that of the first crystal. Distance to from the second crystal to the first crystal is 90 mm – 1 m (along beam direction). The center of the

second crystal should be vertically offset by 25 mm from the center of the white beam. Due to the small minimum distance (90 mm) between the crystals, and the large (6 mm) vertical beam size, a beam-stop cannot be positioned between the two crystals. Thus the design of the second crystal bender should ensure that the bender will not be in the white-beam at all possible rotation angles.

A water-cooled copper Compton shielding, of approximately 3 mm thickness, should be designed to surround the first crystal. The purpose of the shielding is to absorb the Compton scattered x-rays from first crystal, thus minimizing temperature variation on the second crystal and the vacuum chamber.

A removable beam stop will be designed using water cooled copper block. The beam-stop shold be coated with phosphor. A visible light camera should view the beam stop through a quartz window on the vacuum chamber. The beam stop should be at about 1.2 m (z, along beam direction) from first crystal. A vertical motorized stage of +5 mm to -40 mm range should be designed to move the beam stop in the white beam (for monochromator operation) and out of the white beam (for white-beam operation).

A diagnostic flag is provided near the exit port of the vacuum vessel. It will have a 50 mm x 50 mm area to capture both transmitted and diffracted beams from 2nd crystal. A 100 mm vertical motion will allow us to view the transmitted beam from the second crystal at different x-ray energies, and to retract the diagnostic flag from the monochromatic beam. The diagnostic flag should be positioned so that it can not be moved into the white beam.

Figure 67 shows the configuration of the crystal when 111 reflection, with asymmetry angle (χ) of 35.3 degrees, is employed. It is seen that the crystal surface must tilt relative to vertical direction by an angle $\chi - \theta_B$, where θ_B is the Bragg angle. This figure also shows that the second crystal must be at a distance of $G/\tan(2\,\theta_B)$ from the first crystal to maintain a constant offset (G) of 25 mm.

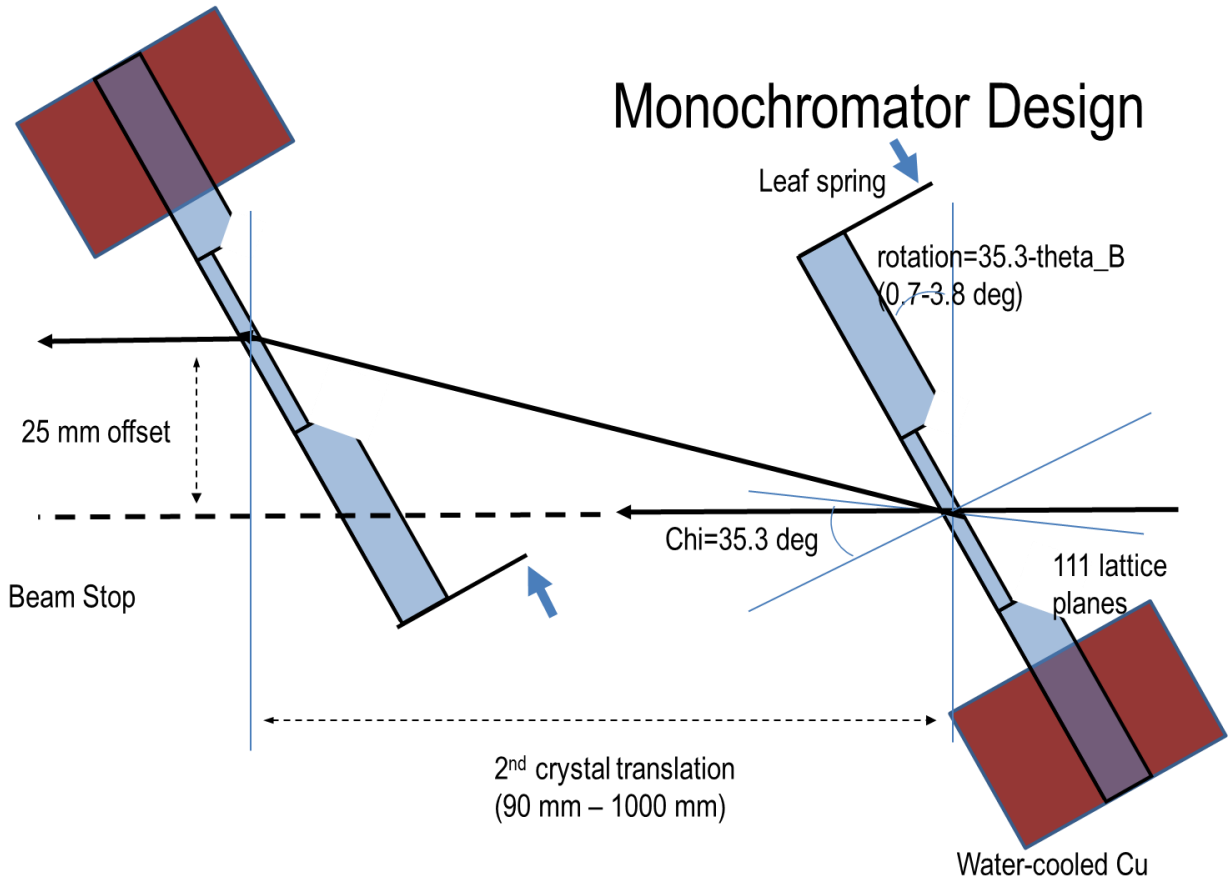

Figure 67 Considerations for tilt of the crystal surface and the second crystal distance

Reflection/Energy	Asymmetry angle (degrees)	Bragg angle (degrees)	Tilt of crystal surface (degrees)	Distance of second crystal (mm)
111 at 30 keV	35.3	3.78	31.5	188
111 at 150 keV	35.3	0.75	34.5	948
220 at 30 keV	0	6.17	-6.17	114
220 at 150 keV	0	1.23	-1.23	580
311 at 30 keV	64.8	7.24	57.6	97
311 at 150 keV	64.8	1.44	63.4	495

Table 12 The calculated crystal surface tilt angle and second crystal distance for 111, 220 and 311 reflections, at 30 and 150 keV x-ray energies

It is seen that the crystal tilt range must be from -6.2 degrees to 63.4 degrees, with a range of 69.6 degrees. Therefore, we specify the crystals to have a +-36 degrees motion.
The minimum range for the second crystal distance is 97 mm to 948 mm to cover 30-150 keV for all three reflections. Therefore, we specify a distance of 90 mm to 1 m.

Based on the above discussions, we summarize the specifications of the imaging monochromator in Table 13.

Component	Specification	Notes
Mask	A water-cooled Copper mask should move +5 mm (up) to -40 mm with the first crystal, to protect the first crystal when it is translated in and out of the white beam. The white beam on the mask can be normal-incidence.	Water-cooling
First Crystal	12 mm (V) by 40 mm (H), 1.8 mm thick +- 36 deg. rotation in plane, 0.001 deg. resolution Minimum crystal surface angle range: -6.2 degrees to 63.4 degrees Bending radius (towards source) 10 m – infinity 2 leaf spring bender +5 mm (up) to -40 mm to move the first crystal out of the beam	Water-cooling required Position sensor required for EPS
Second crystal	12 mm (V) by 40 mm (H), 2.2 mm thick Bending radius (towards source) 10 m – infinity +- 36 deg. rotation in plane, 0.0001 deg. resolution Minimum crystal surface angle range: -6.2 degrees to 63.4 degrees +- 2 deg. tilt, 0.001 deg. resolution 2 leaf spring bender Distance to first crystal: 90 mm – 1 m z translation along beam 25 mm Y offset from first crystal, bender should not be in the white-beam.	Water-cooling not required
Compton scatter shield	Water-cooled copper shielding around first crystal, approximately 3 mm thick	Water-cooling
Beam stop	Water cooled copper block, normal incidence OK, coated with phosphor located at 1.2 m (z) from first crystal +5 mm (up) to -40 mm to move the beam stop out of beam	Water-cooling Position sensor required for EPS
Vacuum vessel and support	0.6 m width x 1.5 m length 2 Quartz view ports of 6 inch diameter	
Diagnostic flag	Near the exit port of vacuum vessel, 50 mm x 50 mm area to capture both transmitted and diffracted beams from 2nd crystal, 100 mm vertical motion to retract from beam	

Table 13 Specifications for the imaging monochromator

3.10. Diagnostics

The purpose of diagnostics is to monitor the condition of the white- and monochromatic-beams in terms of time and position stability, uniformity, and flux. The center branch beam is large with a maximum angular size being 0.2 x 1.0 $mrad^2$ (V x H), thus the white beam is expected to be stable (relative to the beam size along the beamline) and easy to monitor. The monochromatic beam, being created with double bent-Laue monochromator, is potentially subject to errors due to thermal drift, poor uniformity due to mismatch between the bending radius of the two crystals, and relative twist between the two crystals, (twist being a small difference in tilt / pitch angle between the inboard and outboard portion of the crystal), and the absolute twist of just the first crystal (resulting in energy difference between inboard and outboard portions of the beam). It is thus essential to design sufficient diagnostics to monitor and measure the monochromatic beam both at the exit of the monochromator chamber and at the F end-station. Viewing screens will have graticules or cross-hairs that can be surveyed to the beam centerline prior to use, wherever possible. The HEX beam diagnostics are designed with these considerations in mind. Figure 68 shows the layout of diagnostics inside the FOE (initial scope only).

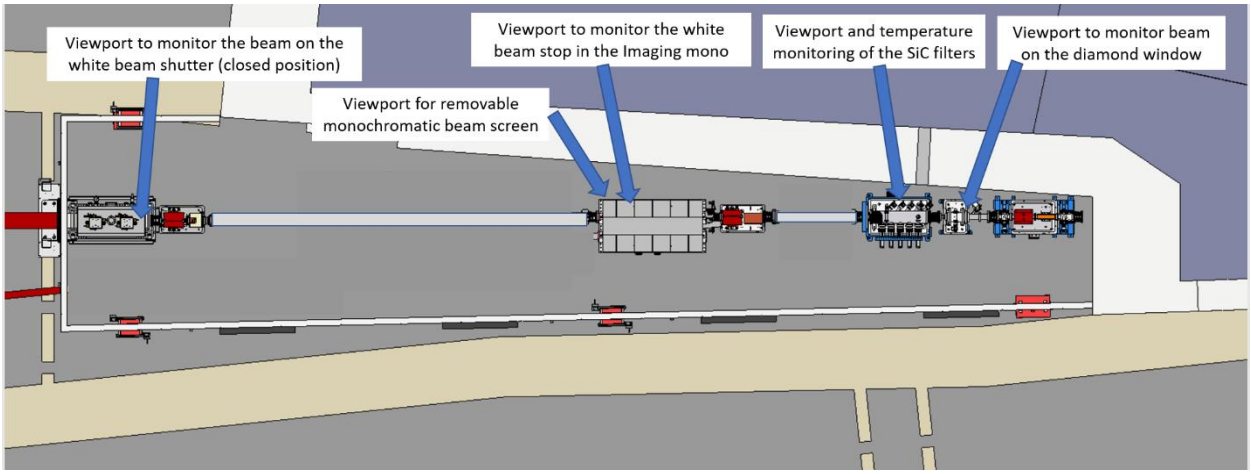

Figure 68 Initial scope diagnostics in the FOE

3.10.1. Diagnostics for the First Diamond Filter

The first diamond filter assembly is exposed to the white-beams of all three branches. The undoped CVD diamond, being 2 mm thick, emits visible light fluorescence that can be imaged with a CCD camera. See Figure 69 below for an example of such a system (the camera is orientated vertically at the right, and encased in shielding, a mirror below the camera prevents scattered x-rays from damaging the camera). The camera image allows visualization of the size and uniformity of white-beam, and the integrity of the diamond filter. The filter chamber should be designed to have a quartz window large enough to allow the camera to see diamond filters for all three branches. Optical filters will be included before the camera to attenuate the visible signal and get better sensitivity to intensity variations. The design of the water-cooling system should incorporate thermocouples at the water inlet and outlet of the filter. Monitoring the temperature difference between the inlet and outlet can further assure the integrity of the diamond filter. The vacuum pressure in this section will be monitored with the EPS, since a pressure spike also would indicate a possible filter failure.

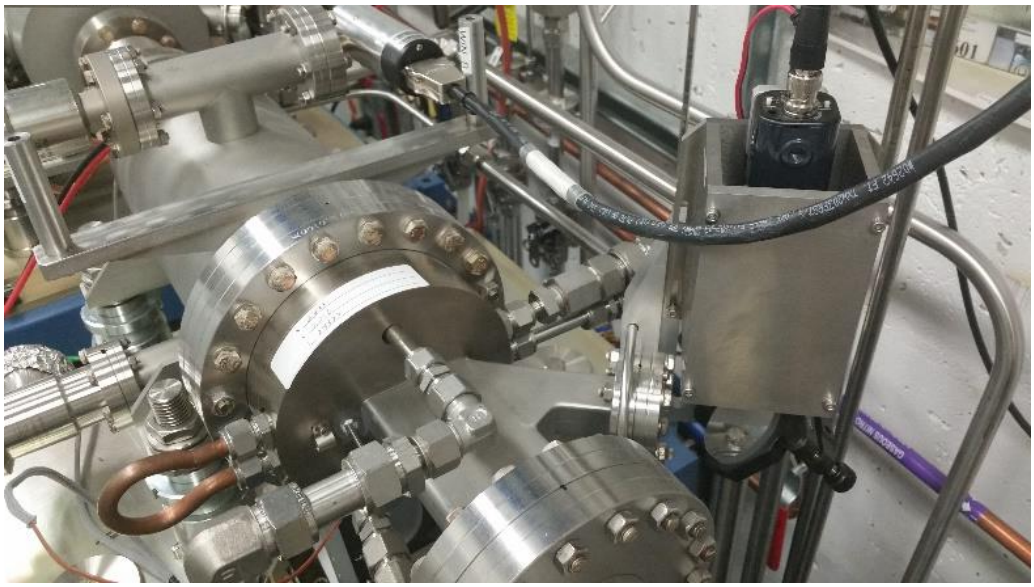

Figure 69 Camera for viewing the diamond window

3.10.2. Fixed Silicon Carbide Filter

The fixed SiC filter for the center branch is exposed to the white-beams of the center branch and is expected to reach a temperature of about 600 degrees C when the front-end aperture is fully open. The design of the water-cooling system for the SiC filter will therefore incorporate redundant thermocouples at the inlet and outlet. Monitoring the temperature difference between the thermocouples allows the assessment of the integrity of the SiC filter. Similar to the first diamond filter, a quartz viewport allows visualization of the SiC filter to check its integrity. The SiC should not be coated with phosphor due to concerns about the phosphor introducing artifacts and phase-contrast to the x-ray beam. The SiC should be single crystal material for the same reasons.
All windows and filters should be optical grade (material will be tested at a synchrotron to select the best material to avoid defects that can introduce artifacts or phase contrast).

3.10.3. White-Beam Stop in the Imaging Monochromator

The imaging monochromator contains a removable beam stop, at about 1.2 m downstream of the first crystal, using water-cooled copper block. The beam-stop will be coated with a durable high-resolution phosphor able to handle the power (e.g. plasma sprayed ceramic coating) or this could be covered with a thin YAG crystal if this is shown to be feasible at the detailed design stage, to allow high-resolution visualization of the white-beam. As the fluorescence from the thick 2 mm diamond filter is expected to be blurry due to the depth effect, the phosphor on the white-beam stop offers the first (and probably the only) high-quality image of the white beam in the FOE. The image allows assessment of the uniformity and stability (both spatial and temporal) of the white-beam. A visible light camera with adjustable filtering should view the beam stop through a quartz window on the imaging monochromator vacuum chamber.
Quantitative measurements of the beam profile will be performed with slits in the FOE to perform a scan, and an ion chamber to measure the beam intensity. This gives an excellent intensity profile of the full beam.

3.10.4. Diagnostic Flag for the Monochromatic Beam in the Imaging Monochromator

A Diagnostic flag is provided near the exit port of the monochromator vacuum vessel. It will have a 50 mm x 50 mm area to capture both the transmitted and diffracted beams from the second crystal. A 150 mm vertical motion will allow us to view the transmitted beam from the second crystal at different x-ray energies, and to retract the diagnostic flag from the monochromatic beam. The motion range of the diagnostic flag should assure that it cannot be accidentally moved into the white beam.
The diagnostic flag at the downstream end of the monochromator chamber facilitates alignment of the tilt angles and bending of both crystals in the following way:

- With both crystals un-bent, the diagnostic flag is driven into the position to intercept reflected beam (e.g. at 50 keV) from the first crystal. The first crystal's tilt angle is adjusted so that the reflected beam is centered on the flag.
- The diagnostic flag is lowered to intercept the second-crystal-reflected beam. The second crystal tilt angle is adjusted so that the monochromatic beam reflected by the second crystal is visualized.
- The first crystal is then bent to a nominal bending radius of 30 m. With the second crystal still flat, the tilt angle of the second crystal is adjusted. The adjustment will result in a left-and-right motion of the monochromatic beam center unless there is no twist (resulting from non-uniform bending) of the first crystal. The differential bending of the two leaf springs is then adjusted to minimize the left-and-right motion of the beam position.
- The second crystal bending is adjusted to a nominal radius of 30 m. The step above is then repeated for the differential bending of the second crystal to minimize the twist of the second crystal.
- In the previous step, if the bending radius of the second crystal does not match that of the first crystal, the monochromatic beam on the diagnostic flag will move up-and-down. If needed, the bending radius of the second crystal is adjusted to minimize the up-and-down motion of the reflected beam.

We note that at 150keV with Si 111 reflection, the separation between the second crystal transmitted and reflected beam is the smallest. In this case, by using a flag-to-first crystal distance of 1250mm, the transmitted beam is 33mm above the white beam. This is sufficient separation with the reflected beam at 25 mm up from the white beam, thus allowing visualization of both the transmitted beam and reflected beam simultaneously. At 30 keV (Si 111), the transmitted beam is 165 mm up from the white beam. Thus we specify a vertical motion range of 150 mm for the diagnostic flag to capture the transmitted beam at low x-ray energies.

3.10.5. Diagnostic on the Shutter in FOE

The shutter at the downstream end of the FOE intercepts both the white- and monochromatic- beams. It is desirable to coat the water-cooled copper block of the photon shutter with phosphor to allow visualization of these beams on the shutter, through a quartz window on the vacuum chamber. This diagnostic can detect abnormalities in the horizontal position of the monochromatic beam. The roll angle of the second crystal will be adjusted to center the monochromatic beam horizontally on the shutter. The copper block can have a machined graticule (prior to coating) with lines at a known pitch horizontally and vertically (vertically spaced to account for the incidence angle) which would provide further absolute information.

3.10.6. Diagnostic Unit for hutches E and F

A diagnostic unit will be constructed for use in hutches E or F. The unit consists of a water-cooled YAG crystal of approximately 30 mm (height) by 120 mm (width) with 0.2 mm thickness. and a visible light CCD camera with zoom lens. The diagnostic unit will be used in hutch E (at the upstream end of the hutch) and/or in hutch F (at the sample position) to refine the alignment of the monochromator according to the procedures outlined above. The unit can also be used to visualize the white-beam (when it is adequately filtered).

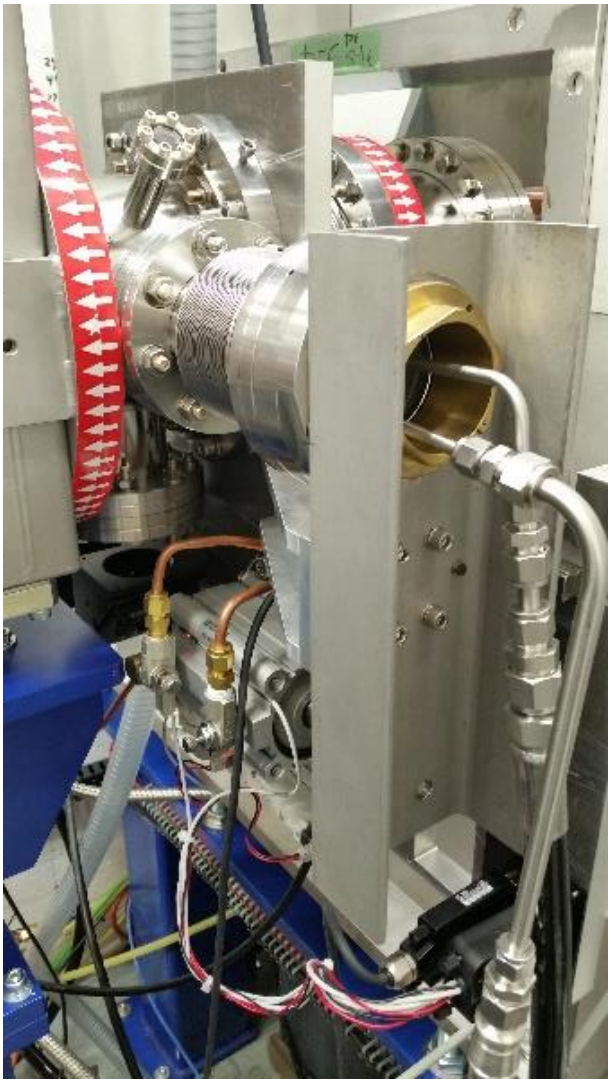

Figure 70 White Beam Viewing System

A picture of a similar diagnostic unit, built in-house at BNL, is used at the ISS beamline is shown in Figure 70. However, these diagnostics, comprising a combined YAG-photodiode-filter assembly, are also available off the shelf (for mono beam), from a number of commercial suppliers. Again, surveyed graticules or cross-hairs on the screen will be used for easy reproduction of the beam position.

3.10.7. Segmented Ion Chamber

A horizontally segmented ion chamber of 0-25 mm (V) x 0-120 mm (H) sensitive area, with 60 mm sensitive depth will be installed on the beam conditioning table in the F hutch. The pitch of each channel is 12.5 mm. The ion chamber can be used to measure both the filtered white beam (for EDXD experiment) and the monochromatic beam (for ADXD and imaging).

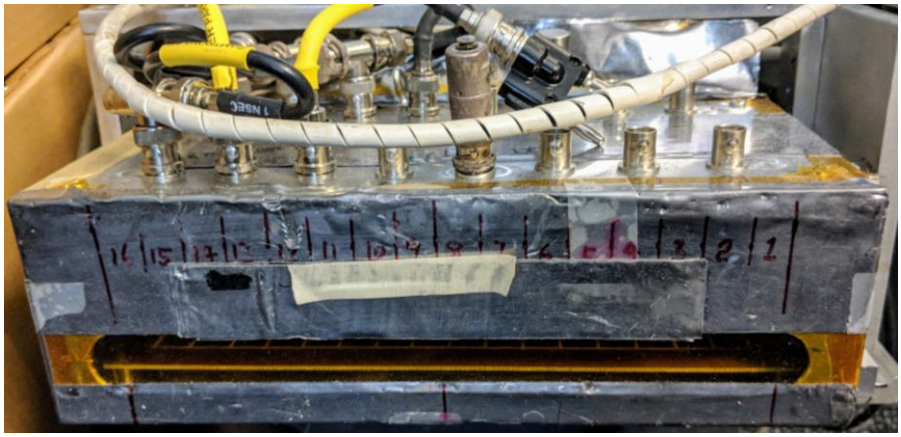

Figure 71 Horizontally segmented ion chamber

A picture of a horizontally-segmented ion chamber used at the imaging beamline X15A of the NSLS is shown in Figure 71. This ion chamber can be re-purposed for measuring and diagnosing monochromatic and white beam at the HEX hutch F.

The ion chamber will be used for the following purposes:

- Alignment of the monochromator: The alignment procedure closely resembles that described previously. Instead of observing the motion of the beam as the second crystal tilt is adjusted, rocking curves of each of the channels in the ion chamber will be recorded by scanning the tilt of the second crystal. By fitting the centroid of the rocking curves, a quantitative and high-precision measurement of the twists in the first- and second- crystals can be obtained. The bending of the crystals can then be refined to minimize the twist.
- Alignment and calibration of the beam-defining slits in the F hutch (for EDXD and ADXD)
- Measurement of the absolute intensity of the monochromatic beam

3.10.8. High-resolution Imaging Detector

Camera systems with different fields of view and resolution will be purchased: the CCD-based camera will be used for high spatial but lower temporal resolution work, and a CMOS-based camera will be used for very high frame rate data acquisition. The imaging detectors can be used as a diagnostic tool for monochromatic beam to assess the temporal stability, and uniformity of the beam. In addition, it can be used to detect small defects in the diamond filter, diamond windows, and SiC filters. We note that, with adequate filtering, the imaging detector can also be used to visualize the white beam at high resolution.

3.11. Vacuum System

HEX is a hard x-ray beamline and will operate in the 20-200 keV range. The average vacuum pressure needed to prevent any measurable x-ray absorption from residual gas is of less concern than for x-rays of lower energy and is eliminated for HEX providing it has an average pressure of $7e^{-6}$ Torr or lower. However, part of the beamline within the First Optics Enclosure (FOE) is windowless and therefore UHV vacuum levels need to be maintained in those sections of the FOE to preserve vacuum in the Front End and Storage Ring. Furthermore, a sufficiently low operational vacuum level needs to be met over the entire beamline to preserve cold cathode gauge and ion pump life and minimize unstable pressure excursions that could close valves and increase maintenance intervals on such equipment. In short, lowering the design vacuum level will help prevent unwanted vacuum intervention.

3.11.1. Overview of Vacuum Requirements

Table 14 below details the standard vacuum components used at NSLS-II:

SUPPLIER	PN	DESCRIPTION
MKS/HPS	937B-BH-CLCLCT-NA	Series 937B controller, Two CCG(CL), Two CEP, NSLS-II Conn
	103170044SH	Series 317 Convention Pirani, 250°C Bakeable, 2 3/4" CF, Baked
	104220036	Series 422, Cold Cathode, 250°C Operating, 2 3/4" CF, Baked
GAMMA	MPC-2-US110-232-HVE-TSPBD	DIGITEL MPC with:
	Part: 360353	HV Supply One: 500-POS-7KV-SC2
		HV Supply Two: 500-POS-7KV-SC2
		Input Voltage: 110-volt, US
		Communications: RS232 Port
		High Voltage Enable: Installed
		TSP/NEG: TSP Upgrade Option
MDC	420033	UHV Burst Disk, 2 ¾" flange, ASME UD certified
VAT		Series 48 All Metal Gate Valve, white/pink beam
VAT		Series 10 UHV Gate Valve, monochromatic beam
VAT	54136-GE02	DN63 Right Angle Valve
KEY or equivalent	BAV-100-F	All metal bakeable valve

Table 14. List of Standard Vacuum Equipment

A complete list of the general vacuum requirements for the HEX beamline is provided in NSLSII-PSD-SPC-001 (Standard Technical Specifications for NSLSII Beamline Components), however the motivation on a select list of these requirements is provided below for clarity of design.

3.11.1.1. Valves

All gate valves that have white or pink beam passing through their aperture are to be all metal series 48 VAT valves. This is to minimize radiation damage (chronic or acute) which could result in valve elastomer seal failure and also minimize the release of unwanted seal material into the vacuum. Gate valves that have monochromatic beam passing through them shall be VAT series 10. All gate valves shall have a

second set of position indicators to accommodate special cases of interface to the EPS (Equipment Protection System).

All manual DN40 right angle valves shall seal using a “soft on hard” copper gasket. This valve has been found to be more reliable in environments where foreign matter can enter the valve. All manual DN 63 right angle valves shall be of the VAT series 54 design.

3.11.1.2. Sputter Ion Pumps

All sputter ion pumps will be noble diode design (one titanium and one tantalum cathode). This will mitigate noble gas instability as a result of leaks in any form, virtual or real. While care is taken to eliminate external leaks in the design of seals and care of assembly, they can and do happen and are well documented throughout the NSLSII complex. Complex internal components can also be a source of virtual leaks. Leaks give rise to argon instability and can occur in pumps removed some distance from the leak source. This is a result of argon enrichment, a phenomenon where pumps further from the leak see a higher proportion of argon in distributed pumping systems and are first to become unstable. This has been observed at NSLS-II beamlines. Due to the unpredictable location and nature of argon instability, all beamline pumps must be of the Noble Diode or Differential-Ion design. This comes at a slightly higher cost and reduction in pumping speed which needs to be accounted for.

3.11.1.3. Gauges

The CCG gauge is susceptible to photoelectrons from scattered light which results in pressure excursions if not oriented in a manner to shield the gauge. Gauges need to be mounted out of line of sight of the x-ray beam, and in a manner to minimize this phenomenon. As a minimum the gauge needs to be mounted on an elbow and in a location that has minimal scatter.

3.11.2. Pressure Calculations

Calculating the outgassing rate of complex systems is difficult, both static and dynamic. Both the material as well as the configuration determine the total outgassing behavior. The quantity of scattered light resulting in PSD (photon stimulated desorption) is difficult to predict and has been found in many cases to raise the pressure a factor of 100x over conditions without light. The expected PSD needs to be accounted for in the vacuum design since the time scales to condition a surface and reduce PSD are significant. Empirical data is the best predictor of static and dynamic vacuum performance, and the performance of similar systems here at NSLSII and elsewhere (Supplier and Facility experience) will be used help to determine if sufficient pumping speed is provided in the design.

Of particular note when calculating pressure is selecting the correct ion pump speed. A pump’s peak speed is always attained at a high pressure ~>e^{-6} and falls to zero at the pumps base pressure ~<e^{-10}. This is commonly referred to as the speed curve of the pump and is a result of the space charge characteristics of the Penning cell discharge. Additionally, the effective speed of the ion pump varies for all gases and is lower for hydrogen, which is the dominant residual gas in UHV systems. A pump is always advertised at the peak speed for nitrogen, but more important is the speed of the pump for the gas it will be pumping and at the pressure it will be operating at. These characteristics are often overlooked.

3.11.3. In-Vacuum Materials

The allowable materials for use in vacuum at NSLS-II are discussed in LT-ENG-RSI-SR-VA-002 (Design and Fabrication of Components for NSLS-II UHV Systems). However, of particular concern is the use of Kapton materials that contain an FEP binder. This fluoropolymer breaks down in a radiation environment and generates CF3 gas. This gas bubbles out from under the Kapton and causes large pressure spikes. It is also an unwanted residual near optical surfaces causing long term degradation of the reflectivity. The cable and wire selected should be rad hard where possible and shielded and routed in a manner to reduce exposure to radiation. Allectra provides a comprehensive selection of radiation hard Kapton insulated vacuum cable.

3.11.4. Vacuum Safety

BNL follows guidelines established for the DOE complex regarding pressure vessels and vacuum systems (Vacuum Systems Consensus Guideline for Department of Energy Accelerator Laboratories, September 9, 2008). The laboratory provides guidelines and requirements for low-pressure-differential, low volume systems as well as for higher risk systems with more constraints. Vacuum Hazards are specifically addressed in the NSLS-II Safety Assessment Document (SAD), where the pertinent requirements are referenced. Vacuum sections that have the potential for overpressure require an AMSE UD stamped burst disk (MDC PN 420033). Glass viewports in exposed locations should be fitted with a clear plastic cover to reduce the potential of external damage.

3.11.5. FOE Vacuum

The FOE vacuum contains similar components to existing NSLS-II beamlines and as a result, the vacuum behavior is well understood:

1. DP (Differential pump). This section is defined by the fixed mask and Bremsstrahlung Collimator. The fixed mask provides a significant conductance limitation and resultant pressure differential. This limits the movement of gas from downstream to upstream and preserves UHV within the FE and storage ring straight section. A permanently mounted QRGA (quadrupole residual gas analyzer) will be located in the Front End, this will monitor the vacuum quality in the Front end and in the differential pump region extending to the diamond windows. The section will utilize two ion pumps as well as two CCG gauges (upstream and downstream of the DP) and a single Pirani gauge.
2. Filtering Module. This section contains fixed diamond filter and two windows followed by Silicon Carbide (SiC) filter elements. The SiC filters are inserted into the beam with external actuators preserving UHV. The design closely follows that of the existing filter module at XPD/PDF with good vacuum performance. An ion pump is installed on the window module and a large ion pump is installed on the filter Module. The vacuum section contains a CCG/Pirani set.
3. Side Bounce Monochromator (out of scope). This section contains the future SBM. There will be a temporary white beam transport pipe with ion pump in place of the SBM for initial construction.
4. Imaging Monochromator and white beam slit. The Imaging Monochromator will be pumped by an ion pump. In addition to the ion pump, a turbomolecular pump will also be fitted since the potential outgassing of the monochromator is high and venting is possible during commissioning

and operation. The vacuum section will contain a single Pirani and one CCG for the monochrometer and one CCG for the temporary white beam pipe.

5. Focusing Monochrometer and Vertical-Focusing Mirrors. The monochrometer chamber is pumped with a large ion pump. The ion pump will have an additional 8" flange in the body. This chamber will be equipped with larger DN63 roughing valve.
6. White beam shutter. The white beam shutter section will be pumped with ion pumps.

3.11.6. White Beam Branch

The initial scope of the central White Beam Branch will include white beam transport extending through Hutches C, D, E and ending in Hutch F. The transport pipe will be pumped and maintained by ion pumps and monitored with CCG gauges. Where the pipe is separated by valves, each section will have a Pirani and CCG gauge. Where the pipe section extends more than 20 meters, a CCG gauge will be located near each end.

The objective specification of the transport pipe pumping is to be able to pump from atmospheric pressure and reach a pressure sufficient to start the ion pumps in under 10 hours and reach a vacuum level suitable for ion pump longevity (e^{-7} Torr) after 100 hours under vacuum. Given the relatively large diameter (> 20 *cm*), shielding requirements and conductance of the transport pipe, there will be no ion pumps external to hutch enclosures and the pipe will extend from the E hutch until it reenters the HEX Satellite building endstation (F) hutch, a span of ~ 33 meters. Furthermore, the vacuum will benefit from large ion pump(s) in the 500 *l/s* range. The transport pipe will have roughing valves and ion pumps at each end within the E and F hutches. To make this possible, the transport pipe must be critically clean for UHV. This will minimize water absorption and retention in an unbaked condition and allow ion pumps to be started in a reasonable time. An analysis to check the feasibility of this design using conservative values for outgassing of unbaked stainless steel was undertaken.

Of particular concern is the evacuation time when dominated by outgassing at pressures of ~10 Torr and lower. The dominant residual gas is water vapor and the outgassing a first order surface desorption, expressed simply as:

$$Q = Q_0 \, e^{(\frac{-t}{\tau})} \qquad \textit{Equation 6}$$

For a clean stainless-steel surface, this normally follows a slope of (-1) when plotted on log-log paper.

Throughout the literature, stainless steel is shown to have a unit outgassing rate of ~e^{-10} torr l/s cm^2 after 24 hours under vacuum. Previous work also found that any performance gain from electropolished surface was minimal, but a benefit from vacuum firing exists (see below, Figure 72. Outgassing Rates for Stainless Steel).

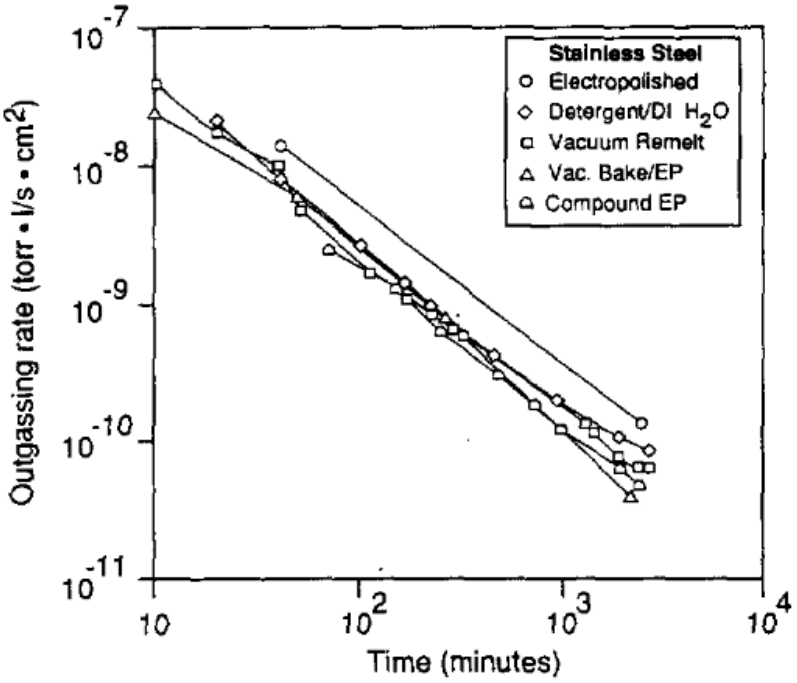

Figure 72. Outgassing Rates for Stainless Steel

It should be noted that after > 1000 minutes, some flattening occurs with the exception of the pipes that were vacuum fired (600-900 °C). The improved performance on vacuum fired (450C, 48 hour) material was also observed on the stainless-steel Half-Cell storage ring chambers of the Spallation Neutron Source, see Figure 73.

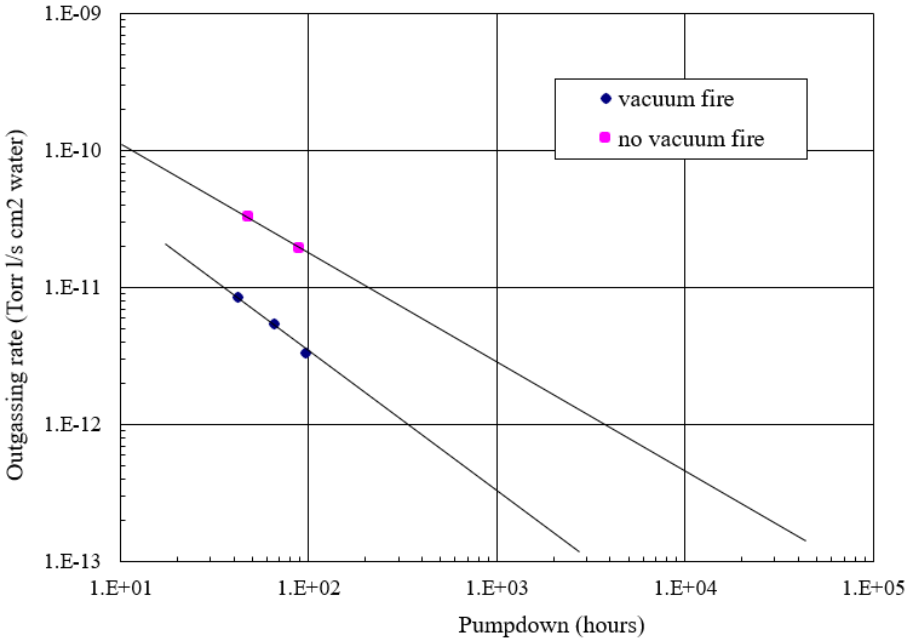

Figure 73. Outgassing of SNS vacuum chambers with and without 450C vacuum degas.

Case 1: Time to evacuate to suitable vacuum to turn on ion pumps and allow beam.

It is expected with a turbocart located at each end, the time to evacuate the bulk gas in the beampipe and reach below one Torr will be roughly one hour.

The pressure at the pump is simply:

$$P_p = \frac{Q}{S_p} \qquad \textit{Equation 7}$$

Where:

$S_p = 5\ l/s$ effective speed of turbopump cart using 1 meter long x 40 mm diameter hose

$q = 5e^{-10}$ *Torr l/s cm²* unit outgassing rate at 10 hours

$D_p = 20.3\ cm$ diameter of beampipe

lp = 1650 *cm* length of half the beampipe

$A_s = 1x10^5\ cm^2$ surface area of half the beampipe

Following (Equation 7), the pressure at the turbopump cart is:

~$5e^{-5}$ Torr l/s ÷ 5 *l/s* or $1e^{-5}$ Torr ($1.3e^{-5}$ mbar). This pressure is sufficiently low to start the ion pump(s).

Case 2. Pressure ~100 hours, after starting ion pumps.

With the transport pipe having pumps of equal speed at both ends, the pressure profile will be symmetrical. The pressure will be a maximum halfway between the two and the gas flow at this point will be zero. Therefore, the analysis simplifies to one finding the pressure profile in a long uniformly outgassing tube pumped at one end. A set of solved equations for this condition is provided by K. Welch.[2] The following equations are only valid for molecular flow conditions (< e^{-7} Torr) in the case of the pipe transport pipe and with the pipe falling well within the solution of a "long tube" (*l /D >10x*), where the conductance is simplified to:

$$C = \frac{kD^3}{l} \qquad \textit{Equation 8}$$

where *k* is dependent on molecular weight and temperature, in this case,

$$k_{water} = 12.1\sqrt{\frac{28.8}{18}}\ l/\sec cm^2 \qquad \textit{Equation 9}$$

The pressure at any given point (x) along the length (l) is:

$$Px = P_p + \frac{\pi q_e}{2kD^2}\ (2xl - x^2) \qquad \textit{Equation 10}$$

and by integrating Equation 10, the average pressure in the pipe is:

$$P_{avg} = P_p + \frac{2}{3}\left[\frac{\pi q l^2}{2kD^2}\right] \qquad \textit{Equation 11}$$

The following family of curves in Figure 74 show the 20cm beampipe is not "conductance limited" and in fact has a higher average pressure than the smaller 10cm diameter pipe given the same pump speed (Figure 75). In this case, higher pump speed is required to offset the lower total outgassing of the 10cm pipe.

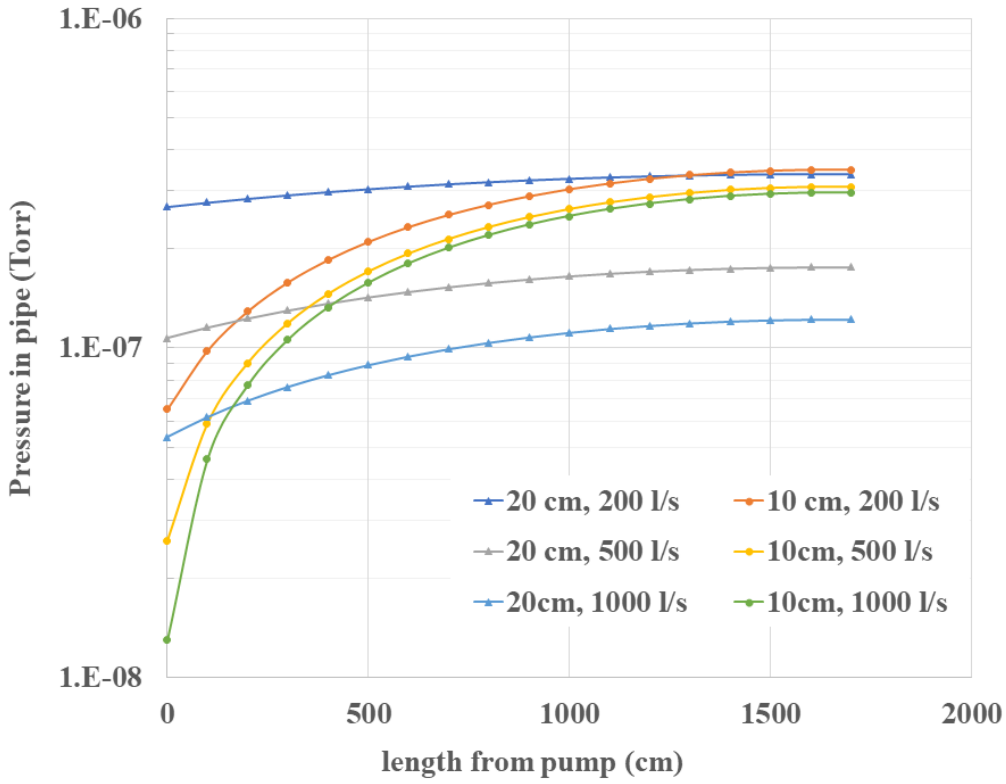

Figure 74. Pressure profiles illustrating effect of pipe conductance and pump speed.

The Figure 75 below shows how the higher conductance 20cm pipe benefits from increasing pump speed to reduce the average pressure over the smaller pipe with lower conductance.

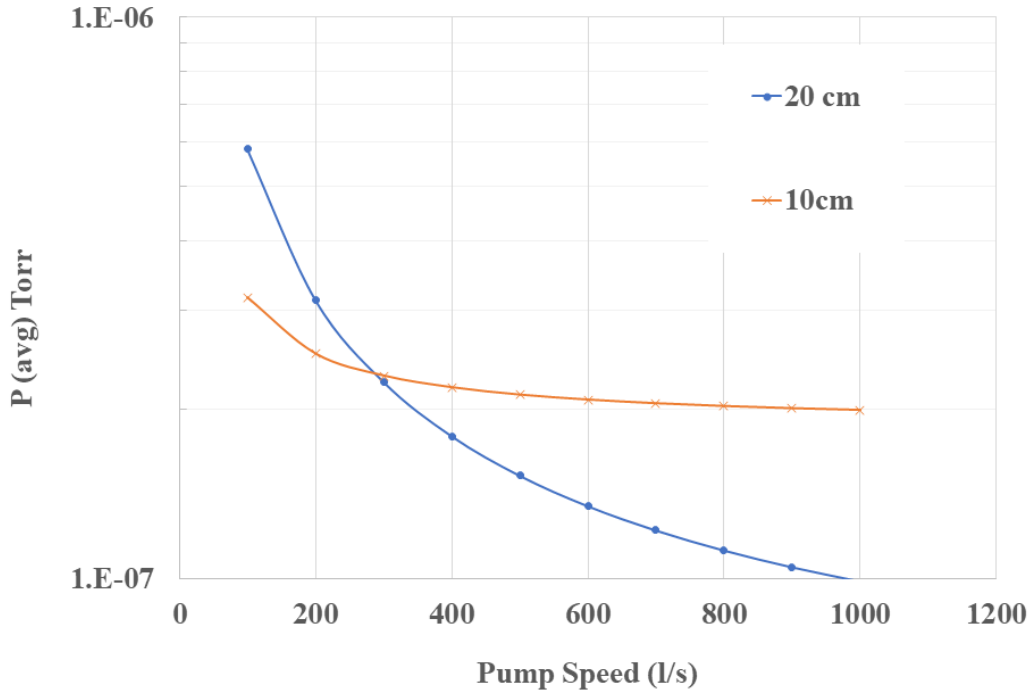

Figure 75. Average pressure as a function of pump speed for the pipe diameters 20cm and 10 cm.

With this in mind, the largest reasonable pump size is selected based on the space envelope and cost:

$S_p = 200\ l/s$ effective speed of 500 *l/s* ion pump

q = 1e^{-10} *Torr l/s cm*^{2} unit outgassing rate at 100 hours

Following (Equation 7), the pressure at the pump is 2.5*e*-7 Torr (3.3e-7 mbar).

Following (Equation 10), the maximum pressure at a point equidistant between pumps (*x=l*) is found to be ~3.4e^{-7} Torr (4.5e^{-7} mbar).

Following (Equation 11), the average pressure in the pipe after 10 hours on the ion pumps is 3.1e^{-7}.

This is in general agreement with computer generated *Monte-Carlo* simulations, which show slightly higher (~2x) values than the generalized solution. shown below (Figure 76):

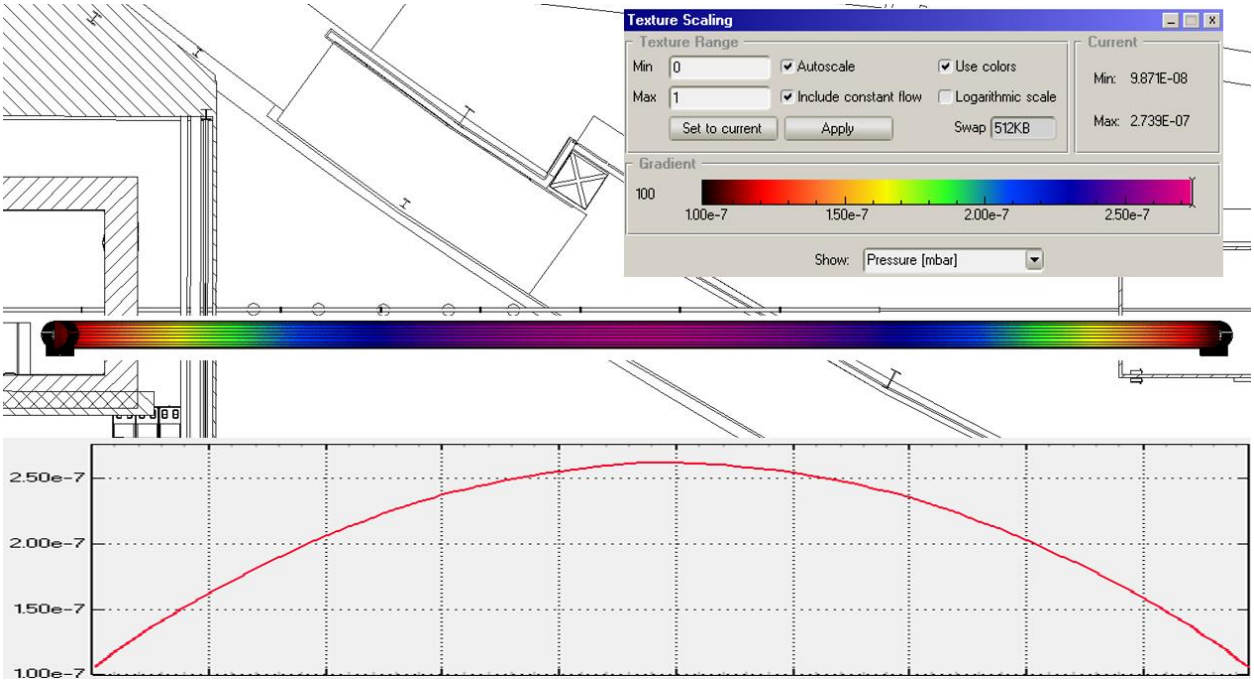

Figure 76. Pressure profile along the 33 m transport pipe after 100 hours under ion pump vacuum.

After >100 hours, the ion pump pressure will fall below ~ e^{-7} Torr where pump lifetime will not be a concern. Again, the average pressure is well below that needed to prevent beam attenuation.

3.11.7. Vacuum Control

Vacuum control is accomplished through the EPICS (Experimental Physics and Industrial Control system) architecture. All of the vacuum devices communicate via RS232 serial interface through a MOXA terminal server gateway to the EPICS IOCs (input/output controllers). The client interface to EPICS is performed on either Unix workstations or PCs. The primary OPI (OPerator Interface) application program to view and control vacuum devices is CSS (Control System Studio). Figure 77 shows a typical beamline vacuum system control page. Vacuum EPS (Equipment Protection System) is accomplished through PLC control with vacuum device relay signal logic to interlock gate valves.

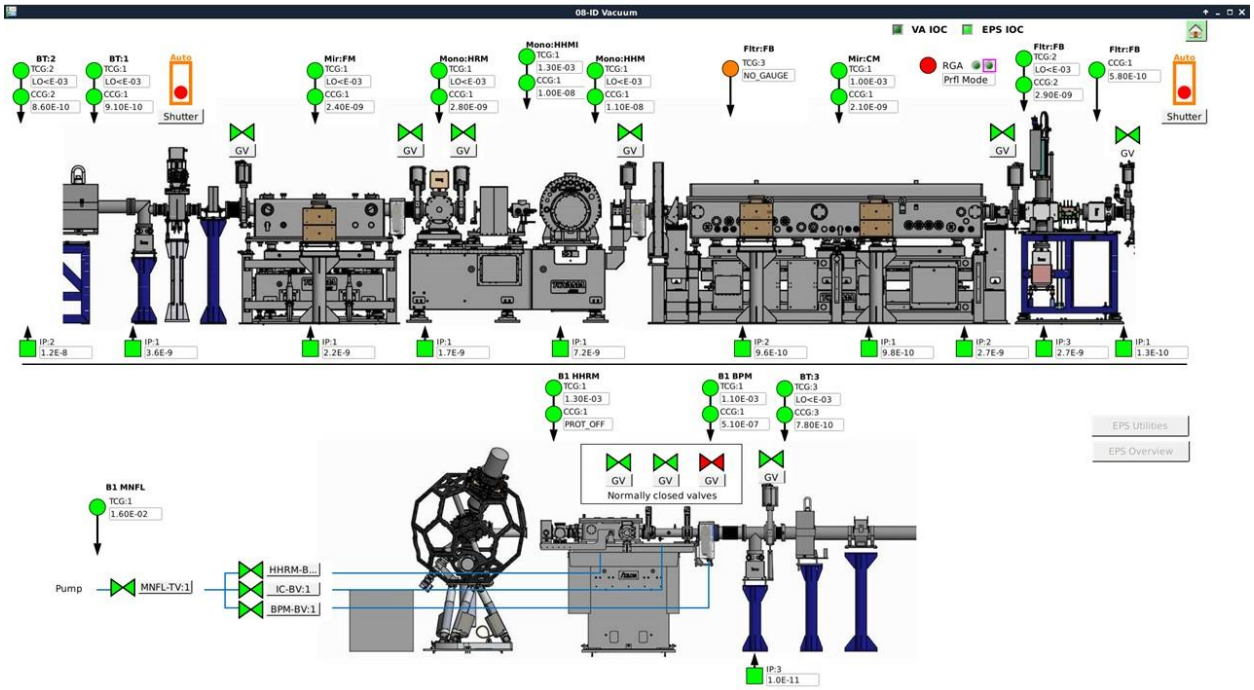

Figure 77: Typical CSS vacuum control page from NSLS-II, ISS beamline

Endnotes:

[1] H. F. Dylla, D. M. Manos, P. H. LaMarche, “Correlation of Outgassing of Stainless Steel and Aluminum with Various Surface Treatments”. J. Vac. Sci. Technol. A 11(5), Sep/Oct 1993.

[2] K. M. Welch, “The Pressure Profile in a Long Outgassing Vacuum Tube”, Vacuum 23(8), 271 (1973)

3.12. X-Ray Shielding

Shielding of the beamline equipment and the experimental stations is required at NSLS-II to avoid personnel being exposed to x-rays. The document "LT-ESH-STD-001: Guidelines for NSLS-II Beamline Radiation Shielding Design" is used as the basis for the design of the HEX beamline. The following paragraph is taken from the document.

Radiation exposure to staff and users resulting from National Synchrotron Light Source II (NSLS-II) operations must comply with Brookhaven National Laboratory (BNL) and Department of Energy (DOE) radiation requirements and must be maintained as low as reasonably achievable (ALARA). Per the Photon Science Shielding Policy (PS-C-ASD-POL-005), in continuously occupied areas during normal operation the dose rate is ALARA, and shall be < 0.5 mrem/h (based on an occupancy of 2000 hrs/year) or less than 1 rem in a year.

Due to the flexible nature of the HEX beamline, an early design decision was taken to make the hutch walls sufficiently thick to avoid having to use the invasive secondary Bremsstrahlung shields at various locations along the length of the hutch.

3.12.1. Safety Components

The HEX beamline includes a number of safety components that are critical to the safe operation of the beamline;

- X-ray beam shutters (white and monochromatic)
- X-ray masks and beam stops
- Bremsstrahlung collimators and stops

It should be noted that secondary Bremsstrahlung shields and a PPS aperture are not included in the above list.

- The hutch shielding calculations have been performed with the assumption that the secondary Bremsstrahlung shields are not fitted; and hence the hutch walls (especially the downstream walls) are of increased thickness to compensate. This will provide increased flexibility in future when the beamline is upgraded or modified.
- The PPS aperture (designed previously to protect an upstream-pointing uncooled copper web between adjacent apertures in a mask) has been rendered obsolete by the use of a new mask design. This is described in Section 3.12.1.2.

Assumptions for white beam component designs.

- All safety critical components that are touched by white beam shall have a Finite Element Analysis performed to ensure that temperatures and stresses are reasonable.
- Calculations assume the full beam, with no allowance made for moveable slits or filters (fixed or moveable).
- Allowable materials for high heat load components include Glidcop, and CuCrZr alloy.
- The peak temperature on any component shall not exceed;
    - 300°C for critical components (eg photon shutters), requiring a long fatigue life (10,000 cycles), and

- 400°C for non-critical components or those with a low fatigue life requirement (e.g. masks where full beam power is not seen under normal operating conditions).

3.12.1.1. X-ray Beam shutters

The white beam shutters are required to switch off the beam to downstream hutches. They are located as follows;

- Front end (one shutter for all three beams)
- First Optics Enclosure (FOE) one white beam shutter for the central branch (stops beam to the E and F hutches).
- First Optics Enclosure (FOE) one white beam shutter for the outboard branch (stops beam to D-hutch). This is not in the scope of the initial build-out of the beamline.
- First Optics Enclosure (FOE) one monochromatic beam shutter for the inboard branch (stops beam to B-hutch). This is not in the scope of the initial build-out of the beamline.
- E-hutch contains one white beam shutter to stop beam to the F-hutch.

The shutter design will be similar to that shown below in Figure 78. These shutters will be fitted with dual lead or tungsten blocks to stop the bremsstrahlung, and each of these blocks are fitted with an angled, water-cooled, photon stop. In addition, redundant and diverse position sensing switches will be fitted to give a clear indication that the stops are in the correct closed position, or not.

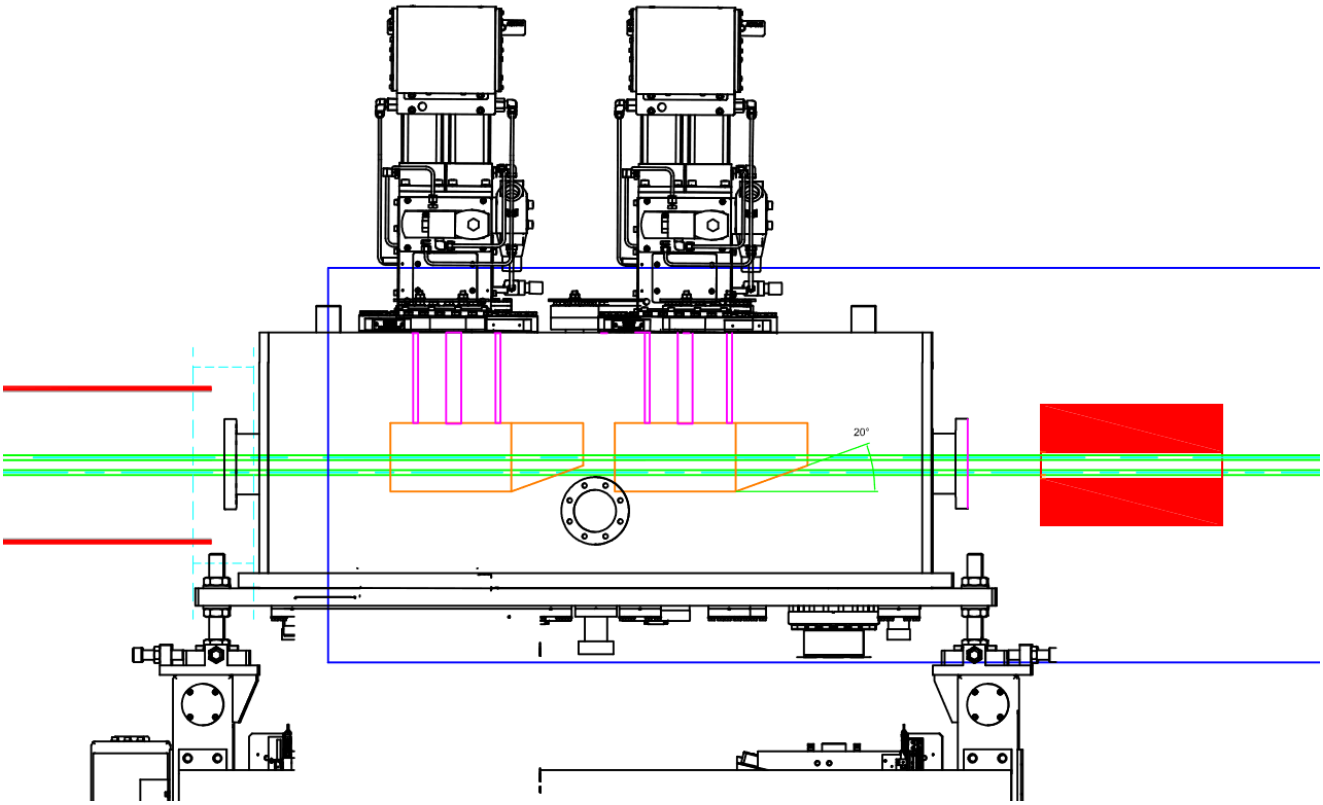

Figure 78 A Design for the Beamline Redundant Safety / Photon Shutter

3.12.1.2. X-ray Masks and Beam Stops

X-ray masks are included in order to tightly collimate the beam to the required size, and prevent the high power x-ray beam from touching any uncooled surfaces. The masks themselves are made from specially selected Copper alloys (Cu-Cr-Zr, or Glidcop) which retain strength at high temperatures. The entrance "throat" is normally angled to spread the heat load and prevent hot-spots, and melting that otherwise can occur.

A new design of mask, pioneered at NSLS-II for the SST beamline, will be used in several places for HEX. This design is used where more than one beam passes through a mask (e.g. for a canted beamline, or in the case for three separate beams), and where (normally) a vertical "web" of copper has a small normal incidence edge that is unable to be cooled sufficiently. The new design tapers the angled surfaces only in the vertical. Figure 79 shows a cut-away section of the Front End mask; this is more fully described in Section 3.7.3.2, however, variants of this design will be used in the beamline in the First Optics Enclosure (FOE). This is a very significant advance, allowing us to avoid use of the PPS aperture (this is a device that trips the PPS in the event of high power x-rays impinging on (and melting) a thin walled capsule shaped to protect critical surfaces. This device needed to be custom made for each beamline, and, it was expensive when all the necessary capsule pressurization and monitoring equipment was included.

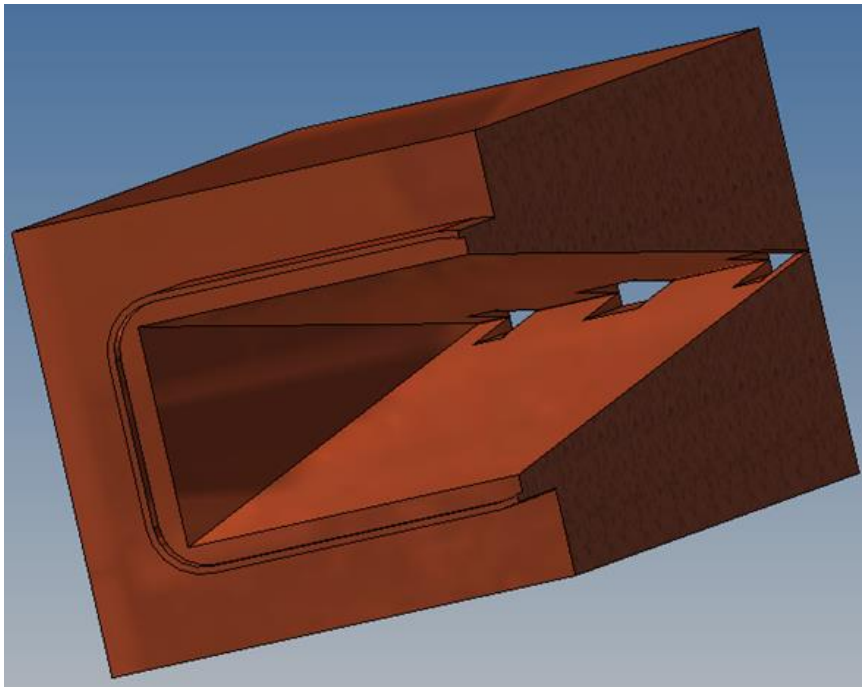

Figure 79 Cut-away model of a three-aperture mask.

The x-ray beam stops are designed taking account of the power density and maximum area of the beam, at the location of the stop along the beam. No account is taken for slits or removable filters. Since white beam is taken into the A, C, D, E, and F hutches, the beam stops in the F-hutch, as well as for the D-hutch (this is out of scope) are designed to handle the high power loads. The beam stop in the B-hutch is needed to stop only the monochromatic beam, and so can be uncooled.

3.12.1.3. Bremsstrahlung Collimators and Stops

The document "LT-ESH-STD-001: Guidelines for NSLS-II Beamline Radiation Shielding Design" lists the following guidelines and assumptions:

- The minimum thickness, along the beam direction, for primary bremsstrahlung stops, collimators and white beam shutters for all NSLS-II beamlines is 30 cm of Pb or 20 cm of W.
- Lateral dimensions for these components shall be based on ray tracings. Distance between lateral edge and the extremal bremsstrahlung ray shall be > 24 mm for tungsten and > 37.5 mm for lead. These are the 3-Moliere-radius distances for tungsten and lead respectively. In most cases, it will be useful to extend the lateral dimensions of these components in order to help manage the secondary Bremsstrahlung.
- The primary Bremsstrahlung stops, collimators, and white beam shutters shall be located inside a white beam enclosure.
- White beam shutter status (open or close) shall be monitored by redundant PPS-interlocked switches and shall be designed to be fail-safe.
- If the shielding is made from smaller bricks, the bricks shall be properly staggered so that the edges and seams are not aligned.

The HEX beamline adheres to these clauses. Due to the large beam fan, and the consequent need for Bremsstrahlung stops and collimators that are of a large size transverse to the beam, we have elected to use lead wherever possible to avoid the high costs of Tungsten.

Figure 80 shows a typical high heat load mask and a collimator assembly as used at the XPD beamline at NSLS-II. The HEX mask and collimator will be quite similar, although wider due to the overall beam width.

Figure 80 A typical high heat load mask and beam collimator

3.12.2. Hutches

The hutches are shielded rooms, required to protect the staff and users from the x-ray beam. The hutches are interlocked with the Personnel Protection System (PPS) which is described in Chapter 9.1. The designs employed follow the usual policies and designs developed at NSLS-II, however the wall panels are thicker than usual because of the higher x-ray energies from the SCW. The hutches on the experimental floor are all constructed from lead, with associated steel support structures; the hutch in the satellite building is of concrete construction, such a hutch fabricated from lead would be prohibitively expensive. The photo in Figure 81 shows a hutch at NSLS-II on completion of hutch construction. Note the two beam exit ports on the downstream wall, and the two double sliding doors.

Figure 81 View slightly upstream of an NSLS-II hutch during construction

The HEX lead hutches are as shown in Figure 82. This is a simplified plan view and doesn't show doors and labyrinths, which are specified to be at least the same thickness as the adjacent panel. The lead thickness is shown in the picture; the calculations validating these thicknesses are covered in Section 3.12.5.

Table 15 shows a list of the hutch drawings; (* note that the B-hutch will not be a part of the initial construction).

Overall Layout	PD-HEX-HU-1000
A-hutch	PD-HEX-HU-1110
B-hutch	PD-HEX-HU-1210 *
C-hutch	PD-HEX-HU-1310
D-hutch	PD-HEX-HU-1410
E-hutch	PD-HEX-HU-1510
F-hutch	PD-HEX-HU-1600 and -1610

Table 15 List of Hutch Drawings

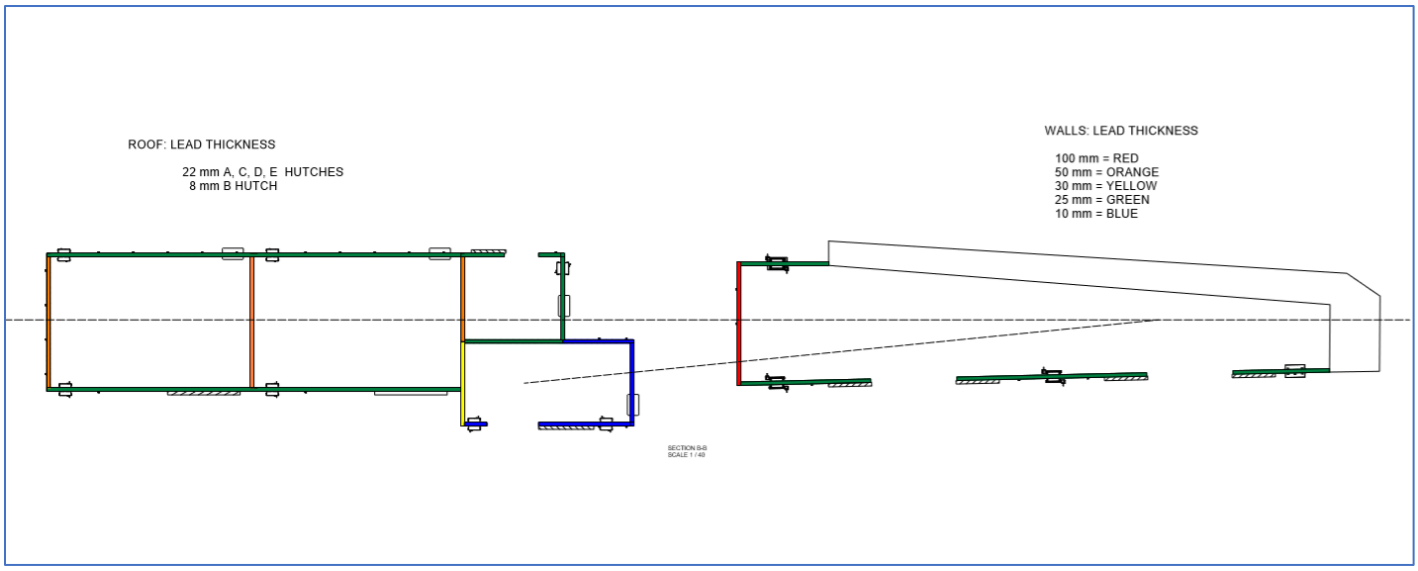

Figure 82 Layout of Lead Hutches for the HEX beamline

The satellite building hutch is approximately 5.5m wide x 18.8m long (internal dimensions) and constructed with thick cast in-situ concrete (walls 0.7m – 1.0m thick, and roof 0.6m thick). The concrete construction is part of the satellite building contract, although the doors, labyrinths, beam stops etc are all included in the lead hutches contract. See Figure 83 for a simplified schematic of the hutch.

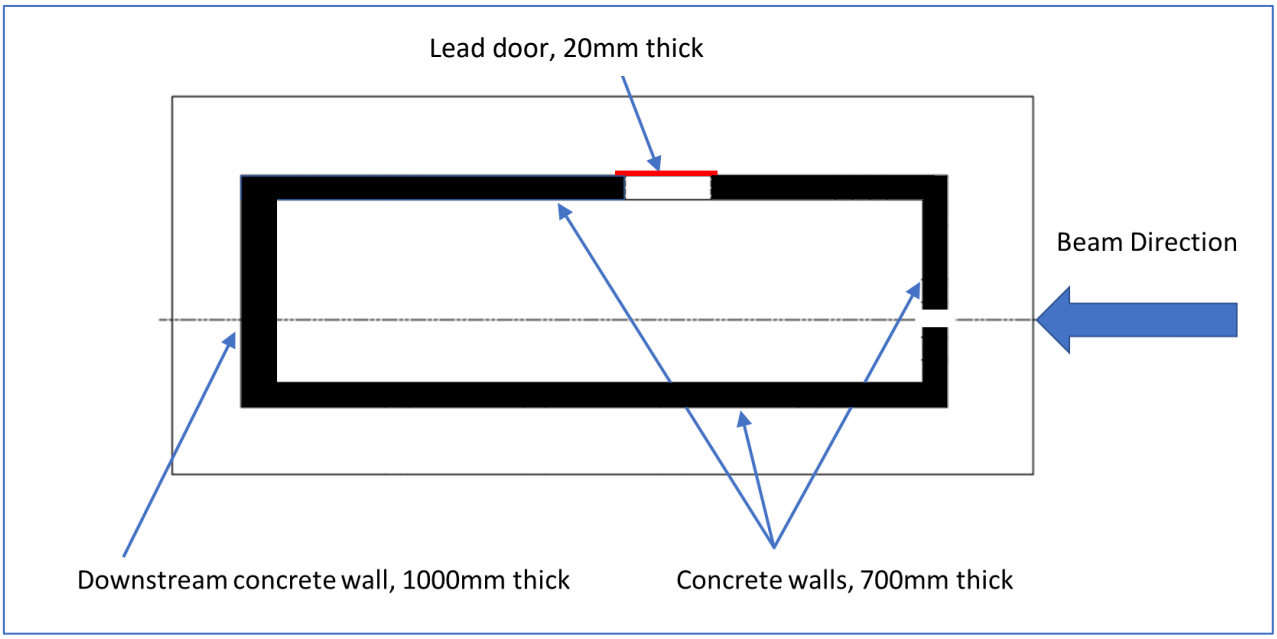

Figure 83 Plan view of the HEX beamline concrete hutch

The inboard wall of the hutch is fitted with a number of wall labyrinths (see Figure 84) designed for User access (with easy to operate access door inside the hutch with a simple interlocked pull switch to gain access), and for the PPS wiring which will be secured under configuration control.

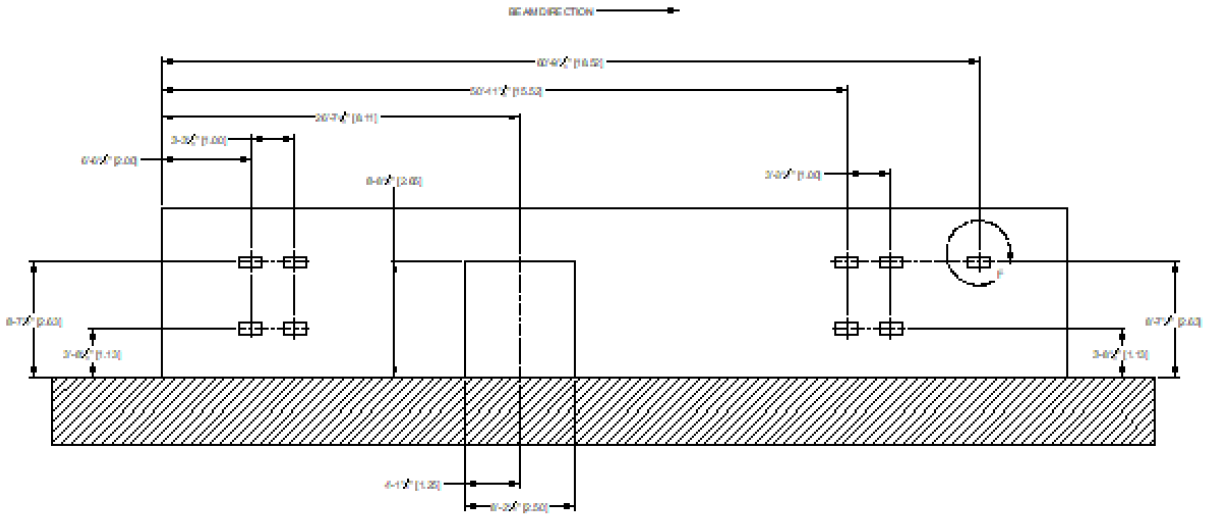

Figure 84 F-hutch inboard wall elevation showing door and wall labyrinths

An important feature of the concrete hutch is the floor labyrinths, and idea taken from the JEEP beamline at Diamond Light Source. The details of this are shown in Figure 85. The width of the trench and labyrinth is ~26" – sufficient for a 24" cable tray with clearance on either side. The trench itself extends from the beam centerline inside the F-hutch to the rack location on the outer wall of the satellite building. This means that cables can be under the floor, and when covers are in place there will be no trip hazards; important in what could become a "busy" hutch.

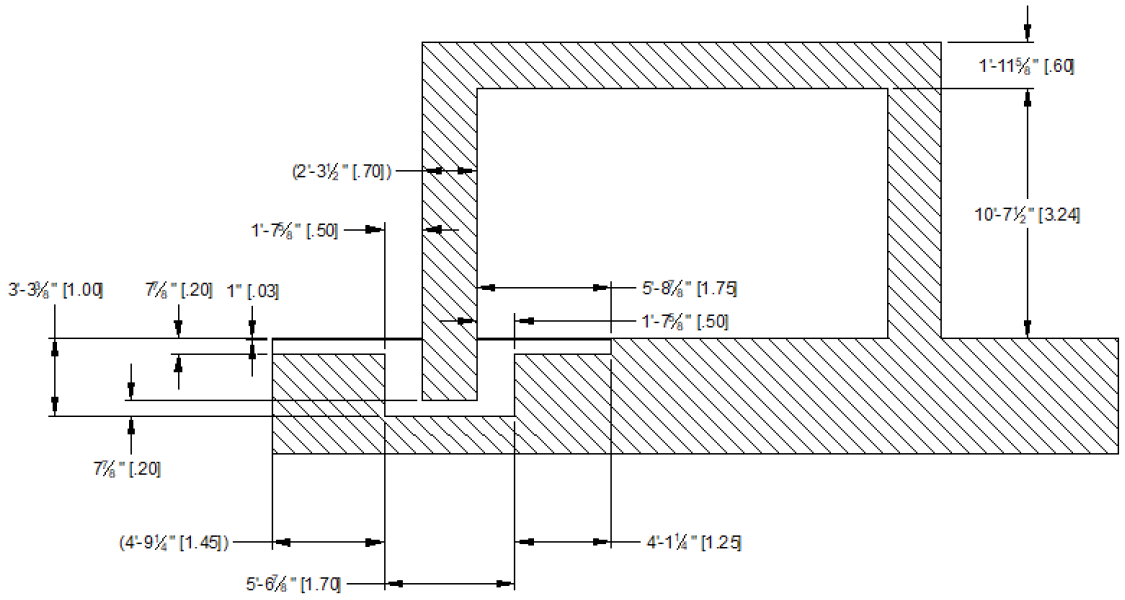

Figure 85 F-hutch floor labyrinth detail. (Beam direction into page).

3.12.2.1. Labyrinths

The hutches are fitted with labyrinths to allow cables and pipes to connect through the walls without leakage of x-rays. These are secured with electrical locks and switches or they are placed under configuration control. These labyrinths are used for the following purposes;

- Control cables (motors and encoders)
- Mains electricity
- PPS cables
- Liquid nitrogen, where required
- Ventilation air (in and out)
- Exhaust gas (where required)
- Chilled water
- DI water (this enters the FOE from the SR tunnel, and is then distributed along the beamline from the FOE; for HEX many hutches will require DI water due to the power of the white beam meaning that many components require cooling).

3.12.2.2. Doors and windows

The HEX hutches will be fitted with standard doors, normally these can be either a swinging single door or sliding single/double door as needed; in the case of HEX all the doors are sliding due to the weight. One door per hutch will be pneumatically actuated. These will be fitted with magnetic locks and switches so they can be incorporated into the PSS. Generally, windows are discouraged on white beam hutches due to the extreme thickness of lead glass needed (around 3" which would cause very poor visibility); HEX will not have windows fitted to the hutch. Figure 86 shows the typical lead-lined floor groove cross section.

Figure 86 Typical hutch floor groove showing groove in concrete floor, steel insert, and the lead shielding

3.12.2.3. Hutch Electrical Equipment

The hutch will be fitted with standard ventilation fans within the hutch contract. Wiring to this equipment (and all other electrical wiring, including lights and outlets) will be performed under the beamline utilities scope.

3.12.2.4. Hutch Roof Access

The hutches are all designed for roof access; features include load ratings compatible with human loads, as well as equipment and utilities, handrails and kick-plates are included for safe access, and swing gates will be used to restrict access to hutch roofs from the mezzanine floor (storage ring tunnel roof) to just beamline staff and other authorized staff (see Figure 87).

Hutches will often be connected by personnel bridges, where this is sensible (i.e., a span of <10 m). In the case of HEX, a bridge will be installed between the A and C hutches. In addition, a short flight of steps from the A-hutch roof to the mezzanine will be installed; egress from the mezzanine to the experimental floor is via the convenient stairs in the 27-BM sector. These stairs and bridges are all included in the hutches contract.

Figure 87 Personnel access gate in the SR tunnel roof railing, raised treat plate over the SR tunnel kick plate, and steps down onto the tunnel roof

3.12.3. Transport Pipes

The beam transport pipes will be included in the beamline contract. The dimensions of the white beam transport pipe, and the required shielding thickness are shown in Figure 88 and Table 16 below.

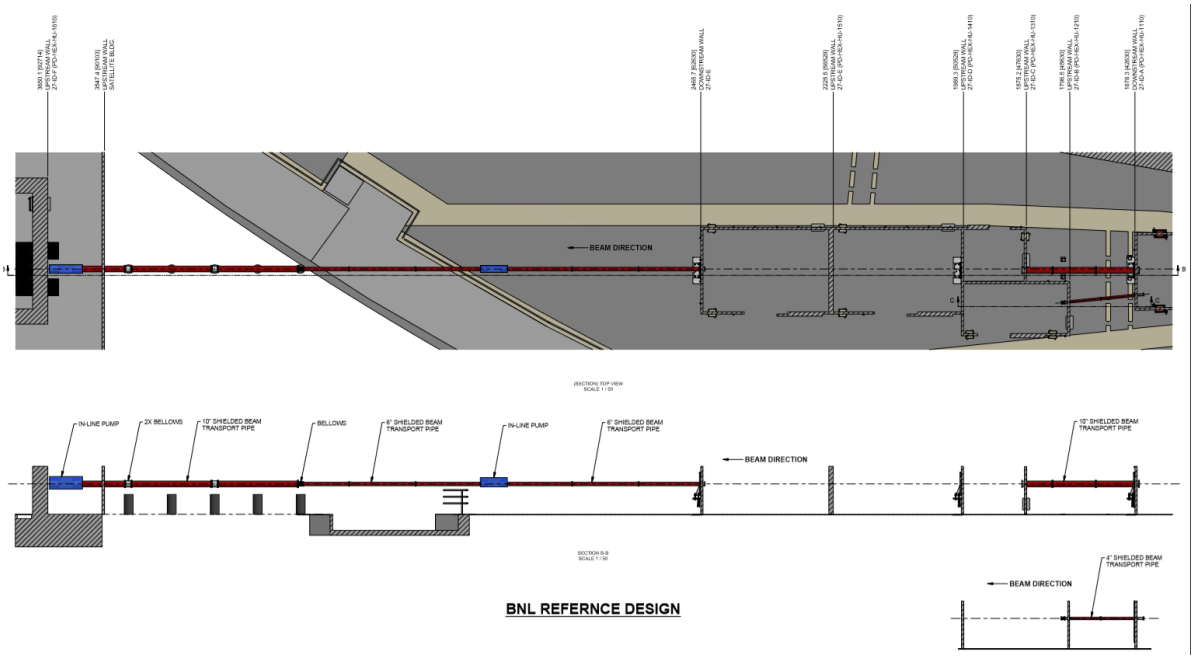

Figure 88 Shielded Beam Transport Pipe

Due to the diverging beam, the diameter increases with distance from the source; additionally, clearances of 20mm from the high-power x-ray beam to the inside wall are required in order to avoid any possibility of the beam striking the pipe and acting as a scattering source (or melting the pipe)!

The shielded pipe for the white beam central branch is in two sections, as can be seen in Figure 88: the section from the A-C hutches, and the longer section from the E-F hutches.

Pipe diameter	6” ID inside NSLS-II building 10” ID outside NSLS-II building Lead thickness: at the time of writing this thickness is to be confirmed, but it is expected to be <20mm
Pumping boxes (shielded)	1 on the edge of the experimental floor 1 adjacent to F-hutch
Bellows boxes (shielded)	Three in E-F pipe, one inside building.
Joint boxes (shielded)	Minimum possible commensurate with design and installation requirements (expected ~2 in A-C pipe and 2 in E-F pipe).
Base pressure	10E-8 mB
Pressure after 100 hours pumping	10E-6 mB

Table 16 Shielded White Beam Transport Pipe Requirements

3.12.4. Synchrotron and Bremsstrahlung Ray Tracing

The synchrotron and x-ray ray tracing follows the normal NSLS-II procedures. Several important points for the HEX beamline are;

- Normally white beam is present in just the FOE (A-hutch), and Bremsstrahlung rays are completely stopped in this enclosure. In the case of HEX, white beam is taken to C, D, E and F hutches, so the Bremsstrahlung rays are stopped as follows;
    - in the D hutch (for the outboard beam),
    - in the F-hutch (for the central beam), and
    - in the A-hutch (for the inboard beam, heading for hutch-B).
- The beamline, in its mature configuration will have three separate branches. Not only do the three branches have to be raytraced, but care must be taken to avoid crosstalk between branches.

The ray tracing is available as a separate document.

3.12.5. Shielding Calculations

Under normal operating conditions the radiation shielding design of the HEX white beam enclosures must consider the following as sources of radiation

a. Bremsstrahlung generated when the electrons in the stored beam interact with residual gas molecules in their path. This is usually termed as Gas Bremsstrahlung (GB) and in the case of HEX beamline it is generated in the straight section of 27ID.
b. Scattered bremsstrahlung generated by the interaction of the primary GB with the beamline components such as masks, collimators, and mirrors.
c. Photo-neutrons generated by the interaction of primary GB with the beamline components.
d. Scattered synchrotron radiation (SR) from beamline optical components.

The enclosures must be designed to reduce radiation dose rates in the occupied areas outside the enclosures during normal operation to less than 0.05 mrem/h. Assuming occupancy of 2000 hours per year, this will keep annual dose limits to staff and users to less than 100 mrem. For any individual not involved in the operation of the NSLS-II facility the annual dose must be kept below 25 mrem considering the occupancy factor. The latter dose requirement affects areas outside the satellite building where personnel not involved in the operation of NSLS-II may be present.

The FLUKA Monte Carlo code [1,2] is used to simulate spatial distribution of dose rates due to GB interactions with beamline components while the analytical code STAC8 [3] is used to estimate the dose rates due to SR interactions with optimal scatter targets. Since the HEX beamline components layout and ray tracing drawings have not yet been finalized, the shielding analysis followed a generic approach with standard scatter targets to mimic components that are typical in a beamline such as masks, mirrors, monochromators and beam stops.

This report consists of two parts, one dealing with the GB as the source and the other with the scattering of the SR. Both cases are constant sources of radiation and the dose rates that are present represent the normal operating conditions.

The source of the primary GB radiation is 1/E energy spectrum that extends up to 3 GeV and sampled with the FLUKA source routine. The full GB power is assumed to be incident on target. The total ambient dose equivalent rates are estimated in a three-dimensional mesh (USRBIN in FLUKA) by scoring the fluence and folding them with the fluence to ambient dose equivalent conversion coefficients. All the

results given herein are on contact with the enclosure walls (and roof) in units of mrem/h. The storage ring parameters used for the GB shielding analysis are given in Table 17.

Electron Beam Energy	3 GeV
Stored beam Current	500 mA
Average pressure in the straight section	1×10^{-9} torr
Length of the straight section	15.5 m

Table 17 Storage Ring Parameters used for the GB Shielding Analysis

The 27ID-HEX beamline shielding enclosures are rectangular except for the first optics enclosure (FOE) where a slanted section of its inboard wall is defined by a storage ring accelerator enclosure. The length of the enclosures varies between 3 m and 19.5 m (inner dimensions not including the shielding thickness). All white beam enclosures have their lateral walls located at least 1.5 m from the beam centerline except for 27ID-C outboard lateral wall which is located at 0.5 m from beam centerline. The roof of the lead enclosures (27ID-A to 27ID-E) is positioned at 2.09 m from beam centerline and at 1.8 m for the concrete enclosure.

The top and side views of the FLUKA model for the 27ID-A enclosure are shown in Figure 89 whose length is approximately 18 m. A white beam stop (WBS R=2 cm, L=3cm) made of copper followed by a lead bremsstrahlung stop (BRS R=10cm, L=30cm) were placed 50 cm upstream from the downstream wall. In this configuration, the WBS/BRS is of little use in stopping the scattered bremsstrahlung from upstream targets. The scatter targets considered in the GB simulation include copper block and a silicon crystal. In Figure 89 the copper target (R=2cm, L=3cm) is positioned at 10 cm from the upstream wall of the enclosure and the silicon target (4cm x 4cm, 20 cm long) positioned in the middle of the enclosure. The results of GB simulation shown in this report correspond to this configuration because it gives the highest ambient dose equivalent rate on the downstream wall of the enclosure. For the lateral walls and the roof, the highest ambient dose rates were obtained with a Cu target that is approximately 20 cm long as well as when GB directly strikes the WBS. Various configurations were simulated that included Cu and Si targets placed at different locations inside each beamline enclosure, varying the length of the Cu target and using either short or long Si targets with different orientations to the beam direction. The thickness of the downstream wall and combination of additional local shielding were also varied. Figure 89 inset shows a downstream wall 10 cm thick reinforced with additional shielding comprising of a 2 cm Pb guillotine (40 cm x 40 cm) on the inside of the enclosure and on the outside 3 cm Pb plate (140 cm x 140 cm) followed by 10 cm polyethylene plate (140 cm x 140 cm).

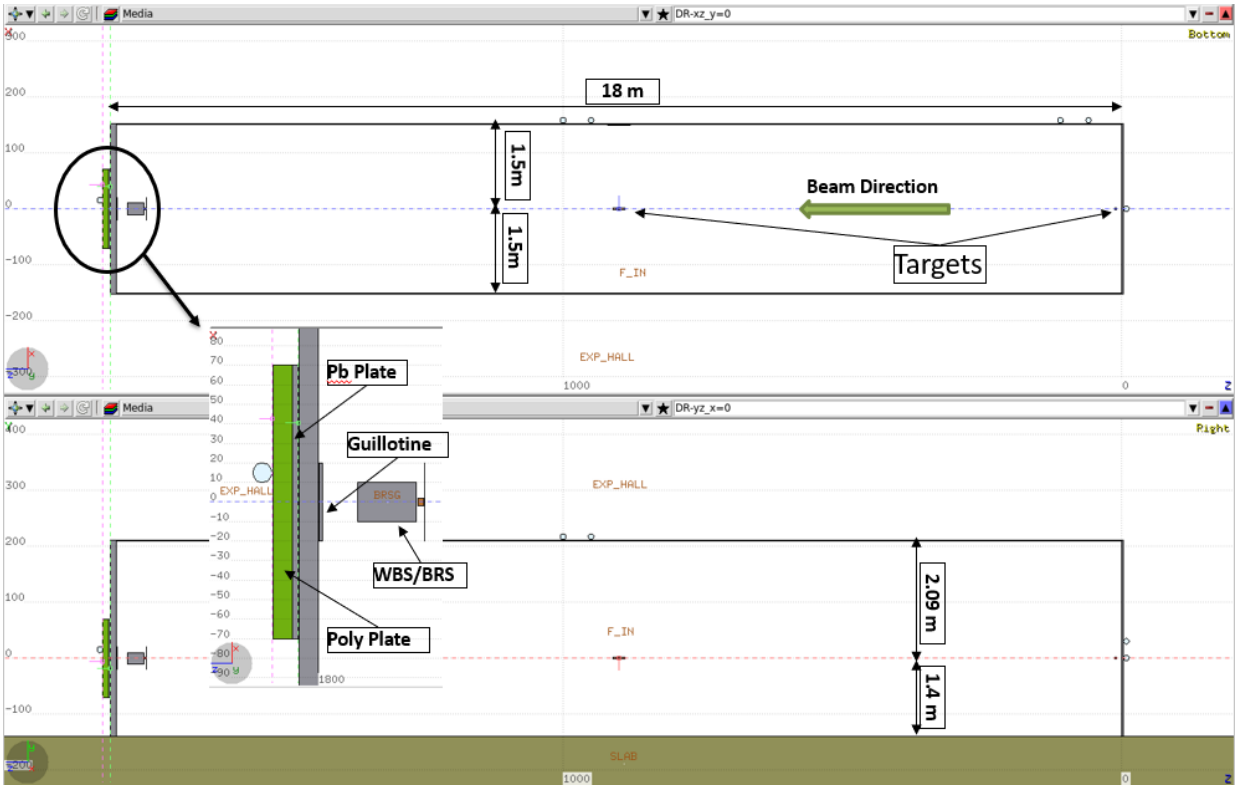

Figure 89 FLUKA geometry for the 27ID-A (FOE) enclosure (top and side views)

3.12.5.1. White Beam Enclosure 27ID-A

The white beam enclosure 27ID-A is the first optics enclosure (FOE) that has both GB and SR entering the enclosure. The shielding configuration for the GB analysis used a 18m long enclosure with 10cm thick Pb downstream wall (no apertures), 25 mm thick Pb lateral wall located at 1.5m from beam axis, 10mm thick Pb roof at 2.09 m above beam axis. The downstream wall is reinforced with a 2cm Pb guillotine (40cm x 40cm) on the inside of the enclosure and on the outside 3cm Pb plate (140cm x 140cm) followed by 10cm Polyethylene plate (140cm x 140cm). In this configuration, the total ambient dose rates in and around the 27ID-A enclosure are given in Figure 90 and the corresponding neutron ambient dose rates are given in Figure 91. The total ambient dose rates on the lateral wall and roof are found to be less than 0.05 mrem/h with the neutrons contributing more to the dose rates. Figure 92 (a) & (b) give the top and side view of the total ambient dose rate away from the downstream wall. Figure 92 (c) & (d) show the total ambient dose rates on contact with the lead plate and polyethylene plate respectively. The left most figure shows the shielding configuration on downstream wall. As seen from Figure 92 (c) and (d) the ambient dose rates in areas accessible to personnel are below 0.05 mrem/h. Figure 93 shows the total ambient dose rates outside the downstream wall of 27ID-A when the primary GB strikes individual components WBS/BRS, Si and Cu. The ambient dose rates are below 0.05 mrem/h with Cu as the target being the worst case.

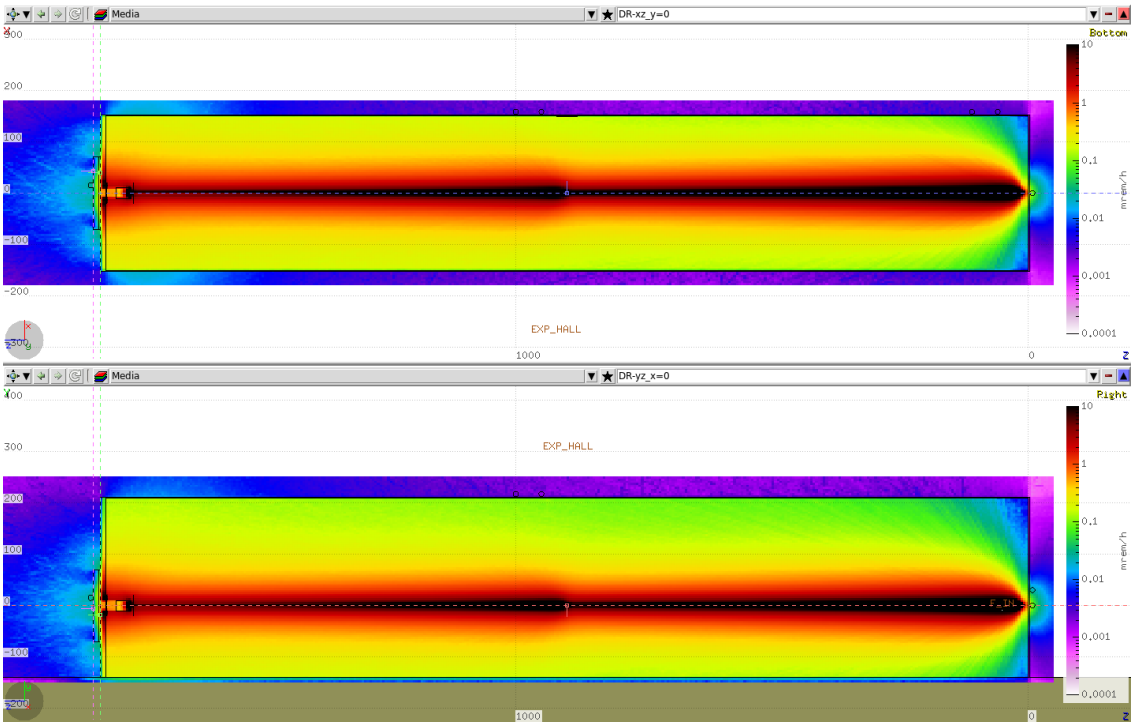

Figure 90 Total ambient dose equivalent rates in and around the FOE when the primary GB strikes the Cu target located at 10cm from the upstream wall with a Si target located in the middle of the enclosure. The top figure shows the horizontal view (y=0.0) and the bottom figure shows the vertical view (x=0.0)

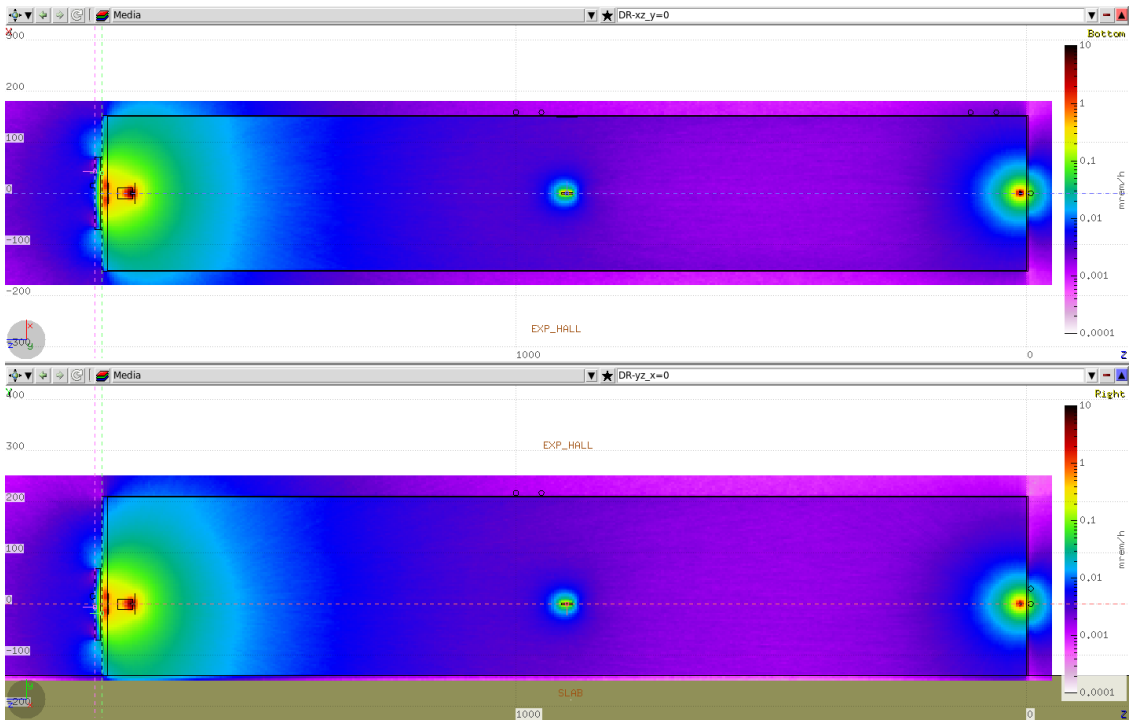

Figure 91 Same as Figure 90. showing only the neutron ambient dose equivalent rates in and around the FOE

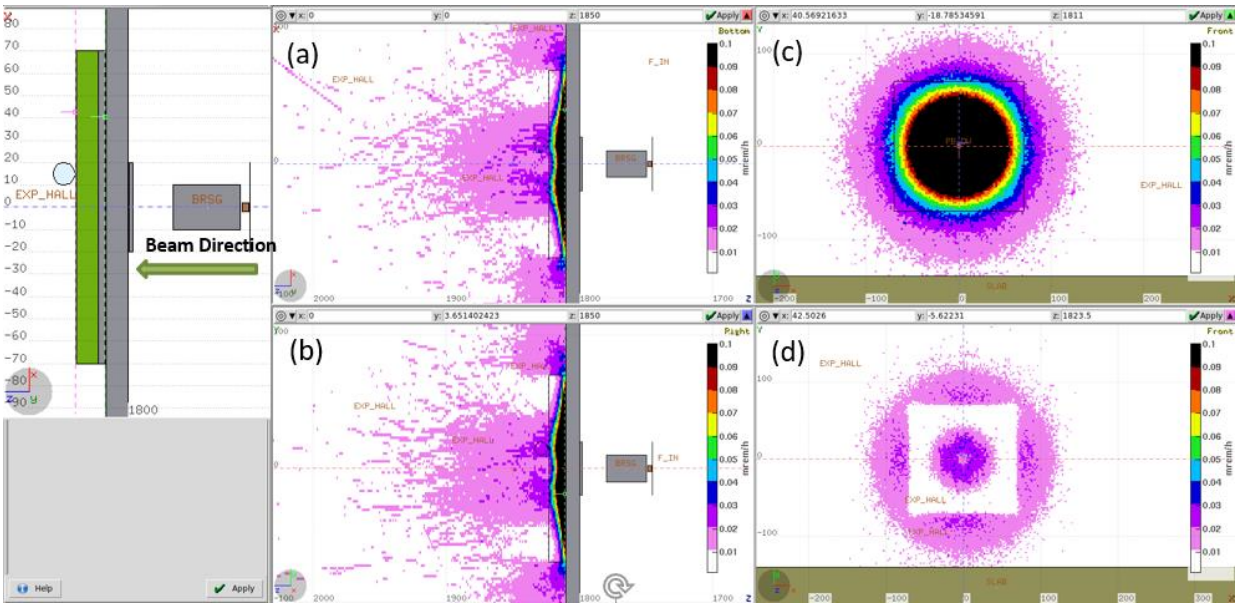

Figure 92 Total ambient dose equivalent rates on the exterior of the downstream wall of 27ID-A (FOE). The additional shielding configuration on the downstream wall is shown in the leftmost figure

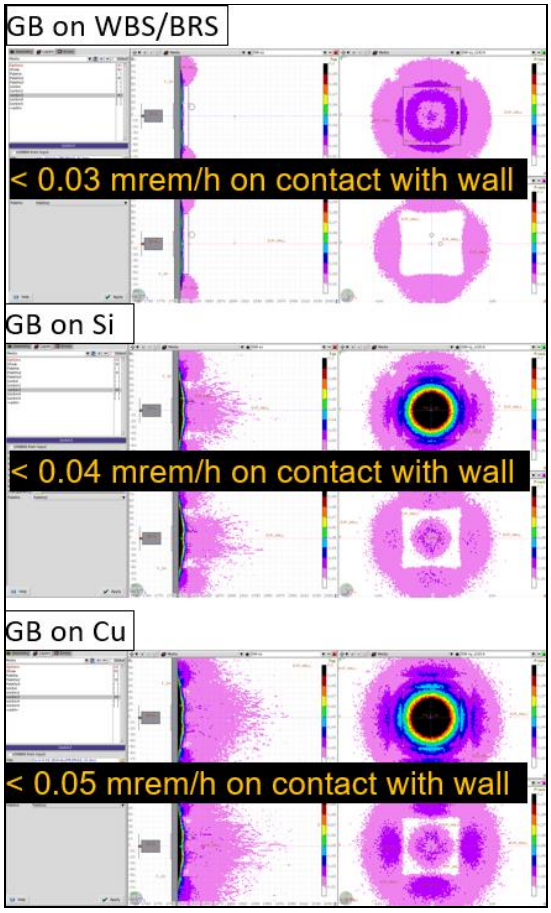

Figure 93 Total ambient dose equivalent rates on the exterior of the downstream wall of 27ID-A (FOE) with primary GB directly striking WBS/BRS (top figure), Si target (middle figure) and Cu target (bottom Figure)

3.12.5.2. White Beam Enclosure 27ID-C

Both GB and SR enter the white beam enclosure 27ID-C. The shielding configuration for the GB analysis used a 3m long enclosure with 5cm thick Pb downstream wall (no apertures), 25 mm thick Pb inboard lateral wall located at 1.5m from beam axis, 25 mm thick Pb outboard lateral wall (reinforced with 6 mm Pb belly band at +/- 50 cm around beam centerline) located at 0.5m from beam axis, and 22mm thick Pb roof at 2.09 m above beam axis. The downstream wall is reinforced with a 7cm Pb guillotine (80cm x 80cm) on the inside of the enclosure and on the outside 3cm Pb plate (120cm x 120cm) followed by 10cm Polyethylene plate (120cm x 120cm). In this configuration, the total ambient dose rates in and around the 27ID-C enclosure are given in Figure 94. Figure 95 (a) & (b) give the top and side view of the total ambient dose rate outside the downstream wall. Figure 95 (c) & (d) show the total ambient dose rates on contact with the lead plate and polyethylene plate respectively. The left most figure shows the shielding configuration on downstream wall. As seen from Figure 95 (c), the dose rate outside the lead is approximately 0.08 mrem/h which slightly exceeds the dose criteria. However, spatially this is very localized and drops to below 0.05 mrem/h at the surface of the polyethylene plate as seen in Figure 95 (d). The dose rates on the downstream wall will be reevaluated once the beamline components are finalized. The total ambient dose rates on the lateral walls and roof are shown in Figure 96. The ambient dose rates are less than 0.05 mrem/h for the inboard lateral wall and the roof. However, the ambient dose rates exceed 0.05 mrem/h on contact with outboard lateral wall due to its shorter distance to the beam centerline of 0.5 m compared to inboard wall which is at 1.5 m. A 10 cm poly belly band (+/- 50 cm around beam centerline) reduces the ambient dose rate to below 0.05 mrem/h within +/- 50 cm around beam centerline but no so outside this area. The polyethylene belly band will need to extend beyond +/- 50 cm. Instead of a belly band, it is more effective to place the shield near the scatter target. Once all the beamline components dimension and position inside 27ID-C enclosure are finalized, the appropriate shield will be designed to keep ambient dose rates below 0.05 mrem/h on outboard lateral wall and upstream wall of the enclosure.

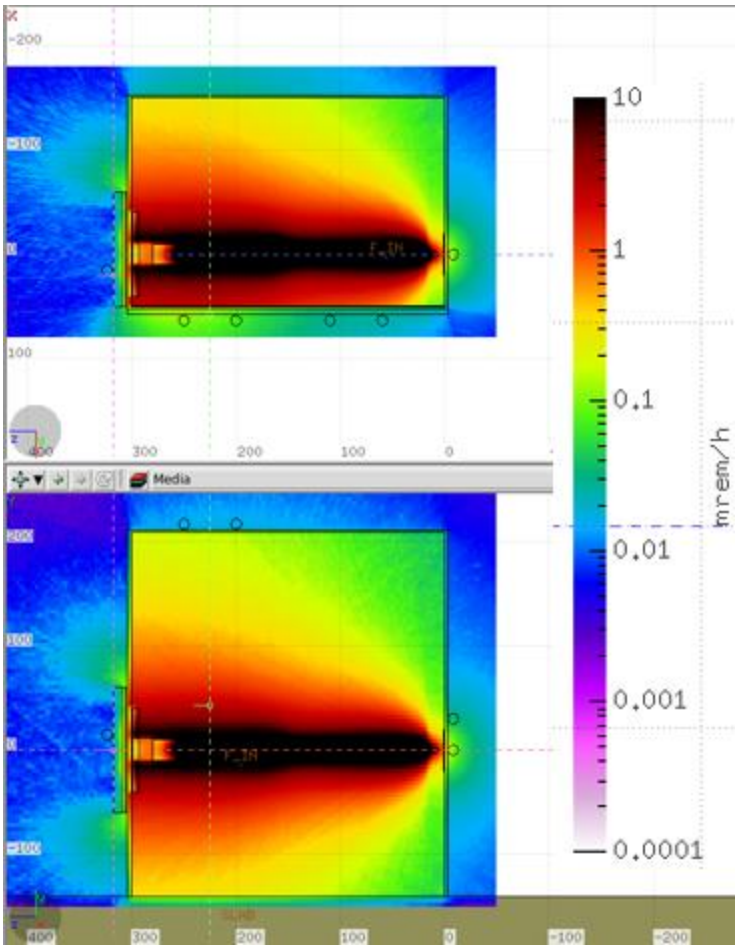

Figure 94 Total ambient dose equivalent rates in and around the 27ID-C enclosure when the primary GB strikes the Cu target located at 10cm from the upstream wall with a Si target located in the middle of the enclosure. The top figure shows the horizontal view (y=0.0) and the bottom figure shows the vertical view (x=0.0)

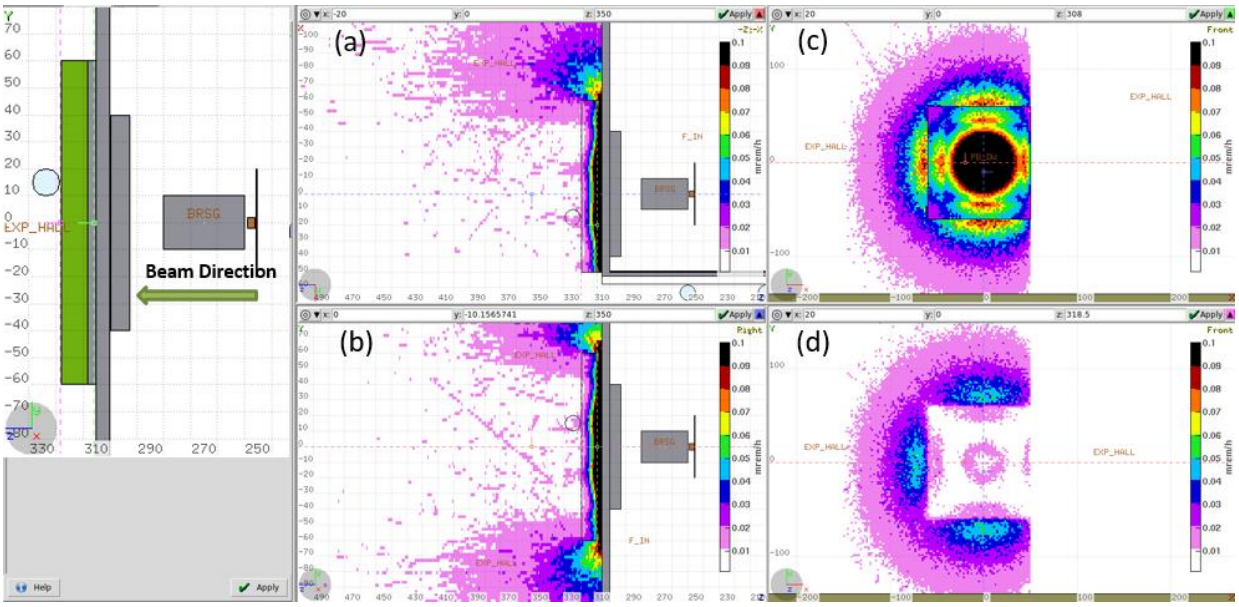

Figure 95 Total ambient dose equivalent rates on the exterior of the downstream wall of 27ID-C. The additional local shielding configuration on the downstream wall is shown in the leftmost figure

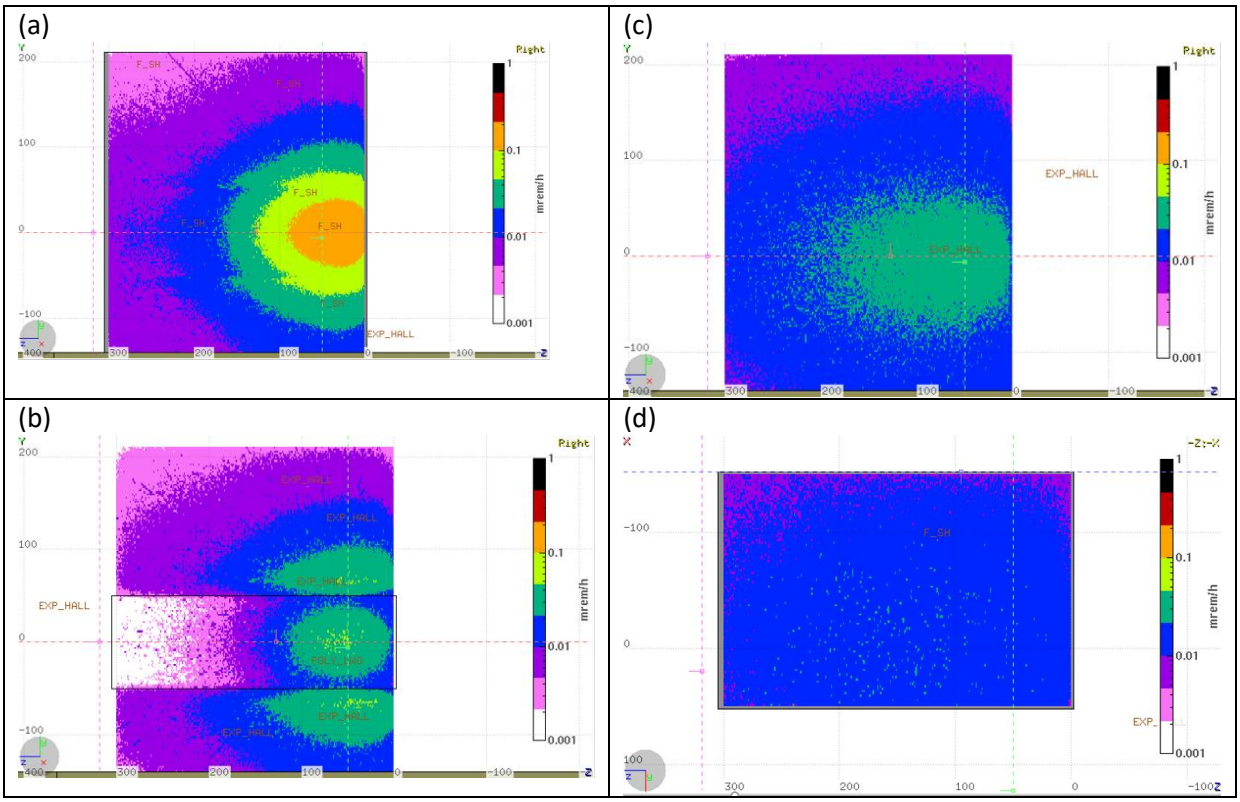

Figure 96 Total ambient dose equivalent rates on the exterior of the outboard Lateral wall without/with additional polyethylene shield (a & b) inboard lateral wall (c) and roof (d) of 27ID-C.

3.12.5.3. White Beam Enclosures 27ID-D and 27ID-E

The white beam enclosures 27ID-D and 27ID-E also have both GB and SR entering the enclosure. The shielding configuration for the GB analysis used a 6m long enclosure with 5cm thick Pb downstream wall (no apertures), 25 mm thick Pb lateral walls located at 1.5m from beam axis, 22mm thick Pb roof at 2.09 m above beam axis. The downstream wall is reinforced with a 7cm Pb guillotine (80cm x 80cm) on the inside of the enclosure and on the outside 3cm Pb plate (140cm x 140cm) followed by 10cm Polyethylene plate (140cm x 140cm). In this configuration, the total ambient dose rates in and around the 27ID-D/E enclosure are given in Figure 97. It shows that the ambient dose rates criteria are slightly exceeded for upstream wall and in a small area near the exterior surface of the downstream wall. However, the upstream wall of 27ID-D is shared with 27ID-C which will be unoccupied by personnel when beam is allowed into the enclosure. In addition, the upstream wall of 27ID-E is shared with 27ID-D. Figure 98 (a) & (b) give the top and side view of the total ambient dose rate outside the downstream wall. Figure 98 (c) & (d) show the total ambient dose rates on contact with the lead plate and polyethylene plate respectively. The left most figure shows the shielding configuration on downstream wall. As seen from Figure 98 (c), there is small amount of radiation leakage just outside the lead plate that amounts to approximately 0.09 mrem/h which slightly exceeds the dose criteria. However, the spatial extent of this dose rate is localized and drops to below 0.05 mrem/h at the surface of the poly plate as seen in Figure 98 (d). Once all the beamline components are finalized the dose rates on the downstream wall will be reevaluated

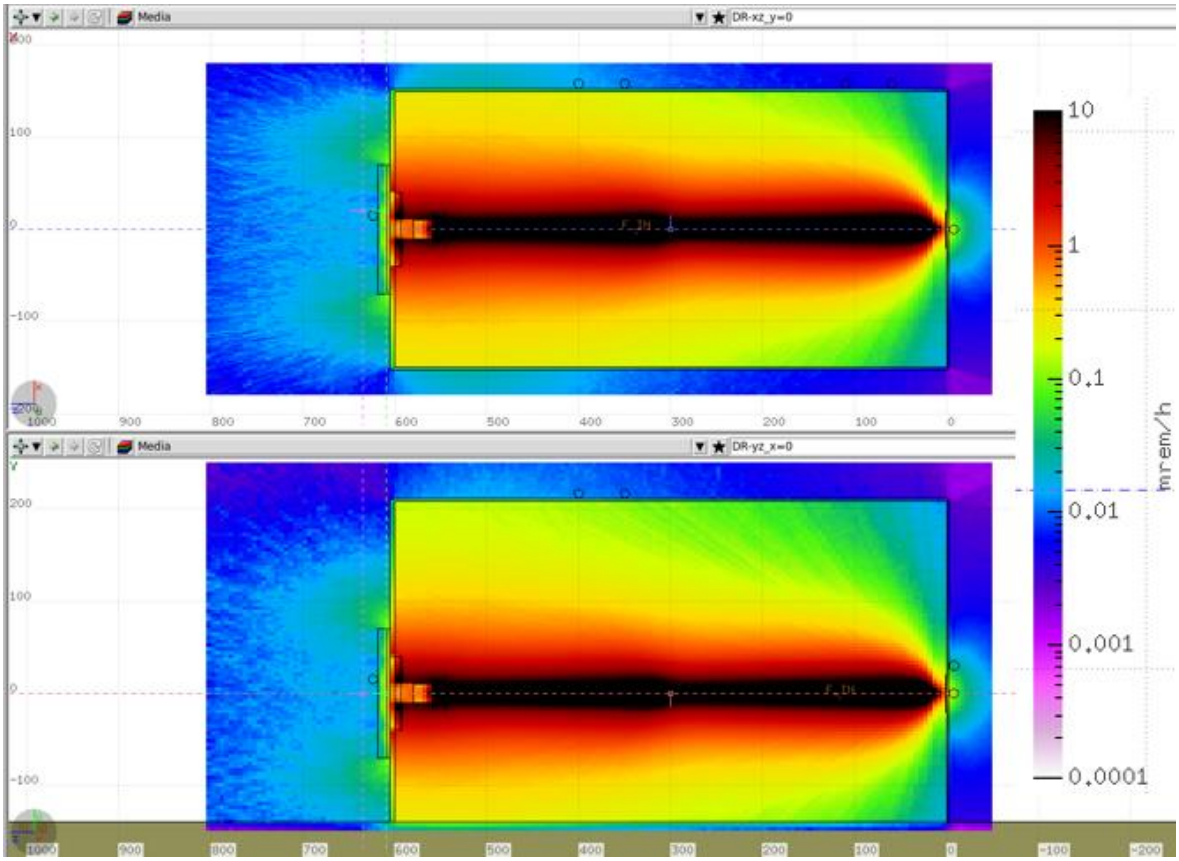

Figure 97 Total ambient dose equivalent rates in and around the 27ID-D and E enclosures when the primary GB strikes a Cu target with a Si target located in the middle of the enclosure. The top figure shows the horizontal view (y=0.0) and the bottom figure shows the vertical view (x=0.0).

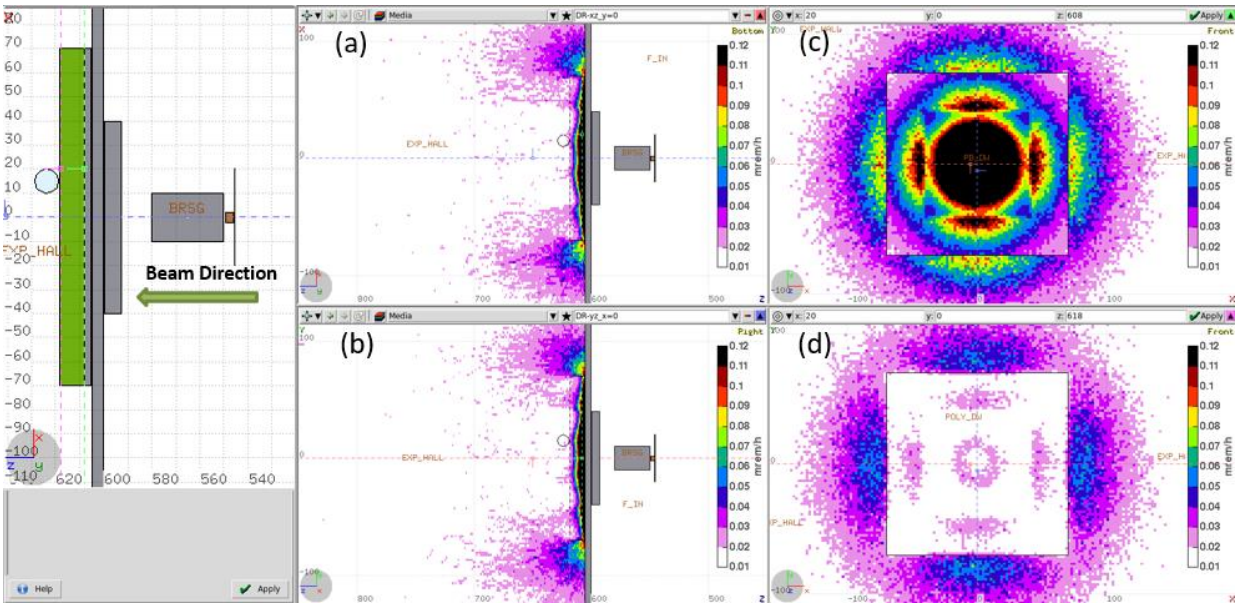

Figure 98 Total ambient dose equivalent rates on the exterior of the downstream wall of 27ID-D and E enclosures. The additional local shielding configuration on the downstream wall is shown in the leftmost figure.

3.12.5.4. White Beam Enclosure 27ID-F

The white beam enclosure 27ID-F has both GB and SR entering the enclosure. The shielding configuration for the GB analysis used a 19m long enclosure using Portland concrete (standard construction material) at 2.3 g/cm^3 density for walls and roof. The downstream wall is 100 cm thick with no apertures and the upstream wall is 70cm thick. The inboard and outboard lateral walls are 70 cm thick and located at 3.5m and 1.5m from beam axis respectively. The roof is 60 cm thick at 1.8 m above beam centerline. The downstream wall is reinforced with a 5cm Pb plate (130 cm x 130 cm) on the inside of the enclosure. In this configuration, the total ambient dose rates in and around the 27ID-F enclosure are given in Figure 99. Clearly the ambient dose rate on the lateral walls, upstream wall and roof are below 0.01 mrem/h. Figure 100 (a) & (b) give the top and side view of the total ambient dose rate away from the downstream wall. Figure 100 (c) & (d) show the total ambient dose rates on contact with the exterior surface of the wall and 1 m away respectively. They are approximately 0.02 mrem/h on contact and below 0.01 mrem/h 1m away from the wall.

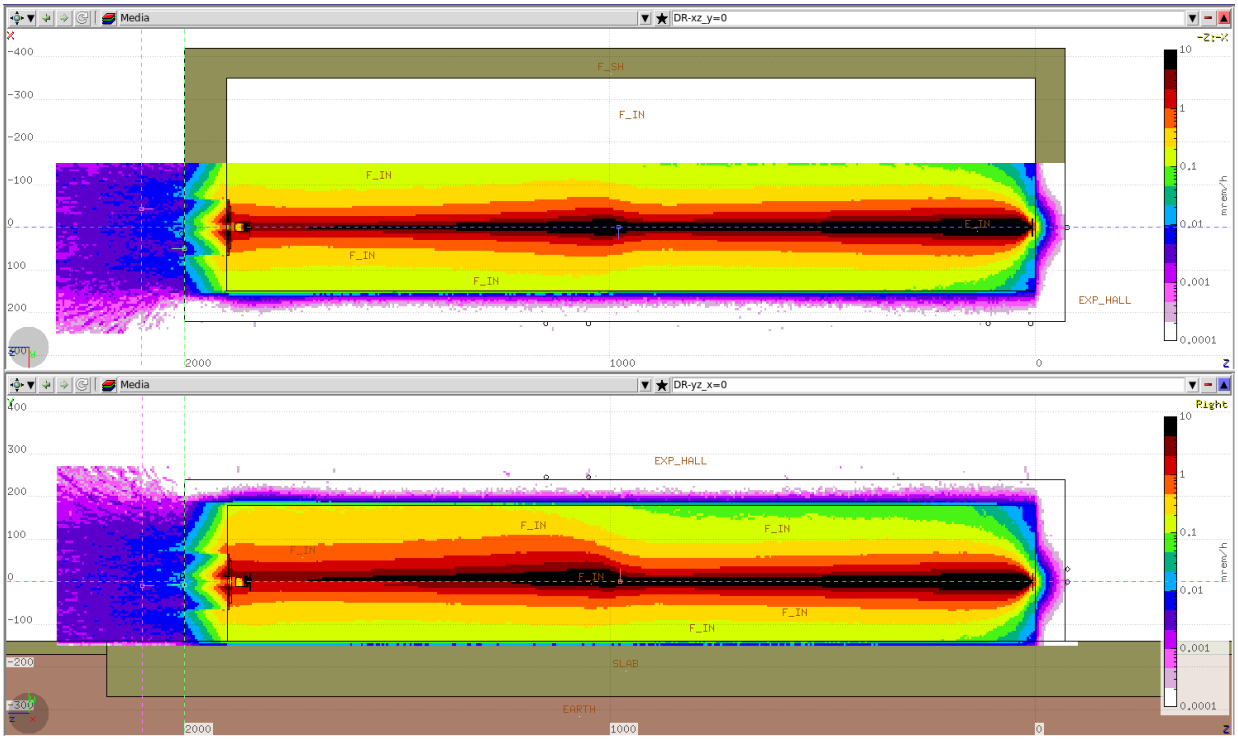

Figure 99 Total ambient dose equivalent rates in and around the 27ID-F enclosure when the primary GB strikes a Cu target with a Si target located in the middle of the enclosure. The top figure shows the horizontal view (y=0.0) and the bottom figure shows the vertical view (x=0.0)

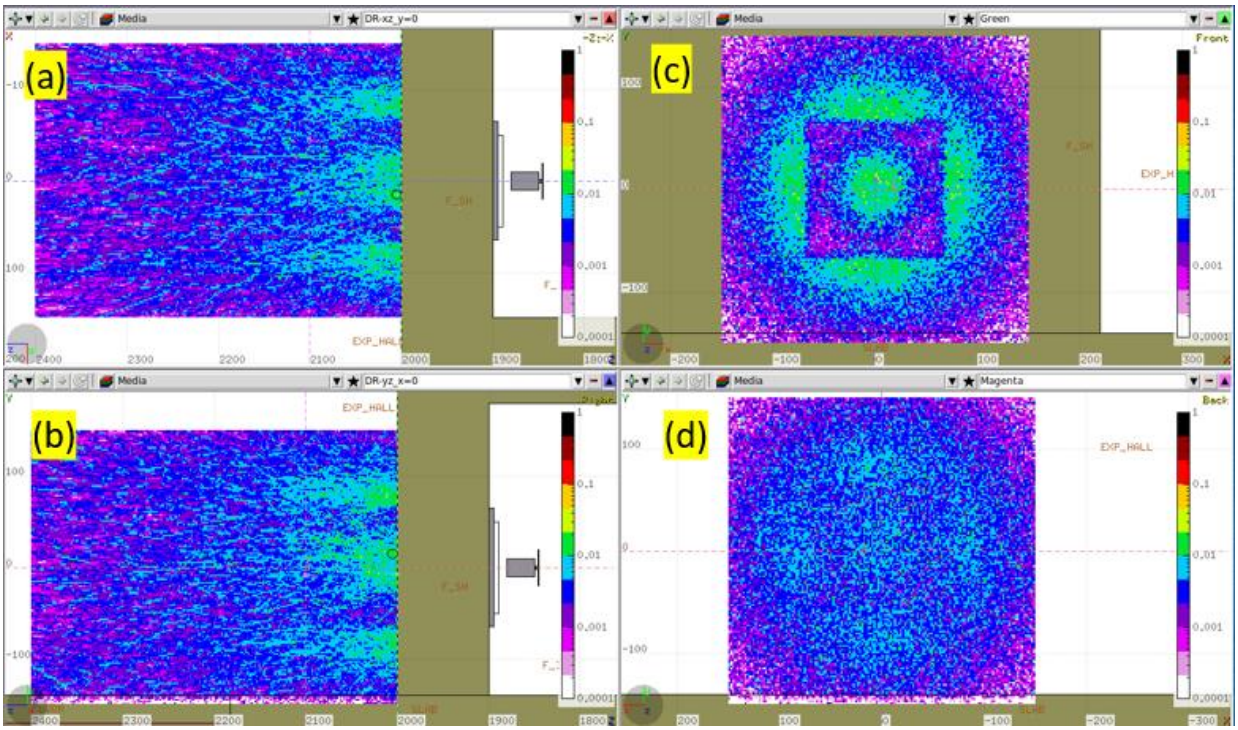

Figure 100 Total ambient dose equivalent rates on the exterior of the downstream wall of 27ID-F enclosure

3.12.6. Synchrotron Radiation Analysis

The 27-ID (HEX) beamline is a Superconducting Wiggler (SCW70) source and the calculations presented here are based on the following accelerator and insertion device parameters:

- Electron Energy: 3 GeV
- Stored beam Current: 500 mA
- SCW70:
  - Period Length: 70 mm
  - Number of Poles: 29
  - Max magnetic Field: 4.5 T
- Horizontal Fan entering the enclosures
  - 27ID-A, 27ID-C, 27ID-D and 27ID-E: 1.4 mradH
  - 27ID-F: 1.0 mradH
  - 27ID-B: 0.2 mradH

The SCW70 will be operating at nominal field of 4.3T and assuming 4.5T field is conservative, allowing for an over-field condition. The SCW70 spectrum calculated with STAC8 using the above parameters is given in Figure 101 and agrees very well with the calculated spectrum using a separate code SRW [4].

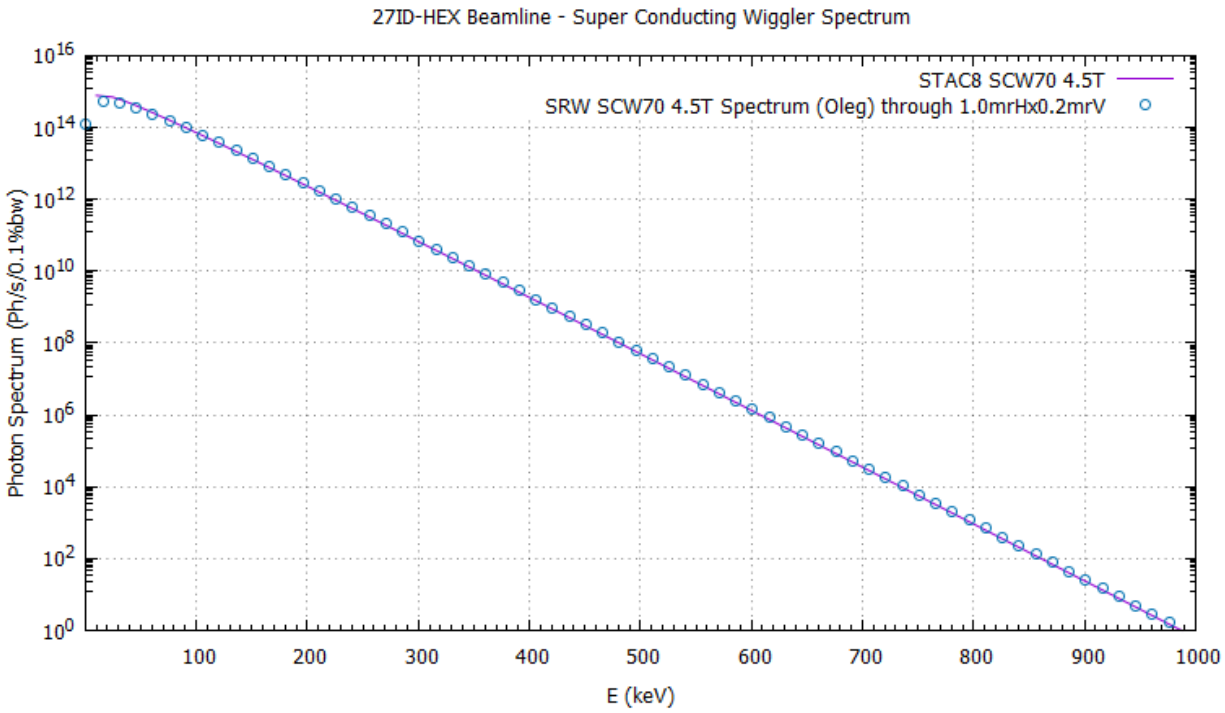

Figure 101 SCW70 photon spectrum as calculated by STAC8 and compared with spectrum generated using SRW by Oleg Chubar

The STAC8 code was used to calculate the ambient dose equivalent rates in the occupied areas outside of beamline enclosures. The build-up factor in the shield was included in the calculation. The results for the shielding analysis for white beam lead enclosures (27ID-A, C, D, E) are summarized in Figure 102 for (a) 25 mm lead lateral wall at 1.5 m from beam centerline (b) 31 mm lead lateral wall at 0.5 m from beam centerline (c) 22 mm lead thick roof at 2.1 m from beam centerline and (d) 50 mm lead downstream wall 1 m from scatter target. It shows that a lateral wall that is at least 1.5m from the beam centerline requires a thickness of 25mm Pb to keep the ambient dose rates below 0.05 mrem/h, shown in purple line in Figure 102. For the lateral wall that is 0.5 m from the beam centerline as in the case of 27ID-C enclosure, the Pb thickness increases to 31 mm. Figure 102(c) shows that a minimum lead thickness of 22mm is required for the roof of the lead white beam enclosures to keep the ambient dose rates below 0.05mrem/h. The results for the downstream wall are shown in Figure 102(d) . A thickness of 5 cm of lead will keep the ambient dose rates below 0.05mrem/h, except for forward scattering angles below approximately 20 degrees. Below 20 degrees the thicker 10 cm Pb downstream wall of 27ID-A enclosure and additional shielding on the downstream wall of 27ID-C, D, E enclosures which consist of a 3 cm Pb plate and 7 cm Pb guillotine will reduce ambient dose rates below 0.05 mrem/h in the forward direction.

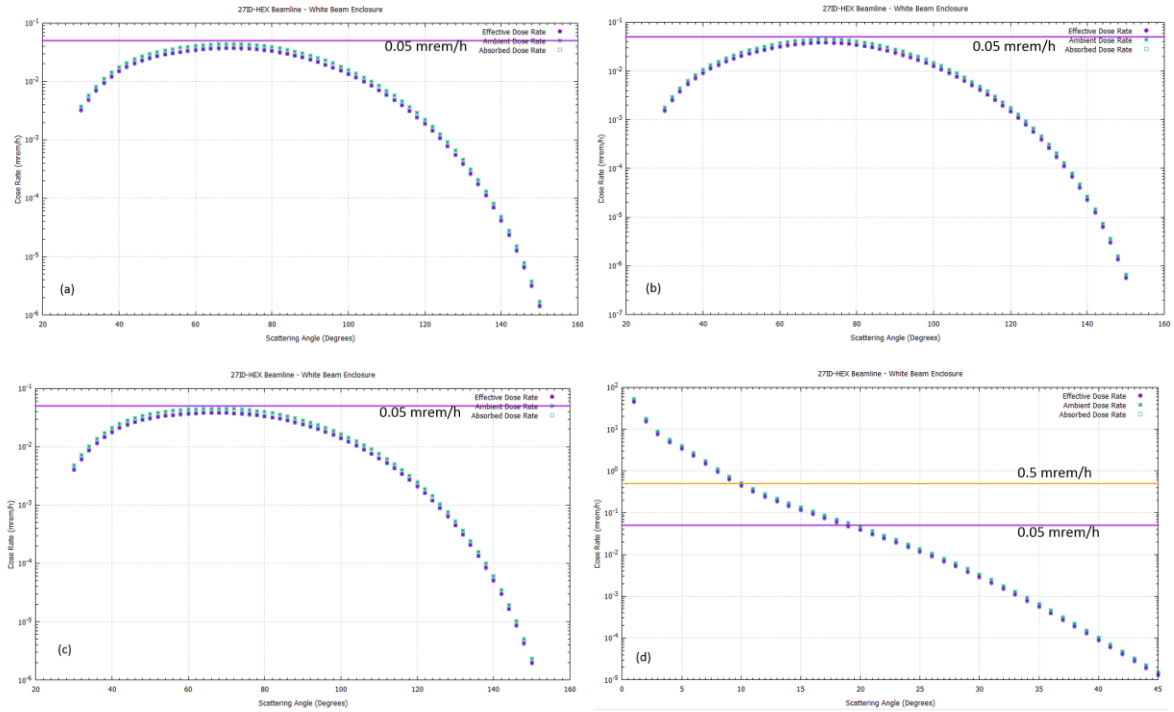

Figure 102. Photon dose rates on contact with the white beam enclosure walls and roof as a function of the scattering angle.

For the concrete enclosure 27ID-F, the SR calculation is carried out using an optimum scatter target assumed at 150 cm from the lateral wall and 1 m from the downstream wall. The results of the calculations are shown in Figure 103 for (a) lateral wall ignoring build-up in the 70 cm thick concrete (red trace) and (b) downstream wall - the purple plot with the (+) sign corresponds to 100 cm concrete and 10 mm Pb. The results indicate that at least 70 cm of concrete is required for the outboard lateral wall and 100 cm of concrete for the downstream wall with a local lead plate to cover small angle scattering. Figure 103 (a) shows that the ambient dose rates are underestimated by over two orders of magnitude without build-up factors in the concrete stressing the importance of build-up in the concrete.

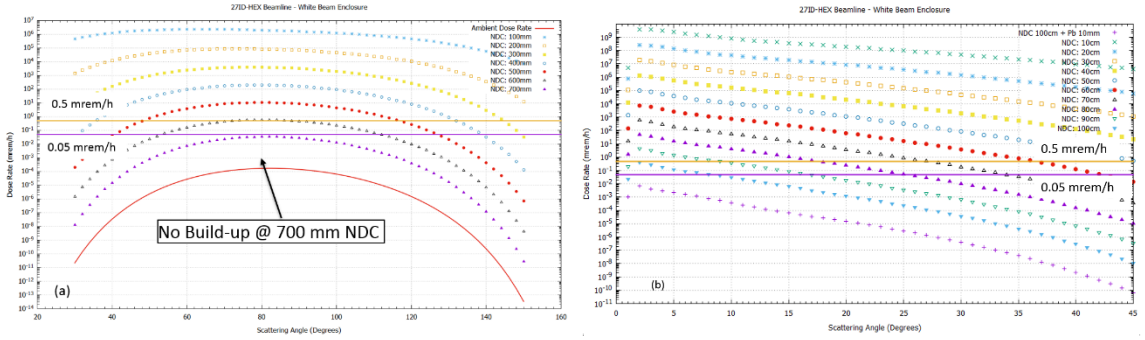

Figure 103. Ambient dose equivalent rates on the exterior of the lateral and downstream walls of 27ID-F enclosure as a function of the scattering angle for various thickness of the concrete.

This shielding should keep ambient dose rates in accordance with NSLS-II shielding policy for staff occupying areas inside the experimental floor and to any individual not involved in the operation of the facility (e.g. maintenance workers) occupying areas outside the satellite building. The requirement for the roof is 60 cm thick concrete assuming a 10% occupancy on the roof of the satellite building (lower dose rates for building maintenance staff) and 20% occupancy on the roof of the 27ID-F enclosure for NSLS-II staff. It is planned to restrict access to the enclosure roof since any equipment requiring routine maintenance will not be located on the roof. The shielding requirements for the inboard lateral wall and upstream wall are 64 cm and 65 cm respectively but it is planned to construct these with the same thickness as the outboard lateral wall.

The monochromatic beam enclosure 27ID-B has only SR entering the enclosure. The dose rates outside the 27ID-B enclosure when the monochromatic beams are scattered from an optimal target are discussed here. The scatter target is assumed located at 1 m from the lateral wall, 1m from the downstream wall, and 2 m from the roof. The ambient dose rates were calculated for the 4 operational energies of the 27-ID-HEX beamline corresponding to 39, 64, 75 and 117 keV, including higher harmonics and assuming any mirrors downstream from the side bounce monochromator are out of the beam, which is more conservative. As an example, results for the radiation shielding analysis for the lateral and downstream wall are given in Figure 104 (a) for 10 mm Pb thick lateral wall at 1.0 m from beam centerline and Figure 104(b) for 30 mm Pb thick downstream wall at 1.0 m from scatter target. It shows that for lateral wall that is at least 1.0 m from the beam centerline require a thickness of 10 mm Pb to keep the ambient dose rates below 0.05 mrem/h. Similarly, the minimum required thickness for the roof was calculated to be 10 mm Pb. For the downstream wall, a thickness of 30 mm of lead will keep the ambient dose rates below 0.05mrem/h, except for forward scattering angles below approximately 10 degrees. Below 10 degrees the monochromatic beam stop (30 cm x 30 cm) that is 35mm Pb thick will keep ambient dose rates below 0.05 mrem/h in the forward direction.

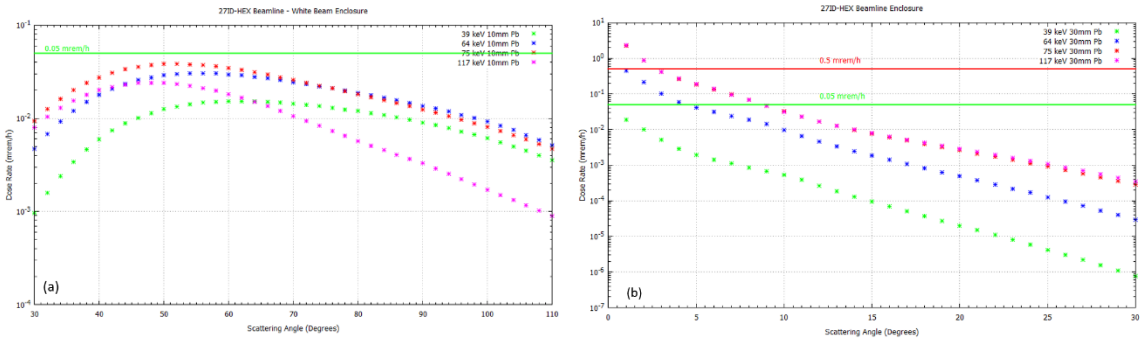

Figure 104. Photon dose rates on contact with the walls of 27ID-B enclosure as a function of the scattering angle and for four operational monochromatic beam energies.

3.12.6.1. Shielding Summary for each 27ID-HEX enclosure.

Table 18 below summaries the minimum shielding requirements for the 27ID enclosures based on the generic approach described above and considering both the GB and SR source of radiation.

Hutch	Upstream wall	Downstream wall	Outboard lateral wall	Inboard lateral wall	Roof
27-ID-A (FOE, White beam enclosure)	NA	10 cm Pb (floor to ceiling) + 3 cm Pb plate (140cm x 140cm) + 10 cm Poly (140cm x 140cm) + Pb Guillotine 2 cm thick (40cm x 40cm) all centered around GB centerline. Poly downstream of Pb	25 mm Pb	NA	22 mm Pb
27-ID-B (Mono beam enclosure)	10 mm Pb	30 mm Pb (floor to ceiling) + mono beam stop 35 mm Pb (30cm x 30cm) centered around the mono beam centerline.	10 mm Pb	Shared with 27-ID-C	8 mm Pb
27-ID-C (White beam enclosure)	25 mm Pb	5 cm Pb (floor to ceiling) + 3 cm Pb plate (120 cm x 120 cm) + 10 cm Poly (120 cm x 120 cm) + Pb Guillotine 7 cm thick (80 cm x 80 cm) all centered around GB centerline. Poly downstream of Pb.	25 mm Pb + 6 mm belly band (+/- 50 cm around beam centerline) + lateral local shielding (poly) near scatter target to be determined when component locations are finalized.	25 mm Pb	22 mm Pb
27-ID-D (White beam enclosure)	Determined by DS walls of 27-ID-C and 27-ID-B	5 cm Pb (floor to ceiling) + 3 cm Pb plate (140 cm x 140 cm) + 10 cm Poly (140 cm x 140 cm) + Pb Guillotine 7 cm thick (80 cm x 80 cm) all centered around GB centerline. Poly downstream of Pb	25 mm Pb	25 mm Pb	22 mm Pb
27-ID-E (White beam enclosure)	Determined by DS walls of 27-ID-D	5 cm Pb (floor to ceiling) + 3 cm Pb plate (140 cm x 140 cm) + 10 cm Poly (140 cm x 140 cm) + Pb Guillotine 7 cm thick (80 cm x 80 cm) all centered around GB centerline. Poly downstream of Pb	25 mm Pb	25 mm Pb	22 mm Pb
27-ID-F (White beam enclosure)	70 cm Portland concrete	100 cm Portland concrete (floor to ceiling) + 5 cm Pb plate (130 cm x 130 cm) centered around GB centerline	70 cm Portland concrete. 25 mm Pb thick labyrinths	70 cm Portland concrete. 20 mm thick lead door and labyrinths	60 cm Portland concrete. 22 mm Pb thick labyrinths

Table 18 Summary of shielding requirements for the 27ID-HEX beamline enclosures

References

1. T.T. Böhlen *et. al.* (2014) The FLUKA Code: Developments and Challenges for High Energy and Medical Applications" Nuclear Data Sheets 120, pp. 211-214.
2. Ferrari A. et al. (2005) FLUKA: a multi-particle transport code, CERN-2005-10, INFN/TC_05/11, SLAC-R-773.
3. Asano & Sasamoto (1994), Development Of Shielding Design Code For Synchrotron Radiation Beam Line, *Radiat. Phys. Chem*. 44, pp. 133-137.
4. O. Chubar and P. Elleaume (1998), Accurate And Efficient Computation Of Synchrotron Radiation In The Near Field Region, proc. of the EPAC98 Conference, 22-26 June, p.1177-1179.

3.13. Mature Scope Equipment – Not Included in the Base Scope

The base and mature scope can be categorized by branch. Mature scope equipment can be added to the beamline as additional funding becomes available.

Inboard branch (monochromatic beam to B-hutch)	**This branch is mature scope**. All components in this branch including, and downstream of the side-branch monochromator (see section 3.13.1).
Central branch (white and monochromatic beam to E- and F-hutches).	**This branch is base scope**. Upgrades can be made later with the addition of: • Focusing monochromator • Focusing mirror
Outboard branch (white beam to D-hutch)	**This branch is mature scope**

Table 19 Mature scope by branch

3.13.1. Monochromatic Side Branch Addition

The monochromatic side branch is not included in the base scope. Designs have been completed to include future equipment, as follows;

- Side branch monochromator
- Vertical focusing mirror
- Monochromatic beam shutter and transport pipe
- Diagnostics and vacuum system.

This section describes the planned design.

3.13.1.1. Side Branch Monochromator

The side branch monochromator will be a single-bounce (horizontal) bent Laue crystal. The monochromator uses the same two-theta angle, 5.8 degrees, as that used at the PDF beamline of the NSLS-II (see Figure 105 below, noting the two exit tubes on the left hand side for the diffracted beam (nearest the viewer), and the straight through beam). PDF will be commissioned in 2018. As such, we will study the performance of the PDF beamline after it becomes operational. If all is satisfactory, we plan to copy the same design for the HEX side branch monochromator.

It is expected that the side branch monochromator will be water cooled, provisions will exist in the DI water system in the A-hutch to add the cooling circuits easily.

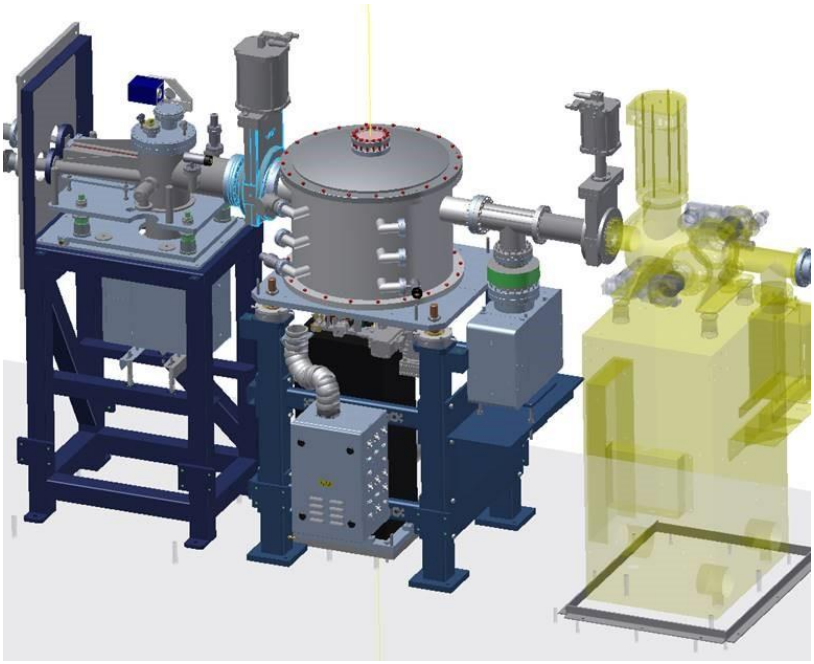

Figure 105 View of the PDF Beamline Side-Branching Monochromator

Table 20 shows the preliminary design parameters for the monochromator crystal.

Crystal	1	2	3	4
Reflection	111	220	311	511
X-ray energy (keV)	39.1	63.8	74.8	117.3
Asymmetry angle (deg.)	35	35	35	35
Thickness (mm)	3.0	5.0	5.0	5.0

Table 20 Preliminary specification for the side-bounce monochromator

We note that the HEX power density is less than that at PDF, and the fan size, 0.2 mrad x 0.2 mrad, is also less than the PDF fan size. Thus, we are confident that an adaptation of the PDF monochromator design, after being proven by experiment to be suitable for high-energy x-rays, can be used with little modification at HEX. Figure 106 below shows a top view, looking downstream showing the green diffracted beam.

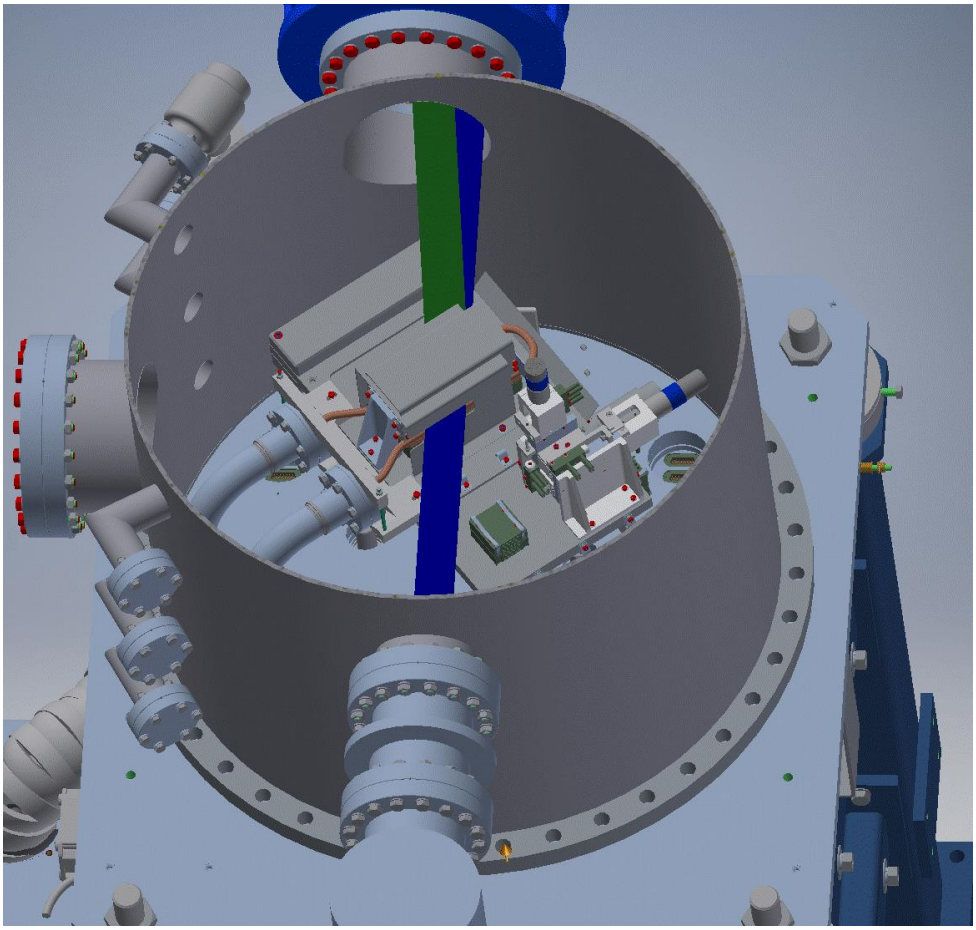

Figure 106 Internal view of the Side-branch Monochromator

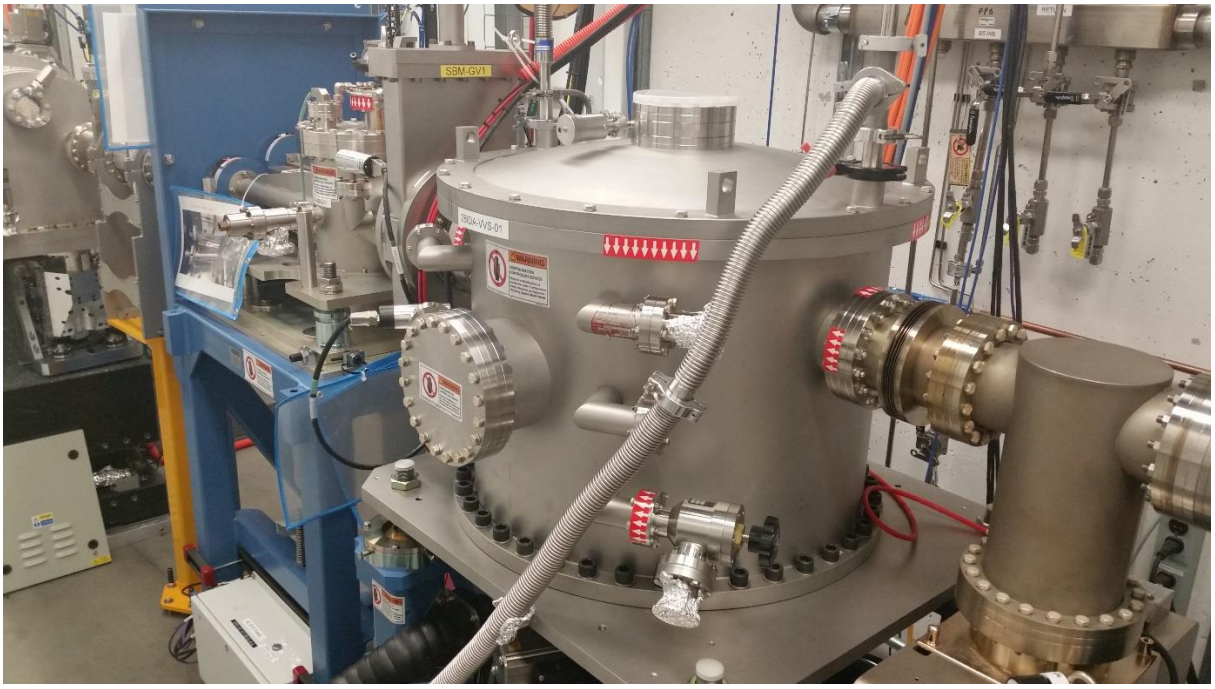

Figure 107 The installed PDF beamline side branch monochromator

3.13.1.2. Side Branch Focusing Mirror

A very similar mirror is described in Section 3.13.2.3. The two mirrors will be installed alongside each other, meaning that care will have to be taken to avoid space conflicts. The side branch VFM is in the bounce-up geometry.

3.13.1.3. Other Monochromatic Branch Components

The monochromatic branch will require a number of other components including a monochromatic beam shutter (the standard NSLS-II device would probably be suitable; any required modifications would be minor). In addition, a shielded transport pipe would be needed from the A-hutch to the B-hutch (this would be monochromatic and therefore less shielding is required compared to the HEX white beam shielded pipes). The branchline would also require diagnostic components and the usual vacuum equipment. The detailed design of these components is left until the branch is funded, although it is very important to be sure that this branchline is feasible and practical without unnecessary additional expense, and without impacting the components installed for the other branch(es).

3.13.2. Center Branch Additions

3.13.2.1. Center Branch Focusing Monochromator

High-energy x-rays are especially suitable for in-situ powder diffraction and PDF measurements, the bread-and-butter experiment performed at the highly-productive XPD beamline The idea of sagittal focusing using Laue crystals was originally developed at the NSLS. Simulations show that it can be implemented at HEX to provide the high-energy x-rays at a flux of 10^{13} ph/s. This allows EDXD (high spatial resolution and depth resolution, low angular resolution) and ADXD (high angular resolution, low spatial resolution, no depth-resolution) on the same sample, greatly enhancing the HEX scientific programs.

The center branch of HEX will be designed with a high-energy focusing x-ray monochromator that, together with a vertically focusing mirror, focuses the monochromatic beam in the E experimental enclosure. The building of the focusing monochromator is not in the current scope. We note that the design of the beamline (FOE layout, beam transport, hutches) must accommodate the future addition of the focusing monochromator. The design effort for the focusing monochromator will be limited to preliminary design. Engineering design and design review of the monochromator design will be required before commencement of procurement/installation in the future, if and when funds become available

X-ray Optics Principles of the Focusing Monochromator

The idea of sagittal focusing using Laue crystals was originally developed at the NSLS a decade ago (Zhong et al. 2001a,b, Zhong et. al. 2002, Zhong et al. 2003). The extent of such focusing is similar to that of sagittal focusing by a Bragg crystal, except for a factor related to the asymmetry angle. The anticlastic bending facilitates the use of inverse-Cauchois geometry in the meridional plane to provide better energy-resolution and to increase the photon flux by an order-of-magnitude compared to traditional sagittal focusing with Bragg crystals. Furthermore, sagittal focusing by a Laue crystal is preferred over a Bragg crystal at x-ray energies above 30 keV because, unlike Bragg crystals, the length of the beam's footprint on a Laue crystal is small and insensitive to energy. The conditions imposed on the asymmetry angle of the Laue crystal to achieve simultaneous sagittal focusing and inverse-Cauchois

geometry in the meridional plane were derived by NSLS scientists for both single-crystal and double-crystal fixed-exit sagittal focusing monochromators.

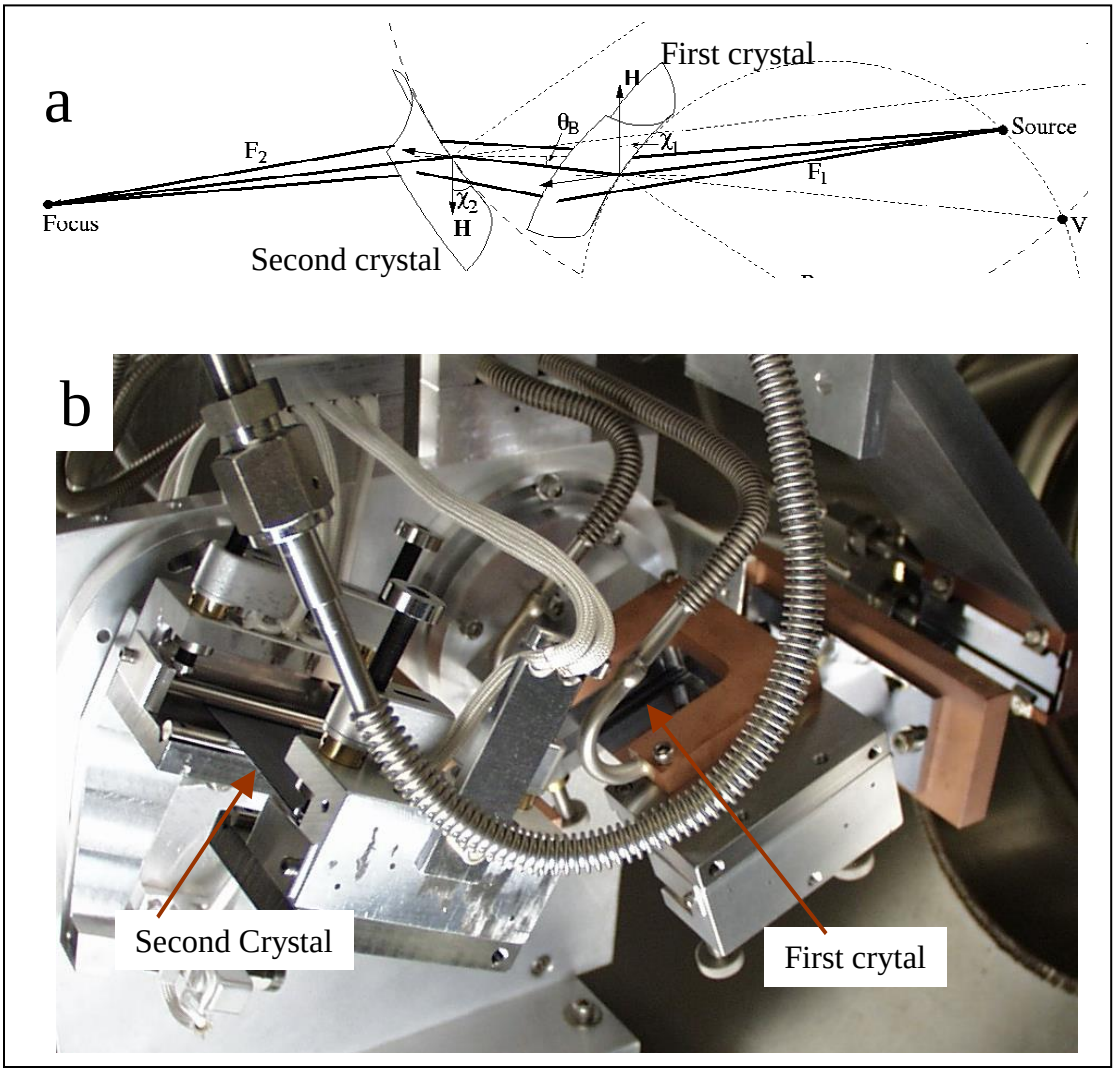

Figure 108 The mechanism for sagittal focusing with asymmetric Laue crystals

Figure 108 shows the mechanism for sagittal focusing with asymmetric Laue crystals;
a) bending of the crystals causes precession of the diffraction vectors (H) around the axis of sagittal bending, and the resulting focusing of the diffracted beams.
b) photograph of a monochromator installed at the NSLS X17B1 beamline.

The use of bent asymmetric Laue crystals to sagittally focus synchrotron x-rays from 15 to 50 keV have been tested at the NSLS X15A, which is a standard NSLS bending magnet line. A four-bar bender, bending a rectangular planar crystal, produced the necessary sagittal- and meridional-bending for this unique application. A double-crystal sagittally focusing monochromator, based on this concept, has been constructed and tested, and was in use at the X17B1 beamline for about 10 years, providing 67 keV x-rays (see figure 4.10). It focuses a horizontal divergence of 3 milli-radians to a horizontal dimension of about 0.4 mm. The x-ray flux-density at the focus was a few hundred times larger than that of unfocused x rays.

The same concept was successfully used at the x-ray powder diffraction (XPD) beamline of the NSLS-II, the X7B beamline of the NSLS, and at InSiTu (F2) beamline at the CHESS facility.

Design Ideas and Goal

As with the imaging monochromator discussed above, a small offset of 25 mm is chosen to minimize the distance between the two crystals, affording compact design and higher stability. The XPD monochromator has the second crystal and its bender in the air. This design was experimentally proven to be convenient. We will consider this option for the focusing monochromator. As with the imaging monochromator, the focusing monochromator and its beam stop must be removable and EPS-interlocked to allow white-beam operation.

The basic parameters and constraints for the focusing monochromator is listed below:

- Source to monochromator distance (f1): 33.210 m
- Monochromator to sample distance (f2): 25.787 m (E-hutch), 70.782 m (F-hutch)
- Focal length f0=1/(1/f1+1/f2)= 14.5 m (E-hutch), 22.6 m (F-hutch)
- Adjustable x-ray energy 30-100 keV, the design should maximize performance at approximately 65 keV

The goal is to focus the 1 milli-radians horizontal fan to approximately one mm horizontal size in the E experimental hutch. For diffraction, it is desirable to have energy resolution of about 10^{-3} dE/E.

The baseline design is a monochromator similar to that used by XPD, with 0.6 mm thick crystals. We will consider using 4 mm thick SiC filter to control heat load on monochromator. This filtering scheme is expected to reduce the heat-load sufficiently to allow water-cooling instead of cryogenic cooling of the first crystal, thus reducing cost and simplifying operations.

As discussed previously, the modified Boomerang design allows for one-motion changing of energy. This option will be considered for the engineering design.

Figure 109 shows the reciprocal space configuration of the Silicon crystal for the proposed sagittal-focusing Laue monochromator. Si 111 and 311 reflections are considered. This design is the same as that of the XPD monochromator at the NSLS-II.

- The crystal surface normal is the 100 direction.
- The bending axis points to the 011 direction.
- Si 111 and 311 reflections are accessible with asymmetry angles of 35.3 and 64.8 degrees, respectively.

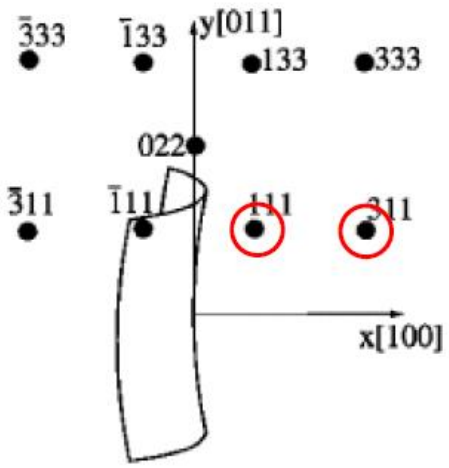

Figure 109 Reciprocal space configuration of the Silicon crystal for the proposed sagittal-focusing Laue monochromator

3.13.2.2. Performance Simulation using 111 reflection

A simulation was performed for the 111 reflection on 100 crystal (the asymmetry angle is 35.3 degrees). The simulation assumes that the monochromator focuses the beam at the center of E experimental enclosure. Both crystals are assumed to be 0.6 mm thick. The distance between the crystals, defined as shift, is calculated assuming a 25 mm offset between the monochromatic beam and the white beam.

Energy (keV)	30	40	50	60	70	80	90	100
Bragg angle (deg)	3.779	2.833	2.266	1.888	1.618	1.416	1.259	1.133
Shift (mm)	188	251	315	378	442	505	469	632
Bending Radius (mm)	2208	1656	1325	1104	947	828	736	662
dE/E ($x10^{-3}$)	0.47	0.82	1.3	1.9	2.3	3.4	4.3	5.4
Integrated Reflectivity (micro-radians)	23	35	46	54	54	49	42	35
Reflectivity (%)	75	97	92	89	76	60	46	35
Flux at Focal spot (10^{12}ph/s/ vertical mm)	2.2	9.1	16	20	17	11	6.0	3.2

Table 21 Focusing mono Si 111 crystal parameters vs energy

Table 21 shows a simulation of shift, sagittal bending radius, energy resolution, crystal reflectivity and integrated reflectivity, and flux at focal spot per 1 mm of vertical beam (assuming that the vertical focusing mirror is not used) as a function of x-ray energy. The simulation assumes using the 111 reflection and that the monochromator focuses 1 mrad of horizontal beam at the center of E-hutch experimental station.

It is seen that the 25-mm offset affords a compact monochromator design with a distance of 631 mm between the two crystals for 100 keV x-ray energy. We will extend the length to about 1 m to allow for extension of x-ray energies to 150 keV.

The sagittal bending radius for focusing 100 keV x-rays is 663 mm. This dictates that the crystal thickness should be smaller than 0.63 mm using the rule-of-thumb that the smallest cylindrical bending radius for a Silicon crystal is about 1000 times the thickness of the crystal. This is the reason for our choice of 0.6 mm crystal thickness in the base design.

Figure 110 shows the simulated photon flux as a function of x-ray energy for focusing in the E hutch using the 111 reflection.

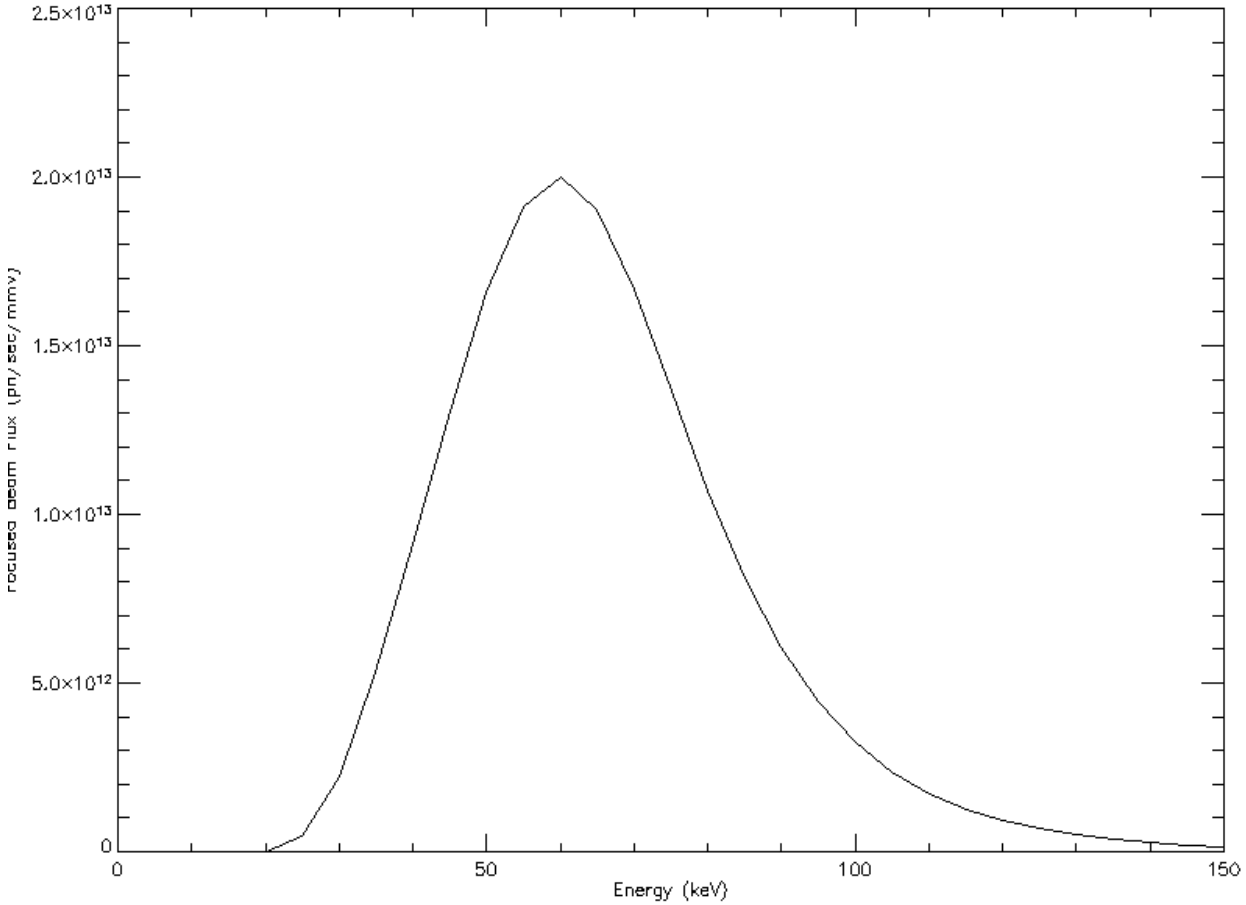

Figure 110 Simulated photon flux as a function of x-ray energy for focusing in the E hutch using the 111 reflection

Figure 111 shows the simulated energy resolution as a function of x-ray energy for focusing in the E hutch using the 111 reflection.

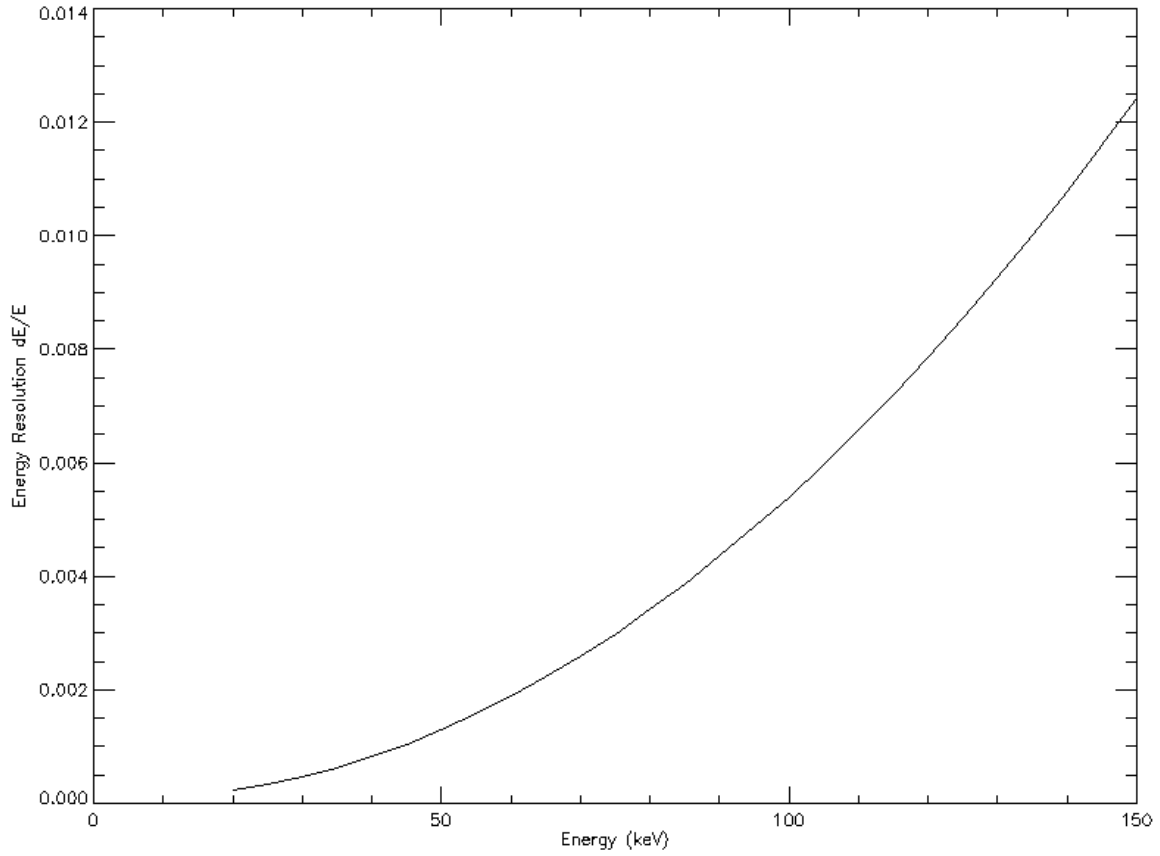

Figure 111 Simulated energy resolution as a function of x-ray energy for focusing in the E hutch using the 111 reflection

It is seen from the figure above that the energy resolution at 50 keV exceeds 10^{-3}. This is due to the combination of two effects: a. as the energy increases, the bending radius must be smaller to maintain the same focal point in the E experimental station, resulting in proportionally increased rocking curve width; and b. higher x-ray energy results in smaller Bragg angle. To achieve higher resolution, especially for high x-ray energies, we consider an additional reflection accessible on the same crystal next.

High-resolution 311 reflection

Figure 112 shows the experimental rocking curves for the proposed sagittally bent Laue crystal, bent to 0.7 m radius, at 67 keV x-ray energy. It shows that the 111 reflection offers a good reflectivity and moderate resolution (proportional to rocking curve width, about 150 micro-radians. Interestingly, the 311 reflection, with asymmetry angle of 64.8 degrees, delivers a higher resolution beam with less flux. The 311 reflections offer higher resolution than 111 for three reasons: its factor-of-three smaller rocking curve width for the same bending radius; it requires larger bending radius that 111 due to larger asymmetry angle, further reducing the rocking curve width; its factor-of-two larger Bragg angle results in smaller dE/E for the same rocking curve width. We thus consider using the 311 reflection (asymmetry angle 64.8 degrees) to achieve about an order of magnitude higher resolution beam that 111 reflection. This can be especially useful for high x-ray energies from 50 to 100 keV.

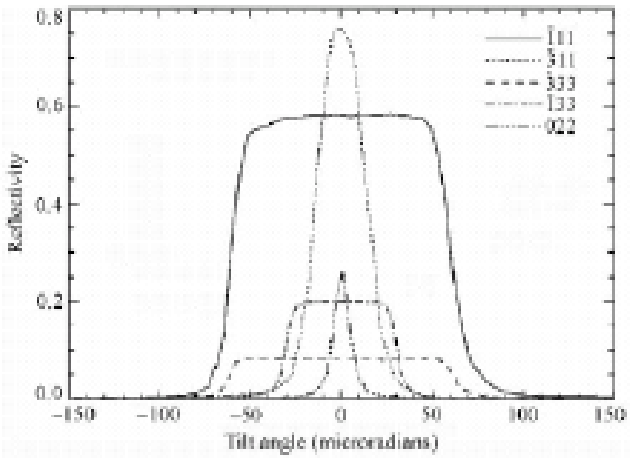

Figure 112 Experimental rocking curves, acquired at the NSLS X17B1 beamline, for the proposed sagittally bent Laue crystal, bent to 0.7 m radius, at 67 keV x-ray energy

A simulation was performed for the case of using the 311 reflection on 100 crystal. As with the 111 reflection, the simulation assumes that the monochromator focuses the beam at the center of E-hutch experimental enclosure. Both crystals are assumed to be 0.6 mm thick. A 25 mm offset is assumed between the monochromatic beam and the white beam for calculating the required shift between the crystals.

Energy (keV)	30	40	50	60	70	80	90	100
Bragg angle (deg)	7.249	5.431	4.342	3.618	3.100	2.712	2.411	2.170
Shift (mm)	96	130	164	197	230	263	296	329
Bending Radius (mm)	6627	4970	3976	3313	2840	2485	2209	1988
dE/E ($x10^{-4}$)	0.42	0.34	0.43	0.97	1.5	2.4	3.4	4.6
Integrated Reflectivity (micro-radians)	0.40	1.1	1.8	2.5	3.1	3.7	4.3	4.9
Reflectivity (%)	0.11	0.38	0.62	0.76	0.84	0.89	0.91	0.92
Flux at Focal spot (10^{11}ph/s/ vertical mm)	0.31	0.63	2.2	4.1	5.5	6.3	6.5	6.3

Table 22 Focusing mono Si 311 crystal parameters vs energy

Table 22 shows a simulation of shift, sagittal bending radius, energy resolution, crystal reflectivity and integrated reflectivity, and flux at focal spot per 1 mm of vertical beam (assuming that the vertical focusing mirror is not used) as a function of x-ray energy. The simulation assumes using the 311 reflection and that the monochromator focuses 1 mrad of horizontal beam at the center of the E-hutch experimental station.

Comparing Table 21 with Table 22 shows that 311 indeed offers an order of magnitude higher resolution than 111 reflection, at the expense of commensurately smaller flux. We note that the 311 reflection requires a very compact monochromator, with a distance of 96 to 325 mm between the two crystals for tuning the x-ray energy from 30 to 100 keV. Table 22 shows that the smallest bending radius is about 2 meters. Thus for a stand-alone device, one can consider using a thicker crystal to offer higher mechanical stability and higher performance at high x-ray energies. As noted before, the current crystal thickness, 0.6 mm, is optimum for the 111 reflection.

Figure 113 shows the simulated photon flux as a function of x-ray energy for focusing in the E hutch using the 311 reflection.

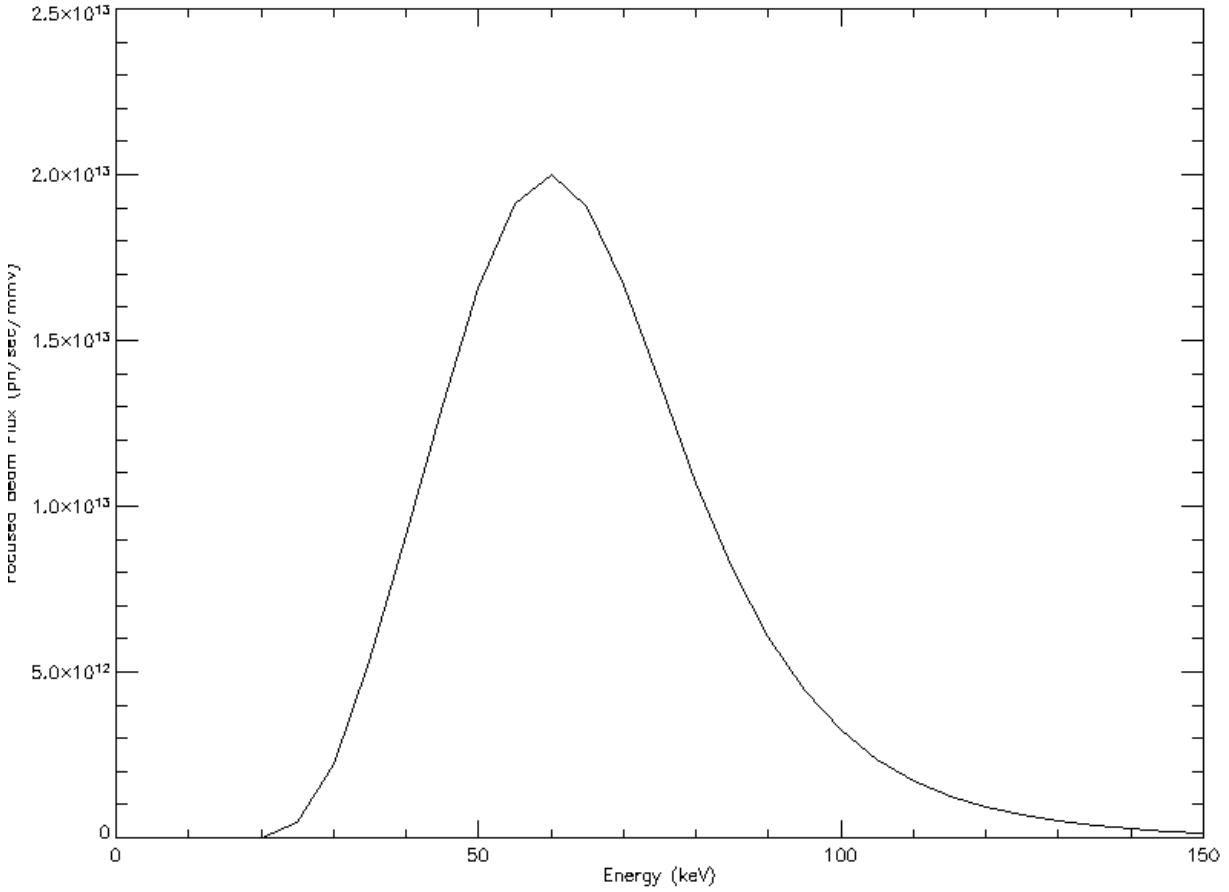

Figure 113 Simulated photon flux as a function of x-ray energy for focusing in the E hutch using the 311 reflection

Figure 114 shows the simulated energy resolution as a function of x-ray energy for focusing in the E hutch using the 311 reflection.

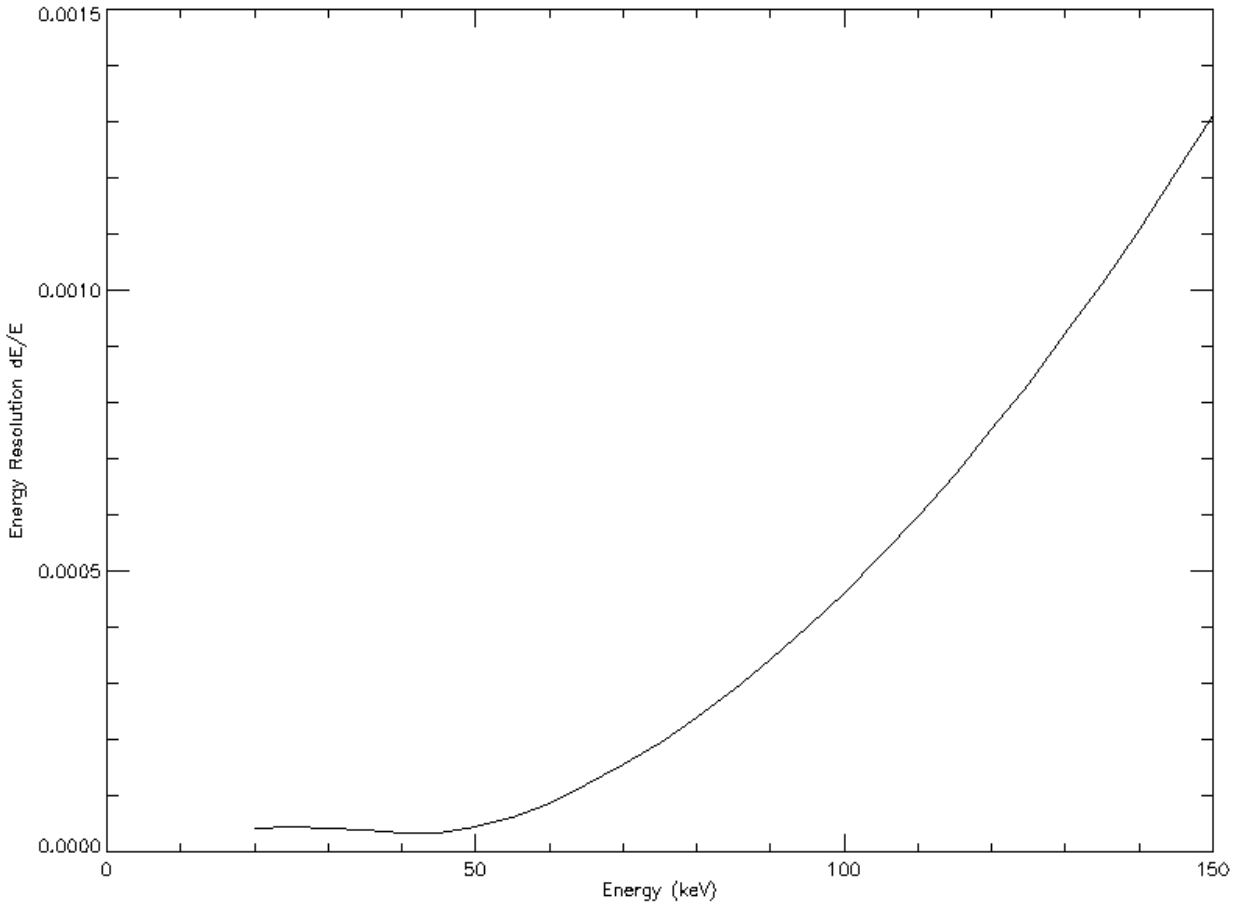

Figure 114 Simulated energy resolution as a function of x-ray energy for focusing in the E hutch using the 311 reflection

We note that while the focusing monochromator is similar in design to that at XPD, the 311 reflection, which is not feasible at XPD due to its cooling design, is important for HEX that desires to achieve x-ray energies of 100 keV and above. Thus, we would focus on making the 311 reflection accessible for the engineering design in the future. We believe that by using simpler water-cooling, as opposed to the cryogenic cooling employed at XPD, it would be feasible to rotate the first crystal by about 25 degrees to access both the 111 and 311 reflections.

3.13.2.3. Center Branch Focusing Mirror

The central branch focusing mirror is a simple bounce-down, vertically focusing, mirror. Given the source and focus distances, a simple meridional cylinder shape is required. The mirror will be fitted with a mechanical bender in order to tune the focus position. Cooling is not required since this will be used only for monochromatic beam.

Figure 115 shows the two vertical focusing mirrors used at the XPD beamline, and the PDF side-branch. The HEX beamline is designed to accommodate two mirrors, side-by-side for the central and monochromatic branches.

Figure 115 View of the two vertical focusing mirrors at the XPD beamline

3.13.3. White Beam Branch Additions

The white beam branch is very basic; in mature scope this branch will have no mirror or monochromator. The simple addition of diagnostics and a white beam shutter in the FOE, along with any necessary beam conditioning equipment in the D-hutch will allow the branchline to operate.

4. End Station

4.1. Introduction

HEX experimental system will eventually consist of three independently operating branches:

- the white beam branch (feeding the D-hutch),
- the center branch (feeding the E and F-hutches), and
- the monochromatic side branch (feeding the B-hutch).

The white beam branch and center branch are white-beam compatible. The side branch offers high-energy x-rays at fixed energy for x-ray diffraction and pair distribution function measurements.

The center branch is in the initial scope. The branch consists of experimental station E inside the storage ring for ADXD, and experimental station F in the satellite building for combined imaging, ADXD and EDXD. The base scope of the project is as follows;

- The white beam branch experimental hutch (D-hutch) is in scope, but the fit-out of this hutch is not in scope,
- The monochromatic side branch hutch (B-hutch), and the fit-out are not in the current scope.

The center branch provides high x-ray energies up to 150 keV for phase contrast x-ray imaging in planar and CT modes. The resolution of about 10 microns combined with a field of view of 100 mm is suitable for most industrial batteries, as well as a wide range of other engineering samples. The ability of phase contrast mechanisms to provide information on microstructure provides a new way for studying batteries.

The center branch will be equipped with special sample environments such as a battery cycler. The design of the end-station will be compatible with the inclusion of equipment such as a large volume press owned by the COMPRES program. The imaging detectors will consist of two types of camera systems: CCD-based cameras for high spatial resolution and a CMOS-based camera for very high frame rate.

4.2. Experimental Station F in Satellite Building (in Scope)

The overall size and design concept of the HEX satellite building is similar to that of the Hard X-ray Nanoprobe (HXN) satellite building at the NSLS-II. The hutch F design is similar to that of JEEP beamline at the Diamond Light Source, with one experimental enclosure consisting of concrete walls and roof.

Techniques offered at the F station include EDXD (with multi-element Ge detector in the future), ADXD, small-angle x-ray scattering (SAXS), and imaging. In the future, SAXS with a sample in hutch E and detector in hutch F can be performed. Imaging capabilities will offer a unique large field of view (especially vertical) of 100 mm horizontal by 20 mm vertical for imaging. Being white-beam compatible, a filtered white beam can be used at the F station for high-speed imaging using filters in the FOE and those in the endstation. The endstation allows for propagation phase contrast imaging that requires a large distance of up to 15 meters from the detector to the sample.

The end-station will feature the following:

- Large hutch size:5 m wide by 20 m long with 8’ x 8’ access doors.
- High ceiling
- Dedicated gas exhaust system for battery and fuel-cell research
- Large-scale samples and/or equipment
- Accommodates large volume press
- Accommodates complex experimental set up such as 3D metal printing
- (Thermal) mechanical loads & contained processing cells
- Accommodates large mechanical testing equipment, load frame/translation stage

The design concept for the end-stations in the F-hutch features a modular concept, with three movable detector modules and a removable sample module.

Figure 116 below shows the beam conditioning table, the sample stack, and the interchangeable experimental tables (going from right to left).

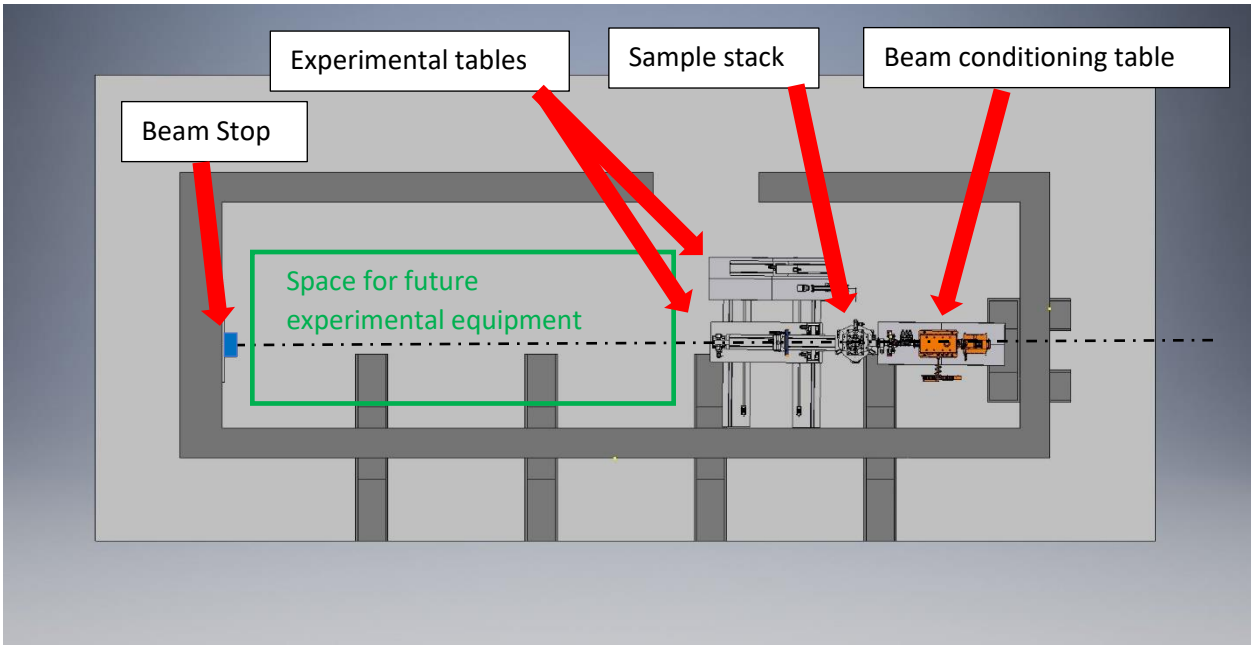

Figure 116 Design of the experimental setup in the F-hutch

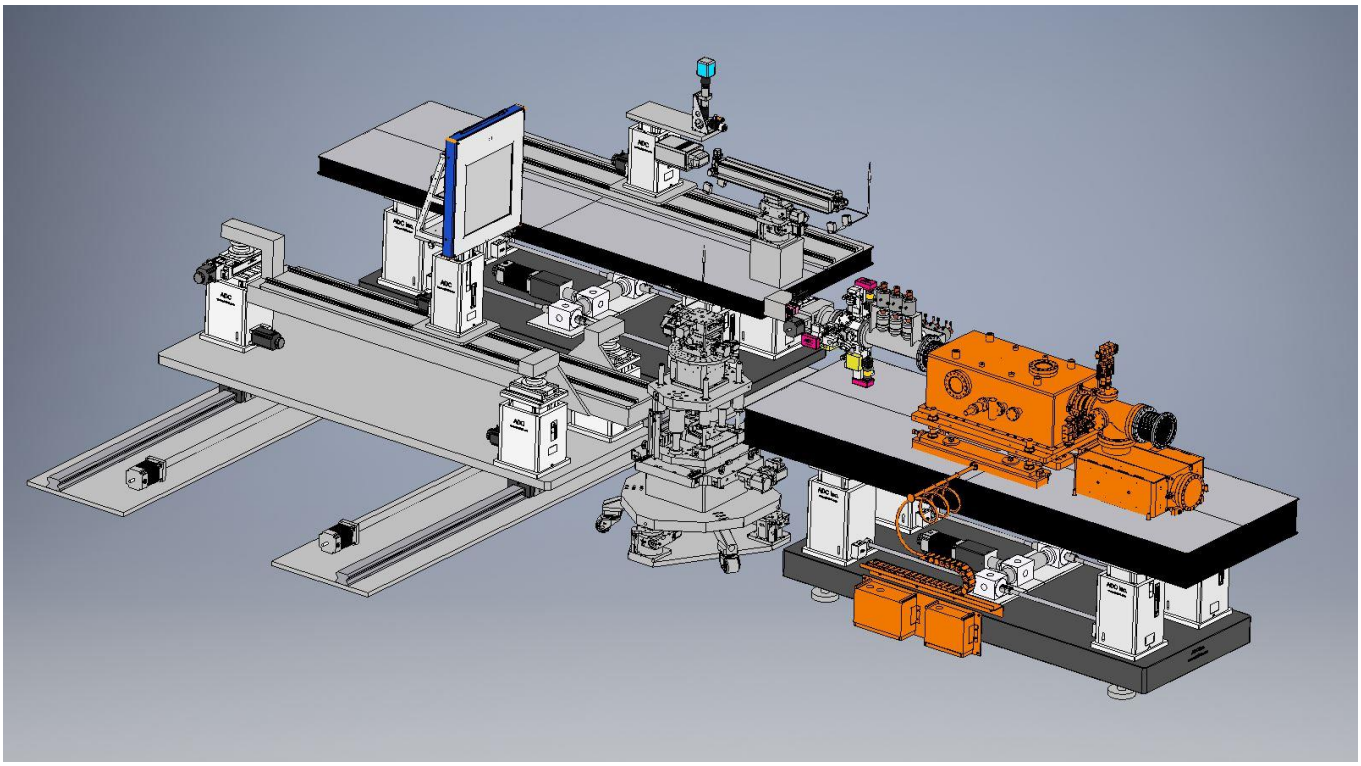

Figure 117 Detail of the experimental setup in the F-hutch

Figure 117 shows the detail of the experimental setup, the KB (focusing) mirror is in the orange tank on the beam conditioning table, the sample stack is separately supported, and may be removed relatively easily with jacking casters to allow access for specialist sample environments, and then on the left hand side, the interchangeable experimental tables are shown. Closest is the ADXD table with a large area detector, and the furthest table supports the EDXD equipment, and the imaging detectors.

4.2.1. Single-detector EDXD system

The single-detector system was decommissioned from the NSLS X17 beamline in late 2014 and subsequently commissioned at the APS 6-BM beamline in mid-2015. The high x-ray energy provided by the APS bending magnet makes in-situ energy dispersive x-ray diffraction (EDXD) possible inside a battery. In contrast to conventional x-ray techniques, where the diffraction angle is varied, in EDXD the incident beam, diffracted beam and sampling volume are fixed (see

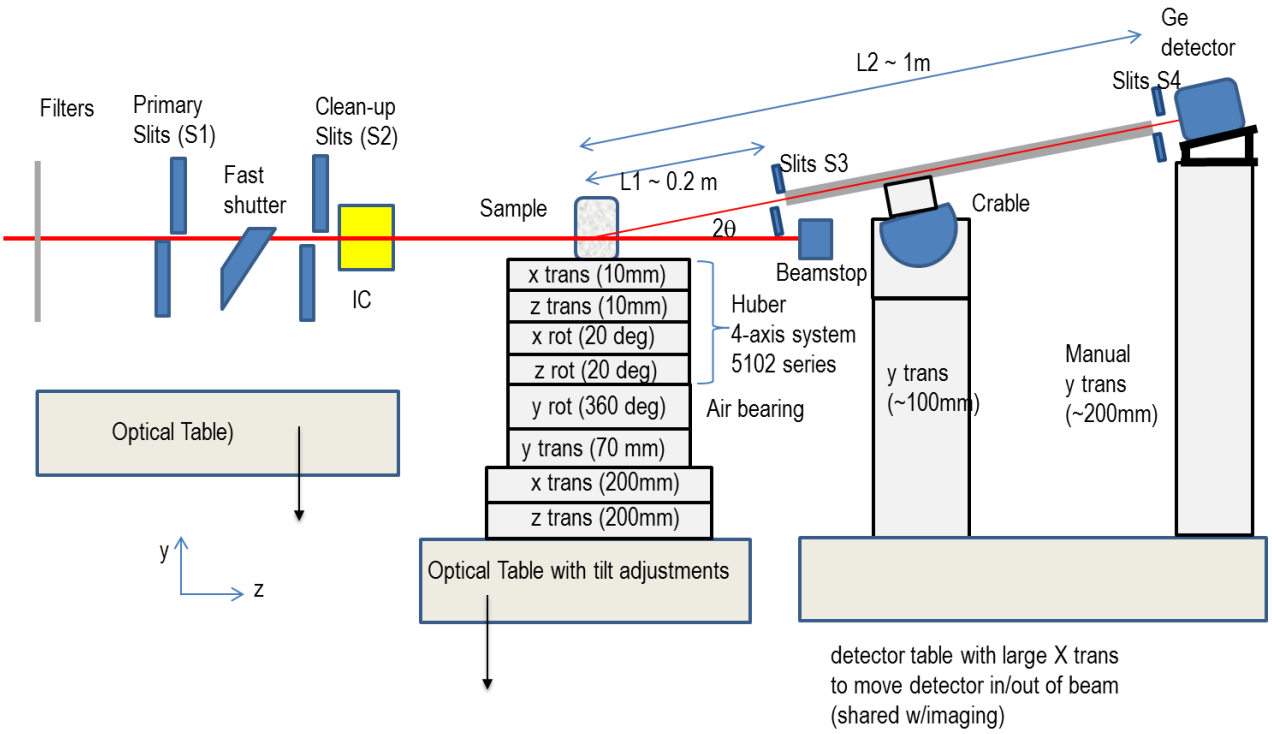

Figure 118 for a schematic of the experimental geometry). The scattering geometry is extremely stable and sample profiling is accomplished by micro positioning of the sample (e.g. battery). The long diffracted-beam path (~1 m) facilitates a well-collimated diffracted beam to define a small gauge volume inside the battery. The volume is currently as small as 10 microns (x) by 10 microns(y) by 100 microns (z, along the beam direction). This volume is extremely small compared to the battery's length scale of up to 50 mm by 50 mm by 200 mm. The sample is micro-swept through this gauge volume while the EDXD spectra are collected by a high-resolution energy-dispersive-Ge detector.

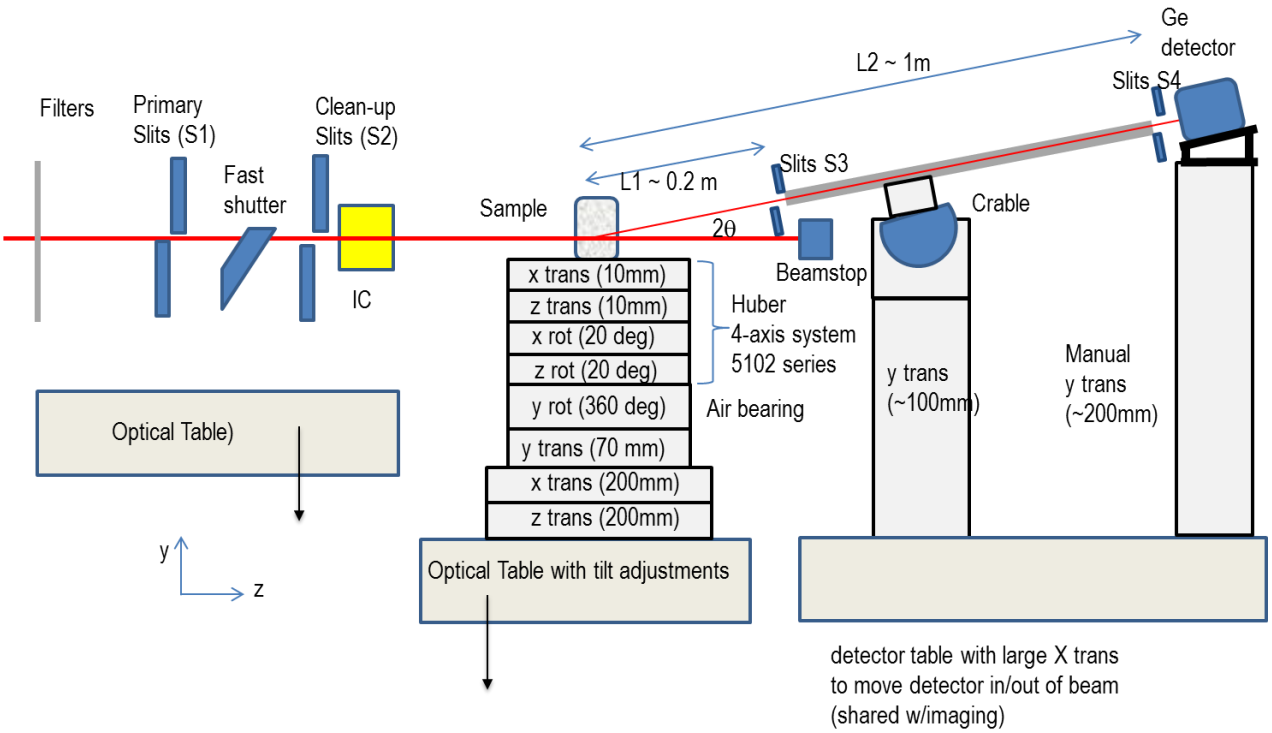

Figure 118 Configuration of the single-detector EDXD system with adjustable two-theta angle

Figure 119 shows a picture of the beam-conditioning components such as the fast-shutter, beam-defining slits (slit 1), clean-up slits (slit2), and ion chamber, currently in use at beamline 6-BM at the APS (Chicago). The beam-transport tube is fabricated with X95 hardware with Lead shielding insert in the bore.

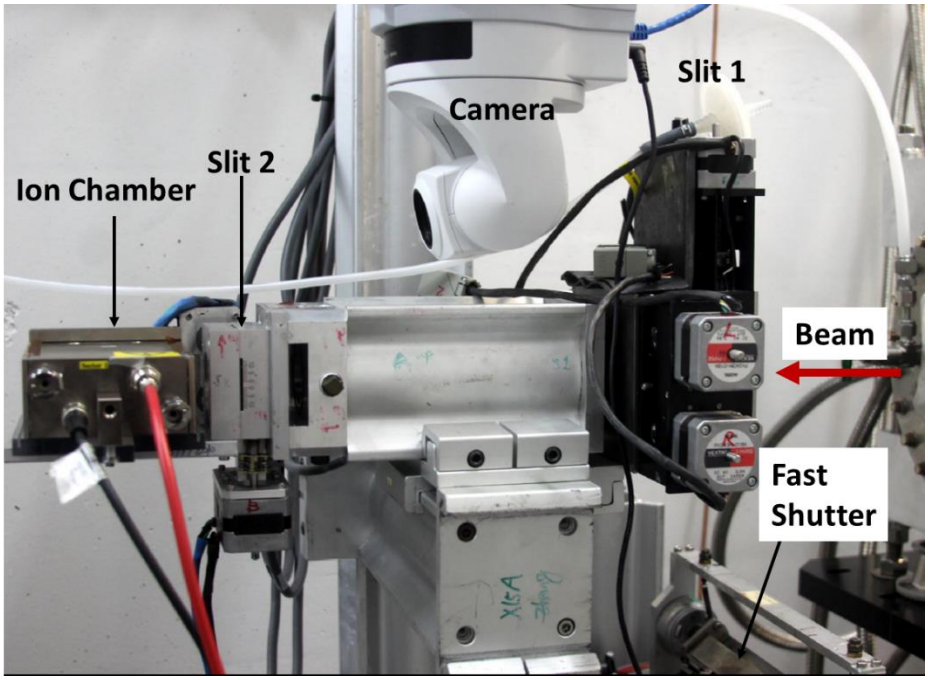

Figure 119 Picture of the fast-shutter, beam-defining slits (slit 1), clean-up slits (slit2), and an ion chamber

Figure 120 shows the sample stage and the two-theta arm. Note that the bore of the 1-m long X95 for the two-theta arm is also shielded to minimize noise in the detector.

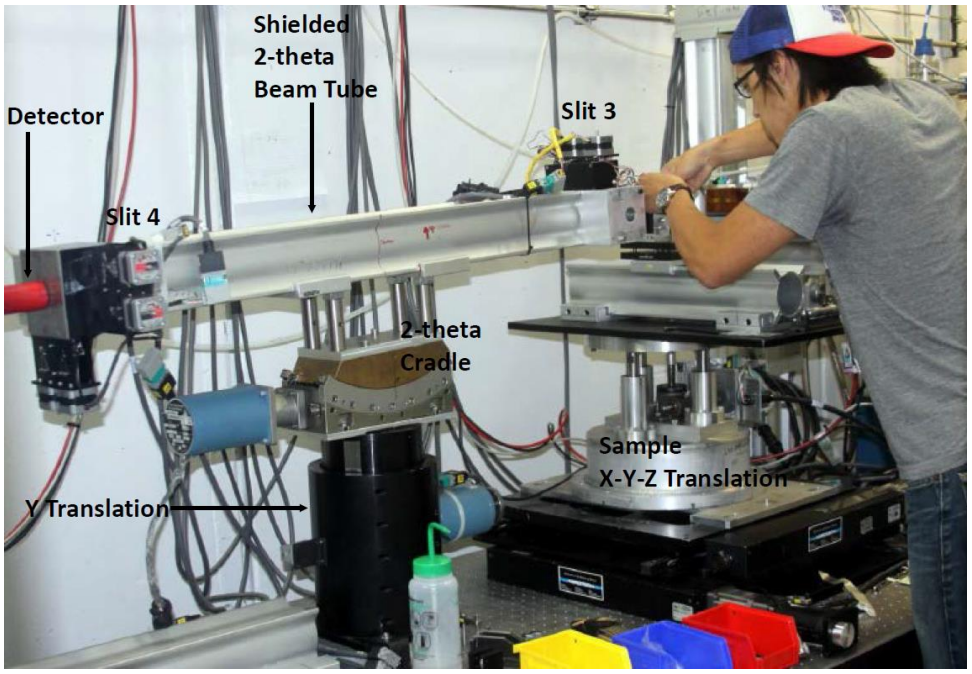

Figure 120 Picture of the sample XYZ translation, two-theta arm with slits 3 and 4

The current system is based on a general purpose two-theta arm with 1-meter length and a vertical scattering geometry. While it offers the most flexibility for proof of principle experiment, the size of the sample, sample heating, and charging equipment is severely limited. The most important flexibility offered by the current system is the ability to change the two-theta angle. Changing the two-theta angle changes the energy of the diffracted beam for the same sample reflection. We experimented with different two-theta angles of 3, 4, 6 and 12 degrees for various battery systems, and found that a four-degree two-theta allows a good balance between the sample attenuation, gauge volume and achievable d-spacing.

A new end-station is planned. With the experience we have gained on the current system, we plan to design and construct the new system based on three optical tables. The beam defining slit, the sample x-y-z stage, and the diffracted beam slit will be located different tables. The detector, its motorized positioning system and its shielding will be supported separately from the two-theta arm to achieve better stability of the two-theta angle.

The individual components are discussed below in the order of the beam travel:

a. Incident beam slit and beam-conditioning system

A new optical table will be acquired. The table will feature a support stand with adjustable height. This optical table is located at the front of the experimental station. It is used to support the incident beam slit and beam-conditioning system.

The incident beam slit defines a well-collimated white beam. The current system uses an incident beam slit consisting of two slits. Each slit has four jaws of 10 mm thick Tungsten. The first slit is used to define the beam, while the second one, 200 mm downstream of the first one, is set to be slightly larger than the first one to reject the scattering by the first slit. We will specify a similar incident beam slits, but with vacuum compatibility to avoid ozone corrosion damage to the mechanisms.

The incident beam slit, along with filters and ion chambers, form the beam condition system as shown in Figure 119. Note that the beam conditioning system is designed to accommodate EDXD, ADXD, and imaging. Thus the maximum aperture sizes for slits and ion chambers are specified to accommodate the imaging beam.

The specification for the beam conditioning system is shown in Table 23. The reason for the specification of the micro-focusing optics is discussed later in ADXD system.

Component	**Specification**	**Notes**
Filter Assembly	SiC, 1, 2, 4 mm, Copper 0.1, 0.2, 0.4 mm Vacuum compatible	Water-cooling required
4-jaw Slits1 &2	0-25 mm (V) x 0-120 mm (H) 1 micron resolution 10 mm Tungsten blade Slit 1 is vacuum compatible	Water-cooling required

Ion Chamber	0-25 mm (V) x 0-120 mm (H) area 60 mm sensitive depth Thin (~50 microns) Aluminum window	IC (with air) response is 0.54 nA for 10^9 ph/s @ 80 Kev
Fast Shutter	25 mm (V) x 120 mm (H) 10 ms response time	
Micro-focusing optics	K-B mirrors (0.5 m length for each mirror) or saw-tooth optics 30-~100 keV, 2m focal length, 1 micro-radians slope error Each mirror individually removable from the beam N2 or vacuum compatible	Desirable to have horizontal line focus
Beam conditioning table	1 m width x 3 m length, at 1 m nominal height 0-100 mm vertical adjustment to switch between monochromatic beam and white beam, 1 micron resolution 200 kg load	

Table 23 The specification of the beam conditioning system

b. Sample stage

A new sample stage, on its own optical table, with motorized XYZ motion and removable rotation on the XYZ will be acquired. It will be designed to position a sample environment as large as the GE NaMx battery. The sample environment will include heating and charging capability, and the capability of housing at least two batteries so that the other battery can be charged while one is being studied in the beam. Since batteries may spend most of the time being charged and discharged, the ability to switch between the batteries improves efficiency. In addition to the minimum required XYZ motions for EDXD, the sample stack has an air bearing for performing CT and XZ translation and rotation for alignment and centering of the sample on the CT rotation axis. The specification of the sample stack is shown in Table 24.

Component	**Specification**	**Notes**
X-Z Translation on X-Z Cradle	+-10 mm translation range with 1 micron resolution +- 20 degrees rotation with 0.001 deg. Resolution 50 kg load	Reference Huber 5102
360 deg. goniometer for CT	360 deg. rotation range with 0.001 deg. Resolution 10 rev./s maximum rotation speed 75 kg load	Reference ESRF ID-19 or APS 2-BM CT rotation air bearing
Y translation	200 mm range, 1 micron resolution 100 kg load	Reference NSLS elephant foot
X-Z Translation	200 mm range, 1 micron solution 150 kg load	

Sample table	0.5 m width x 0.5 m length, at 0.75 m nominal height 0-100 mm vertical adjustment to switch between monochromatic beam and white beam Tilt adjustment +- 1 deg. with 0.001 deg. resolution, needed for alignment of CT rotation axis 200 kg load	Tilt adjustment can be achieved through kinematic mount of 3 vertical jacks

Table 24 The specification of the sample stack

Figure 121 shows the design of the sample stack along with design of the 2-theta arm for the EDXD system.

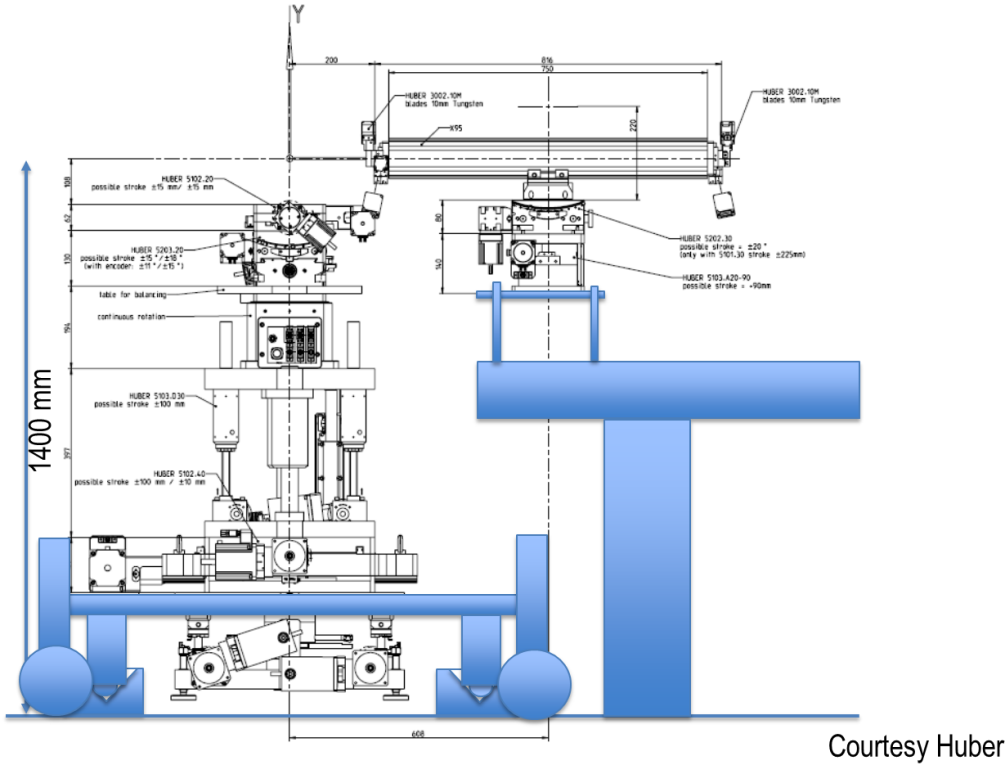

Figure 121 Design of the sample stack and 2-theta arm for the EDXD system

c. Diffracted beam slit

Two motorized four-jaw slits connected by X95 tube, similar to the current incident beam slit, will be acquired. Vertical motion and rotation will be provided to this slit assembly. The combined vertical translation and rotation motion is essential for changing the two-theta angle.

The detector, having a sensitive area of 20 mm diameter (large compared to 0.1-0.4 mm by 10 mm active area), is located in the experimental station that has intense white x-ray beam. Thus, it is important to shield the detector so that the detector only sees the x-rays diffracted from the sample that are transmitted through the diffracted beam slits. Our current system utilizes a ¼ inch lead-shielded beam pipe, custom fabricated by Radiation Shielding Inc., between the collimating slits. We plan to design a collimator using ¼ inch lead thickness that fits inside the bore of X95 tube.

d. Detector

A large vertical translation stage, with a cradle above, will be used to support the detector. The translation stage will share the same optical table as the diffracted beam slit.

Two new Ge x-ray detectors and HV supply and pre-amp electronics will be acquired. the MCA and data acquisition system will also be acquired. The specification of the EDXD detector system is shown in Table 25.

Component	Specification	Notes
4-jaw Slits3 &4	0-10 mm (V) x 0-10 mm (H) 1 micron resolution 10 mm Tungsten blade	In-air
X95 link between slits 3&4	Constructed of X95 of 800 mm length End machined to mount slits Bore hole (~50 mm diameter) lined with 5mm thick lead	
Y translation	100 mm range, 1 micron resolution 50 kg load 1 micro-radians angular stability	Prefer design with center jack and large (>100 mm) footprint to promote angular stability
Cradle for 2-theta arm	+-20 deg. range, 0.001 deg. Resolution 30 kg load	
Detector jack	200 mm range, 10 micron resolution 30 kg load	
Detector angle tilt	0-10 deg. tilt adjustment 20 kg load	Kinematic mount or cradle
Ge detector 2 units	15 mm diameter sensitive area, 5 mm Ge thickness 20- 200 keV	Reference Canberra x-ray detector and XIA MCA
EDXD + Imaging table	1 m width x 3 m length, at 1 m nominal height Large (0-2m) x Translation to move detector in/out of beam. 200 kg load	Height adjustment is desirable

Table 25 The specification of the EDXD detector system

As a scope contingency, the current end station at the APS 6-BM beamline can be moved to NSLS-II. The hardware and software will be updated. In particular, the white-beam slits should be replaced by vacuum-compatible slits to eliminate corrosion by ozone.

Further in the future, at the mature scope stage, this single-detector system will be installed permanently in the experimental hutch D using beam from the white-beam branch, and serve as the work-horse for EDXD. It will be replaced by a multi-detector EDXD system discussed in Sec. 5.4.

At the HEX BAT meeting, the possibility of EDXD with two orthogonal (horizontal and vertical) two-theta arms was discussed. Having two arms is beneficial to strain mapping research, with limited benefit to the battery research. The disadvantage is some loss of adjustability for the first set of slits close to the sample. We will consider this design as a separate development project once the HEX beamline is operational and user demand data for strain mapping is available.

4.2.2. Imaging capability

The work-horse instrument will consist of a very simple and typical micron-resolution tomography set-up. Figure 137 shows the preliminary design for the imaging endstation.

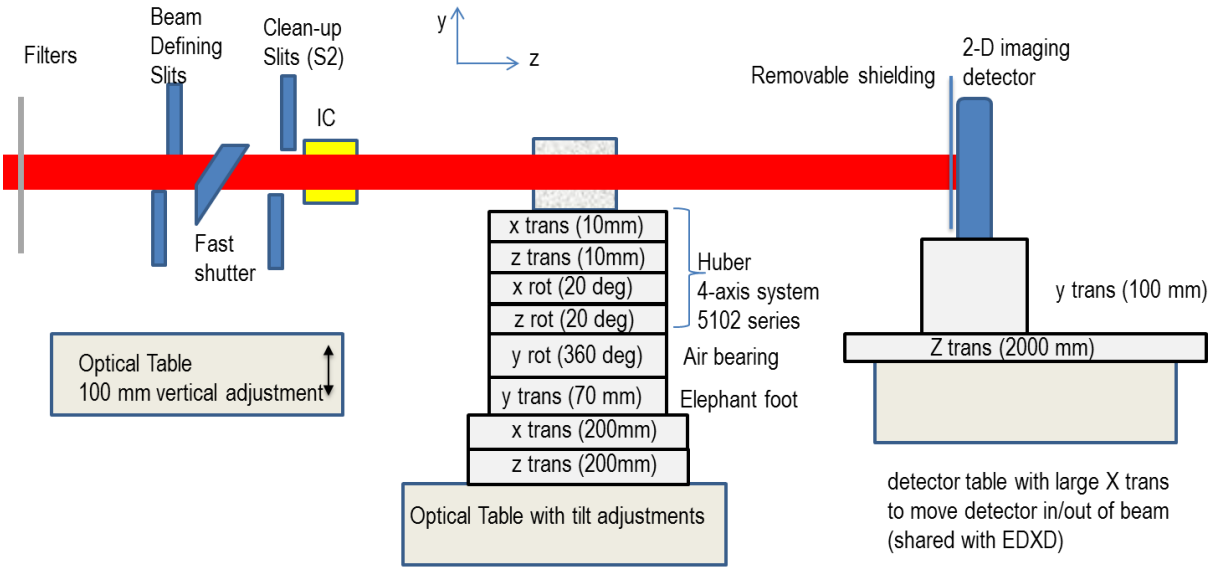

Figure 122 Design of the HEX imaging system

The imaging system will enable both absorption- (by moving the detector close to sample at about 100 mm) and propagation-based phase contrast imaging (by moving the detector away from the sample to a distance of greater than 0.1 m using the z translation under the detector).

Figure 123 shows schematically a typical imaging system consisting of x-ray source, a sample, and an area detector.

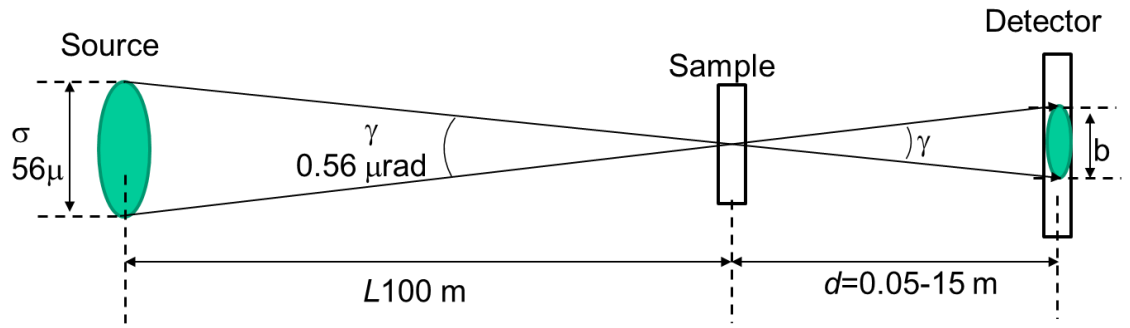

Figure 123 An X-ray Imaging system to Produce Propagation-Based Phase Contrast

For weak phase object, the contrast due to propagation-based phase contrast is

$$I(x) \approx 1 + \frac{\lambda d}{2\pi}\phi''(x) \qquad \textit{Equation 12}$$

where $\phi''(x)$ is the phase of transmitted beam wavefront. The phase contrast increases with sample-detector distance *d*.

The on-axis Penumbral angle is defined as

$$\gamma = \sigma / L \qquad \textit{Equation 13}$$

where σ is the source size and *L* is the source-to-sample distance. The penumbral angle characterizes the phase-contrast sensitivity of a beamline.

Image blurring due to source size is

$$b = d\sigma / L \qquad \textit{Equation 14}$$

Equation 12 and Equation 14 show that to maximize phase contrast, a large sample-to-detector is necessary. Thus, to minimize the blurring, a large source-to-sample distance *L* is desirable.

For the HEX imaging system in the satellite station, *L*=100 m. The penumbral angle (γ) is then 0.56 μrad RMS, and 1.3 μrad FWHM. Using Equation 13, the blurring b is between 0.07μm and 20μm FWHM corresponding to a sample-to-detector distance between 0.05 m and 15 m (with the detector at the downstream end of the experimental station F). Note detector resolution is limited to about 1μm.

Table 26 summarizes the phase-contrast performance, in terms of beam intensity, penumbral angle, field of view and energy range, for HEX and a few existing well-known imaging beamlines.

Beamline	**Flux density (ph/s/mm^2/0.1% bw @ 60 keV**	**FWHM horizontal penumbral angle (σ/*L*2.35)***	**Beam Size H X V (mm)**	**Energy Range (keV)**
HEX	**1.3x10^{11}**	**1.3 μrad**	**100 x 20**	**30-150**
ESRF ID19 W	2x10^{11}	0.9 μrad (on-axis)	45 x 6	20-100

SPRING8 BL20XU@245 m	$3x10^{11}$	2.9 μrad	4 x 2	10-60
APS 32-ID @70 m (RHB)	$1.6x10^{11}$	4 μrad	13 x 2.5	10-60
APS BM @70 m	$4.5x10^{9}$	2.7 μrad	(70) x 8	10-60

Table 26 Performance of HEX imaging compared to imaging beamlines at ESRF, Spring8, and APS

A sample to detector distance of 0.05 m – 2 m d satisfy needs for most experiments according to experience at ESRF19ID and APS 2BM. For example, cracks and voids are usually imaged at *d* less than 0.5 m, insects and solid-fluid interface were successfully imaged at *d* of about 1 m. Thus, we specify a motorized range of 0.05-2 m for the detector longitudinal position (z). For samples requiring larger z, a separate detector positioned near the downstream wall of the experimental station can be used.

a. Incident beam slit

An optical table with height adjustment supports the beam-defining slit, fast shutter and ion chamber to measure the flux of the imaging beam. This optical table is located at the front of the imaging station. The imaging slits and shutters should have large horizontal and vertical apertures to accommodate the 20 mm (V) by 100 mm (H) beam.

b. Sample stage

The sample stage for CT will be positioned on an optical table (see Figure 122). The base of the sample stage consists of a motorized XYZ motion to position the center of rotation in the beam. A large vertical 360 degrees air bearing allows CT imaging of the sample. A small sample XZ stage, and optional tilt adjustments, position the sample at the center of rotation.

d. Detector

Camera systems of different field of view and resolution will be purchased: the CCD-based camera will be used for high spatial but lower temporal resolution work, and CMOS-based camera will be used for very high frame rate data acquisition. A vertical translation stage will be used to support the detectors, allowing rapid changing between imaging detectors of different resolutions. A long 2 meter z translation stage changes the sample-to-detector distance.

Table 27 lists the specification of the imaging endstation.

Component	Specification	Notes
2-D Imaging detectors (large area)	20 mm (V) x 100 (H) sensitive area 30 keV – 150 keV 5 micron – 250 micron resolution	Reference ESRF 19-ID and IMBL modular imaging detector
2-D Imaging detector (high resolution)	20 mm (V) x 20 mm (H) sensitive area 30 keV-100 keV 1-5 micron resolution	Reference ESRF 19-ID and IMBL modular imaging detector

Y translation	70 mm range, 1 micron resolution 20 kg load	
Z translation	2m range, 10 micron resolution 30 kg load	
Table for far detector	0.5 m width x 1 m length, at 1 m nominal height 200 mm vertical translation to move detector in/out of beam	Optional
Table shared with EDXD	1 m width x 3 m length, at 1 m nominal height Large (0-2m) x Translation to inboard move detector in/out of beam. 200 kg load	Height adjustment is desirable

Table 27 Specification of the HEX imaging system

In collaboration with the team at ESRF ID19, we plan to test the SiC and diamond windows/filters for possible wave-front distortion. The windows for the ion-chamber and K-B mirror chamber should also be tested.

4.2.3. ADXD Capability

In the mature configuration, the ADXD system will be served by a sagittal-focusing monochromator and vertical focusing mirror, similar to those used at the XPD beamline. Instead of using dedicated ADXD optics, the initial scope ADXD experimental system will use the imaging monochromator and have an energy range of 30 to 150 keV. The beam used for ADXD will be reduced with an aperture, from the large imaging beam to a size of approximately 0.5 mm by 0.5 mm.

Following a BAT recommendation, the beam can be focused by K-B mirror, compound refractive lens or saw-tooth lens to a spot with a diameter of a few microns. The justification for adding the ADXD system is that the experimental system and micro-focusing optics are relatively inexpensive compared with dedicated focusing monochromator and mirror. The ADXD system will share the same beam-conditioning slits, ion-chambers and sample stage as that of the EDXD system. The beam-conditioning system will need to be raised by 25 mm to be at the correct position for EDXD when moving from ADXD mode to EDXD (i.e., from white beam to monochromatic beam). Figure 124 shows schematically the design of the ADXD endstation.

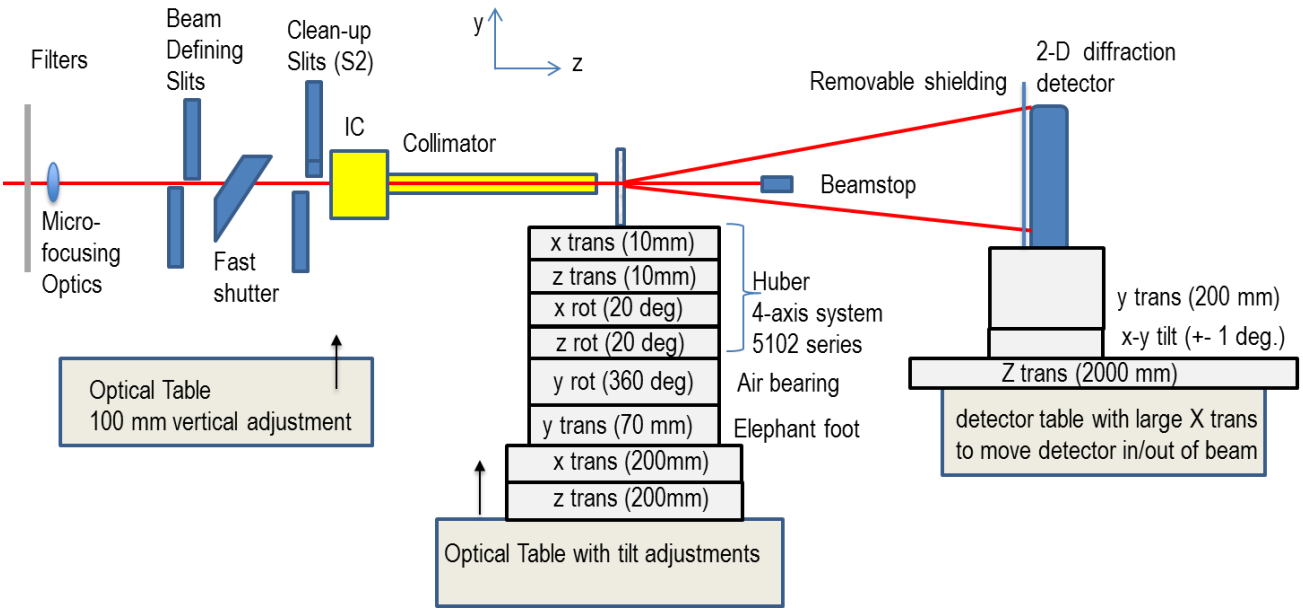

Figure 124 Preliminary design of the ADXD endstation

Options for micro-focusing include: K-B mirror, saw tooth as used at APS-1ID, Kinoform lens pioneered by Ken Evans-Lutterodt, and a compound refractive lens (CRL). The characteristics of the focusing options are summarized in Table 28.

	Aperture	Focal spot size	Line-focus	Energy tunability	Price	In-line
K-B mirror	0.5 mm x 0.5 mm *	1 micron	Yes	Easy	$400k	No
Saw-tooth	1 mm x 1 mm	1 micron	Yes	Relatively easy	$100k, R&D	Yes
Kinoform	0.3 mm x 0.1 mm	0.2 micron	No	Difficult	$100k, R&D	Yes
CRL	0.3 mm	1 micron	No	Relatively difficult	$100k	Yes

Table 28 Comparison of different focusing schemes

*The K-B mirror aperture assumes 0.5 m long mirrors at 1 mrad incident angle.

The requirements for micro-focusing are:

1. Spot size smaller than 10 microns
2. Option for line focusing is desirable
3. Focal distance of about 2 m. The source distance is 100 m.

Based on our discussions with micro-focusing experts Evans-Lutterodt, Chu, and Shi, we are proposing the K-B mirror as the first option due to its commercial availability. We will consider saw-tooth as the second option due to the its excellent performance at APS 1-ID.

To estimate the smallest possible focal spot, the following source parameters were used to simulate the source size for SCW70:

Energy	3.0 GeV
Number of poles	29
Period	7.0 cm
σ_x	.041 mm, Sigma X Assumes low-B straight
σ_y	.0030 mm, Sigma Y
Magnetic field	4.3 T

Table 29 Wiggler parameters used for simulation of the source size.

This results in a peak-to-peak horizontal electron excursion of 0.107 mm. The RMS source size due to excursion $\sigma_{X\_excursion}$ can then be calculated assuming that the excursion is a sine wave.

$\sigma_{X\_excursion}$ =(peak-to-peak excursion)/2.8=0.038 mm

The convolution of this with the RMS of current NSLS-II electron beam (σ_{X_beam}=0.041 mm) results in a horizontal source RMS size of 56 microns, or a FWHM 132 microns. Assuming a demagnification ratio of 50:1, the contribution of source size to focal spot size (sigma) is estimated to be 1.1 microns with a FWHM of 2.6 microns.

Figure 125 shows the design of the focusing optics, demonstrating the effect of the source size and length on the focal spot size for an ideal focusing optic.

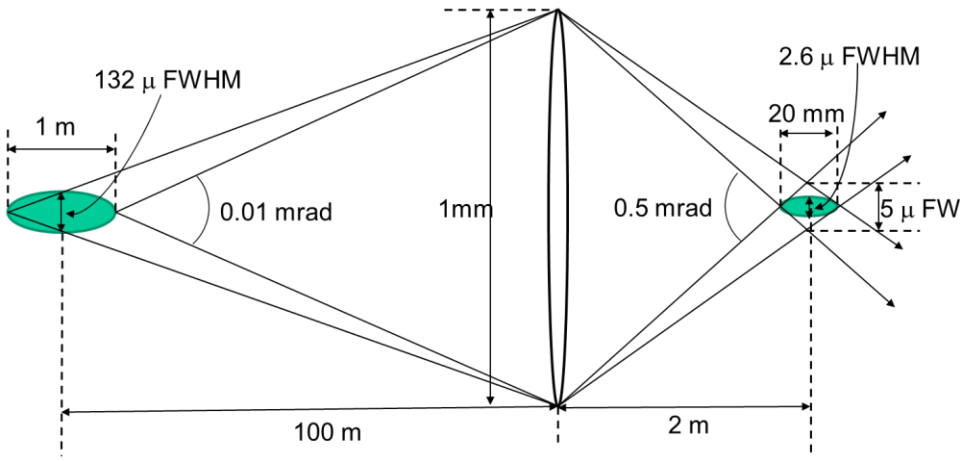

Figure 125 Effect of source length on focal spot size

The 1 m length of the wiggler at a divergence of 0.01 mrad contributes to an additional horizontal FWHM of 100 mm x $0.5x10^{-3}$ rad/2=0.0025 mm. Convolution of this with the focal spot size from source size results in an estimation of the smallest possible focal spot FWHM of 3.6 microns (H) by 2.5 microns (V). Thus we will specify the figure errors of the focusing optics to not contribute to more than 2 microns in focal spot size. This, when combined with a working distance of 2 m, results in a slope-error specification of 1 micro-radians.

Ray-tracing was performed to simulate the focal spot size and shape. Figure 126 shows the simulation results. The simulation assumes a 31x3 micron source of 1 m long, and ideal elliptical cylinder mirrors. The simulation yields a FWHM of 1.2 (H) x0.16 (V) $micron^2$ focal size. It is seen that the focal size is due mostly to the demagnification of the source. Combining the above analytical calculations with the ray-

tracing results gives up confidence that the micro-focusing optics can deliver a focal spot size of less than 10 microns.

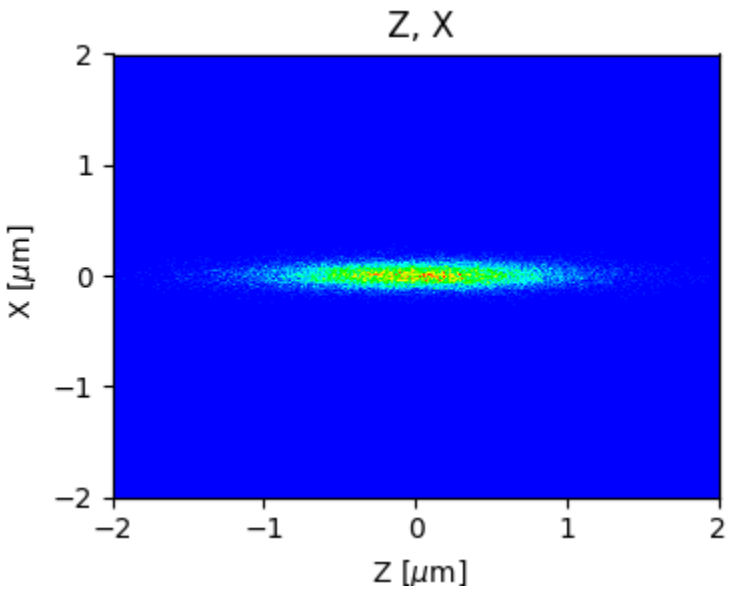

Figure 126 Results of ray-tracing simulation of the focal spot

Focusing with Compound Refractive Lenses (CRLs).

Parabolic compound refractive lenses have better performance than circular or spherical lenses. The RXOptics (https://www.rxoptics.de/design-parameters/) simulation tool was used to simulate the performance of parabolic CRLs. The simulation assumes aluminum lens material which is generally considered appropriate for high-energy x-rays. The x-ray energy is assumed to be 60 keV, desirable energy for micro-focused x-rays for diffraction. The inter-hole distance (thickness at the apex) is assumed to be 30 microns. The thickness of each lens is assumed to be a reasonable 2 mm. The results of simulations with different apex radii showing the transmission and effective aperture, are summarized Table 30.

Radius at apex *R* (microns)	50	100	200	300
Number of lenses	87	177	371	593
Geometric aperture $2R_0$(microns)	628	888	1255	1538
Effective Aperture (microns)	252	255	261	267
Length of CRL (mm)	217	442	928	1482
Transmission	6.6%	2.8%	0.9%	0.4%
Focal spot size (H X V) (microns)	1.3x0.17	1.3x0.17	1.3x0.17	1.3x0.17

Table 30 Simulation results for 2-D parabolic lens.

For the parabolic lens, the radius of curvature at the apex (*R*) determines the lens diameter (also referred to as the geometric aperture) $2R_0$ as shown in the table above. The total transmission is represented by the effective aperture. Table *** shows that the simulated effective aperture of fewer than 300 microns is lower than that of the KB mirrors (500 microns). Table *** also shows that even at

larger radii and correspondingly larger geometric apertures, the effective aperture is relatively constant. This is due to the decreased transmission due to more attenuation of x-rays at larger radii and number of lenses. The smallest radius requires the least number of lenses, which have the largest transmission. At the smallest radius of 50 microns, the transmission is still below 7%. At a radius of aperture at the apex of 500 microns, the length of CRL becomes so large that the focal spot is inside the CRL.

For spherical lenses, simulations using the CLR simulation tool in XOP optics package yields similar results for poor transmission and requirement for a large number of lenses. Thus, we conclude that CRLs, either spherical or parabolic, are not as effective as K-B mirrors for our application of micro-focusing of high energy x-rays at small focal length. We note that the poor transmission and requirements for large number of lenses are due to the combined effects of small focal length (2m) and high x-ray energy (the deviation of the index of refraction from 1 is proportional to $1/E^2$, where E is the x-ray wavelength) in this particular application. Thus, 2D parabolic CRLs should be considered for future applications and upgrades when the required x-ray energy is lower (e.g. 40 keV) and/or the focal length is larger (e.g. 10 m).

ADXD End station Summary Specification.

The specification for the ADXD endstation is summarized in Table 31.

Component	Specification	Notes
Collimator	XPD & PDF design	
Beam stop with embedded photo-diode	~ 2 mm diameter 5 mm Tungsten depth Remote control of +- 3 mm in x-y position	Reference PDF beam-stop design
ADXD flat panel detector	400 mm×400 mm active area, CsI phosphor coating 0.2mm pixel	Reference XPD & PDF flat panel detectors. We will wait for technology to improve
Y translation	200 mm range, 1 micron resolution 40 kg load	Prefer design with center jack
Detector angle tilt	Around x (H) and y(V) axis +-1 deg. tilt adjustment, 0.001 deg. Resolution 50 kg load	For alignment Facilitates changing between apertured beam and K-B focused beam
Z translation	2m range, 10 micron resolution 30 kg load	
ADXD table	0.5 m width x 2 m length, at 0.75 m nominal height Large (0-1.5m) x Translation outboard 200 kg load	Height and tilt adjustment is optional

Table 31 Specification of the ADXD endstation

Although commercial flat-panel detectors are successfully used at various facilities, the implementation of photon-counting CdTe 2D detectors should be considered for future upgrades. The technical advantages are noise free and fast (few 100 Hz) acquisition, allowing the study of high-temperature minority phases (during quench), surface layers, and intermediate phases.

4.3. Multi-Detector EDXD system (Not in Scope)

The experimental system for EDXD, currently installed at the APS 6-BM beamline, was designed and built at the NSLS over the past two decades for the purpose of strain-mapping of engineering materials. As such, it is not optimized for battery research. Among the drawbacks are:

1. It is time-consuming, thus only a line profile can be measured. For battery research, a 2-d or 3-d map is necessary for characterizing the reaction front.
2. The gauge volume is too large due to time constraints.
3. The software was written for strain mapping. It is cumbersome to use and unreliable for battery research.

In the future, the HEX beamline will include a new, novel system to allow parallel data collection. Figure 127 shows the new system proposed. Comparing Figure 127 with Figure 121 shows that they are essentially the same with one key difference: the single-element Ge detector in the current system is replaced by a one-dimensional array of Ge detectors. Currently, the Ge detector of about 20 mm sensitive area is behind a 0.1-0.4 mm (in the diffraction place) by 10 mm (perpendicular to the diffraction plane) slit. The slit size in the diffraction place (vertical) needs to be small in the diffraction plane to define a small two-theta range so that the energy resolution of the measured spectra is not dominated by the divergence of the diffracted beam. Thus, a tiny fraction of the diffracted beam signal and the available detector area is used for the measurement. To profile along the beam direction, the sample is scanned along the beam and measurement is made sequentially at every point. With each measurement taking approximately one minute, the scan time is about two hours for a profile along a line with 100 data points. As such, it is impossible to conduct a two-dimensional scan with 100 x 100 points.

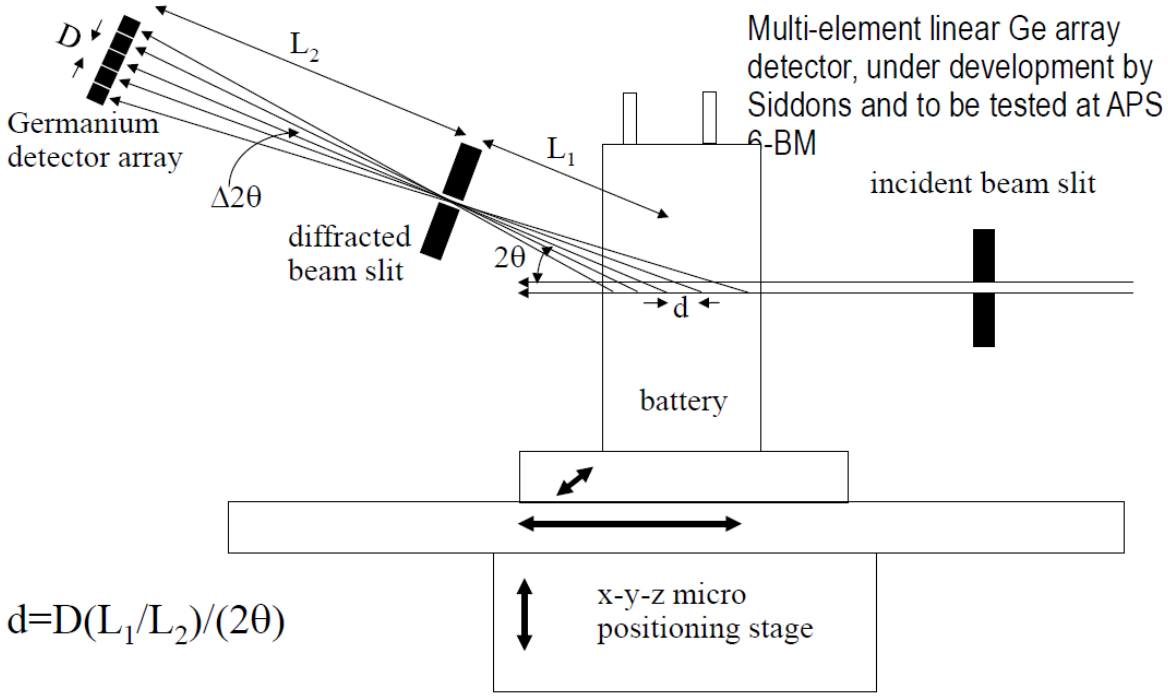

Figure 127 Planned multi-element linear Ge array detector system

About 10 years ago, a collaboration between GE and BNL proposed a new idea of using an array of Ge detectors, each having a dimension of 0.2 mm by 10 mm for the experiment. Figure 127 shows that each detector element acts as the detector in the current setup and measures the diffraction signal from a part of the sample along the beam direction. By using an array, the whole length of the battery along the beam direction is measured simultaneously. Since the measurement at each point is the same as current setup, we can estimate that the measurement time of 1 minute per line is sufficient. Thus, it would take approximately 2 hours to have a two-dimensional profile of the battery by scanning the sample perpendicular to the beam and measuring at each point for one minute.

Figure 128 shows plots the incident x-ray flux provided by the wiggler after filtering by 4 mm of aluminum to attenuate the low energy x-rays. Low energy x-rays are filtered before reaching the sample since they do not have the penetrating power to go through the sample, and will only contribute to sample damage and detector noise. The x-ray flux decreases with x-ray energy. The transmission of x-rays through the battery increases with x-ray energy. Using the battery composition data (120 g Ni, 98 g NaCl, 3.8 g NaF, 0.51 g NaI, 3.8 g FeS, and 115 g NaAlCl4 occupying a volume of 2.8x2.8x20 cm^3), the transmission through the diagonal direction of the sample which represents the most attenuation is calculated and shown in Figure 128. The diffracted x-rays originating inside the sample need to go through the sample in order to reach the detector. Due to the small two-theta angle, the x-ray intensity diffracted by the sample is proportional to the incident x-ray flux multiplied by the sample transmission. The result shows that the most useful part of the x-ray spectra is from 70 to 150 keV, which covers a d-spacing range from 0.12 to 0.26 nm for a two-theta angle of 4 degrees. This range conveniently covers the d-spacing of NaCl 220 and 222, Ni 200, and Mcl2 113 reflections of most interest in battery chemistry. The design will have the flexibility to change between a two-theta of 2 degrees to 6 degrees by translating and rotating the diffracted beam slit and the detector.

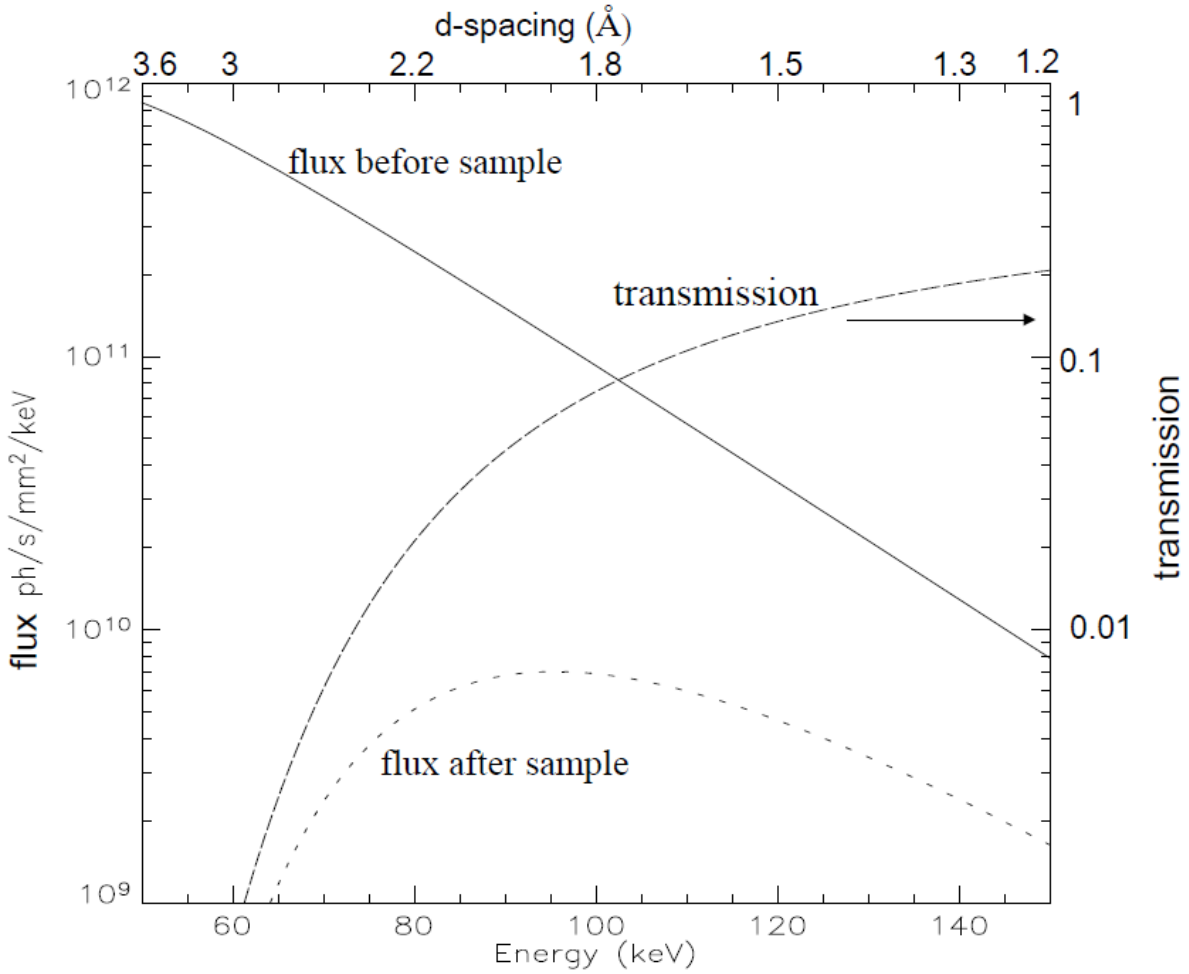

Figure 128 Simulated flux before and after GE NaMx battery, and transmission through the sample as a function of x-ray energy

Figure 128 also shows that the flux through the sample has weak energy dependence in the x-ray energy range between 80 and 120 keV. We plan to construct a standard sample with the same composition as the battery to achieve the same absorption characteristics, but with the phases distributed uniformly throughout the standard. Using data acquired with the standard sample, a calibration curve can be developed for different phases, thus allowing quantitative phase analysis. This algorithm can be incorporated into the data analysis software.

While the new idea of parallel data acquisition speeds up the data acquisition by orders of magnitude compared with the current setup, one noticeable drawback is that different detectors use different two-theta angles. The difference in two-theta between the detector elements, $\Delta 2\theta/2\theta$, needs to be small enough (within 20%) so that the energy difference for the same reflection, $\Delta E/E$, stays in the flat region in Figure 128. From the figure, we have;

$$\Delta E/E = \Delta 2\theta/2\theta = nD/(L_2 2\theta) \qquad \textit{Equation 15}$$

where n is the number of detector elements, and D is the pixel size of the detector.

The gauge volume covered by each detector element is

$$d=DL_1/(L_2 2\theta) \quad \textit{Equation 16}$$

The length of the gauge volume that can be covered is

$$nd=nDL_1/(L_2 2\theta) \quad \textit{Equation 17}$$

From Equation 15 and Equation 17, we have

$$\Delta E/E=(nd)/L_1 \quad \textit{Equation 18}$$

Requiring that $\Delta E/E < 0.2$ and nd = 40 mm to cover the whole battery, we have

$$L_1 > 40/0.2=200 \text{ mm} \quad \textit{Equation 19}$$

For the purpose of design, we choose the minimum required distance between the sample and diffraction slit L_1 of 200 mm. We also impose the condition that the gauge volume, along the beam direction (d), be 0.25 mm, or 5% of battery length along the beam direction. The number of detector elements is then 160 to provide complete coverage of the 40 mm sample length. Using Equation 16,

$$D/L_2=d2\theta/L_1=0.25*(4./57.3)/200.=8.7\times10^{-5} \quad \textit{Equation 20}$$

Equation 19 gives the ratio between the detector resolution and the detector to diffraction slit distance. By using a detector in-plane size of 0.25 mm, slightly less than the detector slit size we currently use (0.4 mm), we have $L_2=0.25/8.7\times10^{-5}=2800$ mm, or 2.8 m. This distance, though large compared to the current detector distance, is conveniently achievable within the limitation of the experimental station size. The detector size of 0.25 mm in the diffraction plane is also convenient for fabrication. For the out-of-plane detector size, we choose a size similar to the detector slit size out of plane that we currently use, 10 mm.

Table 32 provides a summary of the design parameters based on the above discussion.

Design parameter	Quantity	Notes
d-spacing coverage	1.2 – 3.6 Å	
x-ray energy (E)	50 – 250 keV	60-150 energy range with flux above 10^9 ph/s/mm^2/keV
Two-theta angle (2θ)	4 degrees	Variable between 2 and 6 degrees to allow other d-spacing coverage

Two-theta variation between detector elements ($\Delta 2\theta/2\theta$)	< 20%	
Sample to diffraction slit (L_1)	0.2 m	
Sample to detector (L_1+L_2))	3 m	
Energy variation between detector elements for the same d-spacing (ΔE /E)	< 20%	
Detector pixel size	Minimum 0.25 mm (D) in plane, 10 mm out of plane	Smaller in-plane detector pixel size results in higher Z resolution along the x-ray beam
Number of detector elements (n)	160	
Detector size (D)	40 mm in place, 10 mm out of plane	
Sample coverage along beam direction (nd)	40 mm	
Resolution along beam (d)	0.25 mm	
resolution perpendicular to the beam	1-50 microns	Defined by the incident beam slit. Can be very small subject to counting time limitations

Table 32 Preliminary specification of the multi-element detector EDXD system

The proposed Ge strip detector is not commercially available. Since 2010, the NSLS detector group led by Peter Siddons has been working on a prototype Ge strip detector. The first successful proof-of-principle test was conducted at the NSLS X7A beamline using white-beam from the NSLS bending magnet. A next-generation Ge strip detector was tested in late 2017 on the EDXD system at the APS-6-BM beamline, demonstrating the system's capability for diffraction imaging.

As discussed earlier, each detector element uses different two-theta angle around 4 degrees, and thus uses a slightly different part of the incident x-ray spectra. Thus, two-theta angle calibration for each individual detector is necessary to allow absolute d-spacing measurement, and intensity calibration is necessary for quantitative measurement. Since the attenuation of the sample modifies the spectra of the diffracted beam, we plan to construct a calibration sample of the same size as the battery, and with the same attenuation energy dependence. The calibration sample will be constructed with NaCl micro-crystals uniformly dispersed in an amorphous BN or plastic matrix and will be fitted inside the same steel case as our batteries. By acquiring diffraction data from this standard sample, we will be able to calibrate the two-theta angle for each detector element, and normalize the intensity across detector elements.

4.4. White Beam Branch (Not in Scope)

The C branch provides energy-dispersive x-ray diffraction (EDXD) at high x-ray energies up to 200 keV. Spatial resolution is 5 microns in the transverse direction and 50 microns in the longitudinal direction.

The white-beam branch will feature the following:

a. K-B mirror in the hutch for micro-focusing of white beam
b. Workhorse instrument for EDXD with 2 orthogonal detectors (up and outboard)

c. Adjustable two-theta
d. Could re-use mostly endstation being upgraded at 6-BM of APS
e. Compatible with a diamond-anvil cell with white beam

Figure 129b shows an example of the energy-dispersive diffractometer to be installed in the C branch.

Angle-Dispersive Diffractometer

Energy-Dispersive Diffractometer currently at APS

Figure 129 Examples of diffractometers to be installed as part of the HEX experimental system

4.5. Experimental Station E Center Branch (Not in Scope)

In the future, the experimental station E located on the experimental floor will be outfitted for monochromatic high-energy x-ray powder diffraction. The endstation equipment will be similar to that at XPD beamline, with beam-defining slit followed by clean-up slit and ion chamber, sample XYZ-stage and spinner, and an area detector will adjustable detector distance between 0.1 m and 2 m.

4.6. Experimental Station B Side Branch (Not in Scope)

The experimental station B will be dedicated for high-energy x-ray scattering with monochromatic beam. The endstation will be largely similar to that at the PDF beamline, currently being constructed for operation in 2018. Thus, the design and specification of HEX station B can benefit from experience gained at the PDF beamline. The HEX program and the PDF program belong to the same Diffraction and In-Situ Scatting (DISC) division of the NSLS-II. This arrangement facilitates exchange of expertise.

Figure 129a shows an angle-dispersive diffractometer, currently installed at the XPD beamline of the NSLS-II, as an example of HEX diffractometer for the side branch.

5. Controls and Data Acquisition

5.1. Controls

5.1.1. Control Architecture Overview

For the HEX beamline controls, we will employ the established NSLS-II controls standards based on the enormously successful open source EPICS (Experimental Physics and Industrial Control Systems) distributed control framework. We will standardize common hardware components for motion controllers, vacuum pump and gauge controllers, temperature controllers, programmable logic controllers (PLCs) and other input/output devices. We will also follow the standard software standards: Linux based EPICS softiocs with standard NSLS-II features, such as autosave, iocStats etc.

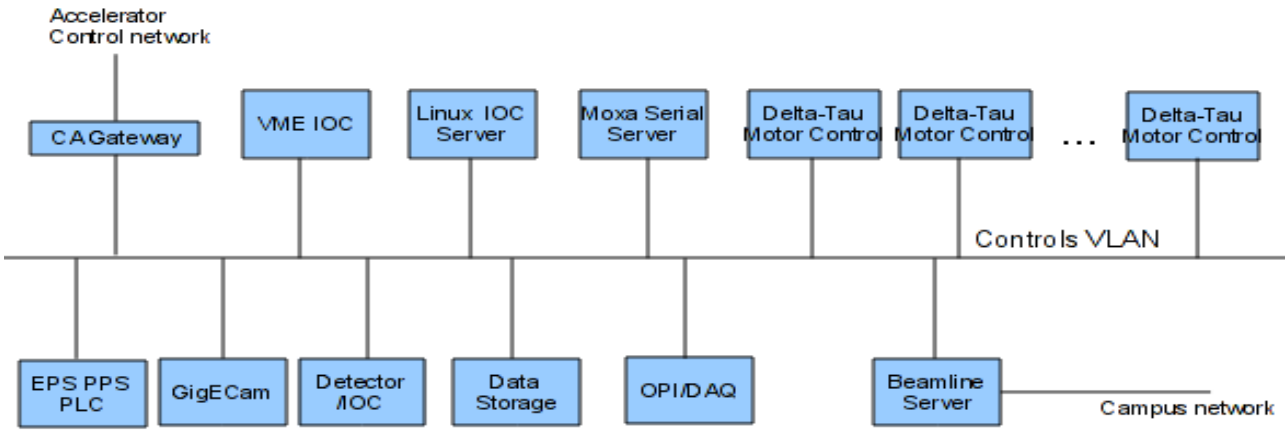

Figure 130 Schematic of beamline controls network architecture

Like every beamline at NSLS-II, the control system at HEX will have an isolated network dedicated for controls and data acquisition. Devices in the beamline, to the extent possible, will be controlled through EPICS Input- Output Controllers (IOCs). A VME crate will be installed at the beamline to support standard Scaler (SIS3820) and an EVR (Event Receiver) which decodes the machine timing information for beamline applications. Standard motion controllers (Delta Tau Geobrick-LV-NSLS-II from Faraday Motion) shall be employed to satisfy almost all motion needs at the beamline. They are controlled through EPICS softIOCs residing on a standardized Linux based IOC server. For ubiquitous serial devices, such as temperature controllers, vacuum controllers and gauges, specialized motors with serial interfaces (which cannot be controlled with the Delta-Tau, such as piezo motors), softIOCs will be developed to communicate with these devices through the use of MOXA terminal servers (www.moxa.com), with EPICS asyn/stream support. For beamline diagnostic imaging applications, standardized GigE cameras with PoE (Power over Ethernet) will be used with EPICS areaDetector support. 2D detectors will be interfaced through the same EPICS areaDetector package. Front end devices that needs to be controlled from the beamline will be through the CA (Channel Access) gateway, with standard EPICS access security feature incorporated in the IOC.

5.1.2. Coordinate Systems

We will follow the coordinate system definitions (Beamline Coordinate System Standards, LT-C-XFD-STD-BL-COORD-001) developed by the controls group. The benefits of having such a common coordinate system include:

1. having a common basis of reference,
2. enabling software sharing and common deployment, and
3. reducing confusion on beamline optics calculations.

The coordinate system convention follows a right-hand rule, with the positive z-axis defined as parallel to the direction of x-ray beam propagation, the y-axis positive in the vertical direction toward the ceiling, and the x-axis as being orthogonal to both the y and z axes.

Common angular definitions are also provided for roll, pitch, and yaw, where roll is rotation about the z-axis (photon beam), pitch is rotation about the x-axis, and yaw is rotation about the y-axis. These angular conventions also follow a right-hand rule.

5.1.3. Naming Convention

We will also follow the naming conventions for equipment, signal, and process variables (EPICS PV) as in document LT-ENG-RSI-STD-002. Having a standardized naming convention facilitates uniformity across beamlines, and enables efficient parsing with archived data.

User-friendly naming of beamline devices will be configured using PV alias feature as needed.

5.1.4. Electrical Cabling Convention

We will also follow the established standards for electrical cabling. All equipment shall conform to the cabling and connection conventions as described in the document, “Beamline Systems Instrumentation Interfacing Standard” [LT-C-XFD-SPC-CO-IIS-001].

5.1.5. IOC Standard Features

Each beamline will be equipped by the controls group with a single, nine-slot VME-64x crate, with MVME-3100 CPU and an EVR (Event Receiver) board that decodes the accelerator timing information. The MVME-3100 CPU shall run the latest stable RTEMS operating system.

Non-VME devices with be controlled through Linux-based softIOCs. The softIOC server is standardized on a 1U rack-mounted server (HP) running the latest stable Debian Linux. EPICS software Debian packages will be installed and configured following the protocols developed by the controls group. The packages mostly contain EPICS synApps applications (motor, asyn, optics, areadetector, etc.) packaged in deb format by the controls group to ensure uniform deployment and coherent version and package dependencies. SoftIOCs will be built and deployed to include the following standard features: IOC health diagnostics (iocstats); autosave/restore for parameter recovery during IOC reboot; conserver/procServ for console access and logging; and autostart script in sysv-rc-softioc package for autostart when the Linux server is rebooted.

5.1.6. PV Archiving

EPICS archiver software will be installed on a Linux server to allow archiving EPICS PV information, such as machine conditions, vacuum/temperature readings, and equipment settings for later analysis. The Archiver will be configured by the controls group, in consultation with beamline scientists to tailor to their specific needs.

5.1.7. Interaction with other control subsystems

5.1.7.1. CA Gateway

An EPICS Gateway server will be configured to interface between the accelerator network and the beamline control network. This server will act as a proxy to control system network traffic, caching accelerator process variables for use by beamline EPICS clients. With CA (Channel Access) Gateway, heavily subscribed accelerator process variables (ex: storage ring current or lifetime) are obtained from an EPICS Gateway rather than directly from the IOC hosting that PV, reducing accelerator network and the IOC resource load.

For HEX beamline, most interaction to the accelerator controls is monitoring of machine status at beamlines. Controls to the front end devices (such as front end slits) are through CA gateway and with the permission (a software flag) given by the control room operator.

5.1.7.2. Timing systems

The NSLS-II timing system consists of a centrally located event generator (EVG) which distributes event-based information synchronously to event receivers (EVR) located at each beamline. The inputs to the EVG include a 500 MHz master-oscillator and a GPS-based, absolute-time signal. This system will distribute beam-based timing information such as fill-pattern and bunch-timing, facility time-stamps. It will also send event-codes and data to EVR modules, all with 8 ns to 400 ps resolution and 25 ps to 5 ps jitter (peak-to-peak). EVR modules have several digital output channels that may be activated by the recognition of event-code reception, and thereby serve as triggers to beamline electronics. It is also possible to have the EVR generate time-stamps when configured to do so for input TTL pulses.

5.1.7.3. Front End EPS (Equipment Protection Systems) and PPS (Personal Protection Systems)

The HEX beamline will have a beamline EPS system for interlock functions. This system will use the standard Allen-Bradley CompactLogix family PLCs. The standard interface to machine (or front end) EPS and machine EPS/PPS are through IO signals passed by beamline EPS.

HEX will have a fast vacuum sensor installed in the First Optics Enclosure (FOE). This sensor will be connected to the fast vacuum valve controller to close the fast vacuum valve in the front end if there is a rapid beamline vacuum failure. This is part of PPS system.

The HEX beamline will require the ability to close and open the front end photon and safety shutters and to monitor the status of those shutters. These functions have been incorporated into the machine PPS design. The operation of such from beamline side is through standard EPICS CA gateway with permission flags from control room.

5.1.8. Standard Controls Subsystems

5.1.8.1. Motion Controllers

Based on requirements from beamline's final designs, beamlines at NSLS-II typically have about 100 to 200 motor axes for each beamline. The NSLS-II project has chosen to standardize on a customized version of the DeltaTau Geobrick-LV motion controller (Geobrick-LV-NSLS-II). This flexible and feature-rich motion controller will be used wherever possible.

Figure 131 Delta-Tau 8-axis motion controller and power supply

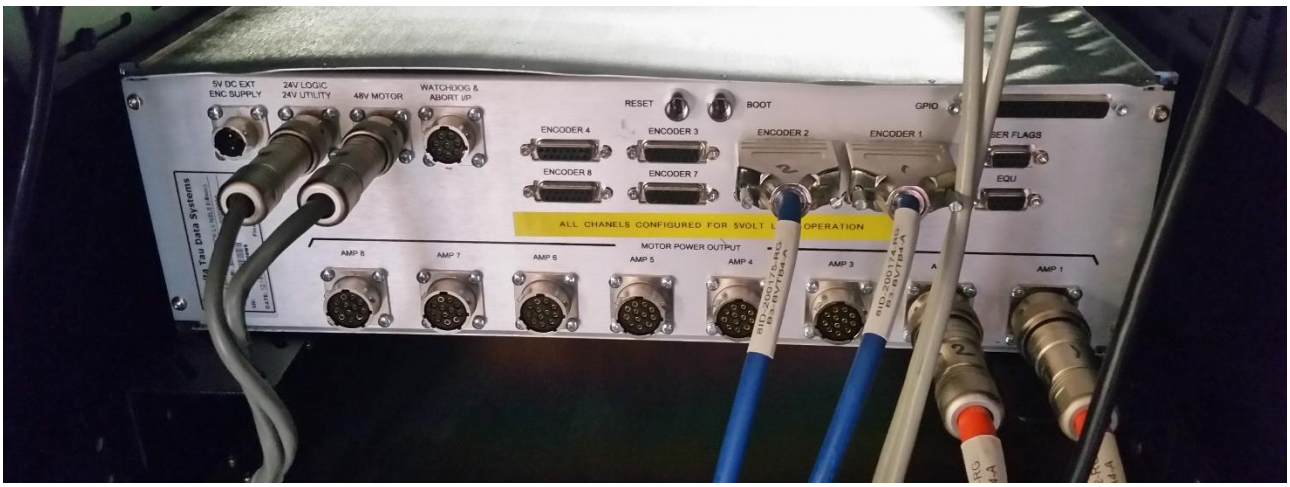

Figure 132 Rear view of the Delta-Tau controller

Each controller includes integrated, low-voltage amplifiers to drive 8 axes of 2-phase stepper or DC servo motors. Each axis can drive motors up to 5A continuous (15A peak up to 2 seconds) and support

standard limits and home signals, digital quadrature encoder inputs, micro-stepping, and 24 channels of digital I/O. We will also standardize on the Delta-Tau Quad-PS switching power supply that is designed to work with these controllers.

Although the controller can be configured to provide pulse/direction to drive standalone 5-phase amplifiers, the use of 5-phase stepper motors is discouraged. It is expected that micro-stepping (software configurable to 2 to 512 micro-steps per full step) of standard 2-phase steppers will satisfy most motion needs at the beamlines.

The standard communication with the motion controller is through Ethernet. This makes it possible to locate motion controllers near motors to reduce cabling lengths. Control is handled by the standard EPICS motor record support, which many beamline scientists/engineers are familiar with.

One of the most interesting features of the Delta-Tau BrickLV controller is that it supports coordinated motion for all axes in the controller, and can be extended to up to 32 axes with MACRO (fiber) interconnection of two or more controllers. The other feature of great importance is that the controller can send triggers at programmed intervals to detectors, with which "fly-scanning" can be programmed to vastly improve data acquisition efficiency.

Many optical components will be purchased as turnkey systems from vendors. To ease integration into beamline control systems, optical component subsystems must conform to standards established for use on the beamlines (e.g., motion controllers and cabling). We will follow the practice of the project beamlines to work with vendors early in the design phase and offered assistance and incentive to encourage adoption, in the form of equipment lending and assistance with configuration and testing. To ensure standardization, control standards will be included in all beamline procurement packages.

5.1.8.2. Optics, Virtual Motors, filters, etc.

We plan to take full advantage of the existing optics module distributed with the synApps (a collection of EPICS-based synchrotron applications). This module includes support for optical tables, mirrors, monochromators, slits, attenuators, and diffractometers. The module includes calculations on the EPICS IOC level to provide additional PVs that are physically meaningful for beamline operations. For example, a virtual motor in units of x-ray energy can be calculated using the EPICS transform record from the Laue monochromator real motor readings.

An alternative is to do these calculations in the motion controller (as pmac motion and PLC programs), which has the advantage of supporting trajectory motion with faster response time than is possible via higher level control.

5.1.8.3. Serial Devices

Many devices to be controlled at the beamlines typically come with a serial interfaces (RS232, RS485 etc.) to connect to computers. The standard solution is to have serial devices connected to a terminal server (ethernet to serial converter), so that the serial communications are translated to ethernet socket communications. The standard serial converter chosen by the controls group is MOXA serial servers (www.moxa.com). Many models are available, but NSLS-II standardizes on the 16-port (for example, nport-6650), for ease of maintenance and extensibility. A common solution is to install a Nport-6650 at each hutch to deal with almost all serial devices.

USB device support for EPICS is very limited at this time, thus their use should be limited to the devices already known to work under EPICS.

5.1.8.4. Counter/Scaler

The standard scaler for NSLS-II is Struck-3820, a 32 channel VME based scaler. It has on-board memory to support fly-scan applications in addition to standard scaler functions.

5.1.8.5. Analog and Digital IO

The ADCs (analog-to-digital converters), DACs (Digital-to-Analog converters), and Binary I/Os are provided by beamline PLCs. If only a few channels are required, the motion controller auxiliary DIO channels can be used (this is rarely done).

5.1.8.6. Spectroscopy and Multichannel Analyzers

There are only a few standalone multichannel analyzers supported in EPICS, some of which are no longer commercially available. For spectroscopy applications, the suggested solution is to use Xspress3 or Xspress3-mini (https://quantumdetectors.com/n/products/xspress-3-mini/). Legacy spectroscopy systems such as XIA Saturn or Mercury (4-channel version) digital spectroscopy amplifiers can also used with EPICS DXP/MCA support. The current models of XIA Saturn/Mercury digital spectroscopy amplify the use of USB connections, which have a limited cable length at 15 ft. The proposed solution is to have a small form (mini-ITX) Linux PC (as softIOC) next to the electronics box, as is done at several beamlines.

5.1.8.7. Imaging and Area Detectors

For diagnostic imaging applications, the standard camera interface is GigE (e.g., Prosilica), supported through the EPICS areaDetector package. For simple viewing applications, PTZ webcams or affordable analog video camera through video servers are planned.

The detector for user data (for example, flat-panel detectors as used in several beamlines) will also be controller through EPICS areaDetector. These detectors typically come with their own control computer/server (in either Linux or Windows) that provides a hook for communication with EPICS areaDetector.

5.1.9. Beamline Vacuum, EPS

5.1.9.1. Vacuum

To the greatest extent possible and practical, vacuum components utilized in the accelerator systems shall be used for beamline vacuum systems. This includes valves, pumps, gauges, associated controllers, PLCs, IOCs, and EPICS software. The hardware standards will be enforced by the NSLS-II vacuum group, who is responsible for instrument procurements. Monitoring and controls (setting interlock limits) are through serial protocols (RS-232) and they are all to be connected to the MOXA Nport terminal server. EPICS integration will be done by the beamline control engineers.

The interlock functions of the vacuum controllers are part of EPS.

5.1.9.2. Beamline EPS

Beamline Equipment Protection System (EPS) are standardized on Allen-Bradley PLC. Typically there is an intelligent EPS chassis in a rack and remote IO boxes distributed at various locations of the beamline. Control engineers will work closely with common systems and beamline scientists to formulate and

document the detailed EPS requirements so that EPS engineer can design and program the ladder logic, and then integrate EPS to the beamline control systems (EPICS IOCS and associated CSS screens).

With the current existing beamlines at NSLS-II, we have a good template for beamline EPS requirements and functions. Typical EPS functions include:

- monitoring high heat load component temperatures
- monitoring coolant flow to components
- monitoring vacuum status in the beamline
- taking protective action as required - closing photon/safety shutters, closing vacuum valves
- reporting status of beamline components to the control system

5.1.10. Front End Subsystems

Beamline Front Ends are those components between the photon source at the storage ring and the vacuum gate valve outside the ratchet wall. The current standard front end design for NSLS-II contains eight axes of motion: a four-axis slit, and a pair of x-ray BPMs with two axes each. The controls requirements for the front ends are defined in the NSLS-II Front Ends Controls PDR (LT-R-ASD-CO-DR-FE-001).

The photon safety shutters (PSS) at the ratchet wall are a critical element of the beamline personnel protection system and will be interlocked with optical enclosure access points downstream of each front end; in addition, they will be interlocked based on the accelerator state. The beamline control system needs to know the status of the front end shutters, and also needs the capability to request shutters to close or prevent them from opening. Refer to the FE Controls PDR document for details.

5.2. Controls Risk and Mitigation

By adopting the established hardware and software standards in developing HEX beamline controls , we expect to see significant reduction in engineering resources than otherwise needed. This is evident in recent NSLS-II beamline buildouts. In particular, for photon delivery systems, we have been and will continue to practice enforcement of standardization by incorporating controls standards in all procurement packages.

Standardization is largely made possible by adopting a feature-rich and flexible motion controller to satisfy almost all motion needs. In the past, this could pose a schedule risk in the integration and testing phase due to its complexity. With control engineers gaining vast experiences from previous beamline buildouts, and beamline control group's excellent track-record in implementing beamline controls, the risks for HEX controls is very small.

5.3. Data Acquisition, Data Management and Analysis (DAMA)

5.3.1. DAMA Introduction

For data acquisition, HEX will employ Bluesky, a new open-source data acquisition framework developed at NSLS-II by the DAMA group. Based on Python, Bluesky features data scanning functions equivalent to

the legacy SPEC software as used extensively at synchrotron beamlines, with much more modern features (such as plotting and saving image array data) by taking advantage of Python developments in data science.

To deal with the large data sets expected to be generated by the large format area detectors at HEX, a standard local storage server with IBM's Spectrum Scale (previously GPFS) file system is in the plans for HEX to provide high-performance simultaneous read and write file operations across all beamline workstations and servers.

The present data collection/analysis system at 6-BM involves three computers: the detector computer; beamline control Computer; and the data analysis computer. The detector computer controls the energy dispersive diffraction spectra collection with a Canberra supplied system. The Beamline control computer controls the settings of the beam-defining slits, diffracted beam slits, and the sample x-y-z position via stepper motors. It issues the TTL logic pulse to the detector computer when a new data collection position is reached in the sample. The macro for the experiment runs on a SPEC general purpose diffraction program. A separate program written in IDL is then used to generate the 2-D intensity map of the energy-position in order to visualize the phase change as a function of sample position.

We will develop software to incorporate these processes into a single user-friendly package using Bluesky. An online display of the preliminary phase analysis based on known position of Bragg line and phase map during data collection will be developed. In addition, a more sophisticated set of software will be developed for any user wishing to perform more detailed analysis. This software will allow much more detailed analysis using refinement of the diffraction pattern, and produce 2-D and 3-D maps of a particular phase.

5.3.2. DAMA Assumptions

In developing the plans, and costs for the HEX beamline, we have made the following assumptions.

- There will be adequate high-performance central storage and archive capabilities available to store all data for a period consistent with the NSLS-II data policy. The local storage situated at the beamline is intended as a cache only (at the level of a few days of storage), and all data will be accessed via the central storage facility.
- There is sufficient computational processing power available centrally within the NSLS-II to serve the requirements of the beamline for near real-time tomographic data reconstruction.
- It is assumed that all the software required to process and analyze the data has been developed elsewhere.

5.3.3. Use Case for EDXD Line Scans and Time scans at Different Charge States

The following Use Case outlines a typical EDXD experiment.

5.3.3.1. Preliminary work

User to fill out an experiment plan. Information could include, sample material, thickness, position in the robot carousel, etc. Also used for metadata and sample tracking.

Calibrations that should be done at the start of each experiment sequence.

- Energy calibration
- Slit calibration

The workflows associated with these calibrations are listed at the end of this document.

5.3.3.2. Assumptions:

NSLS-II Laboratory Information Management System (LIMS) is working.

EPICS layer motion and detector controls hardware are all working.

Detector – point detector Ge detector masked by slit4 to an aperture of about 10 mm (H) by 0.4 mm (V). The detector is analyzed by MCA (multiple channel analyzer) that has 9192 channels.

Data rates are low.

5.3.3.3. Actions;

1	Set the instrument to EDXD mode	
a	Move front-end aperture to smallest aperture position	
b	Move imaging detector out of the beam	
c	Lower the beam conditioning table to white-beam position	
d	Remove the KB-mirror from beam	
e	Move the F-hutch slits to nominal 0.1 mm x 0.1 mm (centered)	
f	Move the EDXD detector/imaging detector table into EDXD position	
g	Remind user (or automate)? to protect the imaging and ADXD detectors	
h	Make sure that the detector 2-theta angle is not zero before the user is allowed to open the shutter	
2	Confirm energy calibration is valid, if not, do this now	
3	Open the FOE shutter	
4	Confirm calibration of slits is valid, if not, do this now	
5	Confirm calibration of anti-scatter slits is valid, if not, do this now	
6	Confirm calibration of slits 3 & 4 is valid, if not, do this now	
7	User (or robot) positions sample (e.g. battery) at the center of sample stage	
8	Move detector 2-theta to user-specified angle, (e.g. 3 degrees)	
9	Set beam defining slits to desired values	(e.g. 0.01 mm vertical by 0.2 mm horizontal)
10	Change slit set 3 and slit set 4 to desired values	
11	Move the sample into the beam using XYZ stages	(Use a phosphor screen taped to the front of the sample for feedback – what about a coated sample holder?)
12	Perform alignment scans for XYZ redefine XYZ in sample's native coordinate system	
13	For each alignment scan:	
a	Plot total intensity as function of motor position	(e.g., I vs. X),
b	Show scatter plot	(vertical being position, horizontal being detector channel, and gray scale being proportional to the log of detector intensity). Figure 133 below shows an example scatter plot of an alignment scan in Y (vertical) direction from the top to bottom of a coin-cell battery, with the gauge volume at the

		center of the battery. The scatter plot is helpful for easy visualization of different phases in the sample.
c	Plot the fitted peak height, peak position, and total intensity as a function of motor position.	It would be desirable to be able to interactively select a region of interest (channel 1000-1050, for example). Figure 134 below shows an example of a scatter plot with regions of interest selected (on the left) and fitted intensity for each peak plotted vs. scan number (on the right).
14	Move sample into region of interest based on the new native coordinate system	
15	User refines the slits, two-theta value, and optional FOE filter (Cu and SiC) to optimize intensity, spatial resolution, and reciprocal space coverage	It would be desirable to develop an algorithm to suggest the optimum configuration based on user-provided information on sample thickness, composition, expected concentration of phases interested in measuring, and desired gauge volume.
16	Remove battery sample, position NIST standard Alumina plate sample at the center of the sample stage	
17	Use the Ge detector total intensity as detector, scan sample z (along beam)	
18	Plot total intensity as a function of Z	
19	Move the sample into the fitted center. The fitted edge length of the trapezoid indicates the gauge volume along the beam	
20	Take diffraction pattern using the Ge detector	It would be desirable to fit the two-theta value using linear interpolation of known d-spacings of Alumina, detector calibration, and initial 2-theta value. This step can be repeated later to assure that conditions have not changed during the experiment
21	User again positions the battery onto the sample stage. The battery is charged to a desired state	
22	Perform a line scan (e.g., X from 0 to 0.1, 21 points, 100 s per point). For each scan	
a	plot total intensity as function of motor position (e.g., I vs. X)	
b	show scatter plot (vertical being position, horizontal being detector channel, and gray scale being proportional to the log of detector intensity)	
c	User to be able to interactively select a region of interest (channel 1000-1050, for example), and plot the fitted peak height, peak position, and total intensity as a function of motor position	
	The following data needs to be saved Intensity vs. channel for each scan Intensity vs. energy using current detector calibration. Intensity vs. d-spacing using current 2-theta calibration An information file containing position of motor being scanned, other relevant motor positions (2-theta pseudo motor, fitted 2-theta, current detector calibrations a and b, slit sets 1, 3, and 4, sample stage positions, filter settings. The information file should also contain the command used for the current scan, as well as time and date at beginning and end of scan.	
	Allow User the option to specify a second oscillation motor, oscillation range (e.g., Y oscillates from -1 to 1 mm at each X). The software adjusts speed of oscillation motor to perform the	

	oscillation in exactly the specified scan time. The software should change the speed back to nominal value after the scan. The software should also warn user if the desired speed to too fast for the motor hardware.	
	Uses moves the battery to a point of interest, and perform time scan	For example, 100 s per data point, rest 500 s in between. The fast shutter should be closed in between acquisition. For each scan, plot total intensity as function of time. In addition, show scatter plot (vertical being time, horizontal being detector channel, and gray scale being proportional to the log of detector intensity). It would be desirable to be able to interactively select a region of interest (channel 1000-1050, for example), and plot the fitted peak height, peak position, and total intensity as a function time. As in line scan, it would be desirable to specify an oscillation motor and perform oscillation for better powder averaging at each time point.

5.3.3.4. Calibrations;

	Energy Calibration	
1	Prompt User to do a calibration	Could this be automated with robot?
2	Perform Energy calibration of Ge detector if desired using Am source	E=a+bN, where N is the detector channel number. This uses linear interpolation and known fluorescence line energies of the Am source.
	Calibration of slits Slits (set 1 to 4) must have backlash correction when opening	would be great if automated, optional if performed recently
1	Position YAG crystal on the sample stage	
2	Zoom sample camera in on the crystal as visual aid. Use the ion chamber as detector	
3	Inform User that the beam defining slits (slit set 1) are being calibrated	
4	Open outboard to 5 mm, scan inboard from 5 to -2, 70 points, 1 s per point, and plot IC intensity. Fit inflection point. Move the inboard to inflection point, redefine inboard slit as 0	
5	Scan outboard from 0.5 to -.5, 100 points, 1 s per point, plot intensity, fit position for 0 intensity. Move inboard to the fitted position, redefine inboard as zero. Now the slits are calibrated to a precision of about 1 micron.	
6	Open inboard and outboard to 0.05 mm (0.1 mm horizontal beam size), repeat steps a and b for top- and bottom slits	
7	For anti-scatter slits (slit set 2): Perform above steps a, b and c for slit set 2 if needed.	
8	We assume that slits 3 and 4 are nominally correct, they do not need to be calibrated often as they are self-defining).	Need a simple algorithm to decide whether or not to calibrate.

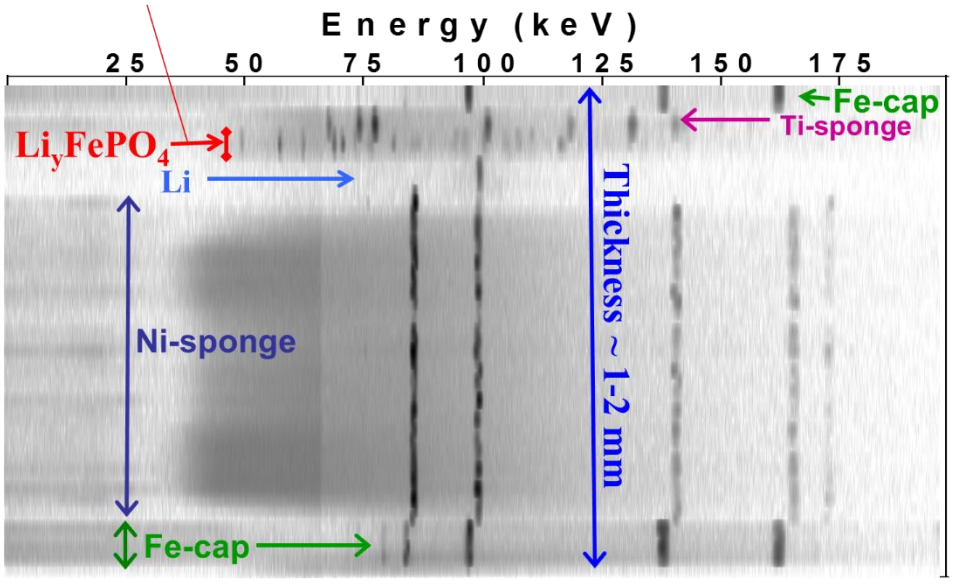

Figure 133 Example EDXD Scatter Plot

Figure 133 shows an example scatter plot with mark-up. The scatter plot is arranged so that the vertical axis is the position of motor being scanned, the horizontal axis is the channel number of MCA or x-ray energy based on current calibration, and the gray scale is the log of the intensity in the MCA channel.

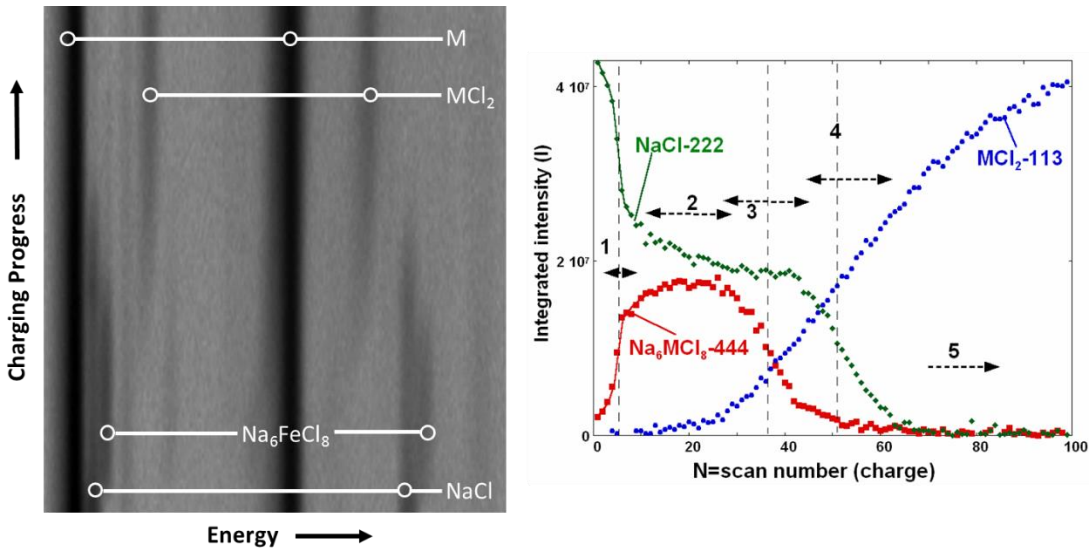

Figure 134 EDXD Scatter Plot with ROI Selected

The figure on the left of Figure 134 shows an example of a scatter plot with a regions of interests (ROI) selected (around a single or a few diffraction peaks). The plot on the right shows the intensity of each region of interest vs. scan number.

5.3.4. Use Case for an Imaging Experiment

5.3.4.1. Preliminary work

- User to fill out an experiment plan. Information could include, sample material, average diameter, the range of height (Y) to be imaged. Also used for metadata and sample tracking.
- Since HEX imaging detector table is moved out-of-way for EDXD and ADXD, the following calibration and adjustment should be done if the imaging table has been moved
    - Calibrate center of rotation (x, horizontal) in terms of detector pixel.
    - Adjust sample stack roll (around the beam, Z) so that the detector rows (horizontal) are perpendicular to the sample's rotation axis.
- If the sample stack has been moved prior to the experiment, the following calibration and adjustments should be performed
    - Calibrate center of rotation (x, horizontal) in terms of detector pixel
    - Adjust sample stack roll (around the beam, Z) so that the detector rows (horizontal) are perpendicular to the sample's rotation axis; Adjust sample stack pitch (around X) so that the rotation axis is perpendicular to the beam
    - Adjust sample stack X (perpendicular to the beam)

The workflows associated with these calibrations are listed at the end of this section.

5.3.4.2. Assumptions:

- NSLS-II Laboratory Information Management System (LIMS) is working.
- EPICS layer motion and detector controls hardware are all working.
- The detector is a 2D imaging CCD or CMOS detectors with different scintillators to achieve different field of views (larger field of view corresponds to lower resolution. The resolution is approximately 0.1% of the field of view, and the optimum scintillator thickness is approximately 10 times the resolution or 1% of the field of view). The 2-D detector is read out in single-frame mode as needed, or in continuous mode at pre-set intervals.
- Data rates are high.

5.3.4.3. Actions

1	Set the instrument to imaging mode.	Most of these steps are performed by software using pre-defined positions with user confirmation at each step that there are no issues such as cable interference.
A	Based on the desired field-of-view, move the front-end aperture to the smallest aperture position that gives a beam larger than the field of view.	
B	Move the four-jaw slits in the FOE to positions yielding a field of view that is slightly (about 5%) larger than the desired field-of-view.	
C	Based on the field-of-view (FOV), suggest to the user the appropriate filtering based on a pre-defined lookup-table.	For example, for 20 mm x 100 mm FOV, suggest 15 mm SiC, for 10 mm x 10 mm FOV, suggest that no additional filtering is needed. The user determines the filter(s) to be used. The control software then moves the appropriate filter(s) into the white beam.
D	Software moves the imaging monochromator to the desired x-ray energy. Both crystals should be bent to a nominal radius of 20 m for imaging. The software presents the user with the suggested bending radius of 20 m. The user selects the bending radius. The software bends the crystals to the desired value based on lookup-table.	

E	Software raises the beam conditioning table to the pre-defined monochromatic-beam position.	
F	Software removes the KB-mirror from beam using pre-defined position	
G	Using the lateral (x, perpendicular to the beam) motion of the EDXD/imaging detector table, move the desired imaging detector (based on the field-of-view and resolution needed) into the beam.	This assures that the EDXD detector is out of the beam.
H	The software adjusts the detector optical zoom and vertical (y) position to position the desired detector into the beam	
I	Move the F-hutch slits to values corresponding to the desired field of view (centered).	This set of slits will be used to define the imaging beam on the sample and detector
J	Ask the user to determine the detector distance from the sample (to optimize phase contrast or attenuation contrast). Software moves the detector to the specified Z (along beam) position	
K	Remind user to protect the ADXD detector	
2	The user opens the front-end and FOE shutters.	
3	Using the diagnostic flag at the monochromator, and the ion chamber in the F hutch, the beamline scientist tunes the second crystal's pitch and roll to optimize intensity and uniformity of the imaging beam.	
4	For imaging, the energy calibration is not critical. Thus the software will present the user with the date of energy calibration at this point.	
5	Using the ion chamber and second crystal's pitch, the user performs the rocking curve. The user moves the pitch to the fitted center of the rocking curve. The user measures the ion chamber for the same time as used for the rocking curve measurement to confirm that the intensity value is approximately (within 5%) the peak intensity of the rocking curve. This alignment can be automated in the future.	
6	The user confirms calibration for center of rotation is satisfactory, if not, do this now.	
7	The user confirms that the alignment of the sample rotation axis (in pitch and roll) is valid. If not, do this now. The required precision is about 0.1 milli-radians. Thus unless the sample stack is removed and re-installed, the alignment should be good.	
8	User (or robot) positions sample (e.g. battery) at the center of sample stage	
9	Single-image: User commands the detector to acquire for a desired period of time, e.g. 1s, the software resets the imaging detector, opens the fast-shutter in the F hutch to illuminate the imaging detector, exposes the detector for 1s, closes the fast shutter, readout and displays the image in logarithmic scale. The user should have the option of saving the image.	
10	The user single-image iteratively while adjusting the x and z sample motors (above the air-bearing rotation) and air-bearing to position the sample into the field-of-view, and to assure that there are air-gaps at both the left and right sides of the image at all rotation angles. At this time, the user may make minor adjustments of the field-of-view using the F hutch slits and FOE slits. The position of the sample stack (with the exception of air-bearing) is defined as the imaging position. The software updates the definition of imaging position.	
11	The user moves the sample out of the beam by lowering it (y-) or moving it laterally (x) to allow the beam to continue un-impeded onto the detector. The user acquires a single-image to verify that	

	no object is in the beam path. This is defined as the air-position. The software updates the definition of air-position	
12	The user opens the CT acquisition program. The acquisition program should have the imaging position and air position information pre-filled. The user is allowed to make adjustments to these positions as needed. The program should allow the user to define acquisition time per-frame, number of pre-image air frames, number of CT frames, air-bearing angular range (usually 0-180 degrees), step size for air bearing as calculated from the range and number of CT frames, number of post-image air frames.	
13	The user launches the CT acquisition program. Without user intervention, the software	
A	Moves the sample stack to the air-position, keep the fast-shutter closed, resets the detector, and continuously expose and readout detector using the pre-defined acquisition time and the number of pre-image air frames. The average of these dark images, defined as Dark, will be used to correct all subsequent air and CT images on a pixel-by-pixel basis	
B	Moves the sample stack to the air-position, opens the fast-shutter, wait for about 30 ms, resets the detector, and continuously expose and readout detector using the pre-defined acquisition time and the number of pre-image air frames. Closes the fast shutter. The average of these images is defined as Air1.	
C	Moves the sample stack to the imaging position. Changes the speed of air-bearing so that the air-bearing rotates exactly the step-size during the acquisition time. Moves the air-bearing to start-ramp, where ramp is a pre-set small angle (e.g. 0.1 degrees) to allow the air-bearing to be at constant speed before imaging. Opens the fast shutter slightly (about 30 milliseconds) before the air-bearing is expected to reach the starting angle. Resets the detector when the air-bearing reaches the starting angle, and continuously expose and readout detector using the pre-defined acquisition time and the number of CT image frames. Closes the fast shutter. Changes the speed of air-bearing back to nominal speed. These images are defined as Data for subsequent discussions.	
D	Moves the sample stack back to the air-position, opens the fast-shutter, wait for about 30 ms, resets the detector, and continuously expose and readout detector using the pre-defined acquisition time and the number of post-image air frames. Closes the fast shutter. The average of these images is defined as Air2.	
E	The raw data are saved as they are acquired.	
F	In a separate information file, the following parameters are saved: the acquisition parameters (x-ray energy, positions of slits in F hutch, # air, # data frames, acquisition time, detector used, pixel size, detector X, Y, Z positions, sample stack positions for air and imaging) and reconstruction parameters.	

The acquisition program should be based on the acquisition BlueSky scripts currently in use at FXI beamline. The program should have the flexibility to allow beamline scientists and users to modify or add additional scripts.

It would be desirable to have the flexibility of using external software/hardware trigger to start a CT acquisition program using pre-defined parameters.

	Separate analysis software is used to view, reconstruct, and analyze the CT data.	We suggest that the reconstruction be based on TomoPy
A	A separate analysis software displays the individual frames as they are acquired. The image can be raw data or background-corrected images. The algorithm for background-correction is BC=(Data-Dark)/(Air1-Dark) on a pixel-by-pixel basis	
B	The analysis software displays the sonogram for a user-selected row using background-corrected data BC. It also gives the user the option to reconstruct a CT slice of the sonogram using filtered back projection for the data frames acquired	
C	At the end of the scan, the analysis software compares the Air1 and Air2. On a pixel-by-pixel basis, the software calculates the Drift_Image as (Air1-dark)/(Air2-dark). The user is presented with a histogram adjustment of this Drift_Image. The histogram is centered around 1. If there is a significant difference (greater than 5% for 50% of the pixels), the software warns the user of beam intensity drift during CT scan	
D	At the end of the scan, the analysis software calculates the background-and-drift corrected data using the following algorithm: BDC=(Data-Dark)/(Interp(Air1:Air2)-Dark), where Interp function linearly interprets between Air1 and Air2 based on the data frame number using: (Air1*(N-n)+Air2*(n))/N, where n is the frame number of current data, and N is the total number of data frames acquired	
E	In addition to the raw-data (Dark, Air1, Data, Air2) that are saved as they are acquired, the analysis software saves the background-and-drift corrected data BDC	
F	In a separate timing file save the following: the starting time for each data frame, the encoder position of the air-bearing at that time, and the ion chamber reading. This can be used for troubleshooting later if there are issues with the synchronization between the rotation hardware and the detector. The ion chamber reading can be used to refine/trouble shoot background correction/beam drift issues	
G	The user has the option of displaying individual data frames, perform histogram adjustment of the individual data frames, display the sonogram of a select slice, reconstructing a slice using TomoPy, change reconstruction parameters used by TomoPy (filtering, the center of rotation) and displaying the reconstructed slide for histogram adjustment	
H	In the analysis software, the user should have the option to reconstruct, using TomoPy, all data frames and save the reconstructed data in tiff format	
I	The user should have the option to navigate the volumetric data and perform histogram adjustment, slice in chosen planes, and screen-grab using third-party image-processing software such as ImageJ or DataViewer	
	For CT of batteries at different charge states, the GUI should give the user the option of performing CT images (described in step 13) automatically and periodically, e.g., every 30 minutes	

	16. In the future, for performing the CT image of very large samples, the user should be given the option of acquiring the CT set above using different sample-stack Y (vertical), and stitching the reconstructed images together. This is a low priority given the large 20 mm vertical FOV in hutch F	

5.3.4.4. Calibrations

Since the HEX is expected change regularly between imaging and diffraction, automatic alignment is desirable in the future. The following calibration/alignment procedures are written with this long-term goal in mind. It is acceptable to perform these manually in the first 1-3 years.

Calibration of the center of rotation

1	Acquisition software brings the sample stack to pre-defined position for calibration of the center of rotation. This position should place the pin phantom at approximately the center of rotation, and allow the pin to be fully in the beam vertically	
2	The user places pin phantom on the sample stack, opens the front-end and FOE safety shutters, and launch the calibration scan. The pin phantom is a Tungsten cylinder with flat top, with 0.5 mm diameter and 25 mm height. The wire should be on a magnetic-base kinematic mount to allow repeatable installation on and removal from the sample stack	
3	Software performs CT of the pin phantom as described in step 13 above, using pre-defined acquisition parameters, for example, air position is 15 mm below current imaging position, 2000 frames with 0.2 s acquisition time, 360 degrees rotation, 10 frames for the air/dark data	
4	Software calculates the background-and-drift corrected sinogram (in terms of -ln(I/I0) for row 1. For each row in the sinogram, software fits the center of the pin's attenuation. Then the software fits the center position as a function of rotation angle to a 360-degree sine-wave	
5	Software performs the above step for all rows. The software presents a plot of fitted center of rotation as a function of vertical position (column number), calculated average and median values. The user can choose between using the average or median as the center of rotation	
6	After determining the center of rotation in terms of detector pixel, the software presents the old value to the user, confirms with the user before replacing the new center-of-rotation value in the database	

Adjustment of sample-stack pitch and roll

1	Acquisition software brings the sample stack to pre-defined position for pitch and roll adjustment. This position should place the flat-head pin phantom at the center of rotation, and place the head of the pin at approximately the center of the beam vertically. The air bearing should be at absolute zero, defined as when the direction of X motor above it is truly perpendicular to the beam	
2	The user places pin phantom on the sample stack, opens the front-end and FOE safety shutters, and launch the calibration scan	

3	Software moves the X motor above the air-bearing to about 3/8 of the horizontal field of view	
4	Software acquires 10 of each set: Darkfield images with fast shutter closed, Air images by lowering the sample stack to move the pin out of the beam, Data with air bearing at absolute 0, 90, 180, and 270 degrees	
5	The software calculates the 4 background-corrected images of the pin sample	
6	The software fits the position of the pin-head in terms of detector row (x) and column (y) for each image. Presents the user with a zoom-in image of the pin with the pin-head position for confirmation for each of the four images	
7	From the 0- and 180- degree images, the roll correction, in radians, is calculated as dy/dx, where dy is the difference in the vertical position of the pin between the 0- and 180- degree images, and dx is the difference in horizontal position. The software verifies that dx is approximately (within 5%) the offset distance when converted to absolute distance using known detector pixel size	
8	From the 90- and 270- degree images, the software calculates the pitch correction, in radians, as dy/dx, where dy is the difference in the vertical position of the pin between the 90 and 270 degree images, and dx is the same value as obtained in the above step	
9	Software converts the corrections to degrees and presents user with the suggested corrections. Upon confirmation, the software makes the correction using the pitch and roll motors at the bottom of the sample stack	
10	Software repeats above steps 4 to 9 to make sure that the new suggested correction is negligible (<0.001 degrees).	
11	Software saves the new pitch and roll motor position into the database	

Adjustment of sample-stack X (perpendicular to the beam)

1	Perform above procedure Calibration of the center of rotation	
2	If the difference between the center of rotation (in pixel) and half of the horizontal total pixel number is more than 5% of the total pixel number, suggest to the user that the sample-stack X position should be corrected. The software calculates the difference in mm using known detector pixel size and presents the user with suggested correction amount	
3	Upon confirmation of user, the software moves the X motor below the air-bearing and updates the X motor position in the database	
4	Repeat procedure Calibration of the center of rotation to ensure that the suggested correction amount is less than 1% of total pixels	

5.3.4.5. Future Developments for Imaging Software and Automation

- Automated detector spatial correction with a dot-grid phantom. This requires some R&D.
- Construction of a plexiglas phantom with embedded steel wires and spheres for automated position registration of the CT image with EDXD gauge volume. This also requires R&D
- Development of an aluminum phantom for determining the absolute CT number.

- Pursuit of an idea from Michael Drakopoulos for fitting the sample stack pitch / row via CT images of offset sample.
- Helical scanning: the HEX beam has high vertical FOV (20 mm), so for most samples helical CT is unnecessary, although a helical scan scheme has some other benefits such as reducing ring artifacts. Helical CT would therefore be a welcome development for the long term.

5.3.5. Use Case for ADXD Experiment

5.3.5.1. Preliminary work

User to fill out an experiment plan. Information could include, sample composition, average thickness, capillary or plate, stationary, oscillation, or spin

Since HEX ADXD detector table is moved out-of-way for EDXD and imaging, the following calibration and adjustment should be done if the imaging table has been moved

- Calibrate beam center on the detector
- Calibrate detector-to-sample distance
- Align the beam stop

If the sample stack has been moved prior to the experiment, the following calibration and adjustments should be performed

- Calibrate detector-to-sample distance

The workflows associated with these calibrations are listed at the end of this document.

5.3.5.2. Assumptions:

NSLS-II Laboratory Information Management System (LIMS) is working.

EPICS layer motion and detector controls hardware are all working.

Detector – 2D flat-panel detector with 4096 by 4096 pixels. The 2-D detector is read out in single-frame mode

5.3.5.3. Actions

1	Set the instrument to ADXD mode.	Most of these steps are performed by software using pre-defined positions with user confirmation at each step that there are no issues such as cable interference.
A	Move the front-end aperture to the smallest aperture position	
B	Move the four-jaw slits in the FOE to positions yielding a beam specified by the user	Typically this is ~0.5 x0.5 mm
C	No additional filtering is needed for ADXD. The control software moves all filters out of the white beam	
D	Software moves the imaging monochromator to the desired x-ray energy. Both crystals should be bent to a nominal radius of 40 m for ADXD. The software presents the user with the suggested bending radius	

	of 40 m. The user selects the bending radius. The software bends the crystals to the desired value based on lookup-table	
E	Software raises the beam conditioning table to the pre-defined monochromatic-beam position	
F	Depending on if micro-focusing is needed, the software removes the KB-mirror to clear the beam using pre-defined position (no focusing) or moves the KB-mirror into the beam (focusing)	
G	Using the lateral (x, perpendicular to the beam) motion of the EDXD/imaging detector table, move the table to the furthest position in-board. This assures that the EDXD and imaging detectors are out of the beam. Using the lateral motion of the ADXD table, the software moves the ADXD table into pre-defined position	
H	The software moves the vertical (y) position and tilt of the ADXD detector to pre-defined position, depending on the if micro-focusing is used	
I	The software moves the X and Y of the beamstop to predefined positions (this depends on if K-B mirror is used) so that it is in the beam	
J	If no focusing is used, the software moves the F-hutch slits to values corresponding to the desired beam size. This set of slits will be used to define the beam on the sample.	
K	Ask the user to determine the detector distance from the sample. Software moves the detector to the specified Z (along beam) position	
2	The user opens the front-end and FOE shutters	
3	Using the diagnostic flag at the monochromator, and the ion chamber in the F hutch, the beamline scientist tunes the second crystal's pitch to optimize the intensity of the beam	
4	Beamline scientist aligns the beamstop using the built-in photo-diode as detector	
5	User positions sample at the center of the sample stage. Using the photo-diode on the beam stop as detector, the user aligns the sample in the beam	
6	User determines the data acquisition parameters for the detector (number of data frames, acquisition time, single image with/without oscillation, or raster scan). The software should provide the following acquisition protocols	
A	Single-image: User commands the detector to acquire for a desired time, e.g. 1s, the software resets the imaging detector, opens the fast-shutter in the F	

	hutch to put diffracted beam on the ADXD detector, exposes the detector for 1s, closes the fast shutter, readout and displays the image in logarithmic scale. The user should have the option of saving the image	
B	Single image with oscillation: the user specifies acquisition time, the motor to be oscillated, and the range of oscillation (from current position). The software changes the oscillation motor speed to a speed that allows the motor to move through the oscillation range, and return to the current position, precisely within the acquisition time	
C	Raster scan with or without oscillation: In addition to inputs specified above, the user specifies the motor(s) to be raster scanned, the start, end, and the number of data points for each motor	
D	Time scan with or without oscillation: In addition to inputs specified above, the user specifies the number of time points and wait-time in-between scans	
7	User launches the acquisition script. The software opens the fast shutter, wait for the pre-determined shutter opening time (e.g., 10 ms), launches the oscillation or spin motor as needed, resets the detector, and performs the acquisition. After an acquisition, the software closes the fast shutter	
8	For raster scan acquisition, the software moves the scan motor to a specified scan position and performs above step 7 with the exception that the fast shutter remains open till the raster scan is finished	
9	For time scan acquisition, the software performs above step 7 at designated time	
10	Data is saved to the pipeline as it is acquired using procedures developed at the XPD and PDF beamlines for powder diffraction data acquisition	

The acquisition program should be based on the acquisition BlueSky scripts currently in use, and being refined, at the XPD and PDF beamlines. The program should have the flexibility to allow beamline scientists and users to modify or add additional scripts.

5.4. References

[1] NSLS-II, 2010. “Beamline Controls,” Preliminary Design Report (PDR).

[2] A. Broadbent, et al., “Beamline Instrumentation Interfacing Standard,” LT-C-XFD-SPC-CO-IIS-001.

[3] NSLS-II, 2010. “Insertion Device Control,” PDR.

[4] D. Chabot. “Tech Specs for the NSLS-II Motion Controllers,” LT-C- XFD-SPC-CO-MC-001.

[5] E. Johnson. “NSLS-II Nomenclature Standard,” LT-ENG-RSI-STD-002.

[6] A. Broadbent. “Beamline Coordinate System Standards,” LT-C-XFD-STD-BL-COORD-001.

[7] NSLS-II, 2010. “Front End Control,” PD

6. Data Storage Requirements

The following estimate of data quantity is included to help with the sizing of storage and network connections. The data to be stored includes the following;

- Sample metadata
- Beamline setup (configuration); several hundred channels of data, sufficient to allow the beamline configuration to be restored.
- Detector data, e.g. CCD frames.

By far the greatest amount of data will come from the detectors; this is very considerable and is summarized below. It is clear that within a very short space of time access to the centralized data storage facility will be required, and local storage at the beamline would be impractical.

2D Diffraction (mono beam):

- Detector 4K x 4K (Varex Imaging: 100 micron resolution, 41cm size)
- 4B/pixel (float 32 bits)
- Image size = 64MB
- 180 angle points x 50 translation points (say a 1mm object with a 20micron beam)
- size = 600GB (1 cross-section)
- size = 30TB (for the 3D view of the 1mm^3 object)
- Now you need to generate the polarization-corrected, masked, dark-subtracted images as well: 60TB
- At 15fps, you can finish this 3D CT in 8 hours
- Therefore total size is 180TB/day
- 5,000 hrs of user time per cycle and assuming 20% of the beamtime is used for this purpose

Total data per annum: 7PB

Full field imaging (mono or white beam):

- Camera is 2.5K x 2K x 2B = 10MB (Sony Sensor)
- 1500 rotations
- 15GB/CT
- 1 CT in 4s (based on Soleil actual numbers)
- 5,000 hrs of user time per cycle and assuming 10% of the beamtime is used for this purpose

Total data per annum: 7PB

In summary we would expect 10-20PB per annum of storage will be required within 1-2 years of the start of commissioning. We anticipate making extensive use of the lessons learned at the FXI beamline (amongst others); this is now (early 2019) starting to produce similar volumes of data.

7. HEX Beamline Sector and Control Station Design

The design for the HEX sector layout on the experimental floor is shown in Figure 135. This would be a rather congested area given the possibility that three User group could be simultaneously working at the beamline, in the B, D and E hutches simultaneously (in the mature configuration). The fit-out of this area will be done when any of the B, C, or D hutches are fitted out; this layout has been completed for planning purposes only.

It should be noted that the bypass corridor is at a lower elevation than the experimental floor. The steps and small lifts (for equipment and disabled access) are shown. Areas are required for User seating, as well as sample preparation and general workbenches.

It should be noted that the B-hutch will not be built in the initial beamline project scope.

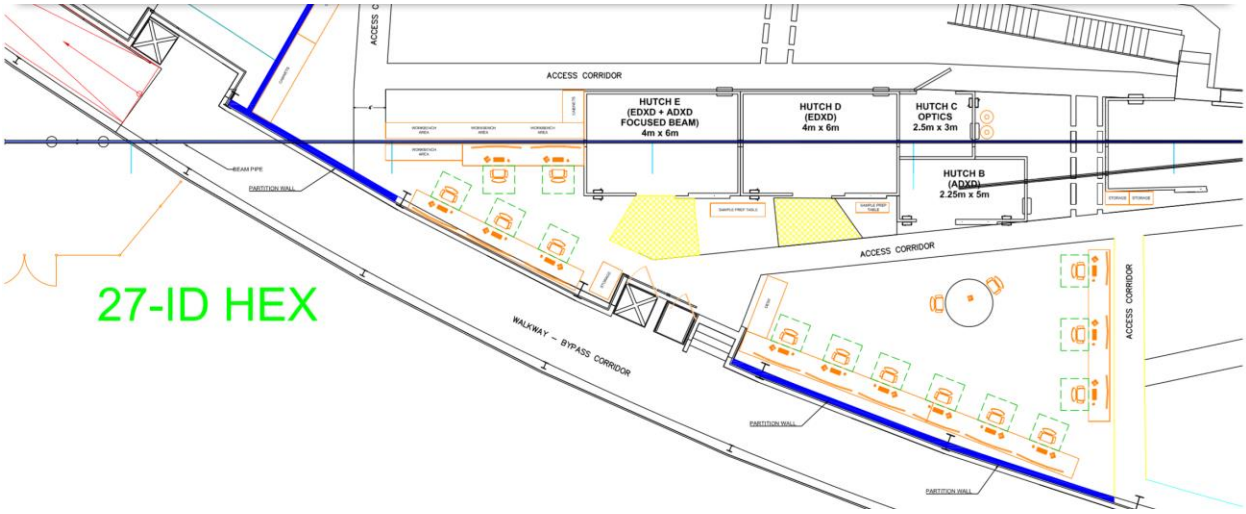

Figure 135 HEX sector layout

The controls station equipment covers the furniture and office equipment not covered in other WBS elements. The following items are included:

- Desktop computers
- Printers
- Desks and chairs
- Small conference table
- Office partitions to section off an area to minimize distractions and noise
- Utility mains wiring and local area network (LAN) built into the desks and partitions
- Whiteboard

Figure 136 shows the proposed layout for the furniture and equipment in the satellite building.

Figure 137 shows the location for the beamline controls racks. These are costed within the controls WBS element, but their locations are included here for completeness.

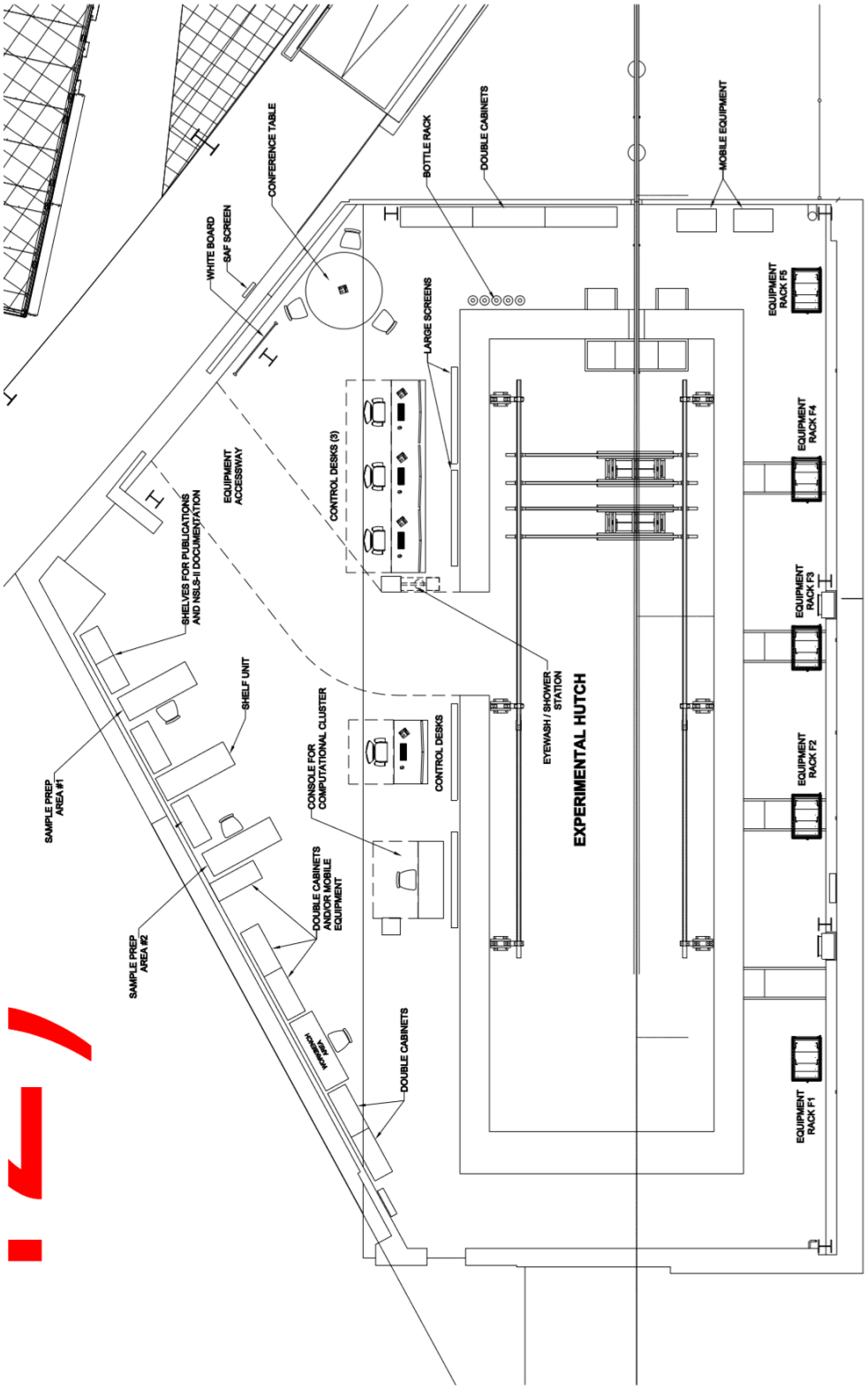

Figure 136 Layout of the furniture and equipment in the satellite building and outside the F-hutch

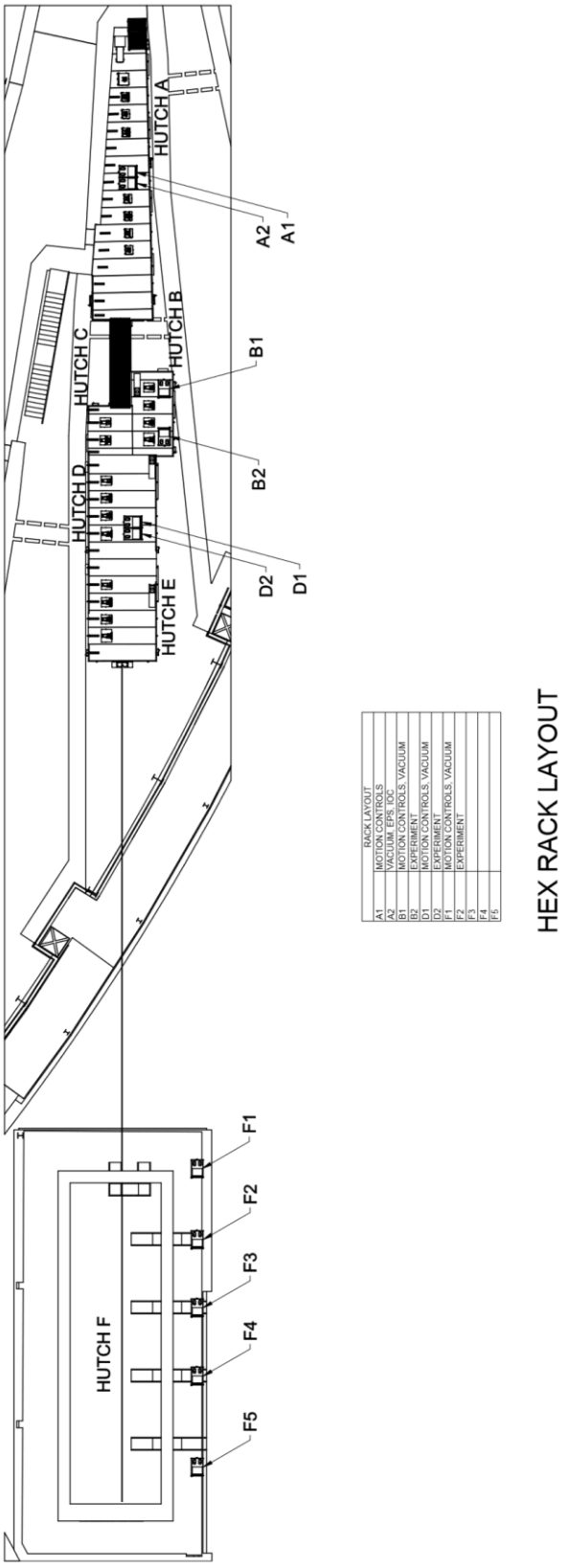

Figure 137 The HEX beamline rack layout

8. Beamline Utilities

8.1. Utilities Overview

The utility systems for NSLS-II beamlines comprise the following services in a standardized (but tailored) "utility pack":

- Mains electrical distribution: 30 kVA total, sensitive and non-sensitive
- Chilled water for electrical racks and user equipment
- De-ionized (DI) water for beamline optical components
- Compressed air, experimental gases, gaseous nitrogen, and liquid nitrogen
- Utility pylons, between hutches, for pipes, electrical conduit, and cable trays

8.2. Mechanical Utilities

The scope includes the supply of air and water in modules (stainless steel for water, copper for air) utilizing purchased standard manifolds, these modules may be added or subtracted as needed by a specific beamline. The scope of mechanical utilities systems is as follows below. Note that some services are not needed on every beamline, such as liquid nitrogen supply, and high capacity compressed air. The specific mechanical utilities requirements for each beamline at NSLS-II are developed in conjunction with the design of each component. An example of the requirements development is shown in Figure 138.

De-ionized Water Distribution

De-ionized (process) water distribution at 45 l/min (12 gpm) (average), 57 l/min (15 gpm) (maximum) at 29.5C+/-0.1C (85F+/-0.2F) and 1 MPa (150 psi) max design pressure at 51C (125 F) and ~0.6 MPa (~80 psi) typical working pressure for beamline components needing cooling due to photon heatloads. Cooled components in the beamline should have the water circuits connected in series in order to limit the total water flow required. The pressure differential across each water cooled circuit should be 0.4 MPa (60 psi) from the point of origin.

Process Chilled Water

Process chilled water at 12C (53+/-2F) and typically 11 l/min (3 gpm) 22 l/min (6 gpm) maximum will be distributed to all equipment racks and end station equipment such as furnaces, compressors, etc. The velocity in the pipe is not to exceed 2 m/sec (6.5 ft/sec). With ~11C (~20F) temperature rise this assumes the removal of ~60% of the 30 kVA per beamline average electrical load with a 24 l/min (6 gallon/minute) flow rate. Typical working pressure 0.3 MPa (50psi). The nominal differential pressure shall be 0.2 MPa (25 psi) with a maximum working pressure of 0.5 MPa (75 psi).

Liquid Nitrogen Distribution

Liquid nitrogen distribution from the local interface point on the storage ring tunnel roof for use with pumped liquid nitrogen cooled heat exchangers (cryocoolers). The system is sized for a minimum flow rate of 12 l/hour (3.1 gals/hr) with 50% of beamlines (20) taking this flow with a supply pressure of 0.2 –0.25 MPa (30–35 psi).

Compressed Nitrogen Gas

Compressed nitrogen gas is available for beamline use with a flow rate up to 10 l/sec (20 scfm), with a nominal working pressure of 0.2 MPa (30 psi) and a maximum pressure of 0.7 MPa (100 psi).

Process Compressed Air

Facility compressed gas (compressed air) is provided at each beamline, with service points distributed at various locations along the beamline. Service is provided at 0.55 MPa (80 psi) nominal, with maximum working pressure of 0.62 MPa (90 psi) and 5 l/sec (10 scfm) flow rate for 5 seconds with 30 second recuperation.

High capacity Compressed Air

For non-critical applications requiring flow rates higher than 5 l/sec (10 scfm), high capacity compressed air service is provided at 0.7 MPa (100 psi), with maximum working pressure of 0.9 MPa (125 psi). The air flow rate varies due to it being dependent upon actual usage within the facility.

Experimental Gases

Experimental gas distribution from gas cylinders is provided to beamlines, as required.

Oxygen Deficiency Hazard (ODH) Sensor

An oxygen deficiency hazard (ODH) sensor and alarm will be installed where required inside hutches. These systems are typically installed inside hutches that have liquid nitrogen supply.

Gas Exhaust System

A gas-exhaust system for the ventilation of fume hoods, etc. is provided by BSA from the user area or from within enclosures to a common exhaust manifold above the experimental floor.

Ventilation System

A ventilation system will be fitted to hutches for forcing filtered experimental hall air into the hutch (this will then leak out via labyrinths and custom air outlets). The fans are mounted on the hutch roofs and air passes in through a vent labyrinth.

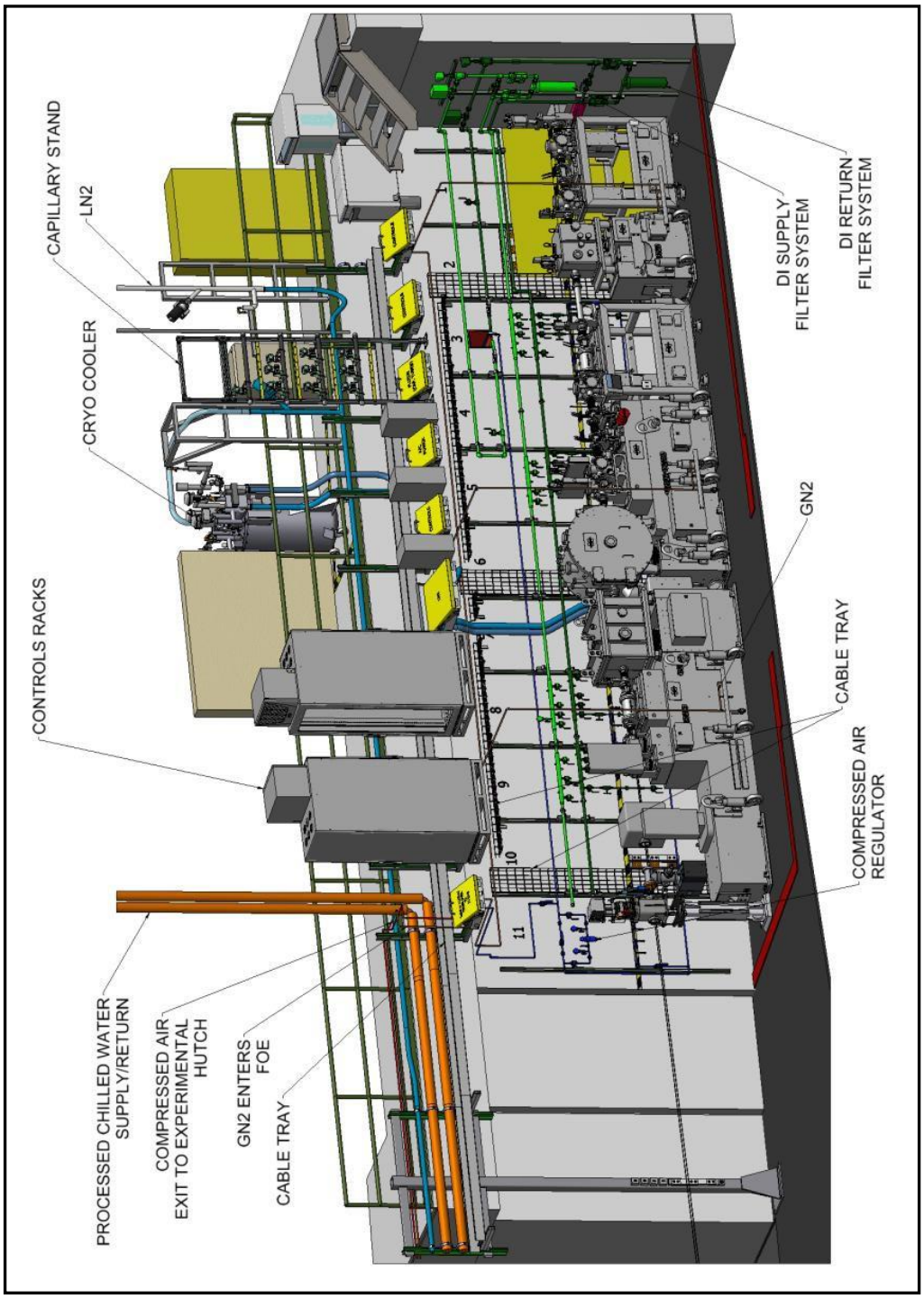

Figure 138 Typical layout of utilities for a First Optics Enclosure

Figure 138 Shows a typical layout of utilities for an FOE; from top: Liquid Nitrogen from a Cryo Cooler, Processed Chilled Water, DI Water flow / return, compressed air, cable trays.

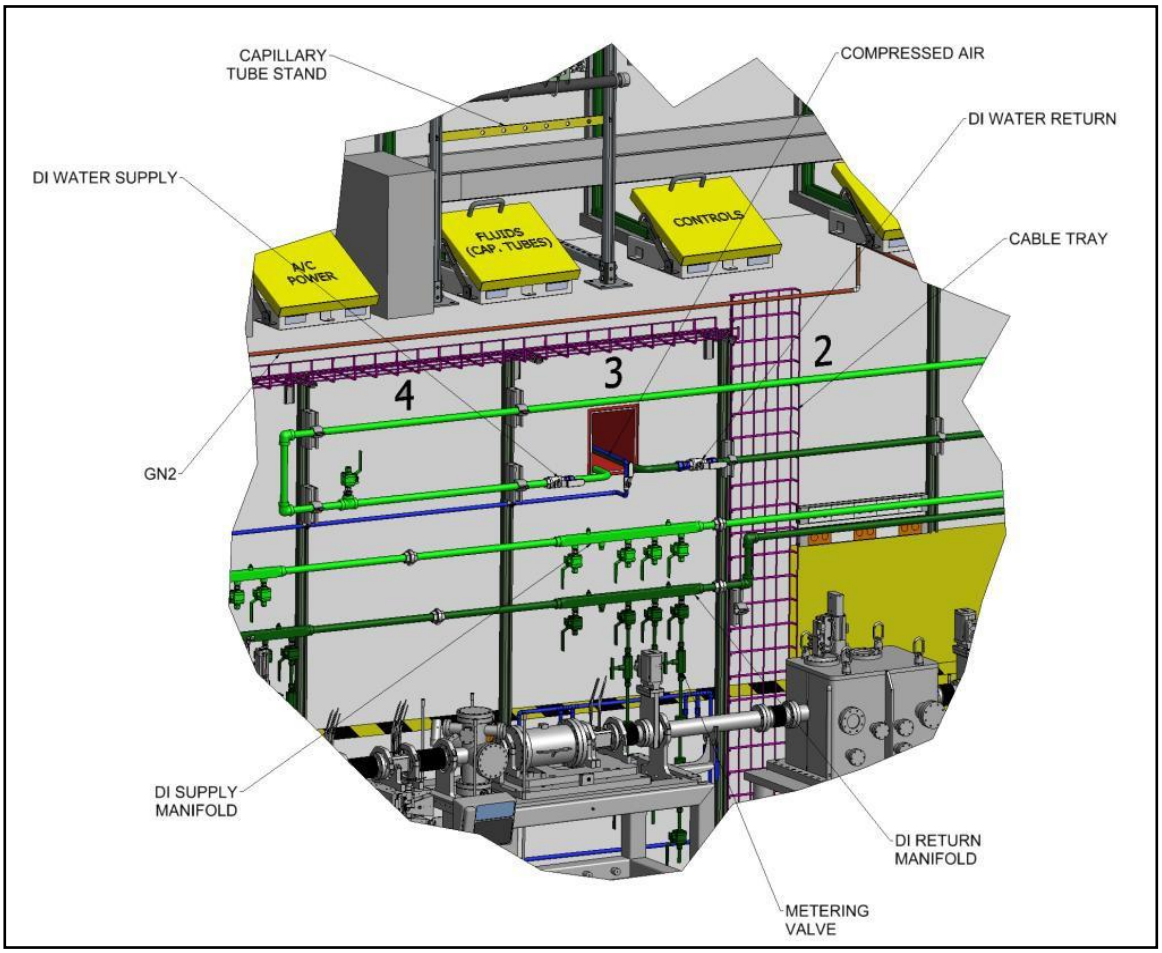

Figure 139 Layout showing the utilities passing through the SR tunnel wall

Figure 139 shows the DI water and compressed air passing through the ratchet wall into the FOE from the SR tunnel, as well as the pipework distribution, along with labyrinth designations.

Figure 140 and Figure 141 (overleaf) show the layout for the following utilities

- De-Ionized (DI) and chilled water
- Compressed air, gaseous nitrogen and liquid nitrogen.

Figure 140 The layout for de-ionized and chilled water

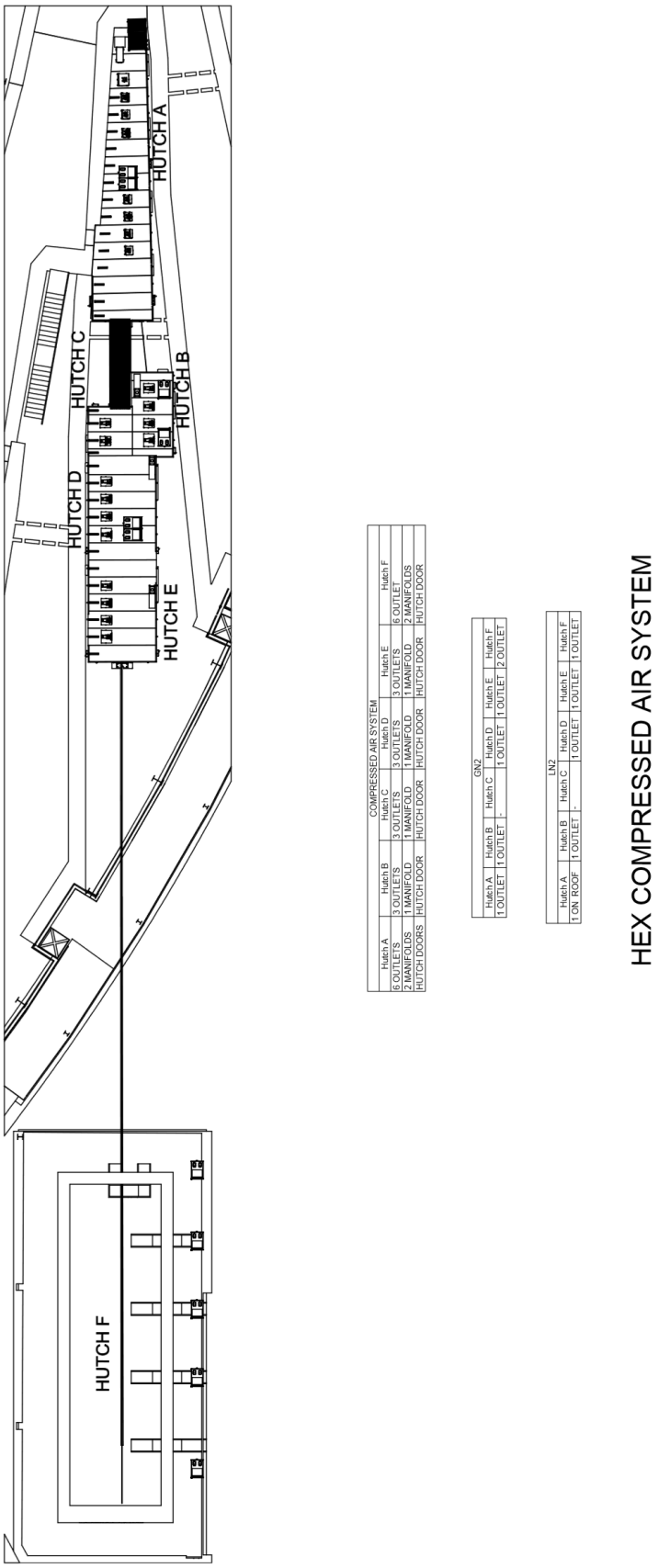

Figure 141 The layout for compressed air, and gaseous and liquid nitrogen

8.3. Electrical Utilities

The scope of Electrical Utilities includes all electrical distribution for a beamline, all electrical grounding to equipment on a beamline, and provisions for cabling (controls, vacuum, network, etc).

Electrical Power

Electrical power distribution to the beamline is comprised of two transformers, each providing 120V (single phase) and 208V (three phase), and 100A.The power distribution includes sub-panelboards with appropriate and properly labeled circuit breakers at each enclosure or experiment area, cable trays, all the electrical outlets in the enclosures and along the beamline and wiring to light fixtures, fans, hoists, etc. inside the enclosures. It also includes electrical power outlets in the hutches, cabins and/or user areas. 480VAC mains is not provided to beamlines as standard, but is available if a specific need for this service is required. Figure 142 and Figure 143 show a typical provisional layout for the electric mains on a beamline.

Electrical Grounding System

An electrical grounding system with busbar distribution is provided inside the hutches, close to the floor and along the inboard wall.

Cabling and Piping Support Structures

Cabling and piping support structures are installed on all beamlines at NSLS-II, including any necessary pylons and roof supports for cable trays, for all utilities, as well as EPS and PPS cables. Figure 145 shows an example of this.

Figure 144 shows the electrical requirements for the HEX beamline. These will be converted into a standard one-line diagram for the electricians a few months before the hutches or the satellite building is complete. The one-line diagram defines the type and rating of the conductors, as well as the breaker panel layouts.

Figure 142 A typical provisional layout for the electrical mains distribution

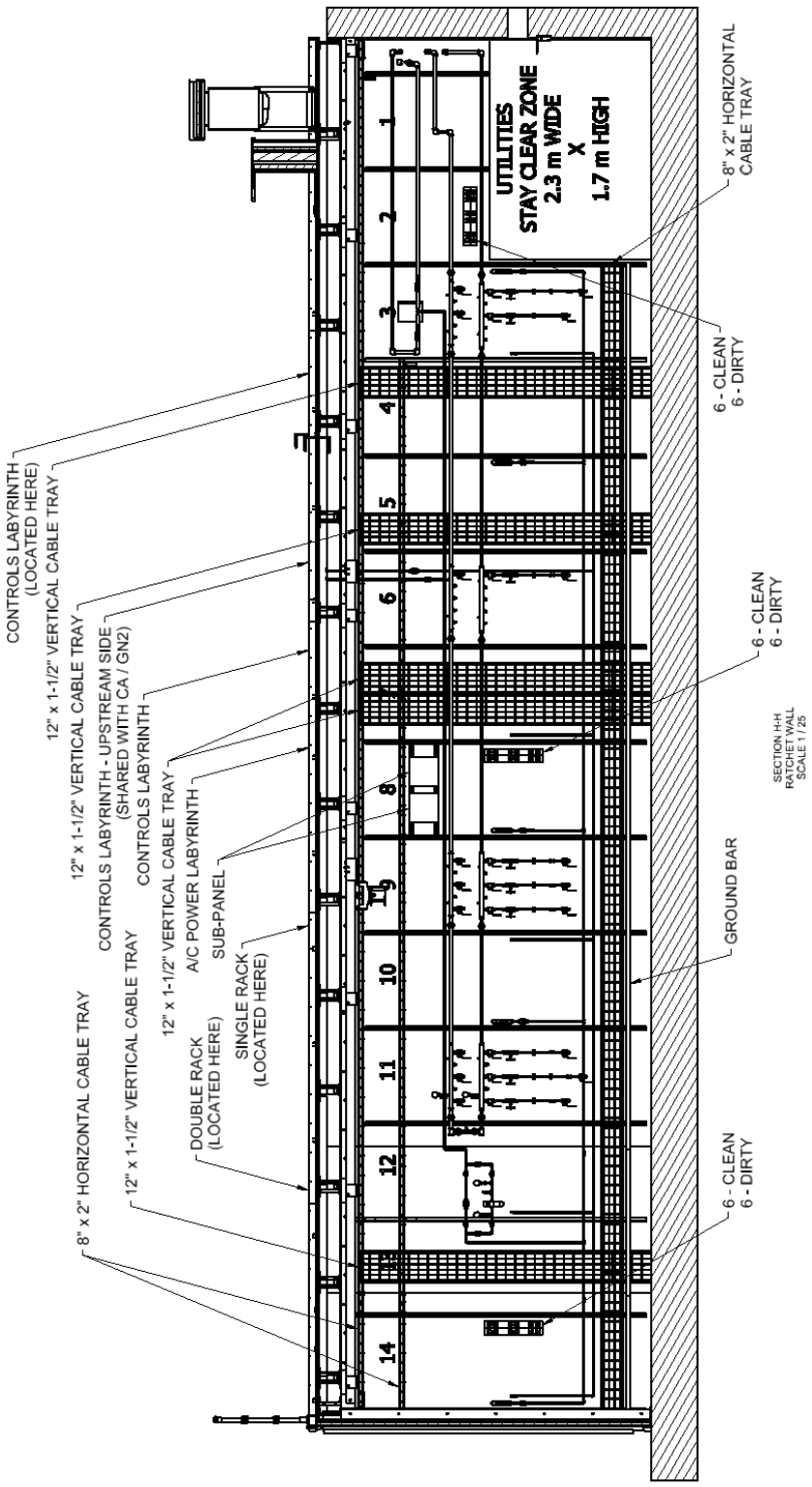

Figure 143 A typical preliminary layout for the electrical distribution within an FOE

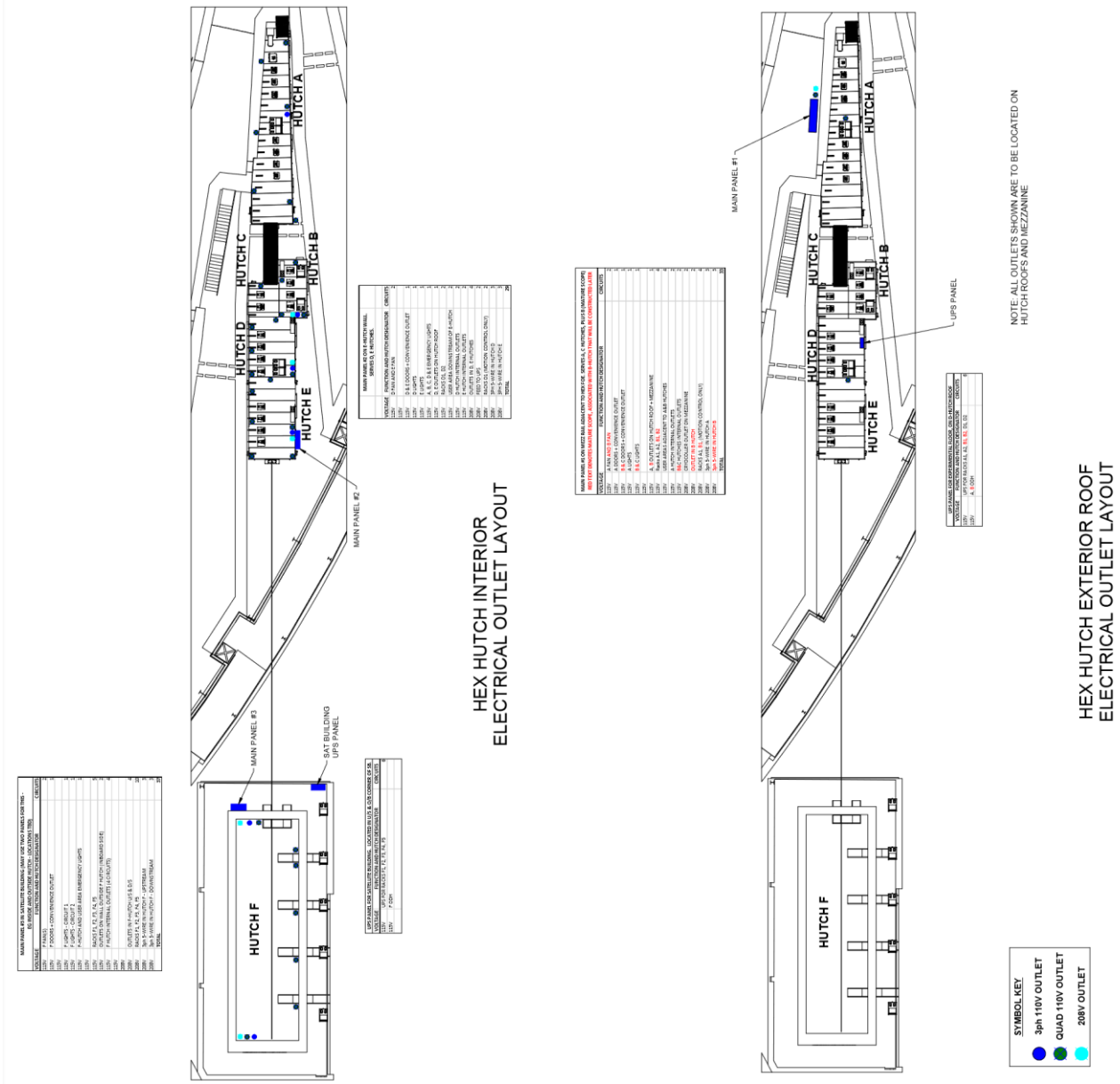

Figure 144 Electrical distribution requirements for the HEX beamline

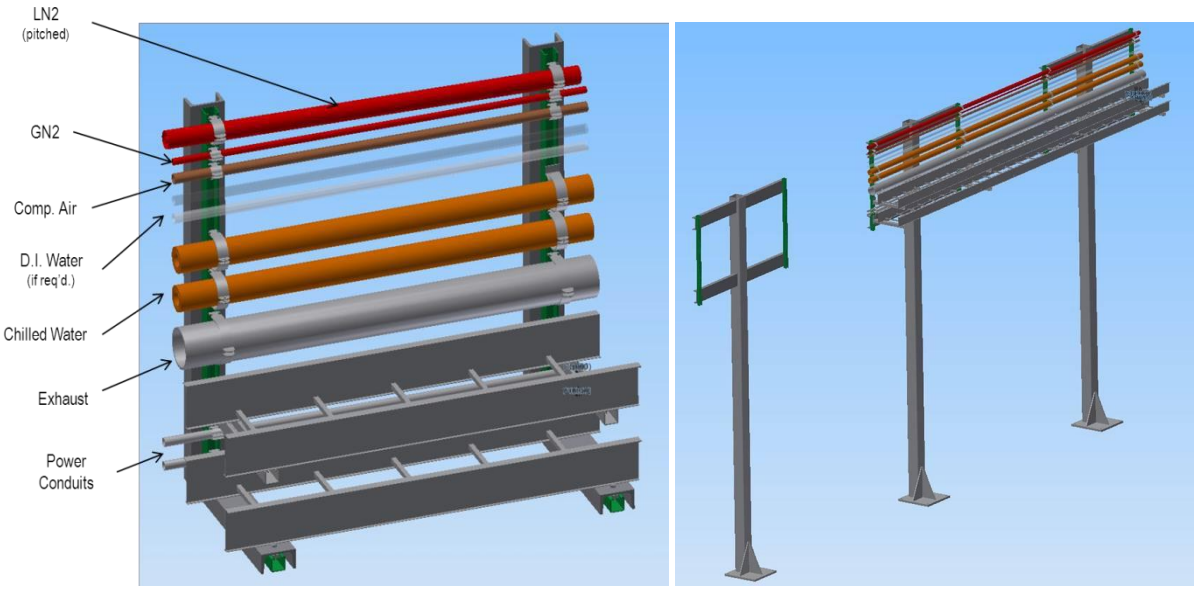

Figure 145 Utility support structures

Figure 145 Shows utility support structures, over hutches and between hutches. The utilities are supported over the hutch roof as shown on the left. Gaps between hutches utilize a pylon system, as shown on the right; the outriggers from the pylons allow a greater cable tray span between pylons and avoid impeding access by forklift or cranes, etc.

9. Protection Systems

9.1. Personnel Protection System (PPS)

9.1.1. Beamline Area PPS

NSLS-II produces intense light from IR, UV, and hard x-rays. Beamlines are designed to use either the bending magnet radiation or the radiation from insertion devices located in the straight sections of the storage ring. Beamlines may have more than one station along the beamline. These stations work in parallel or sequentially. The PPS is an engineered system that provides a means to ensure that personnel are not exposed to the radiation in the beamline enclosures. At NSLS-II, the role of the PPS is specifically to protect personnel from radiation that is present only when there are stored electrons in the storage ring. The PPS will be designed to monitor the various devices installed in the beamline for personnel safety and to provide emergency shutdown in case of any breach of the interlock. The PPS system, along with the required shielding in the beamlines, is designed to provide complete personnel safety during routine operation of the facility and provide protection during abnormal conditions. Figure 146 shows a typical system configuration, in this case for an FOE and two experimental stations, although this is designed to be easily configured to the required number of stations and beamline operating modes.

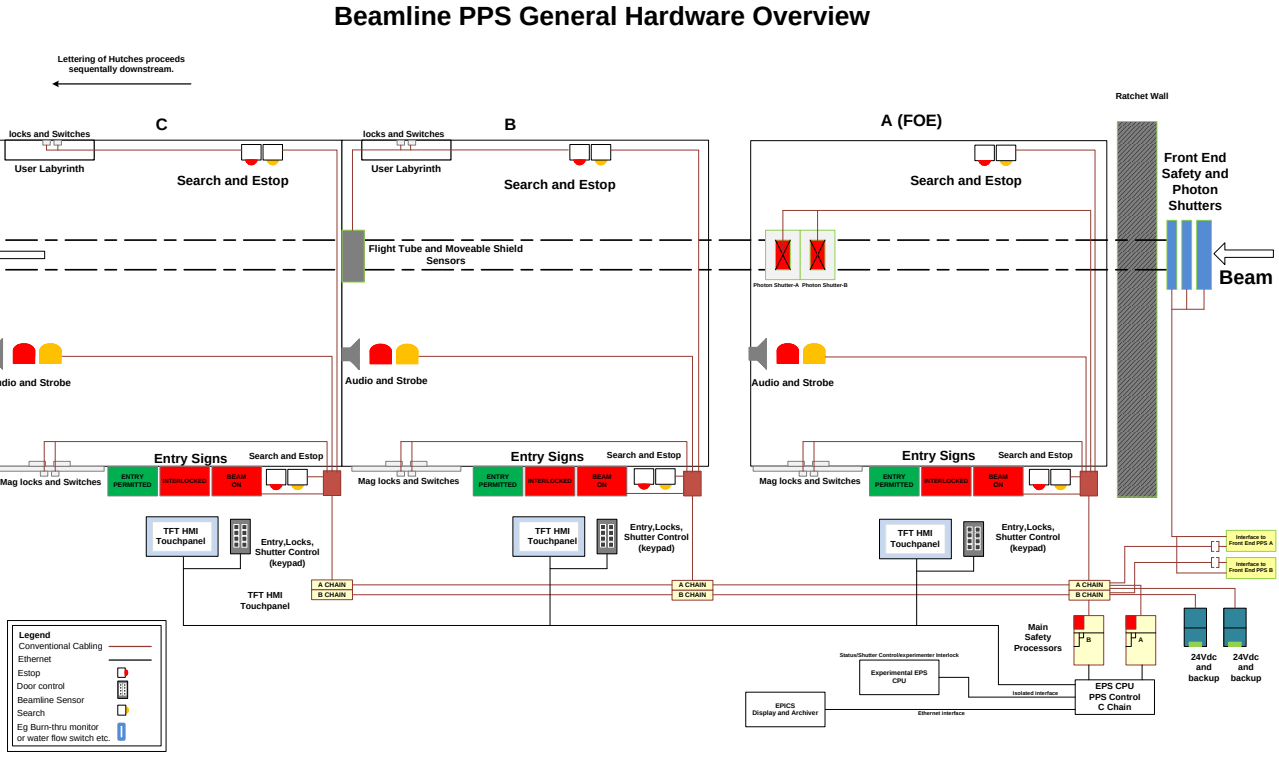

Figure 146 Typical system configuration for a beamline PPS

9.1.2. Functionality

Beamlines will consist of stations where synchrotron radiation is expected to be admitted. The beamline stations shall be constructed of lead-lined walls and roof, as appropriate for the particular radiation characteristics. These stations will house beamline optical components or beamline experimental equipment. The stations are expected to be large enough for personnel to work with the equipment inside. The beamlines will have one or more shutters based on the particular layout, which is expected to vary from beamline to beamline. However, the functionality of the shutters, from the PPS perspective, is expected to be the same and they will be monitored by the PPS. All x-ray beamlines will have shutters in the front-end area inside the storage ring shield wall. The bremsstrahlung radiation emitted by the synchrotron can only be stopped by heavy metal elements such as tungsten or lead. The heavy metal device that stops the bremsstrahlung radiation is referred to as the safety shutter. This is a dual shutter for redundancy. The synchrotron beam, consisting of very high total power and power density, will be stopped by a device that is water cooled, made of copper or alloys of copper, and referred to as the photon shutter. These three devices, the two safety shutters and the photon shutter, will form a shutter cluster and their states (open, closed, or undefined) are monitored by the PPS. Along the beamline are beamline optical elements that will condition the beam, including, for example, monochromators and mirrors. These devices change the characteristics of the synchrotron radiation. The radiation passing through the monochromator will, in most cases, be displaced in either the vertical plane or the horizontal plane from the incident radiation and only a small fraction of the incident radiation with a band pass (of about 0.1% or less) will be passed, with little or no power. In such cases the shutters, located downstream of the monochromator, are known as monochromatic shutters. They will be made of heavy metal and will be much shorter than the safety shutters. Once again, these monochromatic shutters are fully redundant for safety and will be monitored by the PPS.

A major role for the PPS will be to provide a means of ensuring that no personnel are inside beamline stations when the station is opened to synchrotron radiation. Prior to admitting the synchrotron radiation inside these stations, a search of the area has to be performed by a human. It is expected that the station search is performed by one person only. There are PPS devices called “search boxes” inside the station which must be visited as part of the search. Search boxes are strategically placed to ensure that during the search all parts of the station are either visible or visited by the search personnel and no person is left behind inside the station. The search is completed when the station door is closed. The PPS then locks the door. Once the search process is started the PPS will start a beacon and audio signal inside the station, warning all personnel to exit. This signal is expected to last for some time, on the order about 20 to 30 seconds after the station door is closed. The function of the beacon and audio signal is to warn any personnel overlooked by the search person of impending danger. There are very distinct emergency shutdown buttons placed inside the station which, when pressed, will instantly remove the presence of the prompt synchrotron radiation hazard and unlock and open the door.

9.1.3. Design Specifications

The PPS is designed to be robust and provide the emergency shutdown functionality to provide personnel safety from prompt radiation. Like the EPS, the PPS is based on programmable logic controllers. PLCs have numerous advantages over the relay logic scheme of interlocks. They can be reprogrammed to reflect changes in configurations and also have numerous diagnostics. The use of PLCs in safety systems is now best engineering practice. All devices attached to the PPS are designed to be fail-safe—that is, in case of failure the device will fail in such a manner as to either remove the hazard or remove the permit to

generate or maintain the hazard. Every beamline PPS is designed under the same guidelines. The PPS consists of two PLCs, referred to as chains A and B. The two PLCs provide redundancy and independently monitor all the devices. All shutters will have two switches, one for chain A and one for chain B. There will be switches to monitor the closed and open positions. Similarly, all station doors will be monitored with two switches, one each for chains A and B. At beamlines, there are circumstances when a device such as a mask or photon beam stop is provided to absorb the power of the beam, while the radiation safety is provided by lead shielding as collimators or radiation stops. In such cases, the integrity of the masks and beam stops cannot be compromised, as they, in turn, protect the lead shielding which provides the personnel safety. In these cases, the mask or beam stop is monitored by the PPS to ensure that it is not compromised. In most cases, a burn-though monitor is fitted and the water flow or stored nitrogen pressure to these components will be monitored independently by chains A and B of the PPS. In the event that the parameters are not me the beam is dumped. All PPS equipment is clearly identified and secured in locked cabinets. Cabling for the PPS equipment to field devices is on separate closed conduits, which are used exclusively for the PPS. All power to the PPS is backed up by short time uninterruptible power supplies which can back up the system for up to 15 seconds. This time is sufficient to ride out short power interruptions and maintain continuity of operations.

9.1.4. Interface

The PPS must interface with numerous systems. The primary functionality of the PPS is to monitor and provide emergency shutdown. To provide emergency shutdown, the PPS interfaces to the Storage Ring Personnel Protection System (SPPS). The PPS removes a permit to the SPPS to operate the storage ring. In the event of the removal of the permit by the PPS, it is the responsibility of the SPPS to remove the hazard by shutting down the dipole power supply and the RF to the storage ring systems. The Front End PPS, (FPPS) monitors the positions of the front-end shutters located inside the storage ring shield wall. There will be a provision in the FPPS to remove the PPS interactions for a specific beamline. This is in the form of a Kirk Key in the interface box between the FPPS and PPS for each beamline. The FPPS will monitor the closed positions of the Front End shutters when the PPS is not available and will remove the storage ring permit if it experiences any “not closed” status. When the individual beamline PPS is available, the FPPS will ignore the status of that beamlines shutters. This scheme will allow installation and maintenance of the PPS to take place while the machine is in operation. All PPS functions are monitored and data archived using the control system at NSLS-II. EPICS interfaces to the PPS PLCs to monitor their functionality. The EPICS interface is read-only; there is no writing to PLCs from the EPICS interface. Changes to the PLC operating codes are only possible from the field devices or when the PLC software is downloaded to the PLCs during routine validation of the system. All command and control functionality for the PPS resides with the EPS (PPS C chain) for the beamlines and front ends. The EPS interfaces to the PPS and receives signals from the PPS prior to operation of the shutter. In the event the EPS malfunctions, the ESD procedure of the PPS will activate and will remove the permit for the machine to operate. The PPS only provides the ESD functionality and hence it expected to be simple and easy to maintain and validate.

Figure 147 shows the requirements for the PPS for the HEX beamline.

9.1.5. PPS Requirements

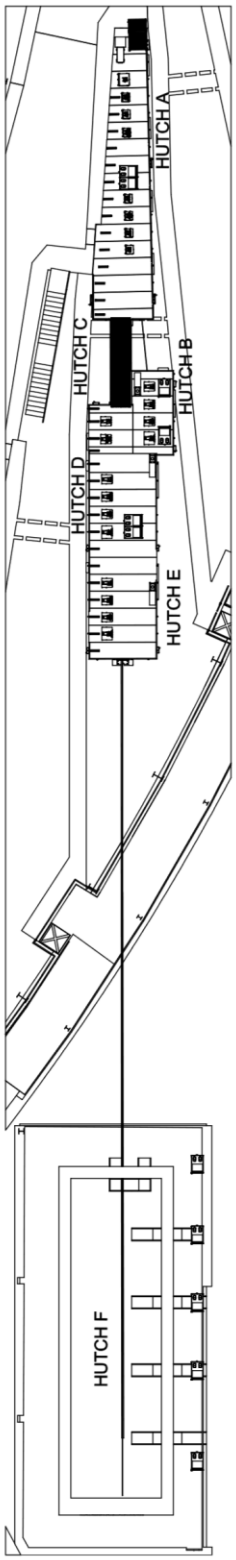

HEX PPS SYSTEM

PPS SYSTEM						
ITEM	Hutch A	Hutch B	Hutch C	Hutch D	Hutch E	Hutch F
Search Buttons	2	2	1	2	2	2
Doors	2	1	1	1	1	1
HMI	Y	N	N	Y	N	Y
Shutter	3**	0	0	0	1(WC)	0
PPS Water Circuit	4	0	1	1	1	1
User Labyrinths	2	1	0	2	2	5

*No Vacuum Sensors in PPS
**Three in full scope, one in initial scope

Figure 147 HEX beamline PPS layout

9.2. Equipment Protection System

The beamlines at NSLS-II are expected to handle x-ray beams with very high power and power densities. Therefore, care must be taken to design the beamline with components that can handle these power loads. Any component that has to handle these high levels of power has to be monitored. The beamline Equipment Protection System (EPS) provides a means of monitoring the components which, when jeopardized, can cause component failure. EPS has the responsibility to act on alarm conditions by mitigating the situation that has caused the alarms.

9.2.1. Functionality

NSLS-II beamline EPS monitors and interlocks the devices in the front end and the beamline. These devices include photon shutters, masks, slits, vacuum gauges, vacuum pumps, vacuum isolation valves, temperature sensors, water flow sensors, water leak detectors, liquid nitrogen pneumatic control valves, smoke detectors, etc. All beamlines at NSLS-II have one Front End (FE) shutter and at least one beamline photon shutter. They are also part of storage ring Personal Protection System (PPS). The beamline EPS communicates with the PPS through related interface signals. In addition,, beamline EPS PLC needs to communicate with FE vacuum PLC and cryocooler PLC through specified interface signals.

Some beamlines also have an x-ray exit window as part of the front end. These x-ray windows provide a vacuum isolation to transmit the x-ray beam. Certain beamlines at NSLS-II, such as the soft x-ray beamlines, share the storage ring vacuum with the front end providing the interface. In such cases, the fast valve, along with the rest of the inline vacuum valves, provides the isolation needed in case of accidents. Due to the large power loads, all components in the front end that intercept the beam have water cooling. These components are typically the fixed mask, photon shutter, and exit windows. The water flow is monitored by flow meters and the signals is fed to the EPS. All vacuum valves are pneumatically operated, and the EPS will operate and monitor their positions. Most beamlines at NSLS-II have some beam conditioning optics upstream of their monochromator. The beam conditioning optics see the large power of the beam and as such, are interlocked by the EPS. The beamline portion of the EPS system will be customized to suit the condition of HEX.

9.2.2. Design Specification

EPS at NSLS-II employs a robust design. The system is based on programmable logic controllers (PLCs), which provide excellent customization capability and also extensive diagnostics. The hardware used is the same as used in the beamline Personnel Protection System (PPS) and the Accelerator PPS. HEX will have its own EPS system, with the sole function being to provide protection from damage of equipment due to synchrotron radiation. The EPS consists of three parts: front-end EPS, beamline-specific EPS, and command/control of PPS components such as shutters and hutch doors. The HEX front-end portion of the EPS is expected to be similar to most other beamlines constructed at NSLS-II, while the beamline portion of the EPS will be customized to meet the specific needs of HEX. Similarly, for the command/control of PPS components, the front-end shutters will be identical to other beamlines constructed at NSLS-II. All front-end components that intercept the synchrotron beam will have water cooling of the components. The water flow of the components will be monitored by the EPS via flow meters. The EPS will be in alarm state if the flow drops below a specified setpoint for more than a defined short duration. Depending on the location of the component it monitors, it will command the

photon shutter to close and – for cases where the flow is upstream of the photon shutter—it will request the stored beam to be dumped.

9.2.3. Beamline EPS Hardware Design

The beamline EPS hardware is based on a Programmable Logic Controller (PLC). Each beamline at NSLS-II is designed to have its own EPS system which consists of only one PLC. The EPS input/output (I/O) signals can be divided into two categories based on their location and signal type. The first category of signals includes vacuum relay signals, smoke detectors, and motion limit switches. These signals are connected to the intelligent chassis or the vacuum chassis. All other signals fall into a second category, and they are wired to remote I/O boxes, or Armor blocks.

9.2.3.1. Intelligent Chassis

Each beamline at NSLS-II is designed to have one EPS PLC, e.g. one controller, which resides in an intelligent chassis, which is a 19" crate, and specified to fit into a standard water-cooled equipment rack local to the beamline. It contains one controller, power supply modules, network modules, I/O modules and other modules. Figure 148 shows the front/rear panel, and chassis module layout.

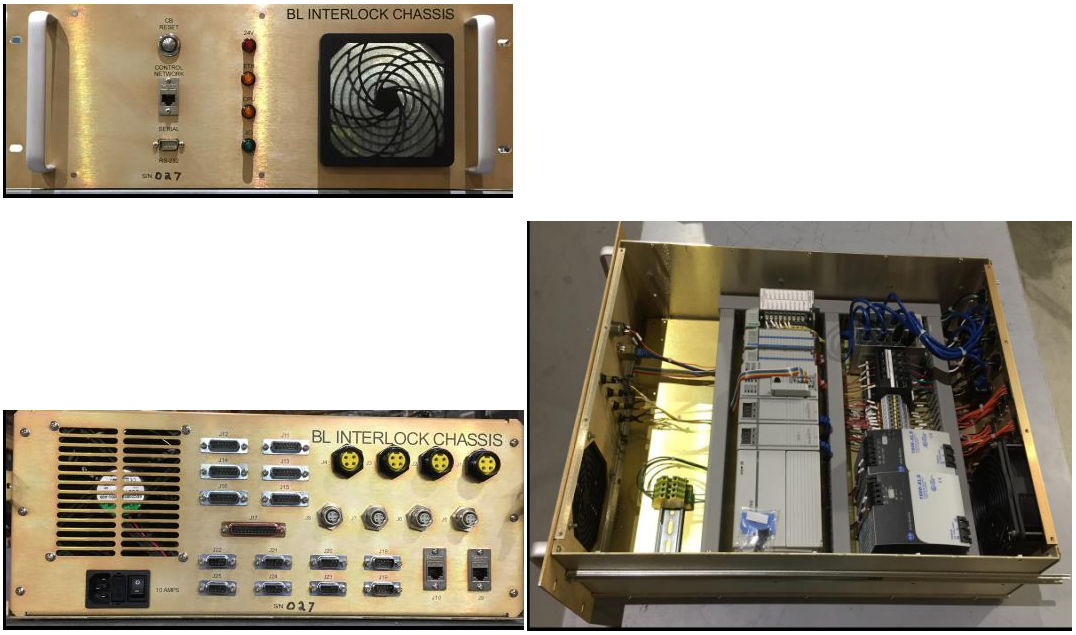

Figure 148 EPS intelligent chassis at NSLS-II

Two power supply modules are used in the chassis. One provides 24 VDC for this chassis and the other provides 24 VDC for distributed I/O modules. The EPS system uses two independent TCP/IP networks. A communication adapter provides EtherNet/IP web server over beamline instrumentation subnet while a ENBT module offers an EtherNet/IP bridge to the beamline private network. All of the PLC data gathering and commanding is on the beamline private network. The instrumentation network handles the communication to users and main control. This assures reliable status and control of hardware on a beamline.

Based on the beamline EPS requirements, the intelligent chassis is designed to provide connection for up to 6 vacuum gauge controllers, 6 vacuum pump controllers, one fast valve controller, four motion controllers and four smoke detectors. It also provides four 24 VDC outlets and four industrial Ethernet ports for the private network.

9.2.3.2. Vacuum Interlock Chassis

For beamlines with many vacuum components, additional vacuum interlock chassis are installed in vacuum controller racks, where needed. The vacuum chassis is the same size as the intelligent chassis. It has front and rear panels that are similar to the intelligent chassis. The chassis module layout can be seen in Figure 149.

Figure 149 Vacuum interlock chassis

The I/O signals connected to vacuum chassis are wired to Allen Bradley (AB) I/O modules. A communication adapter provides connectivity to an EtherNet/IP network. The vacuum chassis provides the same connection capacity as intelligent chassis, with the exception of the 24 VDC ports.

9.2.3.3. Remote I/O Box

A remote I/O box solution is adopted for I/O signals distributed along a beamline. These I/O signals include temperature sensors, water flow sensors, limit switches, coils, etc. The interface signals to PPS and FE vacuum PLC are also connected to an I/O box. The number and location of the I/O boxes vary between beamlines. They are built and installed based on the I/O distribution and density of signals. These boxes also provide enough room for future expansion. Similar to the vacuum interlock chassis, the I/O modules are installed in the remote I/O box, as shown in Figure 150. These boxes are wired to the intelligent chassis for power and network connectivity.

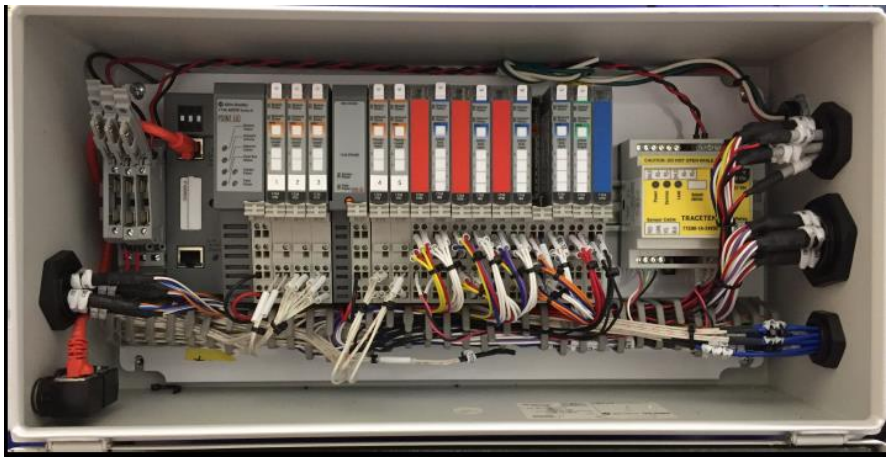

Figure 150 EPS remote I/O box layout

9.2.3.4. EPS Software Development

NSLS-II beamline EPS software development can be divided into three aspects: PLC programming, EPICS IOC (Input/Output Controller) development, and OPI (Operator Interface) development.

9.2.3.5. PLC Programing

The beamline EPS PLC is programmed to take protective actions in the case of detection of unfavorable conditions in the beamline. The controller supports up to 16 tasks. Two tasks run on the EPS PLC: continuous task and periodic task. The continuous task contains PPS logic, vacuum logic, and other time critical logic. The periodic task includes temperature, water, network and other routines where fast response time is not as critical.

Add-on instructions, a powerful feature of RSLogix 5000 used at NSLS-II beamlines, are created for components that are commonly used. They are customized instructions that created for sets of commonly-used logic. Add-on instructions are used for vacuum valves, photon shutters, temperature sensor, and flow sensor contain same functions.

The beamline EPS logic is quite straightforward. Each NSLS-II beamline vacuum section generally is made up of one Cold Cathode Gauge (CCG), one Pirani Gauge (TCG), one Ion Pump (IP) and bounded by Gate Valves (GV). Any detection of poor vacuum from the CCG or IP closes the two adjacent GVs, as well as an additional upstream gate valve. Most beamlines have some beam conditioning optics upstream of their monochromator. To protect the optics and gate valves, the FE shutter must be closed whenever any vacuum loss detected before monochromator. The FE shutter also must be closed in detection of coolant flow loss, temperature elevation, cryocooler loss, network disconnection and so on to prevent the beamline from x-ray damage. The EPS PLC is also programmed to support interlock condition latch to remember status at the moment when interlock happens.

EPICS (Experimental Physics and Industrial Control System) was chosen as the base control system software for all beamlines at NSLS-II. EPS is integrated into this system, and accessible via a customized CSS screen that is visible to the beamline user.

9.2.3.6. NSLS-II Beamline EPS Testing

Several types of tests are done on the beamline EPS system during initial installation work, as well as with future revisions and additions to the existing system. Once the intelligent chassis and vacuum

interlock chassis are received from the manufacturer, all chassis are checked prior to the installation in the equipment rack to verify the proper wiring. After all of the field wiring is completed, the PLC logic program and GUIs are tested with customized dummy loads and simulators. The final test with the completed beamline is carried out before beam commissioning to make sure the hardware and software work properly

All vacuum valves in the front end will also be controlled by the EPS. Setpoints from vacuum controllers that are provided to the EPS will be used to determine when it is permissible to allow opening of the valves. The EPS will determine when it is necessary to close a valve, and will do so if it senses a vacuum alarm based on the vacuum setpoint to the system.

The beamline EPS will be customized based on the user requirements for HEX. Besides monitoring the water flow and controlling the vacuum valves, the EPS system may be used on beamlines to monitor other variables, such as temperature, position, and so forth. The EPS will be used to control the actuation of the shutters. It will monitor the status of the PPS for each shutter and, when a permit is available, it will accept requests to open the shutters. The EPS will be responsible for sequencing the shutters in cases that involve a combination of photon shutters and safety shutters. Any hutch doors that are automated will also be operated by the EPS. The EPS will be responsible for monitoring for the presence of water leaks near sources of water (i.e. DI water inside the hutches, and process chilled water near the cooled equipment racks). If a leak is detected, the EPS will shut the actuated valves for these water systems. The EPS will monitor for smoke and fire inside each water-cooled equipment rack. A smoke alarm will be installed in each rack, and integrated into EPS to provide an alarm and signal via EPICS to the user control station.

9.2.3.7. Interface

The EPS will have Human-Machine Interfaces (HMI) located at the main location of the hardware, which is expected to be located directly above the front end on top of the storage ring tunnel. In addition, there will be a minimum of one HMI per beamline at the beamline stations. The EPS provides the command and control functionality for the beamline PPS. It receives the status information of the PPS and, based on that, can operate the shutters. The PPS, in addition, can request the shutter to close and the EPS will then command the shutter to close. In the event the shutter does not close within a specified time, as determined by the PPS, the PPS will initiate an emergency shutdown (ESD) situation. The EPS will have an EPICS interface to the control system. The EPICS interface will provide both the main control room and the beamlines a complete overview of the status of each beamline. The data from the EPICS interface will also be logged and archived by the central computing systems. The EPICS interface to the EPS will be both read and write. The write functionality will be controlled by the EPICS Channel Access Security. This is essential, to isolate the possibility of accidental control of the wrong beamline EPS via the control system.

This equipment will be purchased as close to the equipment installation start date as possible to avoid possible storage damage or deterioration.

Figure 151 shows the layout for the EPS for the HEX beamline.

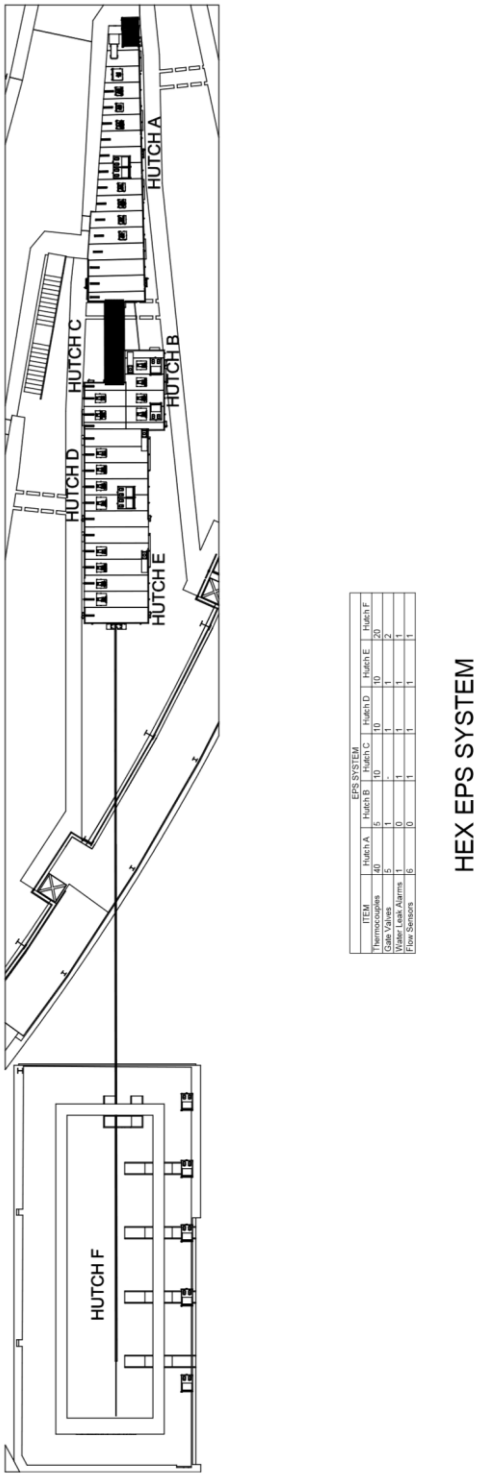

EPS SYSTEM						
ITEM	Hutch A	Hutch B	Hutch C	Hutch D	Hutch E	Hutch F
Thermocouples	48	15	10	10	10	20
Gate Valves	5	1	-	1	1	2
Water Leak Alarms	1	0	1	1	1	1
Flow Sensors	6	0	1	1	1	1

Figure 151 HEX beamline EPS layout

10. Satellite Building

10.1. Introduction

The Satellite Building for the HEX beamline is modelled extensively on the Hard X-ray Nanoprobe (HXN) satellite building. The Requirements, Specifications and Interfaces (RSI) document created for the HEX beamline satellite building notes the required changes, as well as the changes that are permitted in order to reduce cost.

The concrete hutch is a part of the HEX Satellite Building construction contract; the shielding requirements (i.e. the concrete parameters and thickness) are defined in 3.12.5 (which covers the x-ray shielding).

10.2. Key Features of the Building

The following are key features of the satellite building.

- The building is located immediately adjacent to LOB2 at NSLS-II; the air handling systems are located in the LOB2 equipment mezzanine.
- The concrete hutch is approximately 20m long x 5m wide; this is custom designed to shield high energy white beam x-rays.
- The floor under the hutch is >1m thick which helps to minimize vibrations and permits the use of floor trenches for cables and pipes.

10.3. Building Location

The satellite building is located at the north-east part of NSLS-II adjacent to LOB2. Figure 152 shows the location with respect to the overall building and adjacent roadways.

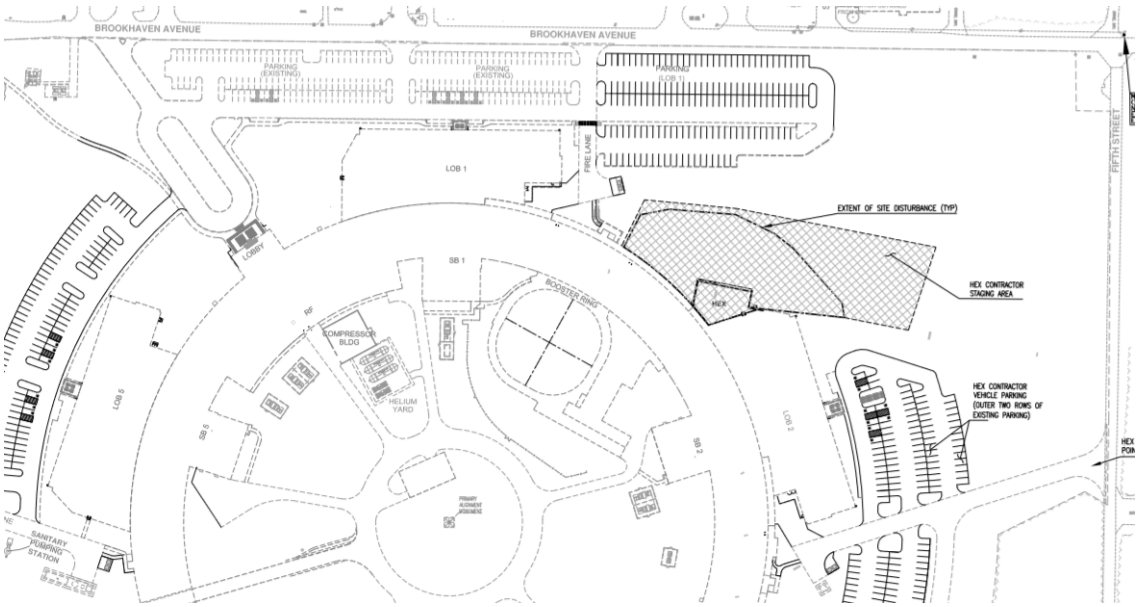

Figure 152 HEX Satellite building location at NSLS-II

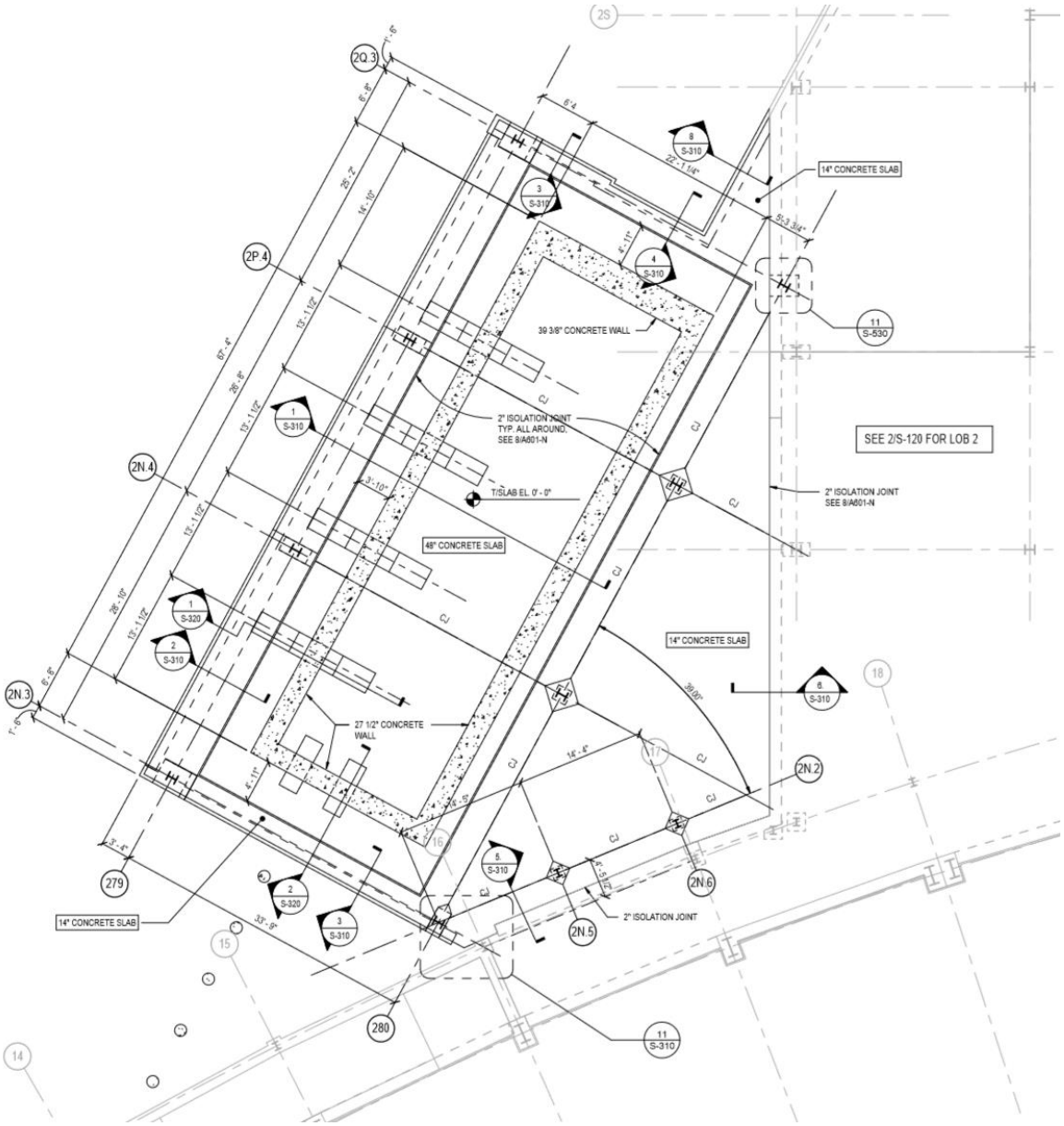

Figure 153 HEX Satellite building concrete and steel layout

Figure 153 and Figure 154 show the plan and elevation views of the satellite building.

The plan view also shows the concrete hutch and floor trench layout (four on the outboard wall, and two on the upstream wall. The triangular area between the concrete hutch and the exiting walls of the LOB and the experimental floor is where the User area will be located.

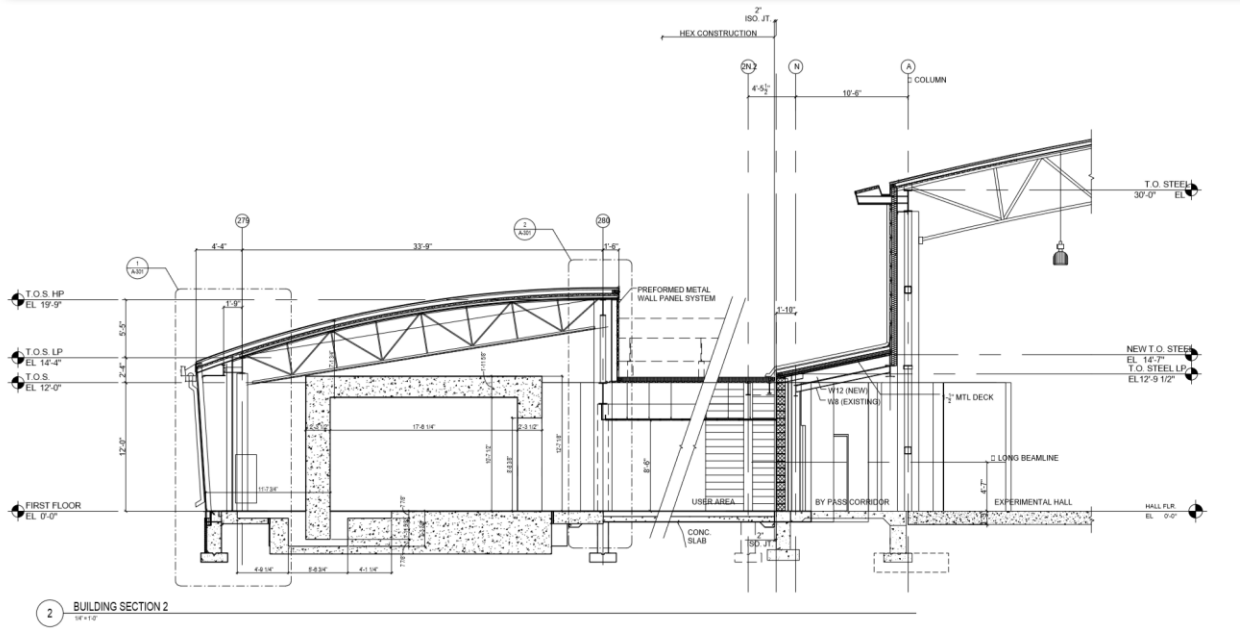

Figure 154 HEX satellite building cross-section

10.4. Satellite Building Egress

Egress from the satellite building is either (preferably) through a personnel door to the LOB, and then immediately through a door to the outside, or through a door onto the experimental floor, and then out of the building through one of the usual exits from the experimental floor. This is shown in Figure 155.

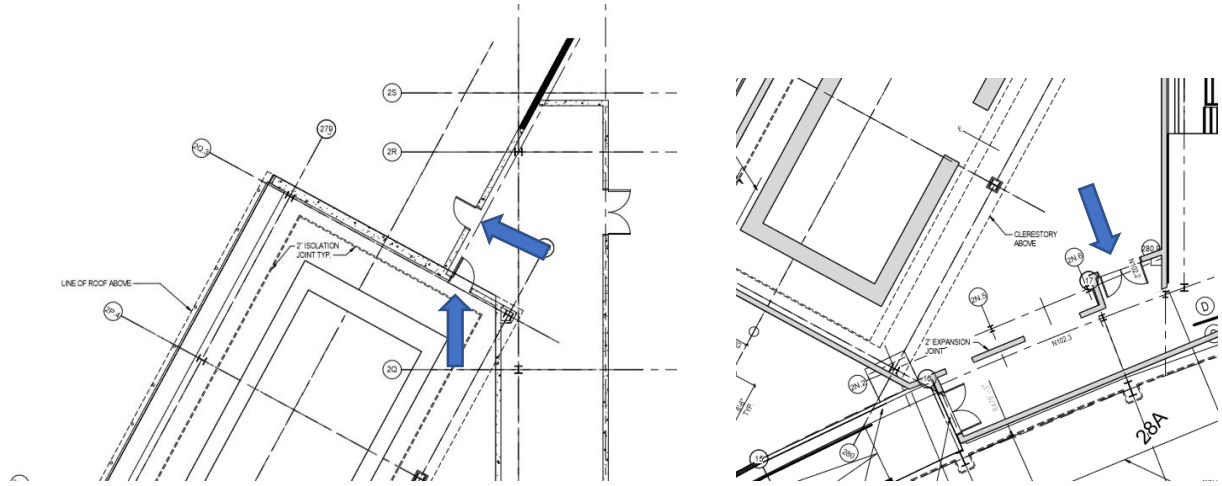

Figure 155 Emergency egress routes from the satellite building

10.5. Shielding Thickness for the Concrete Hutch

Table 33 provides a brief summary of the required shielding thickness for the F-hutch;

Region	**Shielding thickness**
Downstream wall	1.0m of normal concrete
Sidewalls and upstream wall	0.7m of normal concrete
Roof	0.6m of normal concrete
Lead components on inboard wall (eg doors, labyrinths)	20mm
Lead components on outboard wall (eg labyrinths)	25mm

Table 33 Required shielding thickness for F-hutch

Note that additional shielding is required on the downstream wall.

10.6. Scope

The scope of the satellite building is roughly broken down as follows;

- Foundations, structural steelwork, building envelope, concrete hutch, electrical distribution panels, basic electrical layout including lights and convenience outlets will all be included in the satellite building contract.
- Lead additions to the hutch, including x-ray beam stops, shielding doors, labyrinths for User access, PPS, HVAC, utilities, etc will all be included in the lead hutches contract.
- Utilities including cable trays, outlets, lighting inside the hutch, chilled and de-ionized water, compressed air and nitrogen gas, liquid nitrogen, exhaust gas extraction will all be fitted by BNL staff and/or specialist contractors.

11. Major Technical Risks

The requirements on the optics for the HEX beamline are achievable without any of the research and development sometimes required for new beamlines. .The NSLS-II local environment for temperature stability and vibration is now well understood and completely satisfactory for the HEX requirements. No new technical advances are required for delivering the proposed capabilities. These factors help to minimize the risk, although obviously, designs need to be adapted from existing NSLS-II designs (or from designs used elsewhere, including from Commercial suppliers) to the HEX requirements. We anticipate the following technical risks.

11.1. Complexity of the Beamline

HEX will be designed to accommodate three independent branch-lines. However, due to funding constraints, only the center, high-energy white beam branch will be constructed and fitted with an end-station in the current scope. The design of this central branch-line must anticipate the future addition of the two side branches. The HEX facility should be designed to house the additional branch-lines in such a way that a range of possible scientific applications could be accommodated. Thus, there is a risk of missing important interfaces. The risk is highlighted by the fact that many of these interfaces will be to hardware which will not be physically fabricated or in place at the completion of the initial scope of HEX. The strategy will be to ensure that the design of all components is during the preliminary design phase and that the design is feasible and optimized.

Some additional risks (outlined below) are anticipated.

11.2. Impact on Storage Ring

The SCW is expected to have minimal impact on the performance of the storage ring. Preliminary analysis by Weiming Guo (NSLS-II, BNL) see technical note in the Appendix, Section 0, shows that the impacts on both emittance and momentum spread are acceptable. This has been further verified by accelerator physicists as the detailed design and specification of the wiggler, its location, and front-end design have become available, and the risk is now expected to be minimal.

11.3. Superconducting Wiggler

Due to its uniqueness and limited number of suppliers, the purchase or design/manufacture of the SCW poses potential technical risk. In the event of problems, a temporary alternative would be to use a permanent magnet wiggler. Such wiggler could be available from the APS in Argonne National Laboratory. The downside is the lower critical energy; however, it was used successfully at the imaging beamline IMBL at the Australian Synchrotron for a few years before an SCW could be purchased.

11.4. Unique (to NSLS-II) White-beam Shutter

The standard NSLS-II safety shutter is designed for monochromatic or pink beam and does not provide adequate stopping for the very high energy Bremsstrahlung radiation, nor is it designed for the high power, white beam.

This beamline requires a non-standard shutter that is compatible with white beam. Several commercial suppliers have suitable designs for such a component, and this FDR report includes a reference design that could be used by a commercial supplier with minimal risk.

11.5. Unique New Design of Fixed Masks

This beamline will have a new triple aperture mask design. This is based on the (double aperture) design used for the SST beamline, and now in regular operation. The FEA calculations performed indicate that it is feasible and safe for long term operations.

11.6. Heat Load

The heat load for the diamond windows, filters and monochromator crystal is high due to the high power density and large horizontal fan of the white beam. The associated risks include deformation or breakage resulting from the applied heat load on the various components. The mitigation is to ensure that a careful FEA is performed on every component that is touched by white beam.

11.7. Beam Transport Tube

The transport tube poses a technical risk which is mitigated by careful calculations (see Section 3.12.5), and using experienced contractors for the manufacture. We seek to use existing designs for the pipe and the joint boxes, provided by an experienced Contractor (or sub-Contractor).

11.8. Risk Registry

The project actively maintains a risk registry, the current version available on request.

At 16-Mar-2019 the risk registry included the following items (shown overleaf in Table 34).

WBS Code	Risk Code		Risk Description		Risks		Notes
				Cost	Prob	Value	
7.05.01		**HEX Management**					
	HEX0101		Invoicing or funds transfer delays (NYSERDA)	$100,000	0.00	$0	Ignore this risk, now considered very low, NYSERDA pay promptly.
	HEX0102		NYSERDA directed change to scope	$100,000	0.00	$0	Ignore this risk
	HEX0103		Final $15M is not available from NYSERDA	$0	0.00	$0	Risk retired - full $25M approved.
	HEX0104		Inflation rate above projected increases	$1,000,000	0.01	$5,000	Jan-19 Reduced due to contracts placed and escalation included in cost models.
	HEX0105		change to VAB method of accounting	$275,000	0.00	$0	Risk retired: change made
	HEX0106		Lab changes burden structure (increase)	$200,000	0.00	$0	Risk retired: change made
	HEX0107		Devaluation of US dollar	$600,000	0.05	$30,000	Dec-18: risk seems to be reducing. Mar-19, continued risk reduction
	HEX0108		Market driven price fluctuations (general labor & materials)	$300,000	0.05	$15,000	Mar-19, risk reduced, closer to placing contracts
	HEX0109		Industrial actions (strikes)	$0	0.00	$0	Ignore this risk
	HEX0110		Personnel recruitment delays (second Scientist)	$20,000	0.00	$0	Ignore this risk: scientist recruited Mar-19
7.05.02		**HEX Design**					
	HEX0201		Thermal loads cause unexpected design problems	$50,000	0.00	$0	Dec-18: risk retired; this is minimal due to filtering, demonstrated with FEA.
	HEX0202		Changes to shielding requirements	$50,000	0.05	$2,500	Dec-18: risk can be retired after FDR. Most shielding design now complete.
	HEX0203		Limited availability of specialized effort	$200,000	0.00	$0	Dec-18: risk retired since most critical design work is complete
	HEX0204		Higher than expected optical quality is required	$20,000	0.00	$0	Dec-18: risk retired, requirements for high spec optics are understood
	HEX0205		Failure to converge on SCW/FE/BL layout (fan separation)	$50,000	0.00	$0	Dec-18: risk retired since most critical design work is complete
	HEX0206		Late changes to requirements (eg from reviews, BAT)	$50,000	0.05	$2,500	Could be mandated by NYSERDA, or BAT. Mar-19, risk considered to be minimal.
	HEX0208		Design of WB shutter is more complex than expected	$100,000	0.05	$5,000	Design largely complete - Mar-19
	HEX0209		Scope creep due to evolving scientific techniques (eg 3D HE diffraction tomography)	$100,000	0.05	$5,000	Extra stages. Design largely complete - Mar-19
	HEX0210		Ray tracing is more complex than expected	$100,000	0.05	$5,000	Dec-18. Mar-19, largely completed
7.05.03		**HEX Beamline Construction**					
	HEX0301		Underestimated effort or underestimated scope *	$200,000	0.05	$10,000	Scope now fixed, Mar-19
	HEX0302		Accident and injury *	$50,000	0.05	$2,500	
	HEX0303		Limited availability of specialized effort	$5,000	0.05	$250	
	HEX0304		Time of high demand from beamline suppliers	$100,000	0.05	$5,000	
	HEX0305		Underestimated end station equipment costs	$250,000	0.05	$12,500	Design sufficiently mature to reduce this. Mar-19
	HEX0306		Delays to beamline component deliveries	$100,000	0.10	$10,000	
	HEX0307		Design changes after PDR	$50,000	0.00	$0	Retired, Mar-19
	HEX0308		Optics design requires changes to hutch specs	$50,000	0.00	$0	Retired, Mar-19
	HEX0310		Insuffficent mechanical stability of procured components	$10,000	0.00	$0	Retired, Mar-19
	HEX0311		Delays needed to avoid disruption of facility operation	$30,000	0.05	$1,500	
	HEX0312		Hutch price increase due to raw material costs	$50,000	0.00	$0	Dec-18: risk retired, contract about to be placed.
7.05.04		**HEX Beamlines Infrastructure**					
	HEX0401		Underestimated effort or underestimated scope *	$100,000	0.10	$10,000	
	HEX0402		Accident and injury *	$50,000	0.05	$2,500	
	HEX0403		Limited availability of specialized effort	$10,000	0.03	$300	O/T or consultant
	HEX0404		Late optics design changes impact infrastructure	$50,000	0.05	$2,500	
	HEX0405		Late completion of satellite building delays infrastructure start	$100,000	0.00	$0	Retired Mar-19, sufficient float in SB schedule
	HEX0406		Late completion of infrastructure	$100,000	0.05	$5,000	1 month of 6 person standing army, reduced Mar-19
	HEX0407		Additional scope needed to complete central branch	$20,000	0.20	$4,000	2 weeks of 2 electricians
	HEX0408		PPS work is more complex than anticipated	$40,000	0.10	$4,000	2 people for 1 month
	HEX0409		Insufficient DI water flow rate available	$10,000	0.20	$2,000	
	HEX0410		Insufficient electrical capacity for SB from the LOB	$50,000	0.10	$5,000	
	HEX0411		Changes to NSLS-II or BNL safety requirements	$100,000	0.01	$1,000	
	HEX0412		Failure to agree new standard for door actuation before bid	$10,000	0.00	$0	Dec-18: risk retired, this was defined in the hutch bid documents.
7.05.05		**HEX Accelerator Infrastructure**					
	HEX0501		Underestimated effort or underestimated scope *	$100,000	0.10	$10,000	Reduced Mar-19, scope well understood.
	HEX0502		Accident and injury *	$25,000	0.05	$1,250	
	HEX0503		Limited availability of specialized effort	$10,000	0.01	$100	O/T or consultant
	HEX0504		Unable to finalize design and specs of ID and FE	$50,000	0.00	$0	Dec-18: risk retired, the FDR report covers this design aspect.
	HEX0505		SCW has unacceptable impact on the lattice	$25,000	0.00	$0	Dec-18: risk retired, the FDR report covers this design aspect.
	HEX0506		SCW fan requires changes to SR magnet girders or vacuum system	$50,000	0.00	$0	Dec-18: risk retired, the FDR report covers this design aspect.
	HEX0507		FE design is more complex than antipated	$30,000	0.00	$0	Dec-18: risk retired, the FDR report covers this design aspect.
	HEX0508		FE manufacture has cost overrun	$200,000	0.05	$10,000	Probability reduced given design maturity and changes to reduce costs
	HEX0509		FE manufacture is delayed	$50,000	0.00	$0	Dec-18; retire this risk due to good schedule float
	HEX0510		Procurement or fabrication of S/C wiggler causes delays	$100,000	0.05	$5,000	Scheduled manufacturing duration is very generous, low probability
	HEX0511		Poor technical performance of SCW (cryogenic)	$60,000	0.10	$6,000	Assume extra 1 Watt of LHe needed for 1 year
	HEX0512		Poor technical performance of SCW (field quality)	$20,000	0.10	$2,000	
	HEX0513		Lack of cryogenic / SCW engineer expertise	$20,000	0.05	$1,000	Pay a consultant
	HEX0514		SCW cost higher than anticipated	$500,000	0.20	$100,000	Mar-19 - leave for now, review in Apr/May 2019
7.05.06		**HEX Controls**					
	HEX0601		Limited availability of specialized effort	$200,000	0.20	$40,000	Reduced probability given projected controls workload, increased per ZY. Mar-2019.
	HEX0602		Overun of control cables and installation costs	$20,000	0.05	$1,000	Dec-18: review at time of baselining (before FDR)
	HEX0603		New detectors and sample environment controllers require extended software dev	$60,000	0.20	$12,000	
	HEX0604		Experiment control development problems (diffration & imaging)	$200,000	0.10	$20,000	Scope well understood, some work planned to be done early. Reduce Mar-19
7.05.07		**HEX Conventional Facilities**					
	HEX0701		Underestimated effort or underestimated scope *	$220,000	0.05	$11,000	
	HEX0702		Accident and injury *	$100,000	0.10	$10,000	2 week work stoppage, 10% chance.
	HEX0703		Limited availability of specialized effort	$50,000	0.05	$2,500	
	HEX0704		Higher than budgeted bids for satellite building	$500,000	0.00	$0	Dec-18; risk retired since contract now placed.
	HEX0705		Cost additions during SB construction	$200,000	0.25	$50,000	This is in addition to contingency carried in the WBS explicitly
	HEX0706		External factors delay building start date	$100,000	0.00	$0	Dec-18; fixed price contract, work could start early, generous float.
	HEX0707		Weather delays to construction	$100,000	0.00	$0	Dec-18; fixed price contract, work could start early, generous float.
				Total Risk Value		$429,900	

Table 34 HEX Project Risk Register (snapshot at 16-Mar-2019).

12. Environment, Safety and Health Requirements

It is BNL's vision to provide a "Best in Class" Environment, Safety and Health (ES&H) program. We view such a program as essential to the safety of the workers, the public as well as to protect the environment in which we operate. We seek to provide an injury-free work environment and we measure our performance by comparison with only those who have achieved recognition as "Best in Class." To achieve this vision, safe working conditions and practices are an absolute requirement for all staff and contractors. We expect the design of the facilities and facility and experimental operations to be performed with this goal in mind. We will not be satisfied unless our ES&H programs, as well as our new facilities, are both recognized as "Best in Class." To accomplish this vision, it is essential that ES&H be fully integrated into the all aspect of facility design, construction and operations. The BNL program is integrated into all facets of work, from conceptual design, construction, and operations and including decommissioning.

The HEX beamline project work will be performed in accordance with the BNL operating Contract (DE-SC0012704) clause I.131, which implements DEAR Clause 970.5223-1 – Integration of Environment, Safety, and Health into Work Planning and Execution (Dec 2000). BNL utilizes its Standards Based Management System (SBMS), which is an integrated system of Management Systems, Program Descriptions Subject Areas and Manuals, and Facility Use Agreements, to implement Integrated Safety Management (ISM) and its Worker Safety and Health Program required by10 CFR 851. The ISM and Worker Safety and Health Program Descriptions describes BNL's approach to integrating Environment, Safety, and Health (ES&H) requirements into the processes for planning and conducting work at the Laboratory.

Each stage of project development, from conceptual design through operational turnover, has and will continue to reiterate the ISM core functions:

1. Define the scope of work
2. Identify and analyze potential hazards associated with the work
3. Develop and implement hazards controls
4. Perform work within the controls
5. Provide feedback on the adequacy of controls and continue to improve safety management.

Safety through design will be a primary driver throughout the design phases of the HEX project. Through management commitment and leadership, safety in the conduct of activities will continue as fundamental drivers through construction and turnover of the completed beamline.

The design and development of the HEX beamline involves an iterative and uniform review process which includes ESH staff from the central ESH Department - Safety and Health Services, Radiological Control, and Environmental divisions. There are also Subject Matter Experts involved in design reviews and hazard identification and mitigation where necessary.

12.1. Preliminary Hazards Analysis

A Preliminary Hazard Analysis was done for the HEX beamline project. The HEX project is a continuation of beamline construction that has been accomplished over the past several years. Review of the anticipated hazards has shown that there are no new hazards introduced by this beamline construction

or operation. All hazards identified for the construction and operation of the HEX beamline are typical of those encountered with other beamlines and all hazards are currently identified in Section 4 of the NSLS-II Department Safety Assessment Document (PS-C-ESH-RPT-001). No new hazard analysis document is required. The hazards analyzed for construction and operation include:

- Environmental/Waste
- Fire
- Electrical
- Cryogenic and Oxygen Deficiency
- Ozone
- Chemicals and Hazardous Materials
- Vacuum systems
- Pressurized systems
- Material handling
- Noise
- Ionizing radiation
- Non-ionizing radiation
- Working at heights

12.2. Environmental Requirements

In addition, Brookhaven National Laboratory has developed an Environmental Management System (EMS) which is certified under International Organization for Standards (ISO) 14001. BNL is committed to environmentally responsible management of the property and has committed to the EMS methodology for managing environmental aspects of the construction and operation to provide pollution prevention and environmental compliance.

A NEPA evaluation was done in April 2017 which concludes this project falls within the scope of the July 2012 Generic WFO/CRADA/PIQ BNL-520 categorical exclusion and the October 2006 Environmental Assessment EA-1558 which was completed for the NSLS-II facility and included the consideration of several long beamlines. All construction will be within areas already designated for construction of the long beamlines identified in the EA. There will be no significant storage of chemicals, fuels or emissions to water/sanitary nor air.

12.3. Construction Hazards

BNL has a mature construction safety program, with recent experience in constructing the Center for Functional Nanomaterials and the Interdisciplinary Science Building. Lessons learned from these projects, as well as from other construction projects in the DOE complex, coupled with the existing program, will control risk at the HEX facility.

The BNL construction safety program, as outlined in the Standards Based Management System Subject Area–Construction Safety, provides the means to mitigate the hazards presented during the construction phase of a project. Aspects of the construction safety program including: submittal of a Contractor's health and safety plan, preparation of a Phased Hazard Analysis, documentation of a fall

protection program and on-site construction safety oversight are just some of the tools to be used to ensure contracted and on-site personnel are protected from construction hazards.

12.4. Fire and Electrical Hazards

Operational experience at accelerators throughout the DOE complex has demonstrated that most fires in accelerator facilities are electrically initiated, typically by component failure. However, other sources of fire will be considered in the design of the HEX facility. These include the combustibility of building construction materials, the accumulation of combustible materials by occupants, the use of pyrophoric or reactive materials, improper storage or use of flammable materials, lightning storms, and static discharge. Electrical design will follow NFPA 70 and 70E Electric Code, and all applicable building codes. All equipment will follow the SBMS electrical requirements.

12.5. Ionizing Radiation

The HEX beamline will incorporate the requirements specified in 10 CFR 835 and the accelerator-specific safety requirements as set by DOE Order 420.2C, Safety of Accelerator Facilities. The HEX beamline will be designed in accordance with current NSLS-II Shielding Design Guidelines. These guidelines have been developed with the goal that staff will not be exposed to radiation fields exceeding 0.05 mrem/hr. This design will ensure radiation exposure to staff, users, and the general public is within DOE and BNL dose limits and control levels.

13. Cost information

Cost information is not reported in this FDR report due to commercial sensitivities.

This is covered in a separate costing book which may be requested from the Project Manager.

14. Schedule information

The project, in common with all projects at NSLS-II uses the Primavera P6 product for planning and managing the costs and schedule as work progresses.

A so-called “P6 poster” is our summary chart, printed in large format, we can see all activities in the project with start and finish dates, hours, costs etc. A copy of this can be made available on request at any time. This would not be readable on 11”x17” paper.

A summary of the schedule is shown in Table 35. This is current at 22-March-2019.

HEX Partner Beamline Rate Update | IPD - Summary Schedule | 19-Mar-19 11:12

Activity ID	At Completion Duration	Start	Finish	BL Project Start	BL Project Finish	BL Project Total Cost
Total	1145	31-Aug-17 A	04-Apr-22	31-Aug-17	04-Apr-22	$30,000,000
HEX Management	1145	31-Aug-17 A	04-Apr-22	31-Aug-17	04-Apr-22	$5,000,000
NYSERDA Milestones	1006	25-Oct-17 A	02-Nov-21	25-Oct-17	02-Nov-21	$0
HEX Conceptual Design	17	02-Oct-17 A	25-Oct-17 A	02-Oct-17	25-Oct-17	$14,782
HEX Preliminary Design	120	01-Nov-17 A	27-Apr-18 A	01-Nov-17	27-Apr-18	$125,180
HEX Final Design	230	01-May-18 A	02-Apr-19	01-May-18	02-Apr-19	$326,379
HEX Photon Delivery System Procurement and Fabrication	555	02-Jul-18 A	17-Sep-20	02-Jul-18	17-Sep-20	$3,610,612
HEX Photon Delivery System Installation and Test	687	03-Apr-19	30-Dec-21	03-Apr-19	30-Dec-21	$1,146,190
HEX End Station Procurement and Fabrication	251	22-Jan-20	21-Jan-21	22-Jan-20	21-Jan-21	$1,800,498
HEX End Station Installation and Test	125	22-Jan-21	20-Jul-21	22-Jan-21	20-Jul-21	$49,923
HEX Hutches	902	02-Apr-18 A	04-Nov-21	02-Apr-18	04-Nov-21	$23,341
Hutches Procurement	290	11-Jan-19 A	10-Mar-20	11-Jan-19	10-Mar-20	$2,033,467
HEX Mechanical Utilities	478	03-Apr-19	02-Mar-21	03-Apr-19	02-Mar-21	$669,777
HEX Electrical Utilities	413	03-Apr-19	23-Nov-20	03-Apr-19	23-Nov-20	$420,906
HEX EPS	439	22-Jan-20	19-Oct-21	22-Jan-20	19-Oct-21	$194,123
HEX PPS	991	02-Oct-17 A	17-Sep-21	02-Oct-17	17-Sep-21	$769,841
HEX Beamline Furniture and Office Equipment	140	25-Sep-20	20-Apr-21	25-Sep-20	20-Apr-21	$47,862
HEX Front End	764	01-Nov-17 A	20-Nov-20	01-Nov-17	20-Nov-20	$2,560,146
HEX Source	947	02-Oct-17 A	16-Jul-21	02-Oct-17	16-Jul-21	$3,623,462
HEX Straight	584	03-Apr-19	30-Jul-21	03-Apr-19	30-Jul-21	$701,187
HEX Basic System Controls	360	01-Mar-19	04-Aug-20	01-Mar-19	04-Aug-20	$1,034,068
HEX Instrument Applications	173	05-Aug-20	15-Apr-21	05-Aug-20	15-Apr-21	$291,720
HEX Conventional Facilities Design and Bid Preparation	294	02-Oct-17 A	07-Dec-18 A	02-Oct-17	07-Dec-18	$332,774
HEX Conventional Facilities Construction	486	10-Dec-18 A	16-Nov-20	10-Dec-18	16-Nov-20	$4,375,742
HEX Conventional Facilities Commissioning	396	01-Mar-19	24-Sep-20	01-Mar-19	24-Sep-20	$848,021

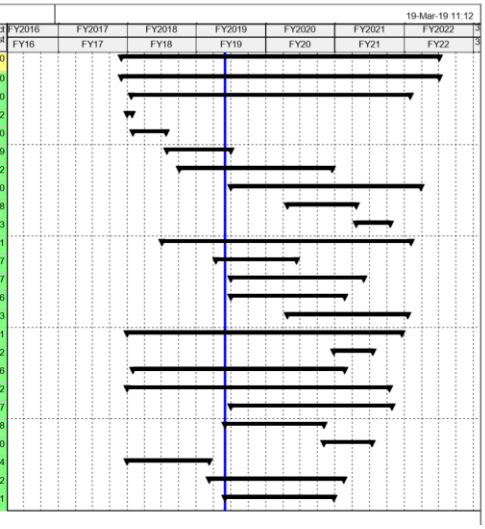

Table 35 The schedule summary by top level WBS

15. Appendices

Appendix 1. Recommendations from Previous Committees and Review Panels

The following list is taken from the HEX beamline recommendation tracking database. This is updated regularly, so this is a snapshot of the status in Dec-2018, at the time of compiling the FDR report.

#	Recommendation	Review	Status	Comment
100	Non-relevant text and WBS dictionary entries should be removed	POB Sub-Panel Review of HEX	Closed	Updated document
101	Consider maintaining the project description in a table of WBS dictionary entries, alongside other key project data, for reference throughout the project execution. Corresponding data would be: WBS number (to the lowest level), descriptions, costs, etc	POB Sub-Panel Review of HEX	Ongoing	This will be done in CEB
102	Include a slide showing top-value items in future project review presentations	POB Sub-Panel Review of HEX	Closed	This is available, should be updated regularly, and will be included in material for future presentations.
103	Conceptual description of shielding should be included in the beamline presentation in future conceptual design reviews	POB Sub-Panel Review of HEX	Closed	A description of the beamline shielding is included in the PDR report, and will be further refined for the FDR.
104	Track design and simulation efforts related to certain out-of-scope items, such as mirrors, that are being addressed outside of the base project scope, if the delivered base scope design depends on them. This should be in place before the PDR review	POB Sub-Panel Review of HEX	Ongoing	This work will continue as the design matures and will be completed by the FDR
105	The process for experimental hazard review should be briefly addressed in presentations in the future. The potential for additional hazards and controls in the satellite building should be acknowledged	POB Sub-Panel Review of HEX	Closed	See https://ps.bnl.gov/phot/ProjectBeamlines/PartnerBeamlines/HEX/Shared%20Documents/IRR%20and%20Exp%20Review.pdf
106	The area where the HEX beam line is external to buildings should be shown as a fenced or otherwise restricted area on the final drawings	POB Sub-Panel Review of HEX	Closed	The layout drawing now includes this.
107	Obtain concurrence that the Site-Office-delegated NSLS-II-authorization-to-operate newly constructed beamlines also applies to HEX. This must be verified prior to the IRR	POB Sub-Panel Review of HEX	Closed	See attached e-mail from Mike Bebon
108	Describe responsibilities and plans regarding the controls which protect the SCW from the electron beam in the Storage Ring and controls which protect the Storage Ring from SCW pressure boundary failure. This should be established prior to the PDR	POB Sub-Panel Review of HEX	Closed	The normal active envelope will be used to protect the SCW, and the SCW will be fitted with overpressure devices to prevent the bore tube being subject to excessive external pressure.
109	Obtain equivalence ruling from BNL Pressure and Cryogenics Safety Subcommittee for the SCW pressure vessel. Documentation requirements for equivalence ruling are defined in SBMS. A design review for safety is needed prior to procurement or fabrication	POB Sub-Panel Review of HEX	Closed	This is a part of the SCW design/procurement activity, and design reviews are stipulated in the SOW
110	A User training program addition needs to be developed and implemented that addresses the added hazards and controls related to the future HEX construction area. This must be completed prior to construction start	POB Sub-Panel Review of HEX	Closed	There are slides in both the Facility Brief and User training which address construction hazards and barricaded areas. In the Facilities Brief it is section 3, and in the User Training, it's slide #16.
111	Describe the configuration management system for drawings (e.g. shielding, SCW and PPS) in future presentations	POB Sub-Panel Review of HEX	Closed	This is a standard procedure and will be included at the next POB review.
112	All NEPA documentation and their basis documents related to HEX should be archived and under NSLS II configuration management. This should be done before the PDR	POB Sub-Panel Review of HEX	Closed	The NEPA review document is not our record to control. It is generated from the Environmental Protection Division, and is their record. We keep a copies on the HEX site and in our Operations shared drive for our use only
113	Work with BNL management to clarify the depth and frequency of future POB Panel reviews, before the end of CY 2017	POB Sub-Panel Review of HEX	Closed	The BNL Management position (from Diane Hatton) is that the POB sub panel reviews are only held as needed.
114	Work with BNL management to decide how POB Panels report to an oversight structure, before the end of CY 2017	POB Sub-Panel Review of HEX	Closed	Not relevant given answer to previous recommendation
115	Work with BNL management to consider constructing a Technical Panel that reports to an oversight structure at least annually, before the Preliminary Design Review scheduled for April 2018	POB Sub-Panel Review of HEX	Closed	Reporting to POB (+ NYSERDA) is now done monthly. Detailed reviews as for any beamline project.
116	Construct a clearer organization chart to present at the next POB review	POB Sub-Panel Review of HEX	Closed	See PDR website (and the PMP)
117	Define a review process for establishing modified scope, and present at the next POB review	POB Sub-Panel Review of HEX	Closed	This has been presented to the POB, and will be presented at the PDR.
118	Re-evaluate the risk of availability of specialized labor and develop a mitigation plan, before the next POB review	POB Sub-Panel Review of HEX	Closed	We don't intend to create a plan to address this, but this is part of our Project Management. Generally most work could be outsourced if required, but the reality is (for the next couple of years) that the BL construction workload is relatively low.
119	Ensure that the SCW working group evaluates the alternatives for the SCW acquisition. Hold an external review of the work of the SCW Task Force, significantly before the Preliminary Design Review in April 2018	POB Sub-Panel Review of HEX	Closed	This was considered in the preparation of the make / buy report, submitted Aug 2018. It is anticipated that a careful review will occur on receipt of the bids (~March 2019).
120	Develop the plans for SCW procurement, including multiple scenarios, to understand the risk and potential cost and schedule impact, for presentation at the next POB review	POB Sub-Panel Review of HEX	Closed	This was completed and document within the make/buy report with several commercial vendors identified.
121	It is important to provide supporting cost documentation that agrees to the P6 summary and if there are differences, it would be helpful to have explanations for any deviations. This should be completed before the PDR Baseline	POB Sub-Panel Review of HEX	Closed	Documentation available on SP site
122	Get assistance from the Business Operations group or use history from previous projects to determine the correct category that high dollar value procurements belong in and what overhead rates to use to ensure proper estimates. This should be done asap	POB Sub-Panel Review of HEX	Closed	Raj and Heather met and resolved this.
123	Obtain a current cost estimate for the Satellite building prior to the PDR (Spring 2018).	POB Sub-Panel Review of HEX	Closed	Costing provided by BM on 4th Dec however we will close this when the independent cost estimate is completed.
124	The bottom-up cost uncertainty and BOE assessment exercise should be completed and summarized. This should be done prior to PDR	POB Sub-Panel Review of HEX	Closed	This is done and summarized in the Contingency Analysis Report (PDR website)

125	Continue to detail out planning packages and refine schedule logic as the project information becomes more defined	POB Sub-Panel Review of HEX	Closed	This has been done (eg SCW preparation phase at the PDR stage) and will continue to be done, as required.
126	As design of the Satellite building becomes defined, subdivide the construction into standard subdivisions. This should be done prior to baselining	POB Sub-Panel Review of HEX	Closed	The MPO staff will work in this direction in line with their normal practice once the contract is placed.
127	Layout a preliminary schedule to build the SCW in house if this becomes a viable option as this should be done prior to the Go-noGo procurement strategy milestone	POB Sub-Panel Review of HEX	Closed	This is now considered to be very unlikely, but the accelerated schedule will permit this in the event of a commercial procurement somehow not working out.
128	Scope deletion / addition decision milestones should be included in the project schedule prior to baselining	POB Sub-Panel Review of HEX	Closed	A plan for phased scope adjustment was presented to POB that allows us to make corrections as the project progresses
150	The majority of research is conducted by external groups with specific expertise in their field; their research needs should be analyzed before costly decisions on set-ups, beam characteristics and detectors are made.	HEX BAT Meeting #1	Ongoing	Reviewing active BDPs and discussing with proposers, discuss further at next BAT meeting
151	The HEX strategy needs to include a detailed proposal about the detectors for the three main techniques taking into account latest developments in-house and externally.	HEX BAT Meeting #1	Ongoing	Pete Siddons presented plans at BAT meeting #2. Work ongoing.
152	Some concerns about getting the beamline operational as soon as possible (may miss the battery research boat).	HEX BAT Meeting #1	Closed	Recent relaxation of the NYSERDA funding profile means we are able to reduce duration by ~6 months.
153	Suggestion to add x-ray lenses for ADXRD using highly focused monochromatic beam. We should consider refractive optics consult Ken Evans Lutterodt	HEX BAT Meeting #1	Closed	Added micro-focusing scope – current design is using KB mirror. Ken was consulted. Kinoform was not chosen due to small aperture (200 microns limited by the depth of etching the lens).
154	High energy should not be limited to 100keV, 150 keV monochromatic beam may be possible.	HEX BAT Meeting #1	Closed	Updated monochromator design and simulation to reflect 150 keV max. energy.
155	Filters. Aim for 30keV as low energy cut-off. Filtering probably fine, maybe consider using less diamond.	HEX BAT Meeting #1	Closed	We simulated impact of Diamond and found that it has little impact for 30 keV x-rays. Current design uses 6 mm Diamond to control the heat-load on SiC filter.
156	Question about heat load and water cooling on the mono first crystal, John Sutter could help with the conversion of FEA data to reciprocal space data to ascertain the theoretical mono transmission.	HEX BAT Meeting #1	Closed	FEA has been completed and included in the FDR report
157	Recommend not to include Diffraction Enhanced Imaging in the base scope.	HEX BAT Meeting #1	Closed	DEI was not in the base scope. We deleted DEI discussion in PDR.
158	Aim to have just one sample position for diffraction and imaging. Switch mode by moving the sample up and down, and moving different detectors in place. [Precise image guided diffraction, morphology-phase-strain determination].	HEX BAT Meeting #1	Closed	PDR reflects one sample position for all three techniques.
159	Samples and environment - aim for two sample stacks - low and high capacity weight-size	HEX BAT Meeting #1	Closed	Current design includes one high-precision, large capacity/weight sample stage. This accommodates both small and large samples. Additional stages could be added later (outside project scope).
160	Recommendation to motorize the vertical stages of the sample tables	HEX BAT Meeting #1	Closed	The tables are motorized in the PDR specifications
161	Special load frames or similar samples will need to have a special stage customized to suit. Jon Almer suggests load frame since this is an "Engineering" beamline. This may have to come later.	HEX BAT Meeting #1	Ongoing	Budget constraints prevent this at present. We will attempt to work with potential User groups – outreach will be ramped up with the BL scientist on-board and after the FDR.
162	The NY State battery consortium has proven solid interest in using HEX. It is now important to critically consult other communities who may benefit from the instrument: Fundamental and applied material science, geophysics including mineralogy and volcanol	HEX BAT Meeting #1	Ongoing	We are reaching out to high-pressure, bio-medical, rock-physics, astronomy, and materials science communities.
163	Although commercial flat-panel detectors are successfully used at various facilities, the implementation of photon-counting CdTe 2D detectors should be better considered. The technical advantages are noise free and fast (few 100 Hz) acquisition, allowing	HEX BAT Meeting #1	Ongoing	Budget constraints currently prevent this from being in the BL base scope. We will look to secure funds from elsewhere. Eric is working on testing a borrowed CdTe detector.
164	Variable field of view (FoV) imaging and (fast) CT using matching detectors and resolution, this including wide FoV to match the maximum beam size. Note that fast CT should be fast enough to deliver 4D data of structural changes.	HEX BAT Meeting #1	Ongoing	Acknowledged, requested quote from Aussietron for such detectors.
166	Motorization of all tables (Z and Y – note that for the IMBL, x is beam direction, y across horizontal, z vertical) and detectors for safety – no pink beam to hit area detectors – and fast pre-aligned switching	HEX BAT Meeting #1	Closed	Yes - done
165	MOST IMPORTANTLY: Design all the beamline equipment to allow fast switching (less than 1min) between all 3 techniques. This requires a few specific things.	HEX BAT Meeting #1	Ongoing	See following recommendations #166 + #167 for specific things needed
167	A dedicated controls engineer to write all the software for the fast switching as the changes should be as close to 'press one button' as possible. I estimate 6 months of continuous work on the beamline, with the scientists. This is vital.	HEX BAT Meeting #1	Ongoing	Controls budget is good, and we have time to develop this. We can do a lot of development work early through collaboration with XPD.
168	ZZ must travel to several synchrotrons during the first design year (2018). This is a must to ensure that the experiment setups are design and implemented properly. These visits must include several days of participation in experiments.	HEX BAT Meeting #1	Open	See next recommendations #169 - #171
169	Visit to JEEP to understand and get familiar with the techniques switching, and see how their mono operates.	HEX BAT Meeting #1	Closed	This was done, plus two visits to the APS (6-BM, 2-BM, 1-ID, 11-ID, 11-BM).
170	Visit to other European synchrotrons, with at least on visit to a bidirectional EDXRD setup as it is essential that ZZ understands how to setup 2 EDXRD systems with very compact 'noses'	HEX BAT Meeting #1	Closed	Eric visited Soleil to discuss this; J-P Itie then visited NSLS-II on 24th Sept
171	Visit to the IMBL for some CT experiments, especially large sample CT and the use of robotics.	HEX BAT Meeting #1	Open	To be planned.
172	ZZ is an optics and beamline alignment genius but he has the old fashioned NSLS 'meccano' approach to experimental setups. I strongly recommend the appointment, or secondment, of a second scientist to this project.	HEX BAT Meeting #1	Closed	Scientist appointment complete - offer accepted.
173	Radiation enclosures: Even though the phase 1 must concentrate on the main line, ensure that the footprints etc. of the side branches enclosures are reasonable and include these in the request for tender, but ask for a price with and without them.	HEX BAT Meeting #1	Closed	This was done. Budget allows purchase of D-hutch, but not B-hutch. This is an acceptable, low impact, compromise consistent with the budget.
201	Recommend revisiting the mission statement for the HEX beamline	HEX CDR Meeting	Closed	Text provided to Richard Bourgeois (NYSERDA) and approved.

202	The Superconducting Wiggler is the most significant risk of the beamline that this review team identifies. The design and procurement needs to be planned out in detail and the route/option needs to be decided urgently.	HEX CDR Meeting	Closed	This will be closed out through natural planned work on the SCW. Specs are being written, and will be sent to potential vendors and BNL magnet division for cost estimations.
203	Complete FEA and thermal analysis of optical design and filters to determine preliminary configuration.	HEX CDR Meeting	Closed	This has been done, to the extent required for the PDR. Fixed filtering will reduce the power levels to something very manageable.
204	Consider both options regarding the mono location and vessel for the side bounce branch in detail before being locked in. Discussion about possible uses of side branch B other than PDF. Explore options and ensure design of infrastructure and space constra	HEX CDR Meeting	Closed	The design is sufficently flexible to allow alternative uses for the single bounce, fixed energy side station. This will be located upstream of other mono since the beam can be stopped / deflected avoiding conflict with other equipment for other branches
205	Consider Compton radiation as possible worst case shielding requirements. Note experience at Aussietron has found at 200 MeV GB becomes 350 keV Compton radiation. Analyze shielding requirements ASAP for endstation/concrete hutch requirements	HEX CDR Meeting	Closed	The analysis of the shielding is in process and the issue of Compton radiation is automatically covered by the Monte Carlo analysis programs.
206	Look into where the beams will end for the side and white beam branch. If feasible, extend the white beam branch to the white beam hutch	HEX CDR Meeting	Closed	Design takes beams to the mono locations, but no further.
207	Use electric cranes/trolleys in hutches	HEX CDR Meeting	Closed	Simplified cranes are included in the FOE only. A crane could be added in the F-hutch later if funds allow.
208	Start recruitment of the beamline scientist immediately. Aim for someone with some seniority.	HEX CDR Meeting	Closed	Position filled Dec 2018.
220	Keep hutch D in scope. Removing hutch D would prohibit access to hutch E roof via the current bridge and additional stairs would be needed.	HEX PDR Meeting	Closed	This is included in the hutch contract. (B-hutch was descoped for budget reasons).
221	Identify equipment that would be needed for endstation de-scoping and properly reserve it for use by HEX.	HEX PDR Meeting	Ongoing	We will complete the inventory of old equipment before FDR.
222	Bring the award for satellite building construction forward to occur before the hutches as funding allows, to better understand contingency situation	HEX PDR Meeting	Closed	New baseline schedule agreed
223	Come up with a prioritized list of scope additions/deletions	HEX PDR Meeting	Ongoing	A plan for phased scope adjustment was presented to the POB and accepted. This work will be ongoing at least to the end of CY2019
224	Consider having the BAT update the scientific case presented in the PDR report and consider the emerging questions in the field that the HEX user community will represent	HEX PDR Meeting	Ongoing	This was discussed at the Second BAT meeting, and an update to the scientific objectives will be included in the FDR report
225	Include a lead shield after the slits in hutch F to prevent background radiation for the detectors	HEX PDR Meeting	Ongoing	We will include a lead shield of approx 0.5m square x 0.25 inch thick, with 110mm (H) by 25mm aperture. An additional removable piece with 5mm diam hole will be specified to cover the large square aperture. This piece will removed for small samples
226	Investigate ion chamber performance working at energy ranges of 30 keV and up	HEX PDR Meeting	Closed	Zhong completed the calculation and has discussed the results at the DISC group meeting.
227	Consider possibility of having imaging and diffraction experiments being performed concurrently	HEX PDR Meeting	Ongoing	The current design allows rapid switching between imaging and diffraction modes. The imaging will be done with dedicated high-resolution detectors. We will consider purchasing a small x-ray eye type detector as an alignment tool in future upgrade.
228	Build a stand that shares the sample stage and detectors. Have precision engineering and nanopositioning group review	HEX PDR Meeting	Ongoing	Highest resolution for focused beam diffraction is 10 microns and imaging about 1 micron. Thus, we believe that the current design, with separate detector & sample tables, is sufficient. We will check with Evgeni during design.
229	The ability to change scintillators should be included in the design	HEX PDR Meeting	Ongoing	The current detector specification calls for detectors of different resolution. There are two model designs, employed by IMBL and JEEP, respectively. They both use changeable scintillators.
230	The review team notes that the multi array detector is in the project cost plan and recommends that multi array detector should be in initial scope. Talk to detector group for costing and general information	HEX PDR Meeting	Ongoing	We are in discussion with Pete and Abdul regarding the Ge array detector. Just recently, they are funded for R&D of a 2D array detector. We came up with a novel way to potentially use this new detector for EDXD at HEX.
231	Consider provisions for in-operando sample environment capabilities. The review team notes that this is not in scope but provisions and space requirement should be considered	HEX PDR Meeting	Ongoing	We will specify the sample stack to be on a kinematic mount, and to be removable from the floor via caster-wheels.
232	Add 1T manual slide/electrical hoist crane to endstation scope	HEX PDR Meeting	Open	This will be installed if funding permits (scope addition), close to the end of the project.
233	A decision on Plan B needs to be made as soon as possible to avoid adverse impact on the project. BNL development of SCW should be pursued separately from HEX, if needed	HEX PDR Meeting	Closed	This is considered to be a moot point since commercial bidders were identified in the make/buy report
234	Regardless of acquisition plan, develop a test plan for characterizing the SCW once it arrives at BNL	HEX PDR Meeting	Ongoing	The test plan will be developed as part of the preparation for the beamline FDR (March 2018)
235	Ensure the cost estimate for SCW includes all associated components including power supplies and utilities interfaces if needed. Investigate if helium recovery system is required	HEX PDR Meeting	Closed	The SCW cost estimates have included the PSU and associated electronics and controls. Utilities are also included. A recovery system is not required, although a vent and PRV will be required outside the tunnel: the cost of this is negligible.
236	FEA analysis on monochromator crystals cooling scheme need to be performed for better understanding of impact of temperature on strain and rotation of lattice throughout the optical volume of the crystal	HEX PDR Meeting	Closed	The FEA of the filters and monochromator crystals is complete and included in the FDR. Results are good.
237	Addition of ADXD capabilities need to be better developed. Currently, significant overlap exists with capabilities at XPD and PDF in both energy range and resolution.	HEX PDR Meeting	Closed	The use of the monochromatic branch is not necessarily reserved for ADXD, several scientific possibilities exist and this branch is not in the current project scope
238	Due to usability with EDXD and ADXD, KB system should be priority. Because of EDXD the KB mirror system should be in vacuum to prevent mirror contamination from exposure to white beam. Budget needs to be updated accordingly	HEX PDR Meeting	Ongoing	KB is the top-choice out of three candidate devices. The budget is $500k, which should be sufficient for a pair of 0.5 m (each) KB mirror system that is vacuum compatible
239	FEA needs to be performed for thermal distortion of the KB mirrors for white beam use	HEX PDR Meeting	Ongoing	We will ask Steve O'Hara to perform this once the filters are finalized and power load on the mirror are known.
240	Consider adding a beam visualization flag/BPM in E hutch	HEX PDR Meeting	Closed	This is described in the diagnostics section of the FDR report
241	Consider adding a beam diagnostics unit in the F hutch to characterize beam stability	HEX PDR Meeting	Closed	See recommendation #240
242	Consider space for future user areas on the experimental floor	HEX PDR Meeting	Closed	This is included in the FDR report, and the drawing will be approved by LSSOC within the Sector Assignment Document (update).

243	Look into the workability based on the size of the E/S hutch door and consider changing it to a sliding door or two swing doors	HEX PDR Meeting	Closed	The double door now has one large section and one small section (for people)
244	Consider the possibility of needing an eye wash station near/in satellite building	HEX PDR Meeting	Closed	We have added this to the project scope and costs are included in the plans
245	Ensure the cost for insulation and fence of section of outdoor beam pipe is included	HEX PDR Meeting	Closed	The fence and gate is included in the SB contract. The shielded pipe is in the optics contract, and BNL workers will do the weatherizing.
246	Check to make sure angle used for BR scatter calculations is the largest it would actually be	HEX PDR Meeting	Closed	This has been included in the shielding calculations included in the FDR.
247	Make sure that all equipment is EPICS compatible and can be controlled by Bluesky	HEX PDR Meeting	Closed	Yes. All equipment will be EPICS compatible, incl in-house developed detectors.
248	Consider adding more data storage	HEX PDR Meeting	Ongoing	This will be done late in the project depending on budget, need, and centralized storage situation.
249	Advanced EDXD collection and analysis tools need to be developed; similarly for tomographic reconstruction	HEX PDR Meeting	Ongoing	Some work is proceeding with this; the FDR report includes Use Cases, that should lead to this work being started sooner than is usual for BL projects

Appendix 2. Requirements, Specifications and Interfaces (RSI) Documents

- RSI for the SCW and Front-End, and
- RSI for the Satellite Building

RSI for the Superconducting Wiggler Source and Front End for the HEX Beamline

(Requirements, Specifications and List of Interfaces)

Compiled by Andy Broadbent and Zhong Zhong, with special thanks to Oleg Chubar.

Version 4

November 2018

RSI for the Source and Front End for the HEX Beamline

SIGNED COPY ON FILE.

Prepared by:

X

Zhong Zhong
HEX Lead Beamline Scientist

X

Andrew Broadbent
Partner Beamlines Portfolio Manager

Approved by:

X

Greg Fries
CAM / Accelerator Division Liason Engineer

X

Sushil Sharma
Mechanical Engineering Group Leader

X

Toshi Tanabe
WPM / Insertion Device Group Leader

X

Charles Hetzel
Vacuum Group Leader

X

George Ganetis
Electrical Engineering Group Leader

X

Oleg Chubar
Insertion Device Specialist

X

Mike Lucas
HEX Beamline Lead Engineer

X

Eric Dooryhee
Diffraction and In-situ Scattering Group Leader

REVISION HISTORY

VERSION	DESCRIPTION	DATE	AUTHOR	APPROVED BY
1	First Issue. .	30-Sep-2017	Z. Zhong and A. Broadbent	See page ii
2	Updated the FE slit description and the tabulated slit openings.	26-Mar-2018	Z. Zhong and A. Broadbent	See page ii
3	General tidy up, correcting a few minor errors, removing FE diagnostic flag from scope and confirming thermal fatigue life of slits and photon shutter.	20-Oct-2018	A. Broadbent	See page ii
4	Small corrections to the FE section, including adding a Flange Absorber, Burn-Through Flanges, renaming Bremsstrahlung Collimator to Lead Collimator for consistency, and correction of small typos.	20-Nov-2018	A. Broadbent	See page ii

Contents

1 DOCUMENT CONTROL

1.1 Identification

This document, *RSI for the Sources and Front Ends for the HEX Beamline,* is part of the Requirement Specification and Interface (RSI) documentation system, mapping to the NSLS-II Work Breakdown Structure (WBS). It captures and summarizes all requirements and specifications for the *Source and Front End* and lists all related technical interfaces with other parts of the project.

1.2 Scope

This document covers the Insertion Device and Front End for the HEX beamline, to be located at sector 27-ID of the NSLS-II, respectively.

2 ACRONYMS

3PW	Three Pole Wiggler
BMPS	Bending Magnet Photon Shutter
BTF	Burn-Through Flange
CED	Cost Estimate Database
EPICS	Experimental Physics and Industrial Control System
EPS	Environmental Protection System
FE	Front End
FM	Fixed Mask
FOE	First Optical Enclosure
FV	Fast Gate Valve
HEX	High Energy Engineering X-ray Scattering (beamline)
ID	Insertion Device
LCO	Lead Collimator
NSLS-II	National Synchrotron Light Source II
PLC	Programmable Logic Controller
RCO	Ratchet Wall Collimator
RSI	Requirements, Specifications, and list of Interfaces
RGA	Residual Gas Analyzer
SCW	Superconducting Wiggler

SGV	Slow Gate Valve
WBS	Work Breakdown Structure
XPBM	X-ray Beam Position Monitor

3 SOURCES FOR THE HEX BEAMLINE.

3.1 Insertion Device Specifications

The insertion device for the HEX beamline is specified below:

Beamline	HEX
Type	SCW
Device envelope length	~1.8 m
Magnetic Length	1.2m nominal (29 main and 4 partial poles)
Canted	No
Period: nominal	70 mm
Nominal (minimum) gap of vacuum bore tube	10 mm
Peak field nominal	4.3 T
Keff: nominal	28.1 (see Note 1)
Energy Range:	8 keV –200 keV
Power total: nominal	55.7 kW (see Note 1)
Max.power per unit solid angle: nominal	28.4 kW/mr^2 (see Note 1)
Straight	Low beta
Device center (see Note 2)	May be offset in the straight to the downstream end.
Fan angle (mrad H) : nominal (maximum) (See Note 3)	9.87 (10.15)
Fan angle (mrad V) : nominal (maximum) (see Note 3)	0.88 (1.47)
Magnetic field variation range	Current adjustment 0 – 100%

Note 1: In assumption of sinusoidal magnetic field distribution in central part of wiggler.

Note 2: The ray tracing should accommodate axial movements of the IDs by +/-5mm, which might be required in the design of the straight.

Note 3: The fan angles of the radiation quoted here are as seen at 16m from the source, and take into account the effects of source length; the worst case fan size is taken. The two values quoted are for the points where the power density falls to values that are 1% and 0.1% of the central value. Designs of the fixed mask entrance shall take into account these fringe power loads.

3.2 Insertion Device Controls

The ID planned for the HEX beamline has no motors. The SCW will require control of the magnet current (for ramp up and ramp down) and monitoring of the conditions within the cryogenic vessel. All of the devices shall follow the requirement in LT-C-ASD-ENG-RSI-001, *Requirements for Design and Electrical Wiring of Insertion Devices for NSLS-II*. The SCW controls interfaces will be in a separate document (Technical Specification for the Superconducting Wiggler).

3.3 Required Fans from the HEX Insertion Device

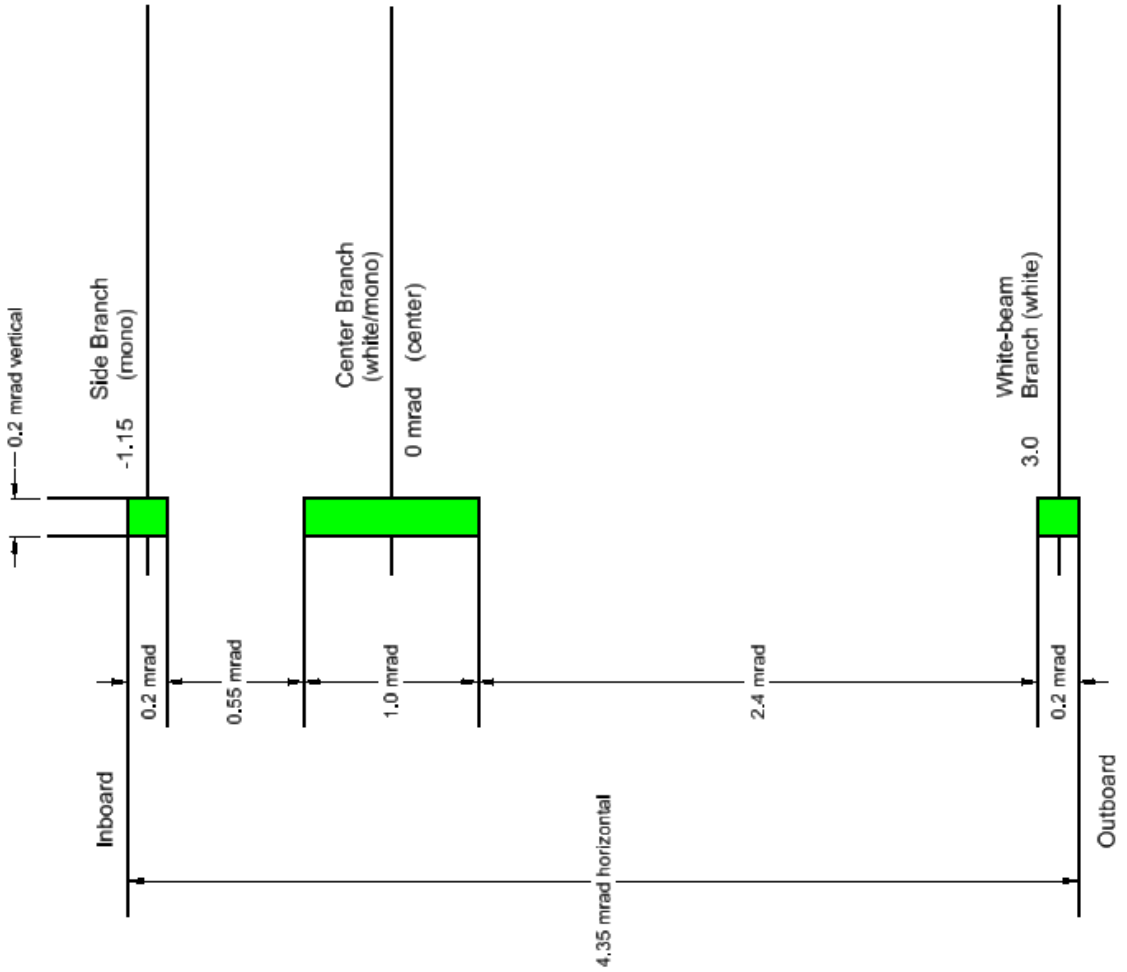

4 SUPERCONDUCTING WIGGLER STRAIGHT SECTION

The straight section shall include all necessary parts required for integration of the superconducting wiggler to the storage ring, as well as all required utilities. The following items are included in the scope for the Straight Section:

Vacuum transitions from the bore tube flanges of the wiggler, to the vacuum chamber at the ends of the straight	Y
Button type BPMs integrated into the straight vacuum chambers (standard stability type)	Y
Canting magnets	N
Vacuum pumps, pressure monitors, and RGA	Y
DI water for cooling the vacuum chambers, as required	Y
Gate valves to be fitted at each end of the straight and on either side of the SCW	Y
Installation of all cables to support the Insertion Device (SCW), to include 2 x ~400A / 10V main power cables, and the low current trim coil cables (as needed), controls cables for LHe and LN2 level sensors (as needed), vacuum sensors, thermal sensors, etc.	Y
Chilled water on tunnel roof for cooling cryogenic re-liquifying compressor	Y
Installation of GHe and GN2 (if needed) exhaust pipes	TBC
ODH Monitoring System	TBC

5 FRONT END COMPONENTS FOR THE HEX BEAMLINE

The components listed below shall be included as a part of the Front End. These are downstream of the Bending Magnet Photon Shutter (BMPS) and the Slow Gate Valve (SGV) that are used to isolate the Front End from the Storage Ring.

Specifications based on the scientific requirements are included in the indented rows.

	HEX
Beam Position Monitor 1 (XBPM1)	N
Beam Position Monitor 2 (XBPM2)	N
Flange Absorber	Y
Fixed Mask (FM)	Y (Mk2 design)
Type	Triple aperture
Source	SCW
Beam apertures (mrad)	
In-board	At 1.15 mrad, 0.2mrad H x 0.2mrad V
Center	At 0 mrad,1.0mrad H x 0.2mrad V
Outboard	At 3.0 mrad, 0.2mrad H x 0.2mrad V
Tolerance on apertures	+/-0.01mrad
Shape	Corner Radius
Burn-Through Flange (BTF1)	Y
Lead Collimator (LCO1)	Y
Water Cooled Beryllium Window	N
Number of X-Y Slit sets (see Note 1)	3
Thermal cycle lifetime	>30,000
X-ray flag	N
Fast Gate Valve (FGV)	Y
Diagnostics Cross	Y
Photon Shutter (PSH)	Y
Thermal cycle lifetime	>30,000
Lead Collimator (LCO2)	Y
Safety Shutter (SS) (x2)	Y
Cycles per year required (bellows)	50,000
Burn-Through Flange (BTF2)	Y
Ratchet Wall Collimator	Y
Gate valve outside Ratchet Wall	N

FOE Fixed Mask 1 (See Note 2)	Y
FOE Bremsstrahlung Collimator 1 (See Note 2)	Y

Note 1: The three independent branches shall have independent control of the beam power entering each branch. Due to the close proximity of the three branches, it is acceptable to have switchable apertures rather than conventional X-Y slits.

Note 2: The mask and collimator may be included in the FE scope at the Project Manager's discretion (rather than in the beamline WBS).

6 COMPONENT DESCRIPTIONS

6.1 Flange Absorber

This absorber protects the Front face of the fixed mask from the wide fan of the bending magnet x-rays.

6.2 Fixed Mask (FM)

The fixed aperture mask shall provide three separate x-ray fans to the First Optical enclosure (FOE) as defined in the table above.

6.3 Burn-Through Flange (BTF1)

The Burn-Through Flange protects the downstream lead collimator from the uninterlocked (max) fan of the Insertion Device.

6.4 Lead Collimator (LCO1)

The lead collimator restricts the Bremsstrahlung radiation fan exiting the shield wall. This should be as tight to the beam as is reasonable, preferably using standard tube sizes, and without undue mechanical tolerances or alignment difficulty. Consideration will be given to amending these specifications to suit standard tubes sizes, if sensible.

6.5 X-Y Slits

The X-Y slits for the three branches shall comprise a beam stop with four apertures, actuated in the vertical direction to switch between the apertures of varying sizes to control power; the aperture sizes are tabulated in the following tables.

The specifications for the slits are as follows:

Material	Water-cooled copper alloy

	Tungsten (or equivalent) blocks for improved beam definition are not required.
Power Protection	A pre-mask is not required.
Maximum Opening	Sufficient to allow the required x-ray fans to continue to the FOE without clipping.
Motorized	Yes to allow selection of any of the defining apertures.
Aperture Position Stability	Δx, Δy = 4 μm or better over any 8-hour period
Aperture Size Stability	0.4 μm or better over any 8-hour period

Slit Apertures		
Outboard Branch	Center Branch	Inboard Branch
0.2mrad H x 0.2mrad V	1.0mrad H x 0.2mrad V	0.2mrad H x 0.2mrad V
0.2mrad H x 0.1mrad V	0.4mrad H x 0.2mrad V	0.1mrad H x 0.2mrad V
0.2mrad H x 0.05mrad V	0.2mrad H x 0.2mrad V	0.05mrad H x 0.2mrad V
0.05mrad H x 0.05mrad V	0.05mrad H x 0.05mrad V	0.05mrad H x 0.05mrad V
0mrad H x 0mrad V	0mrad H x 0mrad V	0mrad H x 0mrad V

6.6 X-Ray Flag

An x-ray diagnostic flag is not required.

6.7 Photon Shutter

The photon shutter is required to stop the three x-ray beams from the FM (one shutter for all branches). This is expected to be water cooled, copper alloy, at a grazing incidence angle and should be fitted with a single actuator.

6.8 Fast Gate Valve (FV)

The fast valve is to shut within 15 milliseconds, once triggered by FV sensors located in the Front End and beamline whenever there is a sudden increase of pressure of a few decades. The stored beam has to be dumped prior to the FV closing, and the cause then investigated and mitigated

6.9 Lead Collimator (LCO2)

See Lead Collimator (LCO1).

6.10 Safety Shutter

The safety shutter is actually a pair of shutters, required for redundancy, air actuated with independent redundant and diverse position sensing. The Safety Shutter, in conjunction with BC1, BC2, and the Ratchet Wall Collimator completely stops the high energy Bremsstrahlung radiation.

6.11 Burn-Through Flange (BTF2)

This burn-Through Flange protects the RCO chamber from un-interlocked (max) fan of the Insertion Device.

6.12 Ratchet Wall Collimator

This device creates a stop for high energy Bremsstrahlung radiation between the beam pipe passing through the ratchet wall and the wall itself. This will use standard tube sizes wherever possible.

6.13 Gate valve downstream of Ratchet Wall.

This valve is not required due to the presence of a double diamond window downstream of the ratchet wall which will effectively terminate the Front End vacuum section.

6.14 Motion Controls

The front end components requiring motion control include

- the slits for each branch (motor and encoder for vertical motion),
- the shutters (3 total) require position sensing switches and a solenoid for the air actuator.

6.15 Vacuum Controls

The Front End vacuum control is part of the storage ring vacuum control through EPICS and the storage ring vacuum PLC. EPICS provides the menu driven on-line control and logging of all vacuum devices, while the PLC provides the control logics for various vacuum devices and interface to EPS PLC for machine protection.

The vacuum system shall be compatible with the LT-ENG-RSI-SR-VA-002, *Requirements for the Design and Fabrication of Components for NSLS-II UHV Systems*, and obtain a vacuum level of $10E^{-9}$ mB.

7 REFERENCES

1. LT-C-ASD-ENG-RSI-001, *Requirements for Design and Electrical Wiring of Insertion Devices*

2. .LT-ENG-RSI-SR-VA-002, *Requirements for the Design and Fabrication of Components for NSLS-II UHV System*

Experimental Facilities RSI for the High-Energy Engineering X-ray Scattering (HEX)

Beamline Satellite Building

(Requirements, Specifications and List of Interfaces)

Version 3

November 2018

SIGNED COPY ON FILE.

Prepared by:

X

Andrew Broadbent
Partner Beamlines Portfolio Manager

Reviewed by:

X

Eric Dooryhee
Diffraction and In-situ Scattering Group Leader

X

Zhong Zhong
HEX Lead Beamline Scientist

X

Mike Lucas
HEX Lead Mechanical Engineer

X

Chris Stebbins
HEX Utilities CAM

Approved by:

X

Tom Joos
Project Manager

X

Brian McCaffrey
Manager, Facilities Engineering Group

X

Lori Stiegler

HEX Beamline Project ESH Manager

X

Chris Channing

Principal Engineer, Energy and Utilities Division

REVISION HISTORY

VERSION	DESCRIPTION	DATE	AUTHOR	APPROVED BY
1	First Issue.	10OCT2017	A. Broadbent	See page ii
2	Clarifications of requirements at Beamline PDR stage.	30MAR2018	A. Broadbent	See page ii
3	Update of requirements at Completion of SB Design.	18OCT2018	A. Broadbent	See page ii

Acronyms

HEX High-energy Engineering X-ray (beamline)
LOB Laboratory Office Building
PSS Personnel Safety System
RSI Requirements, Specifications, Interfaces
SR Storage Ring
WBS Work Breakdown Structure
PD Photon Division

Contents

1 Identification

This document, NSLS-II Experimental Facilities Requirements, Specifications and Interfaces (RSI) for the High-energy Engineering X-ray Scattering (HEX) Beamline Satellite Building is a part of the documentation system, mapping to the Work Breakdown Structure (WBS) for this project.

It captures and summarizes all requirements and specifications for the WBS elements within 7.05.07, HEX Satellite Station, and describes all its technical interfaces with other WBS elements.

2 SCOPE

This document covers the requirements for the High-energy Engineering X-ray Scattering (HEX) Beamline Satellite Building.

The following requirements are covered in this document:

a. Building temperature and temperature stability
b. Beamline and satellite building location
c. Building vibration
d. Acoustic noise

e. Fire safety;

f. Utilities required for the experimental program (and responsibility):

Item	To be included in satellite building contract	Work by others (NSLS-II staff or by separate contract).
Standard lighting and local emergency lighting to comply with codes	Yes, except….	Inside hutch
Electrical power distribution	Yes, except….	Inside hutch
Electrical grounding system	Yes, except….	Instrument grounding
De-ionized (process) water distribution	No	Yes
Process chilled water distribution	No	Yes
Liquid nitrogen distribution	No	Yes
Facility compressed gases	No	Yes
Experimental gases distribution	No	Yes
Ambient temperature sensors	As needed for HVAC system	As needed for instrument monitoring
Oxygen depletion sensors	No	Yes
Communications, Ethernet, and fire alarm system	Yes	No
Cable trays	For utilities under building contract only.	Yes
Gas-exhaust system	No	Yes
Laboratory and other support facilities	No	Yes

3 Experimental facilities requiremenTs for the HEX beamline Satellite building

3.1 General

The Synchrotron Facility is designed to operate continuously 24 hours per day, 7 days per week (≥ 5,000 User Beam Hours per year). The design life of the facility, including the Satellite Building described here, shall be a minimum of 30 years.

The HEX beamline is one of up to 60 beamlines that will be constructed at the NSLS II facility. The nature of this beamline is such that the experimental station must be located outside the main NSLS-II experimental building. This document describes the necessary satellite building to house this beamline's end station and ancillary equipment.

3.2 Beamline and satellite building location

The HEX beamline shall be located on the 27-ID straight, one of the low-beta straights that can accommodate a beamline with an external station. The beamline shall extend in length over the bypass corridor walkway and the satellite building shall be located outside the edge of the Storage Ring (SR) building.

3.3 Requirements for HEX (as compared to HXN)

The satellite building should be very similar to the HXN satellite building, with the following changes:

I. Required Changes

- The hutch concrete wall thicknesses shall be;
  - 0.7m thick for upstream wall and side walls
  - 1.0m thick for downstream wall
    (For reference, HXN walls were ~0.2m thick).
- The roof thickness shall be 0.6m. This will make the roof of the hutch into an exclusion zone. Dose on the building roof is sufficiently low for safe and unrestricted worker access.
- The internal dimensions of the hutch should be unchanged (the thickness of the shielding means the hutch footprint will grow), providing that the walkways around the outside remain legal when racks are located against the outside wall.
- The number of wall labyrinths for Users, PPS, utilities shall be 11 (excluding HVAC labyrinths):
  - 9 on the inboard wall
    (for User access, PPS, spares, etc.)
  - 1 on the upstream wall
    (mechanical utilities (PCW and gases) and/or vacuum)
  - 1 on the outboard wall

The wall labyrinths listed above will have heavy lead labyrinth doors fitted (by NSLS-II) to the inside of the hutch (to simplify the PPS installation; a simple release switch can be fitted avoiding expensive locks

or administrative controls, which was required at HXN). These doors are outside the scope of the conventional construction contract. The conventional construction contract will include the steel sleeves that pass through the wall and finish ½" above flush with the wall surface (onto which the door assemblies will be welded).

- Floor trenches with a cross section sufficient to accommodate a 24" cable tray (actual dimensions 24¼" x 4¼") are required to allow cables and pipes to pass under the walls. Quantities needed: four trenches on the outboard sidewall and two on the upstream wall.
- The unistrut embedded in the wall shall be full height, not just the top few feet of the wall. Fitting these with concrete should be avoided if possible (as happened with HXN).
- Due to the weight of the entrance doors (~1" lead), it is necessary that these are sliding rather than swing doors; care will need to be taken to ensure that there is no interference with adjacent services (electrical outlets etc.). The lead sliding doors (by NSLS-II) are not part of this conventional construction contract.
- Crane – Not needed (a small engine hoist will be used as required for small lifting tasks; it will be specified that all components are fitted with wheels).

II. Permissible Changes (for minimizing cost)

Temperature stability may be relaxed as follows:

- Hutch +/-0.5C over a two hour period, +/-1C over a 24 hour period
- Surrounding area +/-1C
- The hutch entrance vestibule is not required (remove to minimize costs).
- The air handling system is included in the building scope. Air from the main air handler can feed through a roof labyrinth (the labyrinth is part of the lead hutches contract) to two airsocks running the full length of the hutch; the false ceiling is not required. An air outlet labyrinth is required. The scope of the conventional construction contract will include the following;
    - Air inlet and outlet tube through the roof at the downstream / outboard corner comprising a straight through steel pipe of

adequate diameter to meet the ventilation requirements (~16”). This tube shall be cast into the concrete and finish ½” above flush with the surface. The wall thickness shall be >0.5” (adequate for welding the air labyrinth to the outside).

- Exhaust air outlet tube similar to the air inlet and outlet, but ~12” in diameter that can be used for extraction of gas from the hutch..
- The ductwork connections (inside the hutch) from the tube passing through the roof, to the airsock (for the inlet air), and to the return air ductwork shall be in the scope of the satellite building contract.
- The final ductwork connections (outside the hutch) to the air inlet/outlet labyrinths will be done by BNL staff in the event of the labyrinth components being installed after the satellite building contract is completed.

- The vibration requirement is significantly reduced;
  - The use of Concredamp, or similar material is NOT required (this was a requirement for HXN).
  - The floor thickness under the hutch could be reduced to 15” (same as the experimental floor), providing this will adequately support the hutch weight. However, some equipment and/or cable trays may need to recess into the floor. This may call for a floor thicker than 15”, but it could still be thinner than HXN (1m). See detail drawing.
  - The vibration isolation joints should be retained as used for the HXN design.

III. A vacuum pipe shall connect the beamline in the Experimental Hall to the beamline in the Satellite Building. This pipe will be no larger than 10” in diameter (this comprises 6” beam, 1” clearance each side to the tube, and 1” radial allowance for lead). The pipe will be fitted with 10” OD flanges; no allowance has been made for insulation. The pipe shall be connected to the Satellite Building in a manner that permits survey alignment and preserves the building thermal performance. A similar design to HXN/SIX may be employed for weatherproofing. The holes in the building will be made by BNL staff when the pipe is ready for installation.

IV. Further design changes are permissible, especially if costs can be minimized, although these should be approved by the HEX beamline team.

3.4 Labyrinths

The following labyrinth designs are required as a part of the conventional construction work (Figure 3-1). Note that in all cases the blue parts (and ductwork inside the enclosure) are supplied by NSLS-II, and the conventional construction work includes only the steel parts passing through the wall. These should be cast in-situ with the ends ½" above flush with the finished concrete surface to allow the external parts to be welded.

- Wall labyrinth
- HVAC inlet/outlet and exhaust labyrinths

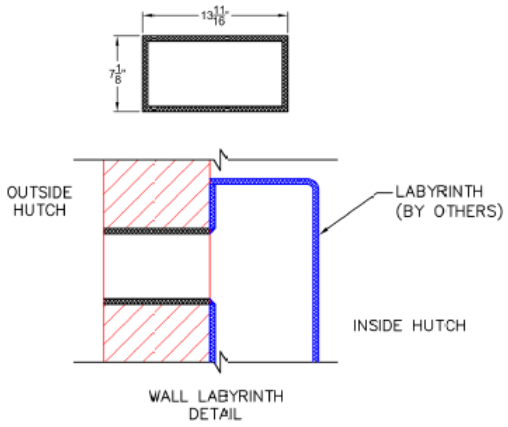

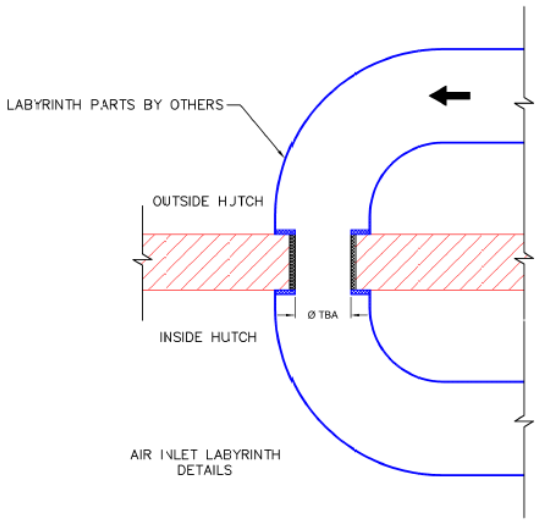

Figure 3-1: Conceptual Labyrinth Designs

3.5 Other Requirements

- An exhaust system with fan (by NSLS-II): will be connected to the main exhaust system above the walkway inside the main ring building.
- LN2 System (by NSLS-II): To be installed under a separate contract by a specialist supplier.
- Gas System Provision (by NSLS-II): Details TBC.
- Trenches in the floor for installation of cables: See Figure 3-2 below. The lids shall be metal and the weight shall not exceed 45 lbs.

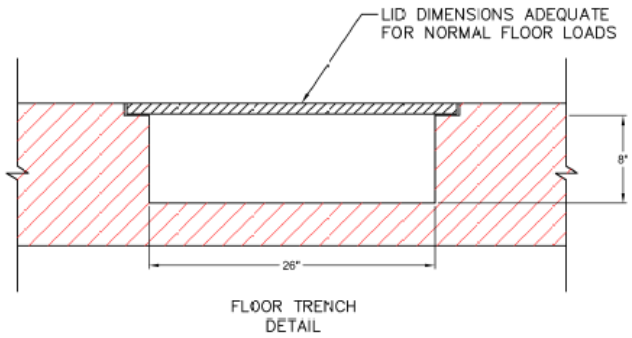

Figure 3-2: Floor Trench Detail (26” wide x 6” deep from underside of lid).

4 Further Considerations

- Review and apply any lessons learned from the satellite buildings for the HXN & SIX beamlines.
- Insulation: The standard of contractor installed insulation was very poor at HXN, the sealing was also poor with significant air leakage. Specific emphasis will be required on this point, with inspection hold points written into the construction contract.
- Access to the building will be via the experimental floor through the roll-up door and via a personnel double width door (same as HXN). A separate single door shall also allow access to the LOB.

- Controls racks will be located behind the hutch (same as HXN).
- No windows to be included in the concrete hutch walls.
- External gutters are preferred.
- Anticipated heat loads;

Item	Heat load
6 people (area outside hutch)	70W (sensible) and 30W (latent) per person
Electrical equipment inside hutch	5 kW
Electrical equipment outside hutch	Use actual loads from HXN, exclude racks.

Appendix 4. Lattice Schemes for the HEX Beamline at Cell 27.

Appendix 3: Lattice schemes for the HEX Beamline at Cell 27

NSLS II TECHNICAL NOTE BROOKHAVEN NATIONAL LABORATORY	NUMBER **289**
AUTHOR Weiming Guo and Yongjun Li	DATE **Nov. 13, 2017**
TITLE **Lattice Schemes for the HEX Beamline at Cell27**	

This Tech-note reports the two lattice compensation schemes for incorporating a superconducting wiggler at cell 27 for HEX beamline.

Part I discusses a global compensation, and Part II reports a local compensation scheme.

Both parts discuss two possible placements for this 1.2m long device, i.e., the center of the device is located at the downstream of the straight center by 1.0m or 1.8m.

Appendix 4. Lattice Schemes for the HEX Beamline at Cell 27.

Placement of the SCW for the HEX beamline

The proposed superconducting wiggler for the HEX beamline is tentatively placed at the center of Straight 27. The parameters that are relevant to electron beam dynamics are listed in Table 1[1].

Table 1. Main parameters of the proposed SCW for HEX beamline

Device envelope length	~1.6 m
Magnetic Length	1.2m nominal
Number of poles	29 (main), 4 (partial)
Period Length	70 mm
Minimal gap of vacuum bore tube *	10 mm
Peak field	4.3 T
Keff	28.1
Energy Range:	8 keV –200 keV
Total radiation power	55.7 kW
Max.power per unit solid angle	28.4 kW/mr2
Fan angle (mrad H)	9.87 (10.15)
Fan angle (mrad V)	0.88 (1.47)

Due to the wide horizontal fan angle the downstream vacuum chamber is exposed to the intensive radiation. It was asked by the Vacuum group that if the device could be shifted downstream so the fan would pass through the straight vacuum chamber. This note addresses the incurred beam dynamics issues.

The SCW is modeled by a kick-map which was calculated by T. Tanabe. In order to explore the possibilities two cases were studied:

- Move the SCW downstream by 1 m;
- And by 1.8m.

For comparison we placed the above two cases in both the bare lattice and the operations lattice which has 15 IDs installed.

The first step is to correct the linear lattice. Using the bare lattice as an example, the beta functions and the phase before and after correction are plotted in Figure 1 and 2. The SCW was moved by 1.8m in the plots.

The beta functions at the center of the SCW when it is moved by 1m are listed in Table 2. Table 2. Lattice functions at the SCW center when it is moved by 1m

Appendix 4. Lattice Schemes for the HEX Beamline at Cell 27.

	betax	Betay	alphax	alphay
SCW center	2.449	2.435	-0.575	-1.205

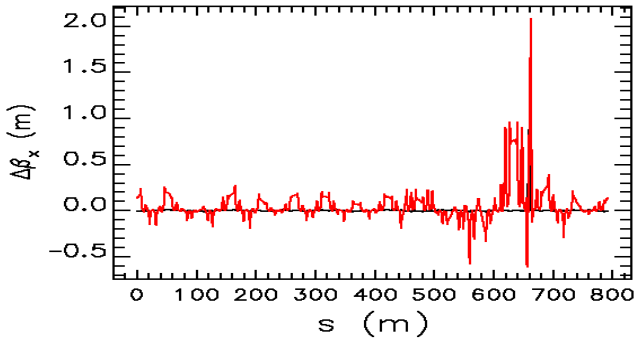

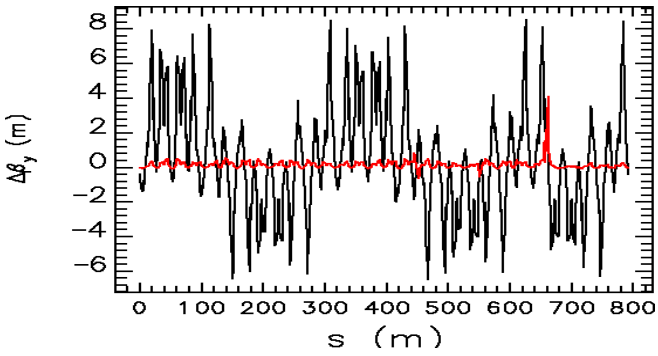

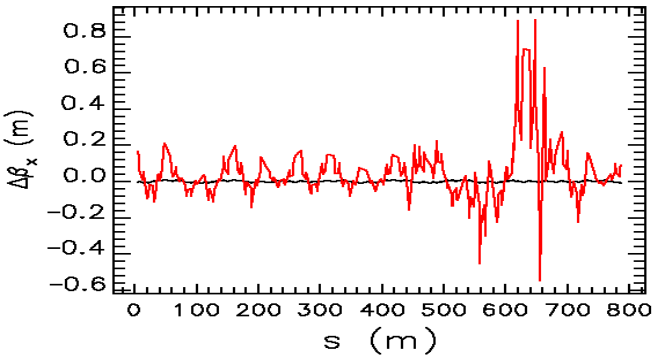

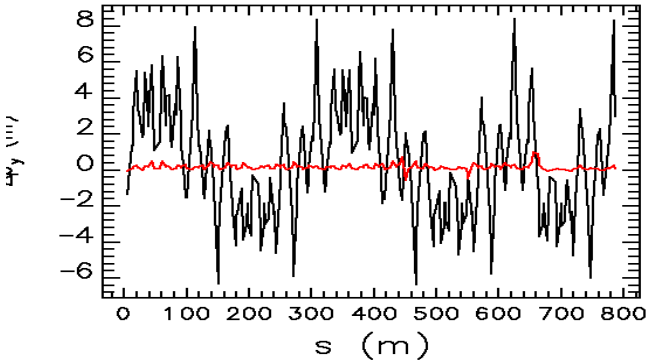

Appendix 4. Lattice Schemes for the HEX Beamline at Cell 27.

Figure 1. the beta functions before and after correction. Black: before correction, red: after correction. Upper: at all the elements, lower: at the sextupole magnet locations.

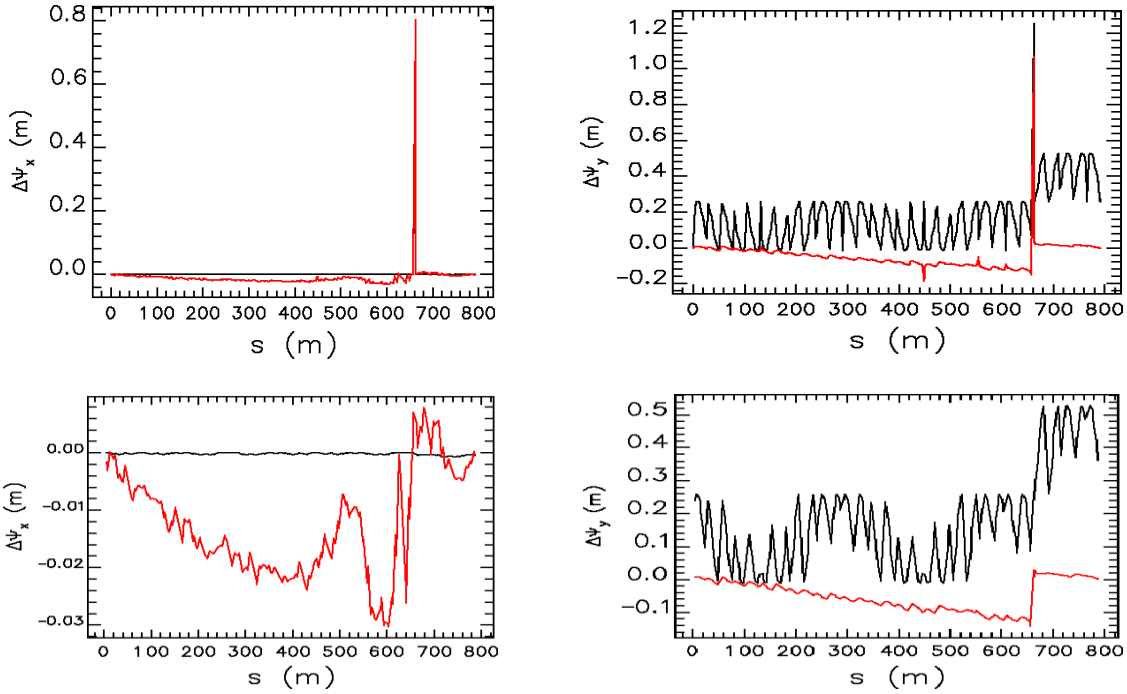

Figure 2. the betatron phase before and after correction. Black: before correction, red: after correction. Upper: at all the elements, lower: at the sextupole magnet locations.

We noticed that the SCW changes the amplitude dependent tune shift significantly. The comparison of these parameters are listed in Table 2. All the detuning terms changed by 30-50%, while the chromaticity coefficients remained at similar values.

Table 2. Comparison of the chromaticity and the amplitude dependent detuning terms for the bare and the lattice with 2m shift.

	Cx1	Cy1	Cx2	Cy2	dnx/dJx	dny/dJy	dnx/dJy
bare	2.0	1.8	-157	28	-2180	-4826	-600
SCW	2.1	1.9	-157	30	-2720	-6339	-1000

Appendix 4. Lattice Schemes for the HEX Beamline at Cell 27.

Frequency map analysis were carried out for 3 cases for the bare lattice.

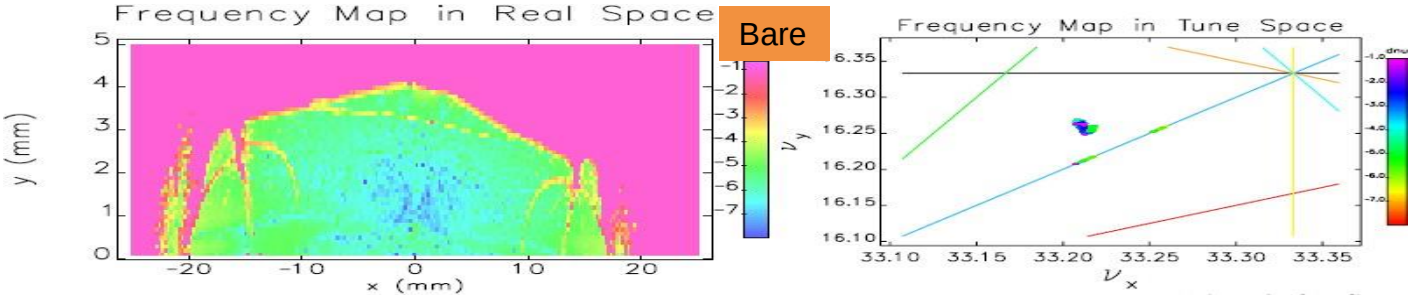

Figure 3. On-momentum Frequency map comparison for the bare, move 1m and move 2m lattices.

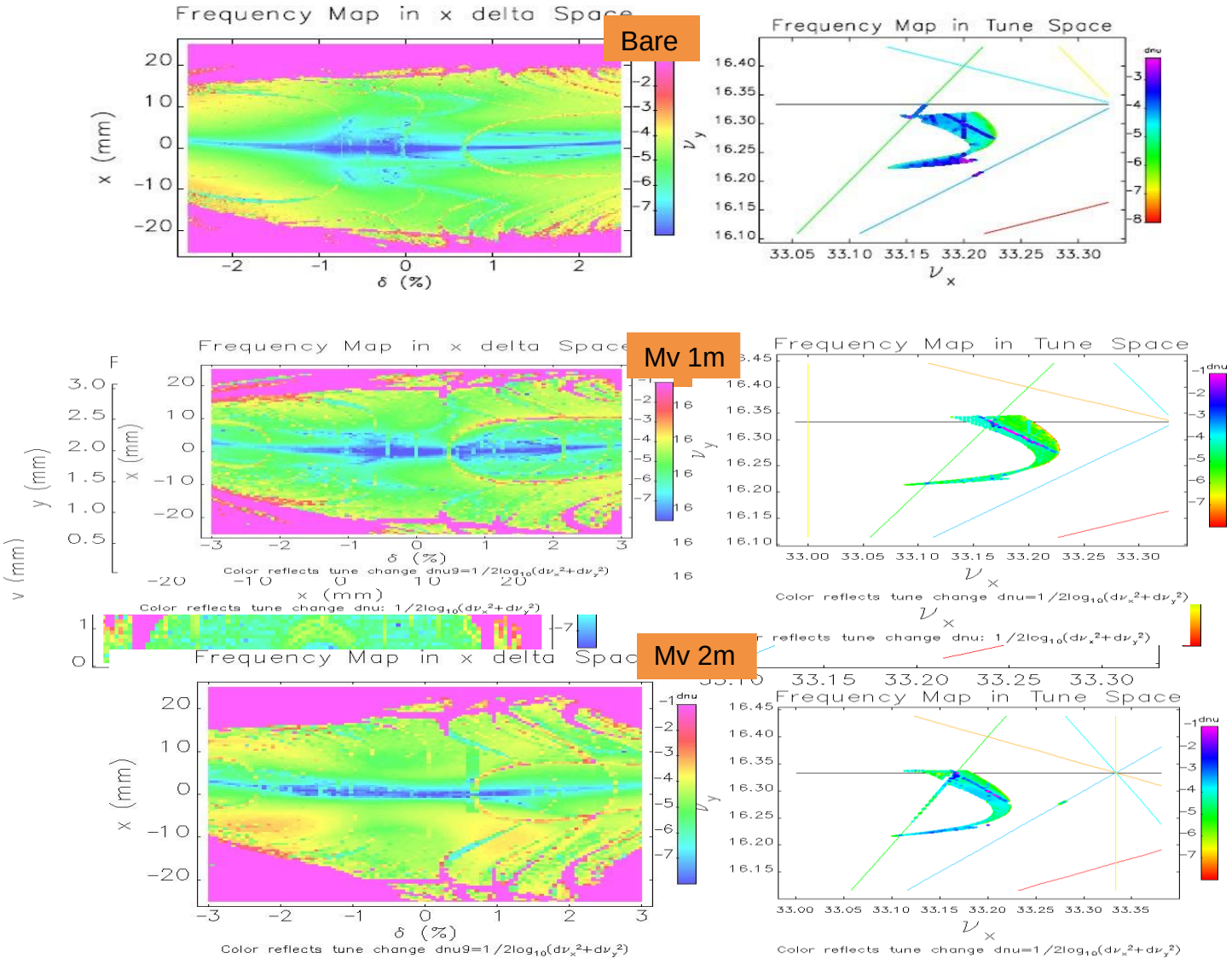

Figure 4. Off-momentum Frequency map comparison for the bare, move 1m and move 2m lattices.

Appendix 4. Lattice Schemes for the HEX Beamline at Cell 27.

Another comparison was made between the bare lattice and the operations lattice. In this case the SCW was moved by 1.8m. The resonance structure becomes severer in the case when SCW is moved by 1.8m.

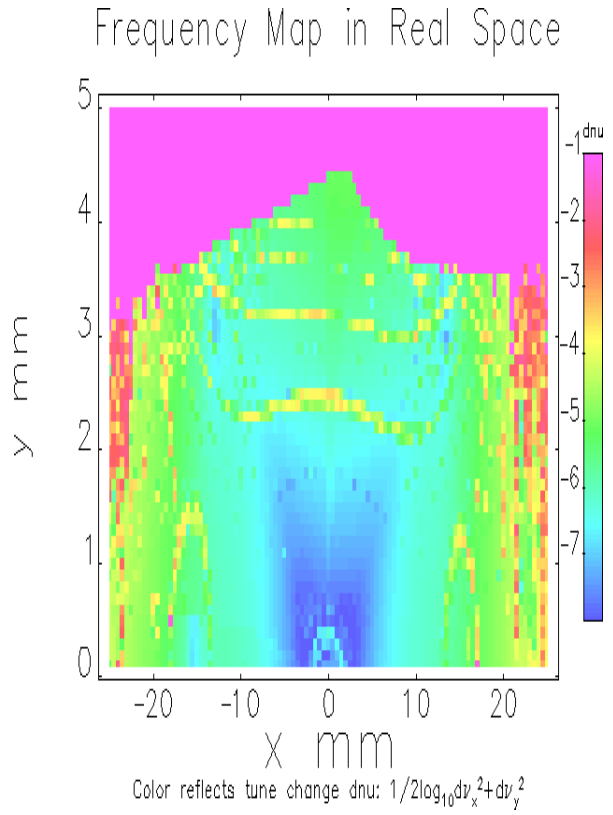

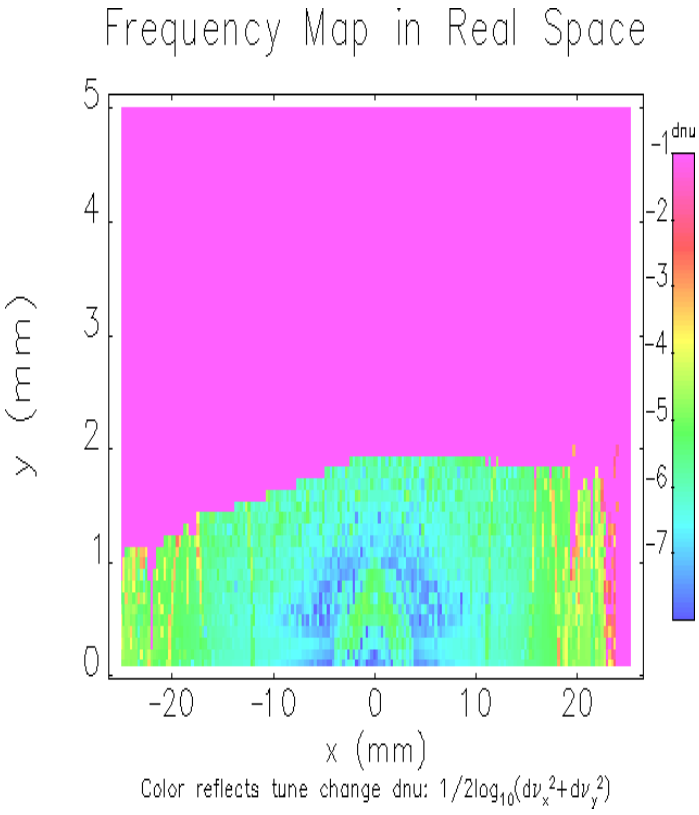

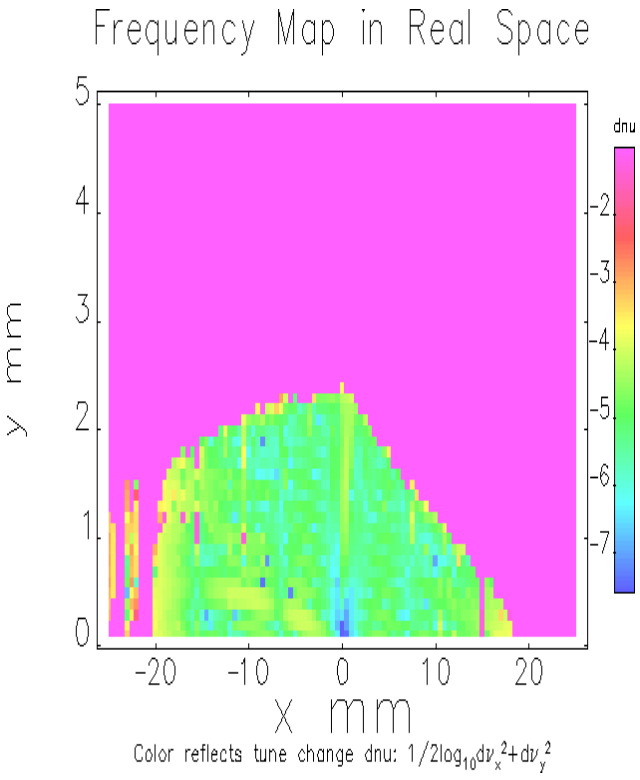

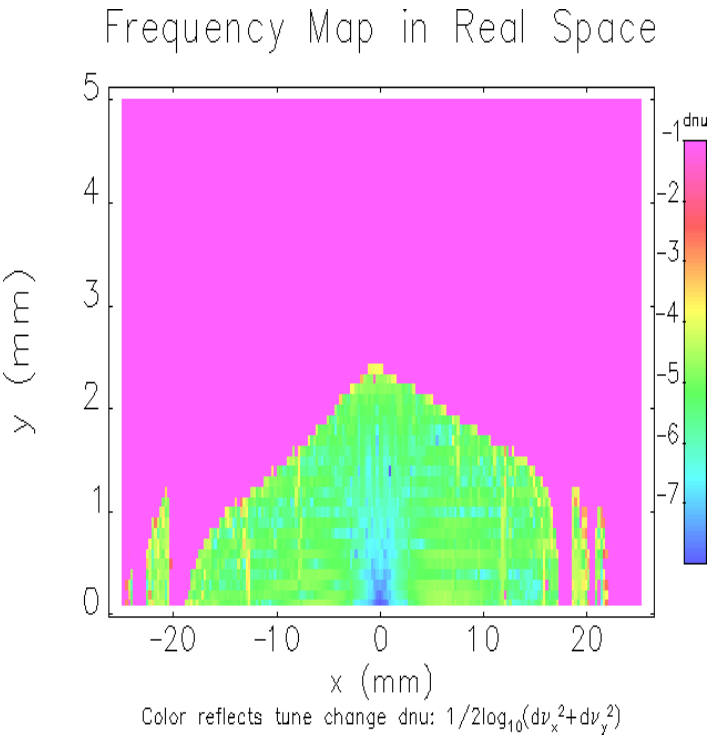

Appendix 4. Lattice Schemes for the HEX Beamline at Cell 27.

Figure 5. On-momentum Frequency map comparison. Upper: bare lattice; lower: operations lattice with 15IDs. Left: no SCW; right: SCW moved by 1.8m downstream.

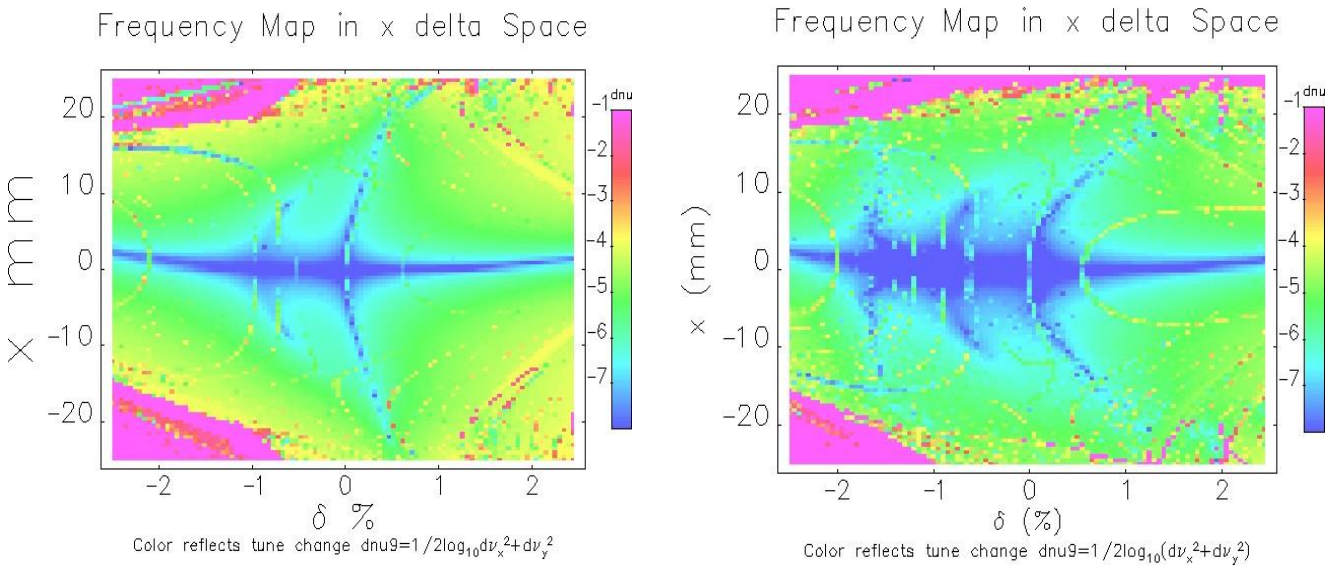

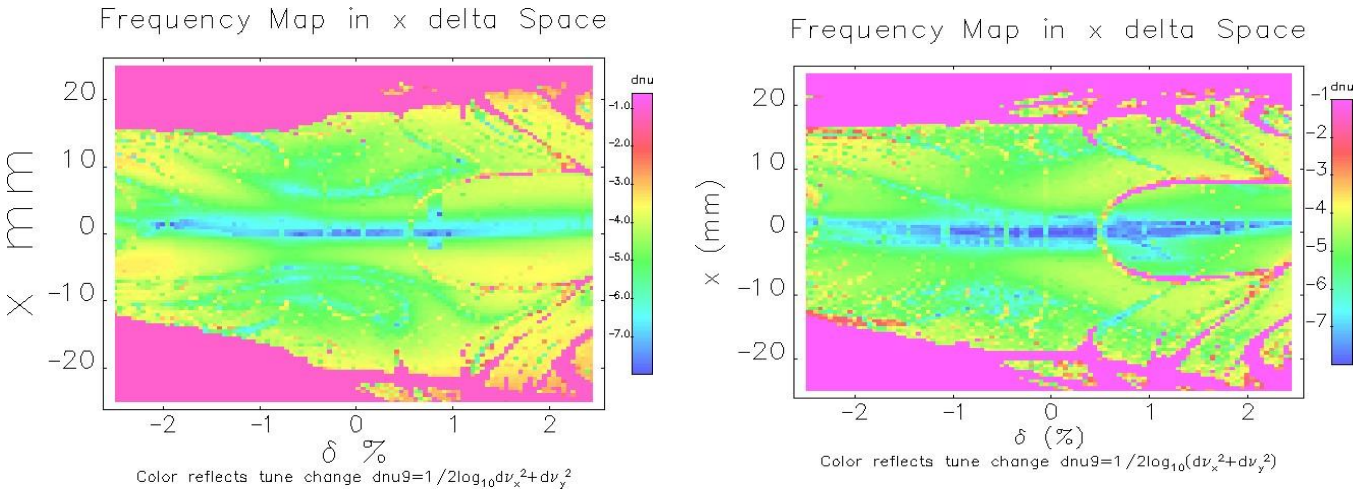

Figure 6. Off-momentum Frequency map comparison. Upper: bare lattice; lower: operations lattice with 15IDs. Left: no SCW; right: SCW moved by 1.8m downstream.

From Fig.5 and 6 it is clear that the impact of SCW to the operations lattice is greater than that of the bare lattice.

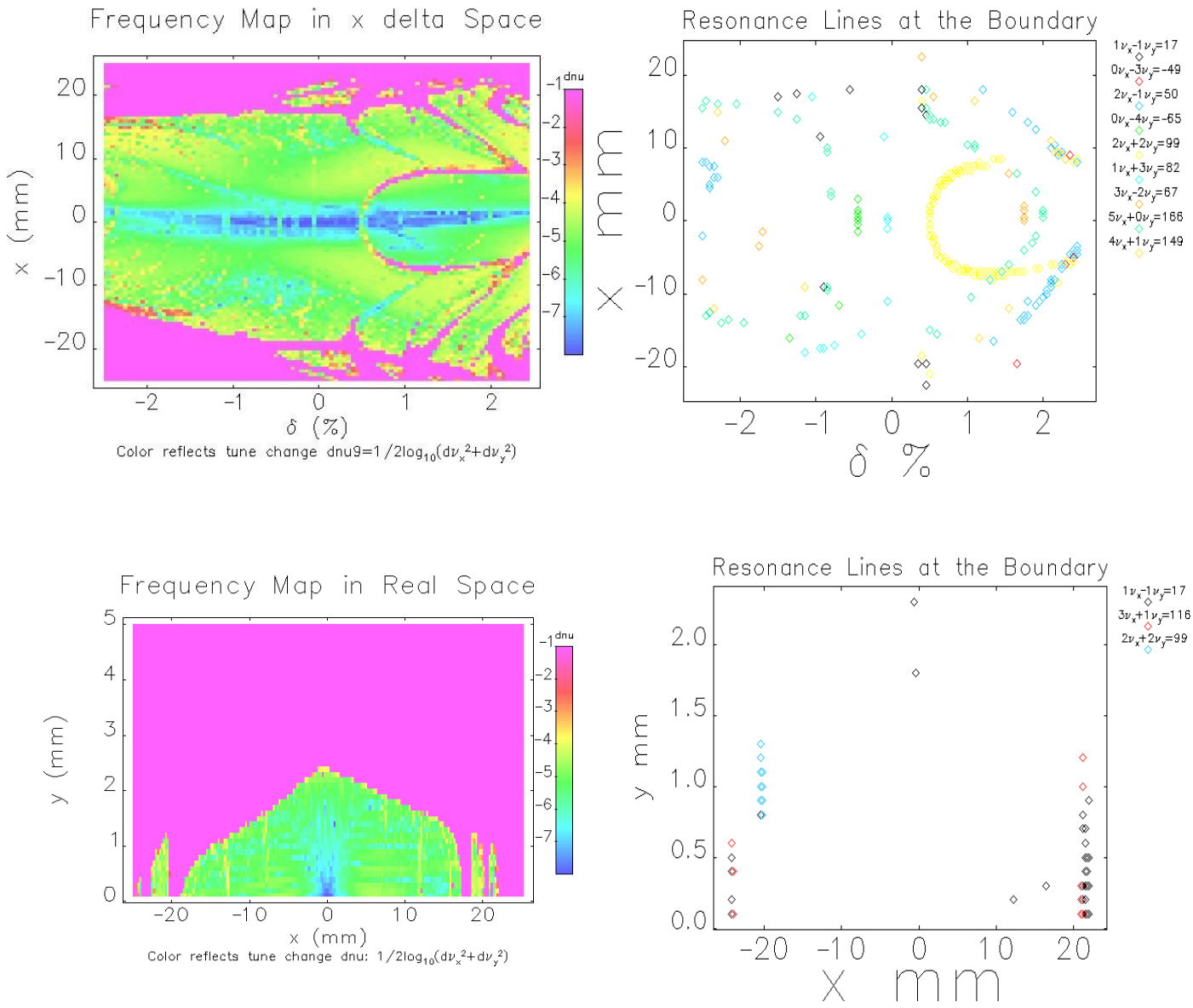

Figure 7. The resonance lines found in the on- and off-momentum frequency maps.

The resonance lines were analyzed and the results are shown in Fig. 7. The line that across dp/p=0.5% to 2.5% is 2nu_x + 2nu_y=99. The limiting resonance line for the on-momentum map is nu_x-nu_y=17.

Conclusion

The SCW introduces 8m peak-to-peak beta beat in the vertical plane and can be restored by all the quadrupoles. Resonance structure becomes severer when the SCW is moved downstream by 1.8m. The effect was not so apparent for the bare lattice. The amplitude dependent detuning terms were changed significantly by the SCW. The limiting resonance lines are nux-nuy=17 and 2nux+2nuy=99.

Reference

[1]Andy Broadbent and Zhong Zhong, RSI for the Superconducting Wiggler Source and Front-End for the HEX Beamline

Appendix 4. Lattice Schemes for the HEX Beamline at Cell 27.

Lattice including SCW in Cell 27 Downstream

Magnet layout

The SCW is 1.19m long. Its center is located at 1.8 m (scheme 1) or 1.0 m (scheme 2) downstream from the center of the straight section (see Fig. 4).

Kickmap

The 2D “radia” kickmap provided by ID group is used to model this device.

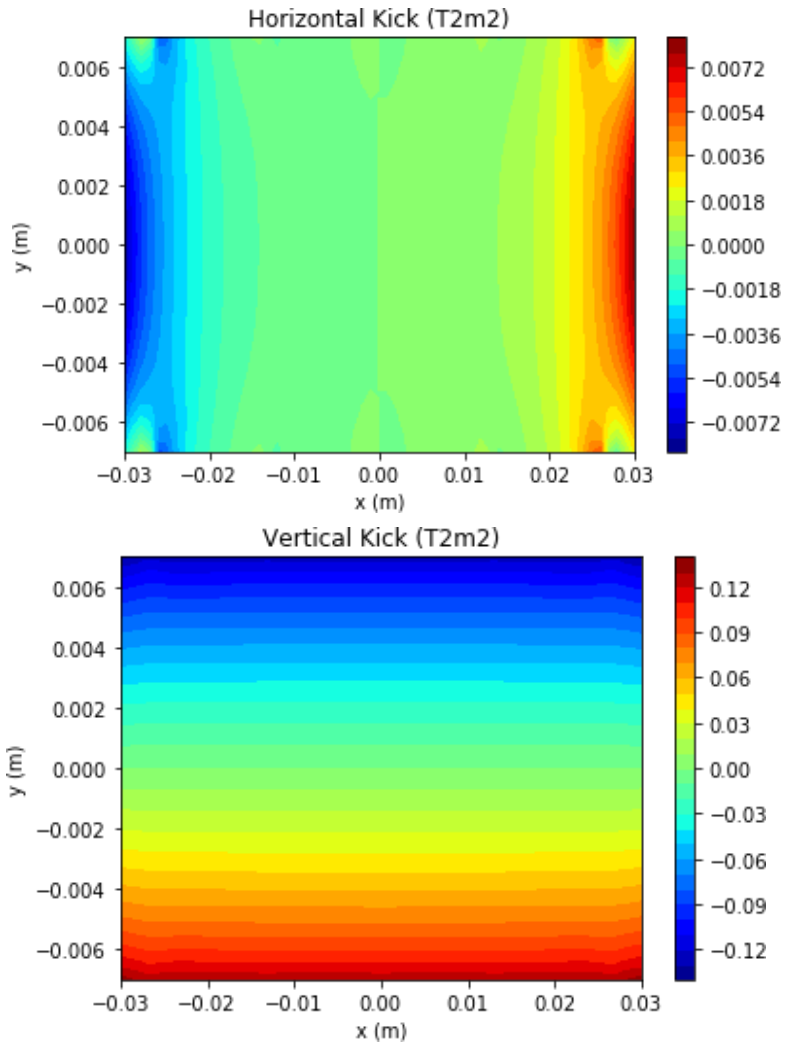

Fig. 1. Kickmap kx/ky of the SCW in the x/y planes

Appendix 4. Lattice Schemes for the HEX Beamline at Cell 27.

Optics distortion without compensation

The horizontal plane

Like other installed wigglers, it has tiny effects in the horizontal plane (see Fig.2).

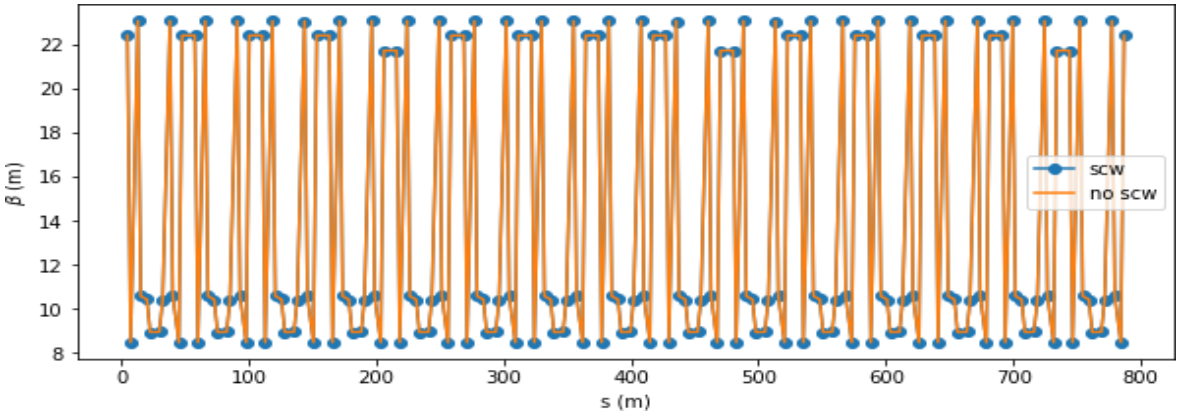

Fig. 2. Optics comparison w/o the SCW in the horizontal plane

The vertical plane

But it affects the optics in the vertical plane significantly. The tune is shifted from16.263 to 16.305. The maximum beta-beat is +8/-6m observed at the location of 180 ring BPMs (see Fig. 3). Therefore an optics re-match is needed.

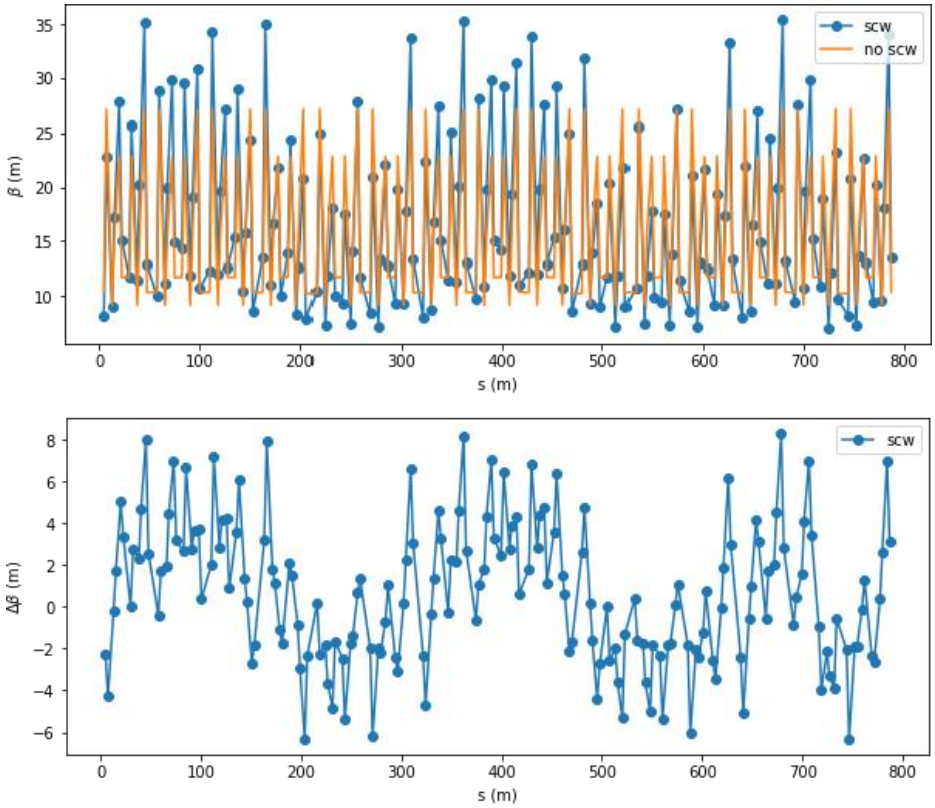

Fig. 3. Optics comparison with and without the SCW in the vertical plane

Appendix 4. Lattice Schemes for the HEX Beamline at Cell 27.

Local optics compensation at ID 27

Here a local linear optics compensation scheme is discussed, which has been proved to be successful in incorporating 3 damping wigglers in NSLS-II. Alternative solution is implementation a global optics compensation, which is discussed separately in W. Guo's tech-note.

Optics without the SCW

Here is the optics with an empty space. The goal is to match the optics at both ends, while maintaining the phase advance to the original value as close as possible.

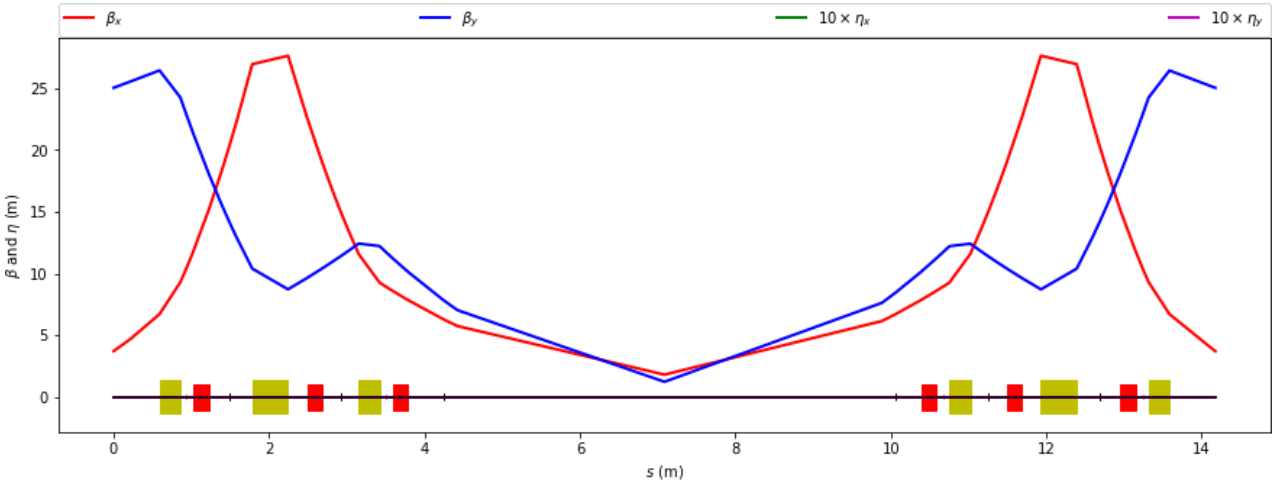

Fig. 4. Optics of the empty ID 27 section

Re-matched Optics for scheme 1 (1.8 m displacement)

Here the optics after a local compensation. The green block is the SCW. The optics distortion is confined within the ID 27 straight section (also see Fig. 7).

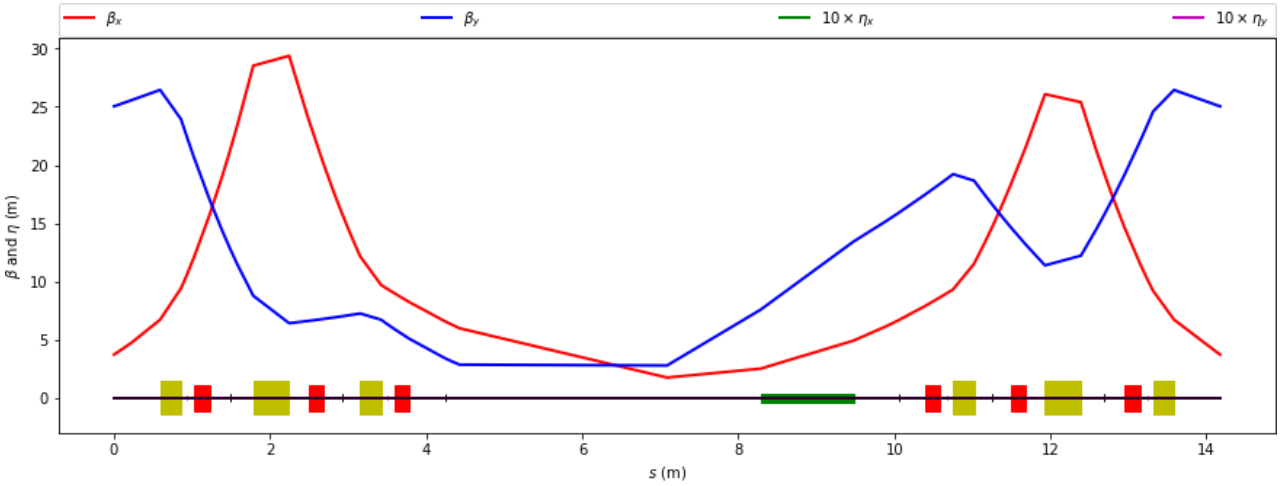

Fig. 5. Optics of the ID 27 section with the SCW (1.8 m displacement scheme)

Appendix 4. Lattice Schemes for the HEX Beamline at Cell 27.

Re-matched Optics for scheme 2 (1.0 m displacement)

Here the optics after a local compensation for the 1.0 m displacement scheme (also see Fig. 5).

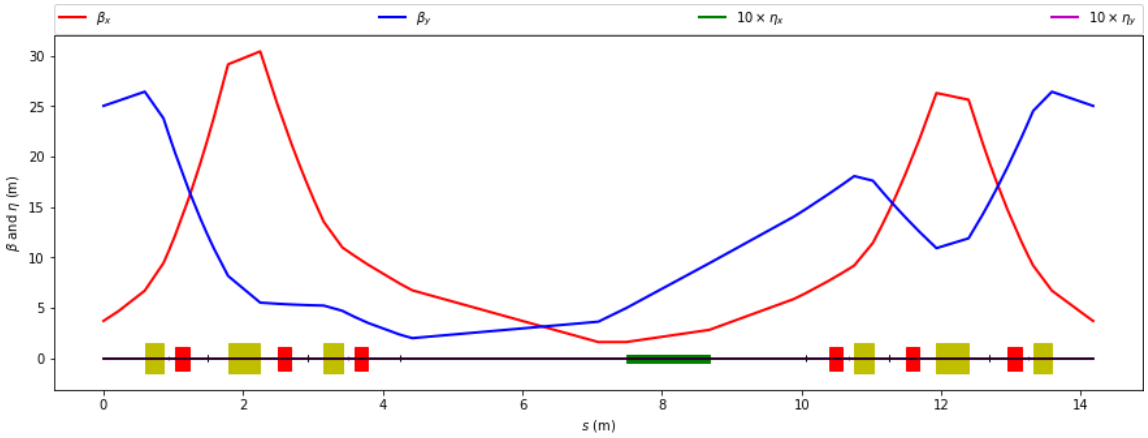

Fig. 6. Optics of the ID 27 section with the SCW (1.0 m displacement scheme)

Appendix 4. Lattice Schemes for the HEX Beamline at Cell 27.

The optics of the whole ring after correction

The optics after a local compensation can be well restored after tuning 6 neighboring quadrupoles (QL1-3 at cell 26 and 27). The vertical tune of the scheme 1 was shifted from 16.263 to 16.283, which should satisfy our previous goal to move the tune apart.

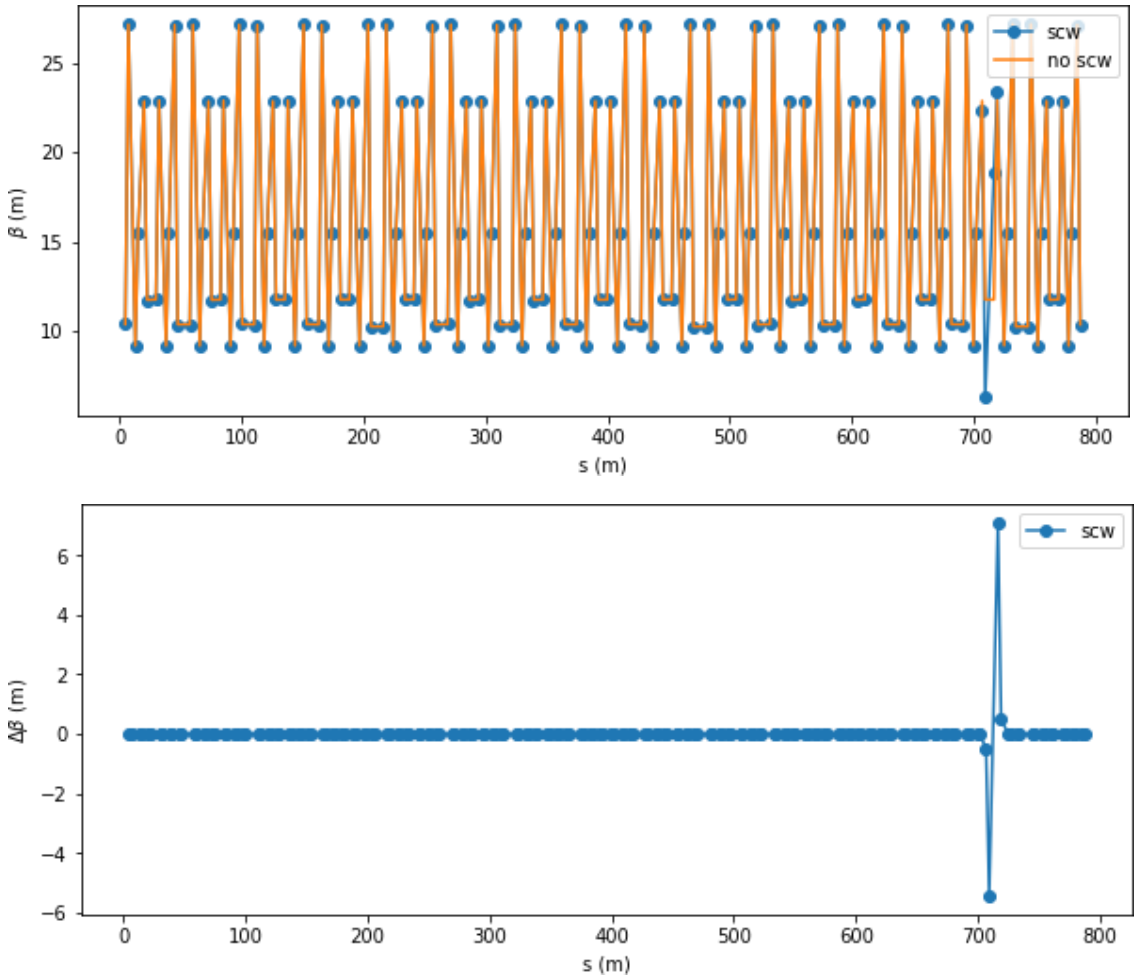

Fig. 7. Optics comparison w/o the SCW in the vertical plane after local compensation for scheme 1

For scheme 2, the tune was shifted as 33.235/16.276.

Appendix 4. Lattice Schemes for the HEX Beamline at Cell 27.

Tune-shift-with-amplitude

The patterns of tune footprint with the amplitude (for scheme 1) are similar as the operational lattice.

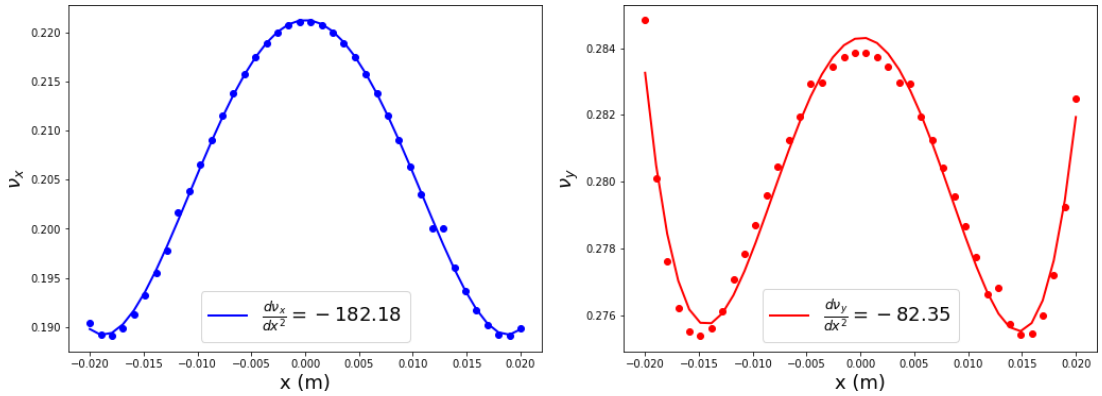

Fig. 8. Tune shift with amplitude in the horizontal plane for scheme 1

Same coefficients are calculated for scheme 2, which has tiny difference from scheme 1.

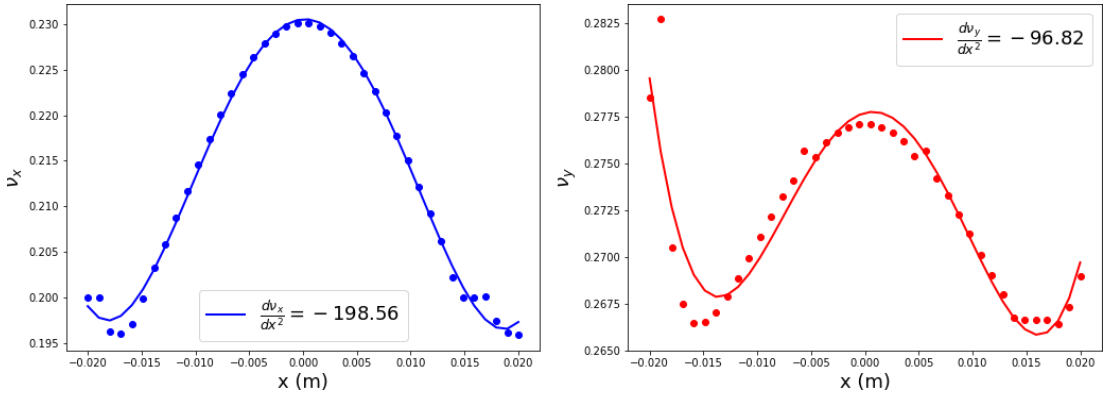

Fig. 9. Tune shift with amplitude in the horizontal plane for scheme 2

Appendix 4. Lattice Schemes for the HEX Beamline at Cell 27.

Dynamic aperture and FMA

Here some tracking studies (dynamic aperture, FMA and energy acceptance) for the error-free lattice.

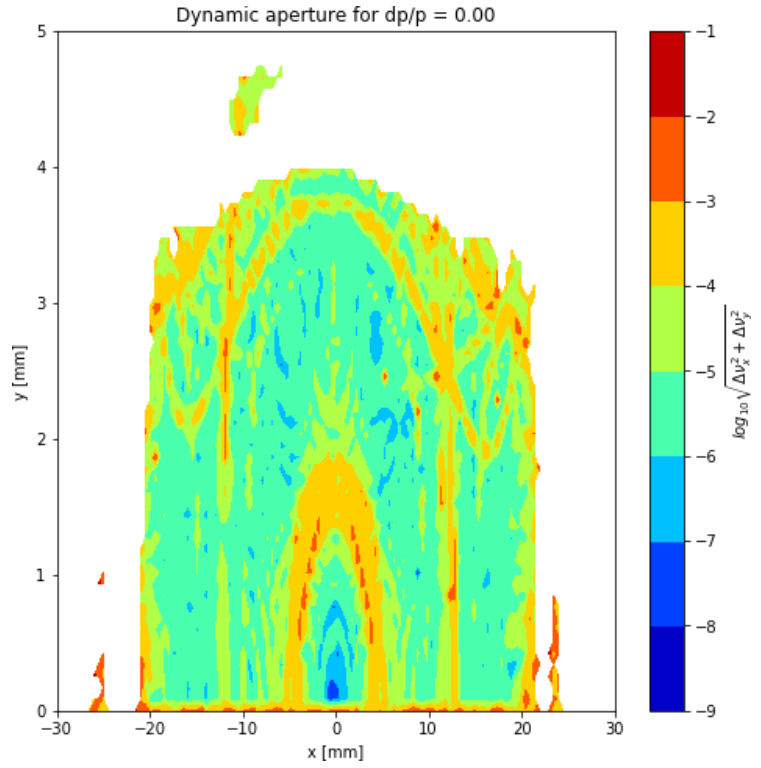

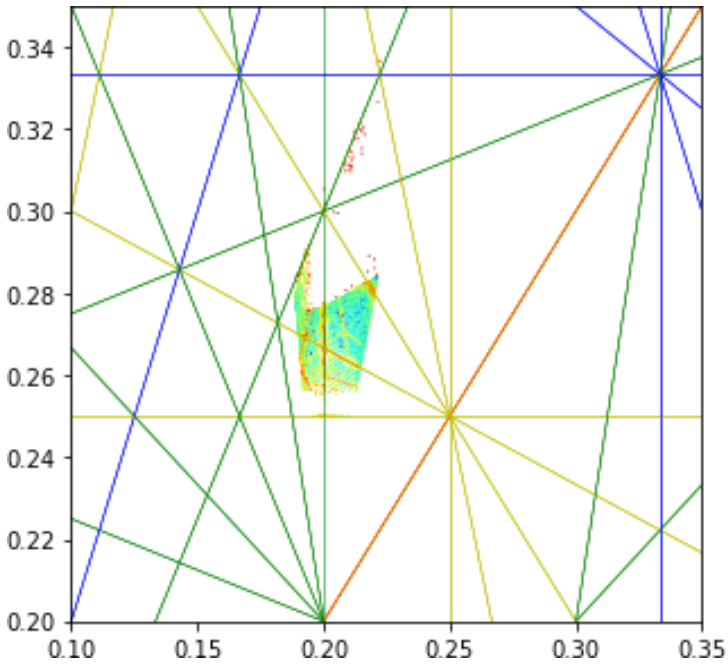

Appendix 4. Lattice Schemes for the HEX Beamline at Cell 27.

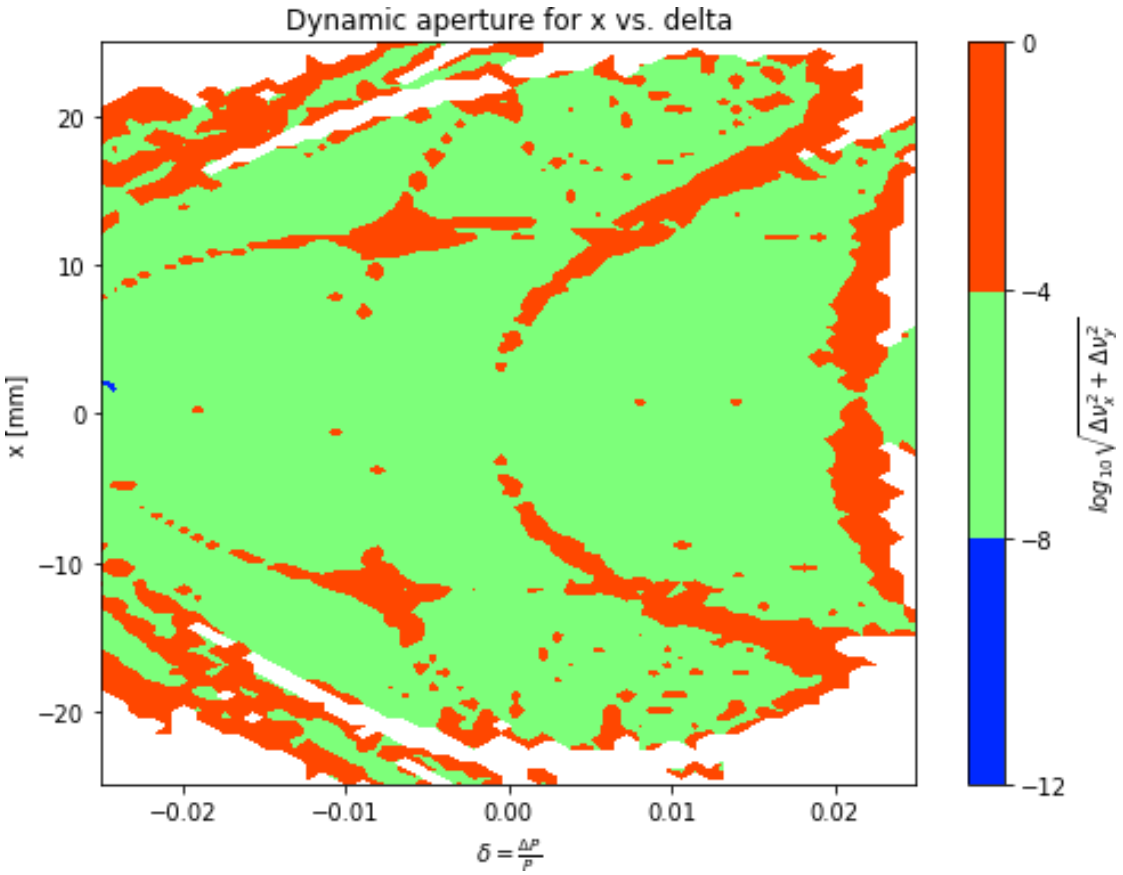

Fig. 10. DYAP, FMA and momentum acceptance for the error-free lattice for scheme 1

Appendix 4. Lattice Schemes for the HEX Beamline at Cell 27.

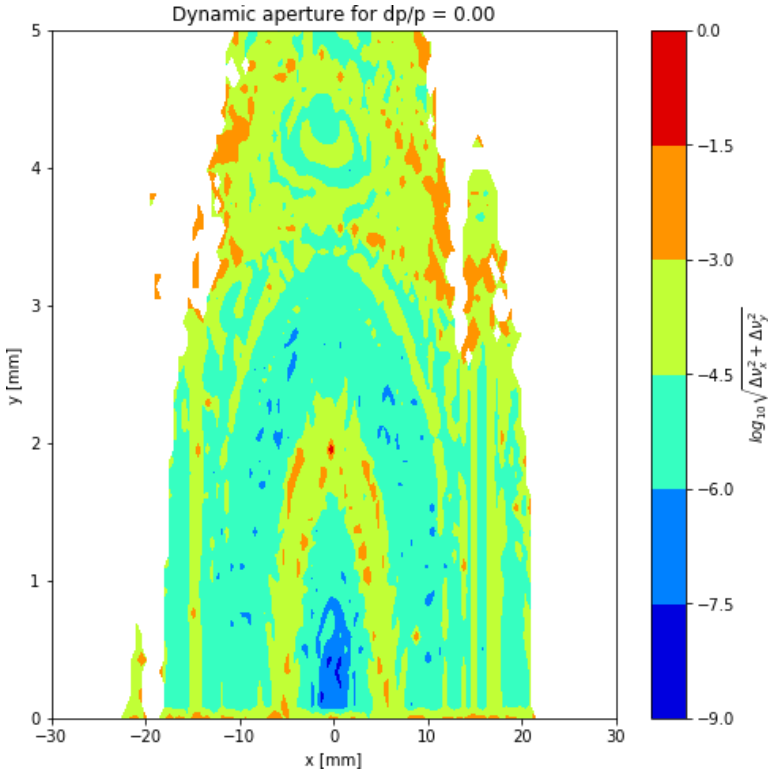

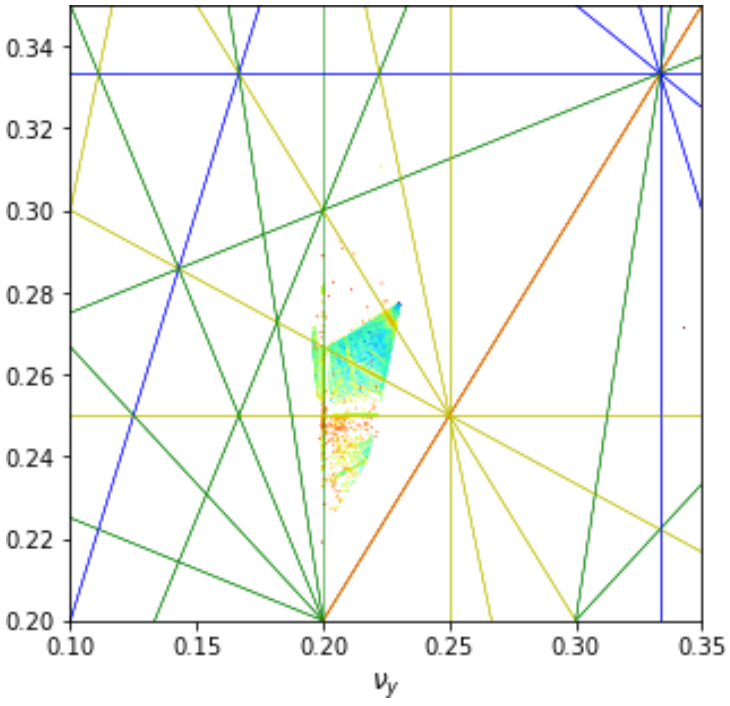

Appendix 4. Lattice Schemes for the HEX Beamline at Cell 27.

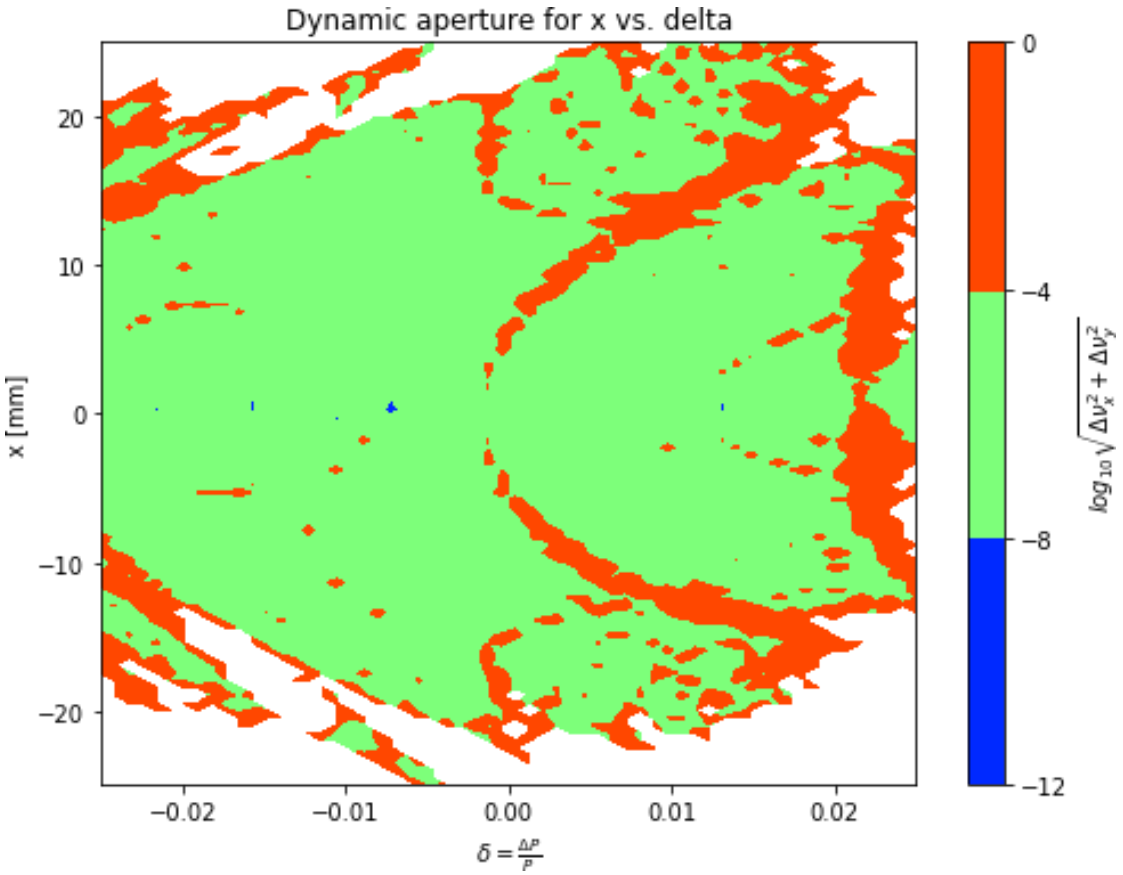

Fig. 11. DYAP, FMA and momentum acceptance for the error-free lattice for scheme 2

Optics at the center of SCW

The linear optics at the center of the SCW is shown below.

For scheme 1: betax = 3.235e+00, alphax = -9.319e-01, betay = 1.566e+01, alphay = -3.078e+00

For scheme 1: betax = 1.953e+00, alphax = -4.871e-01, betay = 7.998e+00, alphay = -2.036e+00

Conclusions

Based on our model, the linear optics can be compensated locally; the tune shift is at the order of 0.01-0.02.

Without a further optimization on sextupole configuration, its dynamic aperture and energy acceptance become smaller comparing with the bare lattice. Some resonances are found stronger as well. But it should be able to satisfy the requirement for top-off injection.

Last, but not least, the current machine deviates from the model already. The nonlinear deviation has not been well calibrated and actually is not well understood yet. The injection efficiency is spoiled by the reduction of dynamic aperture, and this is sensitive to the linear tune during operational run. Some further online sextupole tuning, or re-optimization of sextupole configuration with beam might be needed.

Appendix 4. Drawings

The following drawings are available on request.

Beamline Layout	See ray tracing drawing, front sheet.
Facility Layout, Showing HEX Location	PD-HEX-LAY-1000
HEX User Space Layout	PD-HEX-LAY-1050
Hutches	Drawings listed in Table 15**Error! Reference source not found.** on Page 105
Ray Tracing	PD-HEX-RAYT-0001
Utilities Interface Control Drawings	PD-HEX-UT-1000
Front End Ray Tracing	SR-FE-27ID-1001